Identifying novel anti-ageing targets for the epigenetic reprogramming of hematopoietic stem cells

Quinn Stacpoole

ORCID ID: 0000-0002-5392-7067

Submitted for the degree of Doctor of Philosophy

June 2026

The Walter and Eliza Hall Institute of Medical Research

Department of Medical Biology
Faculty of Medicine, Dentistry and Health Science
The University of Melbourne

Overall Thesis Abstract/Summary

Among the primary drivers of cellular ageing is the loss of epigenetic information that governs a cell's gene expression pattern and overall identity. Multiple generations of healthy animals can be serially cloned by epigenetically reprogramming one adult somatic cell from each generation back to a pluripotent state, demonstrating that ageing is largely an epigenetic phenomenon that can be reset. Pluripotency factors (e.g. the Yamanaka factors Oct4, Sox2, Klf4 and Myc), other transcription factors and even small molecules have been shown to molecularly and functionally rejuvenate many aged cell types and tissues. Importantly, partial reprogramming through transient or cyclical exposure to pluripotency reprogramming factors aims to prevent the loss of cell identity while still retaining some rejuvenating aspects of full pluripotency induction. Furthermore, other transcription factors may have cell rejuvenating properties without any transformation towards pluripotency.

The immune system plays a major role in maintaining tissue homeostasis through clearance of senescent cells, pathogens and cancer cells. However, aged immune cells show a multitude of age-associated alterations that lead to changes in blood composition and immune dysfunction. Hematopoietic stem cells (HSCs) are at the apex of the blood cell hierarchy and display an age-associated expansion of clonally related cells with a myeloid bias and reduced ability to reconstitute the blood. Transplantation assays using aged human or murine HSCs into young mice has revealed intrinsic proliferative and differentiation defects not restored by the young bone marrow environment. However, aged HSCs reprogrammed to induced pluripotent stem cells (iPSCs) using Yamanaka factors, then redifferentiated back to HSCs, appear to be molecularly and functionally rejuvenated. Despite this promising ability, reprogramming to pluripotency comes with complications and risks (e.g. teratomas) and rejuvenation of blood progenitors by partial reprogramming or by other non-pluripotency factors has not been demonstrated.

This thesis describes experiments which explore the feasibility of partial reprogramming of murine HSCs, then describes the use of multi-omic integration and network analysis to generate Hi-C informed gene regulatory networks (GRNs) for aged and young HSCs. These GRNs were then used to identify non-pluripotency transcription factors predicted to epigenetically reprogram age HSCs to a more youthful state.

Declaration

This is to certify that:

(i) This thesis comprises only of my original work towards the Doctor of Philosophy, except where indicated in the preface;

(ii) Due acknowledgement has been made in the text to all other material used; and

(iii) The thesis is fewer than 100,000 words in length, excluding tables, figures, bibliographies and appendices.

Quinn Stacpoole

Preface

In accordance with the regulations of the University of Melbourne, I acknowledge that this thesis comprises my original work, apart from the bioinformatic analyses of Hi-C data in Chapter 3, which was performed by Dr. Hannah Coughlan. In addition, the generation of pre-existing raw ATAC-seq and RNA-seq data was retrieved from GEO and duly referenced in Chapter 4. All sample collection, preparation for the Hi-C experiments, reprogramming experiments, flow cytometry analysis, etc., were performed by me, except for the operation of the flow cytometry sorting machines which was performed by the WEHI flow cytometry facility staff. In addition, sequencing runs on the Illumina were performed by the WEHI genomics facility.

Chapter 4 of this thesis is a manuscript under review as follows:

Stacpoole, Q., Iannarella, N., Johanson, T. M., Coughlan, H. D., & Allan, R. S. (2026). Multi-omic gene regulatory networks informed by 3D chromatin architecture reveal insights into hematopoietic stem cell ageing.

(In revision following peer review by *Cell Reports*, preprint available at *bioRxiv*.)

Acknowledgements

I would like to thank my supervisors Associate Professor Rhy Allan and Dr Tim Johanson for all their support during my PhD project. I would also like to thank my bioinformatics mentor Dr Hannah Coughlan, who provided much needed guidance regarding the computational analysis that I completed but who also did the Hi-C analysis in Chapter 3. It was a pleasure to work in the Allan lab, the members of which were always happy to discuss science but also provide the much-appreciated non-science chat and banter to lighten the days.

All the sequencing for this project was completed by the WEHI Genomics lab and I would like to thank Dr. Stephen Wilcox and Sarah McRaild who ran all of my sequencing experiments.

I would also like to thank and acknowledge Nadia Iannarella and several members of the Bio-services department and the animal technicians, including Jessica Martin, Michael Watters, Natalia Mora and Leanne Johnson, who helped with the care of the experimental animals.

I would also like to thank my PhD committee, Prof. Marnie Blewitt, Prof Stephen Nutt and Prof Louise Purton for their advice, support and extra mentoring.

This research was supported by the Commonwealth through an Australian Government Research Training Program Scholarship, a Walter and Eliza Hall top-up scholarship, an Edith Moffatt stipend extension scholarship and an Edith Moffatt travel scholarship.

Table of Contents

Overall Thesis Abstract/Summary ii

Declaration iii

Preface iv

Acknowledgements v

Chapter 1: Introduction 4

1.1 Background 4

1.2 The ageing of hematopoietic stem cells (HSCs) 5

1.2.1 General features of HSC ageing 6

1.2.2 Lab mice versus wild mice 9

1.2.3 Mitochondrial changes in aged HSCs 9

1.2.4 Cell extrinsic factors and signals associated with HSC ageing 10

1.2.5 Cell intrinsic age-related changes in HSCs 13

1.2.6 Infection history, replication stress as a link between extrinsic and intrinsic drivers of HSC ageing 19

1.2.7 Epigenetics of HSC ageing 21

1.2.8 Current attempts to rejuvenate aged HSCs 24

1.3 Restoration of youthful function using epigenetic reprogramming 27

1.3.1 Loss of epigenetic cell identity as a driver of ageing 27

1.3.2 Age "reversal" using Yamanaka factors 29

1.3.3 Epigenetic memory of a youthful state 31

1.3.4 Potential dangers of pluriopotency factors 32

1.4 3D genome organisation in GRN construction and analysis 34

1.4.1 Gene regulatory networks (GRNs) for studying ageing 34

1.4.2 Hi-C informed gene regulatory networks 37

1.5 Significance and scope of the PhD project 39

1.6 Aims and Hypothesis of the PhD project 40

Chapter 2: Reprogramming of murine HSCs with Yamanaka factors 42

2.1 Introduction 42

2.2 Results 44

2.2.1 OSKM PiggyBac vector does not provide sufficient transfection of HSCs 44

2.2.2 Dox-inducible lentiviral OSKM or OS2-17K vectors do not provide sufficient transduction of LT-HSCs 46

2.2.3 In vitro transcription (IVT) and transfection with polycistronic Yamanaka factor mRNA depends on mRNA size and gene content 51

2.2.4 Nucleofection with DNA plasmids bearing OSK fails to transfect primary murine blood stem cells 56

2.3 Discussion and conclusions 62

2.4 Methods 63

2.4.1 Plasmids for reprogramming 63

2.4.2 Nucleofection of HEK293T cells and primary murine bone marrow cells 73

2.4.3 Lentiviral production and transduction (spin infection) of sorted LSKs 74

2.4.4 In vitro transcription 76

2.4.5 Cell culture 77

2.4.6 Flow cytometry 77

Chapter 3: In Situ Hi-C benefits from extended crosslinking with a double fixation method prior to DNA digestion 79

3.1 Introduction 79

3.2 Results 81

3.2.1 Double fixation shifts library composition toward shorter-range cis contacts and reduces trans-associated signal 81

3.2.2 Differential contact analysis reveals scale-dependent protocol effects 85

3.3 Discussion and conclusions 86

3.4 Methods 87

3.4.1 Low-input Hi-C library preparation 87

3.4.2 Hi-C analysis 90

Chapter 4: Publication in review: "Multi-omic gene regulatory networks informed by 3D chromatin architecture reveal insights into hematopoietic stem cell ageing" 92

4.1 Abstract 94

4.2 Introduction 95

4.3 Results 98

4.3.1 Mitochondrial membrane potential status does not confer differences in 3D genome architecture, but age does 98
4.3.2 Changes in higher order chromatin structures indicate an age-associated increase in disorder 98
4.3.3 Aged LT-HSCs develop chromatin interactions associated with differentially expressed genes 100
4.3.4 Genes that have age-related inappropriate lineage expression overlap with changes in genome organisation 102
4.3.5 AP-1 factor binding motifs are enriched in chromatin that opens and gain interactions during ageing 104
4.3.6 Integrated multi-omic analysis predicts TFs that drive the aged and youthful states of LT-HSCs 105

4.4 Discussion 108

4.5 Methods 112

4.5.1 HSC, monocyte and NK cell isolation 112
4.5.2 LT-HSCs antibody staining and FACS 113
4.5.3 Monocyte & NK cell antibody staining and FACS 113
4.5.4 In situ Hi-C 114
4.5.5 Hi-C DNA library preparation and sequencing 115
4.5.6 Hi-C analysis 115
4.5.7 Gene biological pathway enrichment analysis 116
4.5.8 Topologically associated domains (TAD) analysis 117
4.5.9 Compartment analysis 117
4.5.10 Shannon entropy analysis 118
4.5.11 RNA-seq analysis 119
4.5.12 Determination of lineage inappropriate expression 120
4.5.13 ATAC-seq analysis 120
4.5.14 Motif enrichment analysis 121
4.5.15 Network analysis and transcription factor ranking 122

4.6 Supplementary Figures for the paper in review "Multi-omic gene regulatory networks informed by 3D chromatin architecture reveal insights into hematopoietic stem cell ageing" 126

Chapter 5: Overall discussion, conclusions and future perspectives 132

Bibliography 138

Chapter 1: Introduction

1.1 Background

The majority of global diseases and deaths are now due to non-communicable, age-associated diseases with the top age-associated diseases being cardiovascular disease, chronic respiratory diseases and degenerative neurological diseases (R. Li et al., 2023; Naghavi et al., 2025). Modern medicines and improvements in nutrition and hygiene have all increased the average human lifespan, yet human maximum lifespan remains capped at around 120 years of age (Fulton et al., 2026; Olshansky et al., 2024). However, lifespan among mammals is extremely diverse with the Bowhead whale living more than 200 years, while the forest shrew lives to a mere 2.1 years (Mayne et al., 2019). Among vertebrates, the Greenland shark is thought to live for over 400 years (Nielsen et al., 2016). While this variation in lifespan among animals indicates a strong genetic component, there are also epigenetic mechanisms that modify lifespan. For example, the lifespan of a queen bee is 10 times longer than her worker sisters, even though they are genetically identical (Corona et al., 2005), demonstrating that the epigenetic regulation of DNA can have a dramatic effect on the longevity of an organism.

Humans and other animals accumulate somatic mutations, i.e. random non-germline mutations in individual cells acquired over time as a side effect of normal cell biology or by exposure to everyday genotoxic chemicals or radiation (Cagan et al., 2022). Somatic mutations can give rise to cancer (Anandakrishnan et al., 2019; Martincorena et al., 2017) but can also lead to expansion of clonal populations with phenotypes that are linked to ageing (Bernstein et al., 2024; Cagan et al., 2022; Lawson et al., 2025; Revechon et al., 2025; Zhang et al., 2019). However, serial cloning using somatic cell nuclear transfer (SCNT), demonstrates that somatic cells from adult animals (even very old ones) can be repeatedly reprogrammed back to an embryonic state and give rise to multiple generations of clones with normal lifespans (Malin et al., 2022; Wakayama et al., 2026; Wakayama et al., 2013). These SCNT experiments demonstrate that background somatic mutations are by and large not the major cause of cellular dysfunction during a normal lifespan. Moreover, recent reports have revealed that certain ageing phenotypes can be both accelerated by perturbations to the

epigenome (J.-H. Yang et al., 2023a), but also "rejuvenated" by overexpression of the embryonic transcription factors Oct4, Sox2, Klf4 and Myc (Browder et al., 2022; Gill et al., 2022; Ocampo et al., 2016), thus demonstrating that reversible epigenetic changes are likely the cause of many cellular ageing phenotypes.

Epigenetic regulation of genes is heavily governed by transcription factors (TFs) which act in concert to orchestrate modifications to DNA and histone proteins to coordinate gene expression in different cell types. Construction and analysis of gene regulatory networks (GRNs) and cell-cell communication networks (CCNs) have become important tools to predict the extracellular and intracellular factors that drive cellular behaviours in different cell-types, or in the same cell-type in different conditions. Furthermore, construction of GRNs using 3D chromatin organisation data from Hi-C experiments is an emerging and uniquely useful aspect to GRN inference, as it can provide information about gene regulation that occurs at a distance.

This introductory chapter is broken into 3 sections. The first section will outline the evidence for the effects of epigenetic changes on the ageing of hematopoietic stem cells (HSCs) in the bone marrow compartment. The second section will outline evidence for restoration of youthful function using epigenetic reprogramming in other cell types and why this may be a strategy for restoring function to aged HSCs. The third section will outline the usefulness of Hi-C and 3D genome organisation in GRN construction and analysis. Finally, I will describe the aims and significance of this PhD project and highlight how Hi-C informed GRN analysis can guide future blood rejuvenation strategies.

1.2 The ageing of hematopoietic stem cells (HSCs)

HSCs are multipotent stem cell that give rise to all the mature blood cell types and are found in the bone marrow. In mice and humans, they are rare and represent only 0.005% to 0.01% of all nucleated bone marrow (BM) cells (Mayer et al., 2022). In aged mice or humans, there is an expansion of long-term HSCs (LT-HSCs) due to increased self-renewal, but a skewing of lineage committed progenitors to a myeloid lineage (Karagiannis et al., 2023; Säwen et al., 2018; Sun et al., 2014). In mice, transplantation of aged HSCs into young mice does not appear to correct the repopulating abilities of the stem cells, suggesting a cell-intrinsic component to HSC ageing (Dykstra et al., 2011; Liang et al., 2005; Rossi et al.,

2005). However, other studies have found that transcriptional signatures and some function is partially restored by transplantation into young congenic mice, even non-irradiated ones, while DNA methylation profiles remain unchanged (Kuribayashi et al., 2021), suggesting both a cell-extrinsic and intrinsic dysfunction. Additionally, the commonly observed partial restoration of function after transplantation of aged HSCs into young mice (Ergen et al., 2012; Kuribayashi et al., 2021; Montecino-Rodriguez et al., 2019; Yamamoto et al., 2018), especially after secondary transplantation (Yamamoto et al., 2018), suggests extrinsic components of HSC ageing can modify the intrinsic components. This makes sense if one considers that epigenetic age-related changes, which are perhaps heritable during cell division, remain plastic and malleable depending on the environment. However, the blood cells of recipients of donor bone-marrow during cancer treatment have the epigenetic age of the donor (Søraas et al., 2019; Weidner et al., 2015), reinforcing the observation that epigenetic aspects of blood progenitor aging (namely DNA methylation) are less modifiable by the young bone-marrow environment. In this section of the introductory chapter, I will outline the general traits of HSC ageing, but also define the experimentally validated extrinsic and intrinsic aspects of HSC ageing as follows:

The cell extrinsic aspects of HSC ageing are the external factors and signals in the bone-marrow microenvironment capable of altering the aged HSC phenotype after transplant. Conversely, the cell-intrinsic aspects of HSC ageing are the traits not readily altered after transplantation and exposure to the young microenvironment. However, it should be noted that this is a slight false dichotomy since extrinsic factors shape intrinsic epigenetic memory over time. Thus, HSC ageing is really the interplay of external and internal factors that shapes cell identity and behaviour.

1.2.1 General features of HSC ageing

1.2.1.1 Human features of HSC ageing

Many studies have found that HSCs increase in frequency with age, while common lymphoid progenitor frequencies decrease (Amoah et al., 2022; Kuranda et al., 2011; Pang et al., 2011; Rundberg Nilsson et al., 2016; Woolthuis et al., 2014), although there is actually a decrease in circulating $CD34^+$ progenitors (Fali et al., 2018). More recently, Amoah et al. (2022) demonstrated that HSCs (Lin^- $CD34^+$ SSc^{low} $CD38^-$ $CD90^+$ $CD45RA^-$) from people

between 58-82 years of age (median age 66 years old) increased in frequency, as did the overall population of hematopoietic progenitor cells (HPCs) ($Lin^- CD34^+ SSc^{low} CD38^-$), but not the overall frequency of $Lin^- CD34^+ SSc^{low}$ cells within the BM. The same study demonstrated that the increase in HSC & HPC frequencies correlated with an increase in the activity of the Rho-GTPase, Cdc42 and that aged HSCs had a delayed time to first division (Amoah et al., 2022). There is also a report of an age-associate loss of PIDD1, a protein that promotes caspase-2 mediated cell-cycle arrest and apoptosis, which may encourage the aged-associated over-proliferation of HSC (Schwab et al., 2021).

By using single cell multi-omic analysis on PBMCs from people 20-106 years old, Karagiannis et al (2023) were able to confirm the shift to a higher myeloid ratio, but also identified increased expression of certain protective genes in centenarians, including apotosis regulator STK17A and inflammation regulator S100A4 (Karagiannis et al., 2023). While there is a consistent age-associated increase in the frequency of $CD34^+$ HSCs in humans and a decrease in the frequency of lymphoid biased progenitors, it is noteworthy that most studies mentioned do not examine people over the age of 85 and most look at people under 80 years old. So, the question of whether human HSCs reach a proliferation limit and begin to decline in normally aged humans over 85 is still up for debate.

Recently, it was also demonstrated that, in humans and mice, age-related loss of A20/TNFAIP3, a protein with deubiquitinating protease and E3 ligase activity that responds to DAMP and PAMP signals by negatively regulating excessive NF-κB signalling, leads to HSC expansion and increased myeloid-biased differentiation (Smith et al., 2020). What causes the age-related loss of TNFAIP3 is unclear, but the answer could be cell intrinsic or cell extrinsic.

1.2.1.2 Murine features of HSC ageing

H2B-GFP-based lineage tracing shows that only severe radiation or chemotherapy-induced myeloablation could stimulate murine HSCs to divide (Munz et al., 2023). Similarly, lineage tracing by genetically labelling murine HSCs with tdTomato at 2, 6 and 12 months of age, then monitoring PB at 4 week intervals, demonstrated that aged HSCs contribute less to mature blood cell types and myeloid-bias can be explained by the gradual loss of a lymphoid-biased MPP population (Konturek-Ciesla et al., 2023).

Many studies have discovered specific changes in aged HSCs, particularly murine HSCs, including loss of PU.1, increase in Taz and concomitant increase in Clca3a1 surface expression (Kim et al., 2022), gradual build up and switching to Ezh2 (over Ezh1), possibly used as a molecular memory of divisions (Bernitz et al., 2020), loss of Igf1 (Young et al., 2021; Young et al., 2024) and decrease in the histone acetyltransferase Kat6b (also known as MORF) (Khokhar et al., 2020).

Aged murine HSCs also become more transcriptionally active and express many non-HSC membrane proteins, most notably *Selp (CD62p)*, which codes for a P-selectin transmembrane adhesion protein (Flohr Svendsen et al., 2021). scRNA-seq data of HSCs from young (10-week-old), middle-aged (12-month-old) and aged (20-month-old) mice confirms upregulation of age-related genes previously reported, such as *Selp*, *Mt1*, and *Vwf*, but also showed that Clusterin (Clu), a secreted chaperone protein, may be a marker of myeloid biased HSCs (Koide et al., 2021). Aged HSCs also show a loss of *miR-146a*, which is associated with higher sensitivity to IL6 stimulation and thus inflammatory signalling (Grants et al., 2020) and increased expression of *miR-132*, possibly to enhance survival (Mehta et al., 2015). Cryptic transcription, aberrant transcription initiation from non-promoter regions within the gene body is also elevated in aged mouse HSCs, consistent with an age-related opening of the chromatin (McCauley et al., 2021).

Single-cell expression analysis of young and aged murine hematopoietic stem and progenitor cells (HSPCs) revealed within the primitive HSC cluster a downregulation of differentiation genes *Cd34* and *Cd48*, upregulation of platelet-lineage genes *Vwf* and *Clu*, delayed differentiation pseudotime and upregulated cell cycle arrest genes, which explains the delayed differentiation and myeloid skewing observed in transplantation studies (Hérault et al., 2021). Additionally, differentiation trajectories suggested that myeloid bias is a result of increased erythroid/megakaryocyte development driven partly by increased Gfi1b transcription factor activity (Hérault et al., 2021).

Many markers of aged myeloid-biased HSCs have been discovered including, CD150 level (Young et al., 2021), the α-integrin CD41 (Gekas & Graf, 2013), NEO1 (Gulati et al., 2019), Vwf (Koide et al., 2021) and CD49b negativity (Su et al., 2024). Interestingly, functional differences and fate decisions in these HSCs may be epigenetic since $CD49b^-$ and $CD49b^+$ HSCs, which are myeloid and lymphoid biased, respectively, are transcriptionally

similar but have distinct chromatin accessibility profiles (Su et al., 2024). Also, it should also be noted that while the $CD150^+$ $CD48^-$ $CD41^+$ lineage negative Sca-1^+ cKit^+ cells (LSKs) are expanded in aged mice (Gekas & Graf, 2013), there is a $CD41^+$ "latent-HSC" which is initially myeloid-biased but that become multipotent upon secondary transplantation (Yamamoto et al., 2018). However, the antibody used to identify CD41 (MWReg30 clone) is a blocking antibody that might interfere with bone marrow engraftment as it is a receptor for several ECM proteins (Purton, 2022). Interestingly, another α-integrin, CD61 is upregulated in aged LT-HSCs and appears to mark myeloid-biased HSCs (Mann et al., 2018), but these $CD61^+$ HSCs appear functionally superior, i.e. capable of more long-term engraftment when transplanted (Skinder et al., 2024). On the other hand, the decrease in repopulation potential in LT-HSCs (but not myeloid bias) is associated with the level of surface expression of the P-selectin Selp (CD62p) (Yang et al., 2025).

1.2.2 Lab mice versus wild mice

Aside from mice and humans having species specific differences in their immune systems, most of our knowledge about mouse hematopoiesis is a result of studying lab mice in controlled sterile conditions. However, humans live in the wild, exposed to sundry pathogens and non-pathogenic substances that our immune systems react to, thus findings from lab raised mice in sterile conditions may not reflect real world biology. For example, wild mice have different blood composition to lab mice (Muir et al., 2023), partially attributable to differences in gut flora complexity (Y. H. Chen et al., 2023; Oh et al., 2025). Therefore, if mouse ageing is to be a good model for human immune ageing, comparison of aged versus young HSCs from wild or rewilded mice may be an important area of research that needs to be addressed.

1.2.3 Mitochondrial changes in aged HSCs

In aged mice, there is a fraction of HSCs that have low levels of autophagy and accumulate mitochondria, while also having high metabolic activity (Ho et al., 2017). HSCs lower their expression of Drp1, a regulator of mitochondrial fission, after several rounds of division and lower Drp1 levels are associated with larger, but less distributed mitochrondria that are located more polarly within the cell (Hinge et al., 2020). The same study showed that the

mitochondria are asymmetrically segregated, whereby the altered mitochrondria are preferentially retained by the daughter HSC that returns to quiescence, thus indicating another possible mechanism of divisional memory in HSCs (Hinge et al., 2020).

Quiescent HSCs also have low mitochondrial membrane potential (MMPot), low reliance on glycolysis, and DRP1-mediated mitochondrial fragmentation partly mediates the suppression of mitochondrial activity in MMPot low HSCs (Liang et al., 2020). Furthermore, MMPot low HSCs sequester mitochondria, thus suppressing mitochondrial function, and do not degrade them, while MMPot high HSCs, which are more activated, turnover mitochondria more readily (Liang et al., 2020). Human HSCs with the lowest MMPot also have the highest engraftment potential (Qiu et al., 2021). Additionally, mitochondria in aged murine HSCs have low MMPot which correlated with myeloid bias, and pharmacological enhancement of mitochondrial membrane potential using mitoquinol increased engraftment and reduced the myeloid skewing of transplanted HSCs (Mansell et al., 2021). As will be discussed in Chapter 4, I used Hi-C to examine whether MMPot status in HSCs is reflected within the 3D chromatin architecture.

1.2.4 Cell extrinsic factors and signals associated with HSC ageing

1.2.4.1 Immune cell activation in the niche

The stem cell niche in the bone marrow plays a major role in dictating the activation state, transcriptional profile and fate determination of HSCs. For example, analysis of ligand-receptor interactions in single-cell data from human bone marrow have revealed that ageing is accompanied by a systematic decrease in supportive niche interactions, followed by the emergence of maladaptive, inflammation-associated communication networks in the bone marrow (Feng et al., 2024). Furthermore, there is also a remodelling of the arteriole network in the aged mouse bone-marrow niche, which is associated with altered HSC positioning and clustering of HSCs closer to sinusoids (Saçma et al., 2019). Interestingly, the most quiescent, slowest dividing HSC subpopulation reside predominantly in perisinusoidal niches and appear the most protected from ageing (Saçma et al., 2019).

Analysis of the aged murine BM microenvironment also found increased Il-1β levels produced by cells of the endosteum (Mitchell et al., 2023). Increased Il-1β is associated with loss of efferocytosis in aged murine bone-marrow resident macrophages and increased

caspase-1 activity in phagocytes, which is sufficient to cause myeloid/megakaryocyte-biased skewing of the neighbouring HSCs (Frisch et al., 2019). In addition, plasma cells are increased in the bone marrow of aged mice and exhibit high expression of inflammatory cytokines that likely influence the skewing of HSC differentiation (Pioli et al., 2019). Similarly, age-related loss of the extracellular matrix glycoprotein, osteopontin, is associated with HSC expansion and other ageing phenotypes of mouse HSCs (Guidi et al., 2017). Loss of Netrin-1, a protein expressed mainly by arteriolar endothelial cells and periarteriolar smooth muscle cells in the BM niche which protects HSCs from exhaustion by increasing NF-κB activation, is associated with age-related denervation of the BM leading to HSC exhaustion and eventual depletion (Renders et al., 2021).

1.2.4.2 Mesenchymal stromal/stem cells (MSCs) ageing

Age associated changes to HSC supporting mesenchymal stromal/stem cells (MSCs) also influence HSC ageing phenotypes. For example, it has been demonstrated that aged mouse HSCs have a loss of mTor signalling due to loss of upstream Igf1 signalling specifically from aged MSCs in the bone marrow niche (Young et al., 2021). Furthermore, the myeloid bias of transplanted aged mouse HSCs can be rescued by Igf1 overexpression whereby Igf1 selectively expands lymphoid biased HSCs and restores mitochondrial function (Young et al., 2021). Later reports show that even by middle age murine MSCs in bone marrow downregulate stem cell factor and Igf1, which was associated with reduced lymphoid output in surrounding HSCs (Young et al., 2024). Reduced expression of CXCR4 on aged MSCs in the bone-marrow is also associated with reduced hematopoiesis and myeloid skewing (Singh et al., 2020). SPP1 from human bone marrow MSCs and MMP9 from macrophages have also been identified as ligands driving the upregulation of myeloid-bias inducing AP-1 factors in human HSCs (Feng et al., 2024).

A more recently described kind of pluripotent-like mesenchymal progenitor known as multilineage-differentiating stress-enduring (MUSE) cells (Kuroda et al., 2010) likely has a role in supporting HSCs during ageing. Muse cells express the mesenchymal markers such as CD105, but also the pluripotency marker SSEA-3, and support HSCs in the bone marrow in times of stress (Alessio et al., 2017; Jeong et al., 2018). For example, it has been shown that after 5-FU depletion of immune cells and subsequent stimulation of HSC activity, there

is an increase in SSEA-3 positive mesenchymal cells that also upregulate Jag1, possibly to stimulate HSC self-renewal and replenish the HSC pool (Jeong et al., 2018). How muse cell populations change with age and whether they contribute to changes in the supporting HSC niche is still a major gap that warrants further exploration.

1.2.4.3 Advanced glycation end products (AGEs)

Advanced glycation end products (AGEs) are random sugar-protein crosslinking events that form non-enzymatically over time and have been shown to build up in the extracellular matrix of human bone during ageing (Arakawa et al., 2020; Miyata et al., 1996; Yang et al., 2015). Receptors that detect AGEs (RAGEs) are found on animal cells, including humans (Neeper et al., 1992) and activation of RAGE receptors triggers a robust inflammatory state in monocytes and macrophages, stimulating the secretion of pro-inflammatory cytokines IL-1β and Tumor Necrosis Factor-alpha (TNF-α) (Hofmann et al., 1999). Interestingly, RAGE receptors are significantly upregulated in human bone-marrow MSCs with age (Stolzing et al., 2008) and AGEs likely skew the osteogenic potential of MSCs (Zheng et al., 2024). Despite the seemingly important contribution of AGEs to increased inflammatory signalling, MSC dysfunction and loss of bone structure, no studies have yet explored how increased AGEs might impact the ageing of HSCs.

1.2.4.4 Chronic infection of bone marrow niche cells

A survey of viruses found in human bone marrow from people aged 36 to 85 years old demonstrated that bone marrow cells can be chronically infected with a number of different viruses, including high prevalence of Parvovirus B19 (B19V), Torque teno virus (TTV), but also medium level prevalence of Epstein-Barr virus (EBV), Merkel cell polyomavirus (MCPyV) and human herpesvirus 7 (HHV-7) (Toppinen et al., 2021). TTV establishes a chronic, high-level replication cycle in mature lymphoid and erythroid lineages and is associated with chronic inflammatory signalling known to affect HSCs (Cianfruglia et al., 2026). B19V has high tropism for a number of cell types, including MSCs, where chronic infection causes increase in expression levels of IL-11 and thrombopoietin (TPO) to alter HSC behaviour (Fard et al., 2021). Furthermore, chronic infection with murine

cytomegalovirus (MCMV) increases system wide inflammatory signalling in mice, which caused reduced reconstitution capacity in HSCs (Hirche et al., 2017).

1.2.5 Cell intrinsic age-related changes in HSCs

Heterochronic transplantation is often used to isolate the cell intrinsic age-related changes of HSCs from changes that may be due to the aged environment of the HSC niche. For example, early studies showed that aged LT-HSCs transplanted into young lethally irradiated congenic mice retained the characteristic increase in frequency and bias towards granulocyte-macrophage progenitor (GMP) differentiation, indicating a cell intrinsic fault in HSC turnover and differentiation potential (Rossi et al., 2005). More recent studies have also found similar reduced engraftment capacity and impaired lymphoid output leading to myeloid-biased reconstitution after transplantation, but also that certain molecular characteristics of the chromatin are also refractory to exposure to the young bone-marrow environment. For example, 3 to 4 months after transplantation, old murine HSCs showed only partial restoration of chromatin accessibility and retained age-associated γH2AX and fibrillarin (FBL) foci (Ho et al., 2021).

1.2.5.1 DNA methylation changes in aged HSCs

Other intrinsic aspects of HSC ageing include the accumulation of somatic mutations, telomere attrition, but also refractory epigenetic changes, such as DNA hyper- or hypomethylation. For example, a 5% reduction in global DNA methylation was found in mouse HSCs, but certain genes (*Kiss1r*, *Nav2* and *Hsf4*) which are normally unmethylated but kept repressed by polycomb repressive complex-2 (PRC2) were found to be hypermethylated in older HSCs (Taiwo et al., 2013). Furthermore, aged HSCs transplanted into young mice have a restored youthful pattern of transcription but not restored DNA methylation (Kuribayashi et al., 2021), suggesting epigenetic memory of the aged state is more difficult to restore. Interestingly, it has been found that DNA methylation at CpG sites fluctuate in a circadian rhythm, and it is hypothesized that this continual demethylation and methylation could allow for the observed age-related epigenetic drift (Oh et al., 2018; Oh et al., 2019).

Measurement of DNA methylation age by use of the Horvath clock (Horvath, 2013) has revealed that the reconstituted blood of recipients of transplanted bone marrow is the same DNA methylation age as the original donor blood (Søraas et al., 2019), suggesting that HSC ageing is a cell-intrinsic property. This result was also found in a previous study using a different DNA methylation clock which noted that replicative stress during blood reconstitution in recipients likely aged the donor cells both in terms of telomere length and epigenetic ageing (Weidner et al., 2015). DNA methylation clocks that measure mitotic age of blood cells indicate that accelerated methylation age (mitotic age) is strongly associated with Parkinson's disease and immune system ageing (Paul et al., 2021). In terms of post-transplant age-acceleration, blood reconstituted from cord blood whose age is effectively zero undergoes DNA methylation age-acceleration ageing twice as fast as chronological age progression due to rapid expansion of cell numbers (Onizuka et al., 2023).

Despite the fact that epigenetic clocks reveal DNA methylation age patterns are preserved in donor blood cells, albeit with some age acceleration after transplant, it is still unclear whether quiescent human LT-HSCs that remain dormant undergo some epigenetic ageing, as do other non-dividing cells like neurons and cardiomyocytes. Unlike neurons and cardiomyocytes which are post-mitotic but still have a high metabolic load, quiescent LT-HSCs have low levels of metabolic activity and so may be somewhat protected from ageing. However, recent experiments using a mouse specific DNA methylation clock suggest murine LT-HSCs do in fact age epigenetically, although more slowly than average (Bogeska et al., 2022). Furthermore, the same study demonstrated that intermittent stimulation with the TLR3 agonist polyinosinic:polycytidylic acid (pI:pC) resulted in an accelerated DNA methylation age, approximately doubling their epigenetic age.

1.2.5.2 Transcription Factor activity in aged HSCs

As mentioned, DNA methylation patterns are not restored after transplanting aged HSCs into young mice (Kuribayashi et al., 2021). TF activity, inferred from the combined enrichment of the TF's binding motifs within accessible chromatin and the TF's target gene expression, plays a role in shaping cell identity by establishing and maintaining epigenetic patterns during differentiation and cell division. For example, single-cell analysis shows that certain subsets of lymphoid-biased HSCs have high Zbtb1 TF activity (Elias et al., 2025).

Examination of aged HSCs exposed to young blood factors showed that while cytokine receptor-ligand networks are restored, the TF activity of a certain set of TFs was not restored, indicating further epigenetic mechanisms that make aged HSCs refractory to young environments (Ma et al., 2022). Furthermore, there is a characteristic decrease in TF activity of PU.1 in aged HSCs which is not rescued upon transplant into young recipients (Kim et al., 2022). TF activity evidently plays a strong role in mediating the intrinsic epigenetic component of HSC ageing. However, an assessment and ranking of which TFs have the most influence on the transcriptional changes in aged HSCs has not yet been reported and will be discussed in Chapter 4 of this thesis.

1.2.5.3 Clonal hematopoiesis of indeterminate potential (CHIP)

A special case of an intrinsic aspect of human HSC ageing is clonal hematopoiesis of indeterminate potential (CHIP) characterised by the gradual expansion of blood cell clones harbouring specific acquired somatic mutations. CHIP increases the risk of developing blood cancer (Gu et al., 2023; Weeks et al., 2023), and has been implicated in stroke (Bhattacharya et al., 2022), heart failure (Yu et al., 2021) and atherosclerotic cardiovascular disease (Jaiswal et al., 2017), primarily due to inflammasome-mediated innate immune activation (Khetarpal et al., 2019). Human CHIP mutation carriers also have a strong association with age-acceleration, all-cause mortality and heart disease, based on DNA methylation clocks trained on health parameters, morbidity and mortality (Nachun et al., 2021).

CHIP is associated with mutated genes, including mutations in *TET2*, *DNMT3A*, *SF3B1, SF3B2, ASXL1, JAK2* and *IDH1* (Genovese et al., 2014; Jaiswal et al., 2014; Xie et al., 2014). For example, scRNA-seq of HSPCs from patients undergoing hip joint replacement surgery showed that progenitors with mutations in both DNMT3A and TET2 or with biallelic TET2 mutations have an enhanced clonal advantage than other types of single mutations (Nakagawa et al., 2021). Interestingly, the different mutational patterns were associated with different clonal expansions. For example, compound TET2/DNMT3A mutations were significantly enriched in the erythroid cluster, while another clone with double TET2 mutations were more enriched in the HSC-like cluster (Nakagawa et al., 2021). Intriguingly, even surrounding non-mutated cells acquired altered gene expression patterns that favour clonal expansion, suggesting non-genetically encoded factors contributing to clonal

hematopoiesis (Nakagawa et al., 2021). As another CHIP example, certain mutations in *ASXL1* appear to give HSCs a disadvantage in competitive transplantations assays but an advantage with physiological ageing, likely due to deubiquitination of H2AK119Ub and subsequent overactivation of AKT and mTOR signalling, which promotes myeloid leukemogenesis (Fujino et al., 2021).

Some studies report a mild CHIP-like phenotype in mouse HSCs, but the rate of mutation appears to depend on the method used to calculate them. For example, Chin et al. (2022) found the mutation rate is 8.5 fold higher than in humans but due to the shorter lifespan of mice, the number of mutations in the HSCs of aged mice is actually 5 fold lower than in human HSCs and clonal hematopoiesis was not apparent unless the HSCs that harboured the CHIP mutations were transplanted and allowed to age even further (Chin et al., 2022). On the other hand, Kapadia et al. (2025) used a more sensitive method but found that the mutation rate in murine HSCs was only ~2–3-fold higher than the human rate and clones only become dominant if the mouse is subjected to chronic inflammatory stimulation, chemotherapy, or transplantation (Kapadia et al., 2025).

Clonal hematopoiesis could confound attempts to study the epigenetics of ageing, since a small population of clones may have large changes in their epigenome which skew the overall results. However, clonal populations are usually a very small proportion of the overall population of blood cells, even in people aged 70 years and older (Steensma et al., 2015). Despite the low frequency of mutated clones, CHIP may be a major limiting factor for any therapy or intervention that proposes to epigenetically restore the blood, since CHIP mutations may actively oppose the intervention and genetically aberrant clones may come to dominate the population. Clearance of clonally expanded HSPCs which harbour potentially malignant mutations using as yet undeveloped targeted therapies will likely be a parallel strategy to restore youthful function to the blood.

1.2.5.4 Age-associated bone marrow failure

The flip-side to age-associated expansion of myeloid-biased HSCs is age-associated loss of HSCs leading to cytopenias and possible bone-marrow failure. Loss of HSCs in ageing could be due to genetic or epigenetic changes that lead to alterations in the homeostasis of HSC quiescence, differentiation and self-renewal. For example, some CHIP mutations have

been associated with aplastic anemia (Q. Liu et al., 2026). In severe aplastic anemia, depletion of HSCs and HSPCs leads to peripheral cytopenia (Young, 2018), and has been associated with insufficiency of FZR1 (also known as CHD1) which is associated with a loss of quiescence of HSCs, but also a loss of self-renewal (Zhou et al., 2022). Whether the FZR1 insufficiency is caused by somatic mutations or epigenetic silencing is still unclear.

Myelodysplastic syndromes (MDS) are common in ageing and lead to both multilineage cytological dysplasias but also cytopenias (Aoyagi et al., 2022; Cheng et al., 2019). For example, MDS has been associated with expansion of myeloid-derived suppressor cells (MDSC), which secrete S100A9, a pro-inflammatory signal which can cause death of HSPCs, but also express PD-L1, which also leads to suppression and death of PD-1 expressing HSPCs (Cheng et al., 2019).

1.2.5.5 Chronic infection of HSCs in ageing

Aside from the extrinsic effects of chronic infection of HSC-supporting niche cells in the bone marrow, HSCs themselves can harbour long-term and latent infections which likely skew lineages fates and cause cytopenias in the elderly. For example, it has been well established that 90% of the global population has been infected with EBV, that it often exists for life in latent form and that EBV has a high tropism for B cells (Damania et al., 2022), but recent evidence indicates EBV can also infect HSCs themselves (Wang et al., 2024). In humanized mouse models receiving human $CD34^+$ HSCs, granulocyte-biased skewed differentiation of donor HSCs was observed only in mice infected with EBV (Katahira et al., 2019). It has also been shown in B cells that the EBV nuclear antigen 2 (EBNA2) protein can bind host DNA acting like a transcription factor to reprogram B cells (even autoreactive ones) to promote survival an immune evasion (Younis et al., 2025). It is therefore conceivable that some ageing phenotypes of HSCs stem from EBV infected HSCs, but this has not yet been studied in the context of ageing.

Surprisingly, human parvovirus B19 has also recently been found to infect HSCs themselves and was a driver of pancytopenia in transplant patients (Pei et al., 2026). Considering the high prevalence of B19V found in the BM of elderly humans (Toppinen et al., 2021), the link between B19V and age-associated lineage skewing or cytopenias with eventual bone marrow failure also warrants further investigation.

1.2.5.6 Telomere attrition in HSCs

Of all the human blood progenitors, HSCs express the most telomerase (Chiu et al., 1996); Morrison et al., 1996) and telomerase activity decreases in later progenitors, particularly in myeloid progenitors (Hohaus et al., 1997). Despite this basal level of telomerase expression, the telomeres of human HSCs still shorten over the lifespan (Vaziri et al., 1994), suggesting that telomere shortening may be preserved in HSCs to limit the number of divisions they undergo. Modelling of this telomere attrition suggests HSCs divide on average 56 times over a normal human lifespan, mostly in the first 24 years of life, after which they divide less than once every two years (Boyle et al., 2023). Therefore, telomere attrition is likely a major cell intrinsic component to HSC ageing. Interestingly, mature lymphocyte subsets have the unique ability to re-lengthen their telomeres. For example, memory B cells have longer telomeres than naïve B cells (Martens et al., 2002). Furthermore, antigen presenting cells (APCs) can re-lengthen the telomeres of activated CD4 T cells by conveying telomere loaded vesicles across the immunological synapse (Lanna et al., 2022). Thus, the gradual telomere attrition in HSCs may not affect downstream memory lymphocytes established early in life, but may impact the development of new naïve lymphocytes, and may be a mechanism to limit the proliferative lifespan of autoreactive and pro-inflammatory immune cells.

Quiescent HSCs acquire DNA damage upon activation during infection or blood loss (Walter et al., 2015). Compared to more differentiated HSPCs, LT-HSCs in mice (both young and old) actively suppress the G1 to S phase checkpoint during the DNA damage response, and may have a higher tendency to apoptose after DNA damage, a finding that suggests a LT-HSC-specific mechanism that ensures genomic integrity (Moehrle et al., 2015). The same preference of HSCs for apoptosis over repair mechanisms is also seen in human $CD34^+$ $CD38^-$ HSPCs compared to $CD34^+$ $CD38^+$ linage committed progenitors (Biechonski et al., 2018). Moreover, the study by Moehrle et al. (2015) also showed that levels of oxidized guanosine (8-oxo-dG), an indicator of oxidative DNA damage due to an increase in the oxidant/antioxidant ratio, were similar between young and old LT-HSCs, likely indicating that LT-HSCs are spared from 8-oxo-dG-induced senescence that affects other cell types. However, senescence can likely be induced by a sudden increase in ROS whereby oxidation of guanine in telomeric 5′-TTAGGG-3′ arrays to form 8-oxo-guanine rapidly activates ATM

and ATR kinases and downstream effectors p53 and p21 to induce non-replicative senescence (Barnes et al., 2022).

1.2.6 Infection history, replication stress as a link between extrinsic and intrinsic drivers of HSC ageing

The increase in extrinsic inflammatory signalling and structural changes in the BM lead to increased HSC activation and division, while the intrinsic telomere attrition, somatic mutations and epigenetic changes in aged HSCs are predominantly a result of this replicative history. Thus, infection and replicative history likely connect the extrinsic and intrinsic aspects of HSC ageing. For example, early lineage tracing of genetically labelled HSCs suggested a model in which LT-HSCs with full lineage and reconstitution potential symmetrically divide only four times over the lifespan of a mouse, after which they move into a permanent state of dormancy, while HSPCs continue cycling and replenishing blood cells as needed (Bernitz et al., 2016). Interestingly, only green fluorescent protein (GFP) label retaining HSCs with low replicative history from old mice could fully reconstitute the blood in primary and secondary transplants, while GFP-low cells could only reconstitute the blood of primary transplants (Bernitz et al., 2016). As dormant label retaining LT-HSCs divide, there is also a progressive enrichment of transcription factors E2F1, E2F4, FOXM1, and MYC near the promoters of upregulated genes involved in lineage priming (not cell-cycle genes), suggesting that HSC division inherently prime future lineage decisions of HSPCs (Bernitz et al., 2020).

In other scenarios where the HSPC pool is diminished, such as after blood loss or during chemotherapy, LT-HSCs become active to replace the lost multipotent progenitor pool, whereby the Pip3-AKT-mTorc1-ROS pathway and a parallel Mek1 phosphorylation pathway create an essential feedback loop to take the activated HSC back to quiescence (Baumgartner et al., 2018). In another study in mice, lineage tracing of HSCs using GFP-conjugated histone H2B showed that HSCs do not contribute to blood reconstitution after infection or blood loss and only severe radiation or chemotherapy-induced myeloablation could stimulate HSCs to divide (Munz et al., 2023). Hinge et al. (2020) also demonstrated mitochondrial morphology and position dictate a kind of divisional memory in HSCs

whereby the altered mitochondria are preferentially retained by the daughter HSC that returns to quiescence (Hinge et al., 2020).

Chronic viral infection has been shown to stimulate HSC out of quiescence leading to an accelerated ageing phenotype characterised by LT-HSCs with reduced engraftment potential, myeloid bias and DNA damage (Walter et al., 2015). Furthermore, experiments in mice mimicking chronic infection demonstrate that chronic interleukin-1 exposure (once daily for up to 70 days) does not deplete the HSCs, but causes exhaustion, as exhibited by poor reconstitution potential and hyperactivation of the transcription factor PU.1 (Pietras et al., 2016). In addition, chronic elevation of IFN-γ causes myeloid-biased differentiation (Matatall et al., 2016). Conversely, despite the expansion of HSCs in aged lab mice, mice exposed to repeated acute infections actually display a decrease in LT-HSCs (Bogeska et al., 2022; Matatall et al., 2016), indicating timing and recovery period may be a factor in HSC dynamics.

Single-cell studies of human blood progenitors have shown that quiescent HSCs generally do not contribute to the cycling HSC pool (Varesi et al., 2026). Among the heterogenous human LT-HSC population, other studies show that INKA1 through direct interaction with PAK4 and SIRT1 was shown to downregulate CD112, which generates a CD112 low subset of LT-HSCs with higher self-renewal and regenerative capacity (Boutzen et al., 2024; Kaufmann et al., 2021). The presence of these CD112 low HSCs indicates a mechanism by which blood stem cells ensure both blood cell replacement during stress but also preservation of the stem cell pool.

While it is difficult to replicate findings of replicative stress and infection from mouse studies, human patients with inborn errors that lead to recurrent infections and inflammatory events show upregulation of interferon pathways in HSCs leading to dysfunction and accelerated ageing phenotypes (Sobrino et al., 2023). Furthermore, human donor cord blood ages twice as fast as chronological age, according to DNA methylation clocks, due to the required rapid expansion of cell numbers (Onizuka et al., 2023). Serially transplanting young human cord-blood HSPCs into immunodeficient mice mimics replication stress and causes the young cord blood $CD34^+$ HSCs to phenotypically resemble the aged HSCs by the 2^{nd} transplant, highlighting replication stress as a contributor to HSC ageing (Lettera et al., 2026).

In summary, while the most quiescent HSCs attempt to minimize their rate of proliferation, repeated activation through chronic infection, systemic and local inflammation, blood loss and cytotoxic cell death, appears to directly contribute to intrinsic aspects of HSCs ageing (somatic mutations and epigenetic changes) that alter cell fate, leading to expansion of myeloid-biased clones and depletion of lymphoid-biased clones. Furthermore, due to the limits of replicative lifespan, repeated activation may also ultimately lead to HSC depletion and eventual bone marrow failure.

1.2.7 Epigenetics of HSC ageing

Epigenetics refers to the mechanisms that regulate which genes are expressed in a cell, mechanisms which include DNA methylation, histone modification, chromatin organisation and TF-based gene regulation. Chronic inflammation, telomere attrition and replicative stress over the lifespan all likely contribute to a gradual expansion of dysfunctional HSCs with permanently altered epigenetic modifications that render aged HSCs refractory to restoration upon transplant to a young BM environment. Broadly speaking, there is a loss of trimethylation of lysine 9 on histone-H3 (H3K9me3) in aged murine and human HSCs due to reduced expression of the histone methyltransferase SUV39H1 (which catalyses the methylation of H3K9) leading to altered heterochromatin and derepression of endogenous retroviruses and transposable elements (Djeghloul et al., 2016). Furthermore, aged HSPCs exhibit a significant spatial redistribution and loss of DNA methylation at heterochromatin regions marked by H3K9me3, a phenotype that appears to be driven by the DNA demethylase TET2 (Hong et al., 2023).

As previously mentioned, there is a 5% reduction in global DNA methylation in aged mouse HSCs, but hypermethylation of genes normally repressed by PRC2 (Taiwo et al., 2013). Other groups have also shown increased DNA methylation at genes regulated by PRC2 in aged HSCs (Beerman et al., 2013). In fact, the hypermethylation of PRC2 targets is a general finding in many other aged cell types (Dozmorov, 2015) and is so consistent that highly accurate biological ageing clocks can be constructed from PRC2 target methylation alone (Lu et al., 2023; Moqri et al., 2024).

Aged murine HSCs display loss of DNA methylation and opening of chromatin regions around regulatory elements and genes involved with stress response pathways, indicating an

epigenetic memory of previous infection or stress that primes the HSCs towards a particular fate (Itokawa et al., 2022). Aged human HSCs display loss of H3K27ac, H3K4me1 and H3K4me3 activating marks particularly at enhancers involved in activating genes for transcription factors with tumour suppressor function and genes involved in epigenetic modification (Adelman et al., 2019). Aged human HSCs also have elevated levels of cryptic transcription (transcription from non-promoter regions within the gene body), which is consistent with age-related opening of the chromatin and changes to histone modifications (McCauley et al., 2021).

Loss of asymmetrical division in aged HSCs is associated with loss of polarity of tubulin and certain histone marks due to overactivation of Cdc42 and is not restored by transplantation into young mice (Florian et al., 2012). Aged HSCs also display increased volume, loss of nuclear invaginations, increased distance between homologs of chromosome 11, decreased H4K16ac and loss of H4K16ac polarity (as it associates mainly with chromosome 11) (Grigoryan et al., 2018). These changes in chromatin structure and histone mark polarity were associated with a Cdc42-mediated loss of Lamin A/C, and were rescued by Cdc42 inhibition using the small molecule CASIN (Grigoryan et al., 2018). In HSCs from female mice, age-associated loss of Lamin A/C also leads to derepression of the inactivated X-chromosome (Grigoryan et al., 2021). The importance of Cdc42-mediated ageing is demonstrated by the fact that CASIN injections also increased the remaining lifespan of already aged mice (Florian et al., 2020). However, questions remain as to what causes the age-associated upregulation of Cdc42 that leads to loss of LaminA/C and polarity.

Transcription factors likely dictate much of the epigenetic changes seen in aged HSCs. For example, aged human HSCs show both a loss of H3K27ac at the upstream enhancer of KLF6 and downregulation of KLF6, which was subsequently linked to loss of reconstitution capacity after KLF6 was knocked out in young donor HSCs (Roisman et al., 2019). In addition, EGR1 expression progressively increases with age in human HSCs and is linked to age-related changes in cell cycle progression (Desterke et al., 2021). AP-1 factors have been implicated in HSC ageing in several papers (Feng et al., 2024; Itokawa et al., 2022; Patrick et al., 2024). Interestingly, in 22 different murine cell types (including HSCs) regions of chromatin that significantly close with age are enriched with TF motifs for known cell identity defining TFs while chromatin regions that significantly open with age are enriched

with AP-1 motifs, suggesting a mechanism of ageing common to many tissues (Patrick et al., 2024).

As previously mentioned, TF activity may be a better measure of a TFs role in biological processes. For example, high Zbtb1 TF activity in certain HSC subsets is associated with lymphoid-biased output (Elias et al., 2025), while the decrease in PU.1 activity in aged HSCs is not rescued upon transplant into young recipients (Kim et al., 2022). TF activity is usually calculated using the magnitude of differential expression of the TF's target genes, and the number of targets, to gauge how influential the TF is within the GRN. Interestingly, analysis of HSCs from old mice that had been exposed to young plasma via heterochronic parabiosis showed a set of age-associated DEGs that were not rescued by young plasma (Ma et al., 2022). The TFs in the GRN associated with these non-rescued DEGs included Yy1, which was then overexpressed in aged HSC using a lentiviral system to demonstrate some restoration of the refractory elements of the aged HSCs (Ma et al., 2022). However, it has been shown by other groups that plasma does not adequately access the HSCs in the bone-marrow microenvironment (Ho et al., 2021), which casts doubt on the use of heterochronic parabiosis to study HSCs.

Hi-C is a technique to look at both the broad changes in chromatin architecture and the more specific interactions between regulatory elements and gene promotors. However, it has only recently been used to study the biology of ageing. For example, in mouse skeletal muscle stem cells (MuSCs), ageing leads to loss of interactions between TF binding sites and genes associated with maintenance of quiescence (B. A. Yang et al., 2023; Zhao et al., 2023). Hi-C analysis has also highlighted the decay of heterochromatin domains and activation of transposable elements in aged neurons (Kriukov et al., 2024; Zhang et al., 2022). In mouse B cell precursors, early Hi-C studies demonstrated chromatin remodelling and a shift from active A to repressive B compartment of the Irs1 gene, a component of the Igf signalling pathway (Koohy et al., 2018). In aged pro-B cells, a similar repressive compartment switch from A to B was found for the B cell identity TF, Ebf1 (Ma et al., 2024).

In summary, TFs play a role in maintaining cellular identify and the changes in TF activity in aged HSCs, along with the DNA methylation changes, likely explain much of why aged HSCs remain refractory to exposure to the young BM environment. Rejuvenation of the

intrinsic epigenetic aspects of HSCs ageing will likely require reprogramming interventions to loosen the refractory GRNs and promote a shift to a more youthful GRN state.

1.2.8 Current attempts to rejuvenate aged HSCs

1.2.8.1 Addressing the extrinsic aspects of HSC ageing

As discussed in previous sections, extrinsic inflammatory signalling plays a substantial role in HSC ageing. For example, in mice, age-associated intestinal permeability and microbiome changes increase systemic innate immune signalling, including Il-1β signalling, which contribute to LT-HSCs ageing phenotypes (Kovtonyuk et al., 2022). Il-1β receptor knockout mice show a much reduced myeloid bias (Mitchell et al., 2023) and long-term pharmacological inhibition of Il-1β appears to somewhat restore LT-HSC reconstitution ability (Kovtonyuk et al., 2022; Mitchell et al., 2023). Similar results have been found using inhibition of Il-6 (Valletta et al., 2020) and TNFα (Rundberg Nilsson et al., 2023). However, long-term immunosuppression may pose significant risks and pharmacological inhibition of Il-1β, Il-6, TNFα, etc., does not address the root cause of the chronic inflammation.

Successful restoration of function of aged HSCs by addressing the extrinsic aspects of HSC ageing have also been demonstrated by exogenous delivery of Igf1 (Young et al., 2021), Osteopontin (Guidi et al., 2017) and Netrin-1 (Ramalingam et al., 2023; Renders et al., 2021). However, long-term systemic delivery of these growth-promoting signalling molecules comes with risks and does not address the root cause of why they are diminished with age. Furthermore, extracellular vesicles derived from young MSCs or aged AKT-inhibited MSCs (but not normally aged MSCs) were shown to functionally restore aged HSCs (Kulkarni et al., 2018). All in all, addressing intestinal permeability, systemic inflammation, chronic infection of BM niche cells and niche cell senescence may prove to be essential approaches to restore the niche's ability to properly support aged HSCs.

1.2.8.2 Mitochondrial restoration to rescue aged HSCs

Mitoquinol increases mitochondrial membrane potential (MMPot) in aged myeloid-biased MMPot low HSCs restoring youthful gene expression and engraftment potential (Mansell et al., 2021). Additional strategies to increase mitochondrial health have been attempted. For example, one study claimed that supplementation of aged mice with nicotinamide riboside

increases NAD^+ levels in HSCs and causes enhanced lymphoid potential (Zong et al., 2021). NR supplementation also improves mitochondrial function but, while it partially restores myeloid skewing at the progenitor level (LMPPs increased GMP reduced), the percentages of differentiated lymphoid and myeloid lineage cells was not altered (Sun et al., 2021).

1.2.8.3 Telomere restoration to rescue the replication effects of HSCs ageing

Transient transfection of fibroblast and myoblasts with modified telomerase reverse transcriptase (TERT) RNA lengthens telomeres, allowing for an increase in proliferative capacity without immortalization (Ramunas et al., 2015). However, TERT overexpression in human HSCs does not prevent telomere shortening (Wang et al., 2005), suggesting alternate mechanisms that HSCs use to ensure telomere attrition. Patients with a genetic mutation in PARN have a deficiency in the proper maturation of the long non-coding RNA component of the telomere lengthening ribonucleoprotein called TERC, leading to accelerated telomere attrition. Inhibition of PAPD5, an enzyme in the pathway that degrades TERC, restores telomere length in PARN-deficient human $CD34^+$ HSCs and improves engraftment dysfunction causes by telomere attrition (Nagpal et al., 2020). Similarly, exogenous delivery of an engineered form of TERC also improves the TERT-mediated telomere lengthening in PARN-deficient human $CD34^+$ HSPCs, which in turn improves differentiation output *in vitro* (Nagpal & Agarwal, 2025). However, TERC overexpression or PAPD5 inhibition in physiologically aged human HSCs has not been reported. Interestingly, in both mouse and human HSCs, overexpression of Pot1a, a telomere protecting shelterin complex that diminishes with age, prevents the DNA damage response (DDR) and lowers production of reactive oxygen species and maintains self-renewal, thus highlighting an alternative way replicative stress in HSCs could be reduced (Hosokawa et al., 2017).

1.2.8.4 Restoring polarity to rescue aged HSCs

Remarkably, systemic inhibition of Cdc42 with only a 4 day treatment of CASIN in 20-month-old mice was enough to restore the tubulin and H4K16ac polarity of HSCs to youthful levels and restore their ability to better reconstitute the blood of immunodeficient NBSGW mice, thereby increasing the recipient mice's health-span and lifespan (Montserrat-Vazquez et al., 2022). CASIN restores polarity and asymmetrical division (Grigoryan et al., 2018),

restores youthful levels of X chromosome inactivation (Grigoryan et al., 2021) and increases lifespan of aged female mice (Florian et al., 2020).

1.2.8.5 Transcription factor-based reprogramming of aged HSCs

It has been demonstrated that replication also causes the downregulation of particular HSC identity genes are targets of PRC2, whereby there is a gradual switch from Ezh1 to Ezh2, indicating that Ezh1 activates HSC identity genes, while the gradual switch to Ezh2 likely suppresses them and acts as a marker of proliferative history (Bernitz et al., 2020). Furthermore, pharmacological inhibition of Ezh2 increases the regenerative capacity of the HSCs with higher proliferative history (Bernitz et al., 2020). This indicates a mechanism that links proliferation history to epigenetic changes in aged HSCs that would naturally have a longer proliferative history. However, whether overexpression of HSC identity TFs can also restore the regenerative capacity of aged HSCs is an open question. However, some clues are emerging. For example, overexpression of Zbtb1 can improve aged-HSC lymphoid reconstitution (Elias et al., 2025). Furthermore, overexpression of Yy1, a TF whose activity in HSCs was not restored upon exposure to young plasma during heterochronic parabiosis, was also demonstrated to partially restore long-term engraftment of aged HSCs transplanted into young, irradiated mice (Ma et al., 2022).

As will be discussed in the next section, overexpression of the Yamanaka factors Oct4, Sox2, Klf4 and Myc (OSKM) is often used to rejuvenate cells *in vitro* and *in vivo*. As an example of an indirect effect of Yamanaka factor reprogramming on aged HSCs, targeted epigenetic reprogramming of stressed and senescent cells in mice using viral delivery of OSK (without M) in an accelerated ageing mouse model, resulted in a systemic reduction in proinflammatory cytokines, including Il-1α, Il-1β, and Il-6, which then led to partial rescue of the myeloid biased LT-HSCs (Sahu et al., 2024). Interestingly, direct epigenetic reprogramming of aged myeloid-biased HSCs using Yamanaka factors has not been reported and this will be discussed in the next section.

1.3 Restoration of youthful function using epigenetic reprogramming

1.3.1 Loss of epigenetic cell identity as a driver of ageing

A cell's specific pattern of gene transcription is largely determined by the highly organised way the DNA is folded, coiled and packaged in the nucleus of the cell. The ability of a cell to "remember" its identity-specific pattern of DNA structure after mitosis, despite the immense changes to DNA structure during cell replication, is testament to the primacy of DNA methylation, cell-type-specific transcription factors (TFs) and cell-type-specific non-coding RNAs (ncRNAs) that remain relatively stable during division (Liotti et al., 2022). For example, the DNA methyltransferase enzyme DNMT1 can read the hemi-methylated strand of DNA during DNA replication and apply the methylation to the newly synthesized strand to ensure that daughter cells will carry the same DNA methylation pattern (Jurkowska et al., 2011). Hemi-methylated DNA may also be stably inherited (Xu & Corces, 2018), although the mechanism and function is less well understood.

Cell type-specific TFs and ncRNAs that recognize and bind specific sequences on the DNA to give the cell its particular transcriptional identity, are stochastically partitioned into the daughter cell during symmetrical cell division, thus ensuring that, on average, the cell retains its parent's transcriptional identity (Fuchs & Chen, 2013). However, even small differences in random partitioning of low copy number TFs and RNAs, which creates a heterogeneity among the progeny, can also result in a divergence of cell fate (Huh & Paulsson, 2011). Indeed, cell-identity needs to be somewhat malleable, to allow, for example, the differentiation of stem cells into fully differentiated cells. Active asymmetrical partitioning of organelles, transcription factors and non-coding RNAs can facilitate this process (Loeffler et al., 2022; Sunchu & Cabernard, 2020). Furthermore, the expression of different transcription factors and non-coding RNAs, perhaps due to external signals in the tissue niche, can influence the redirection of the cell's transcriptional identity (Chacón-Martínez et al., 2018; Mannino et al., 2022). These transcription factors and non-coding RNAs can also influence the downstream expression and activity of DNA methylation enzymes, such as DNMT1, DNMT3A/B and TET1/2, which can alter the DNA methylation pattern of the cell to further preserve the cell's new identity (de la Rica et al., 2013; Parry et al., 2021; Yang et al., 2022).

The transcriptional and functional dysregulation of aged cells is associated with epigenetic changes within the cell, including both loss and gain of DNA methylation, changes in histone modifications and levels of histone modifying proteins (Lee et al., 2019; Liu et al., 2022b; Moqri et al., 2024; Zhang et al., 2015). An emerging idea in ageing research is the progressive age-associated loss of distinction between heterochromatin and euchromatin, which has also been coined "convergent alteration of the epigenomic landscape during ageing" (CAEA) (Liu et al., 2022b). This CAEA phenomenon is interpreted as an increase in informational entropy, or Shannon entropy, which has been shown to increase in DNA methylation data from aged skin and blood (Jenkinson et al., 2017). In chromatin accessibility data, for example, CAEA manifests as a general reduction in the height of strong peaks and an increase in height of weak peaks, or emergence of weak new peaks (Liu et al., 2022a). A similar "smoothening" or convergence of frequencies (peak heights) between active marks and inactive marks can be seen in ChIP-seq data during accelerated ageing (J.-H. Yang et al., 2023a).

In Hi-C data, which examines the frequency of chromatin interactions, this loss of distinction between active and inactive chromatin may manifest as a general convergence of interaction frequencies between different parts of the chromosomes, leading to erosion of TAD boundaries and shifts in A/B compartments, commonly observed in many ageing studies (Koohy et al., 2018; Kriukov et al., 2024; Ma et al., 2024; B. A. Yang et al., 2023; Zhang et al., 2022; Zhao et al., 2023). However, increases in Shannon entropy have also been noted in late-passage senescent human mesenchymal progenitor cells (MPCs), an *in vitro* model for ageing (Liu et al., 2022b).

It is hypothesized that continual demethylation and methylation during circadian rhythm could allow for the slow degradation of DNA methylation patterns (Oh et al., 2018; Oh et al., 2019). However, other models to explain the "smoothening" of the epigenetic landscape have been proposed, including the relocalization of chromatin modifiers (RCM) hypothesis (Oberdoerffer et al., 2008). The RCM hypothesis proposes that proteins such as SIRT1, SIRT6, HDAC1, and PARP1 have a dual role in both chromatin stabilization and DNA repair, but during DNA repair, particularly after DNA double-stranded breaks (DSBs), these chromatin stabilizers must be relocated to the site of the DSBs, leaving the abandoned chromatin susceptible to alteration until the DSB is repaired and the chromatin stabilizers are homeostatically returned to their positions on the chromatin (Oberdoerffer et al., 2008). For

example, SIRT6 has a dual role deacetylating histones to promote formation of heterochromatin (Ghosh et al., 2015; Liu et al., 2012; Michishita et al., 2008; Tasselli et al., 2016), silencing LINE1 elements (Simon et al., 2019; Van Meter et al., 2014), but during the DNA damage response, is recruited to DNA breaks to promote formation of γH2AX foci (Meng et al., 2020; Rasti et al., 2022) and catalysing the mono-ADP ribosylation of and recruitment of PARP1 (Mao et al., 2011; Van Meter et al., 2016). Similarly, HDAC1 is required for silencing of genes at the nuclear lamina (Milon et al., 2012), but is recruited to break sites during DSB repair to suppress transcription (Miller et al., 2010) and activate SIRT1 (Dobbin et al., 2013). Similar dual roles can be found for PARP1 (Ciccarone et al., 2017; Giansanti et al., 2022; Maya-Mendoza et al., 2018).

This shuffling of DNA binding proteins during DNA repair is hypothesised to result in a very slow but incremental epigenetic drift, generating increasing amounts of transcriptional noise and an averaging, or smoothening, of the epigenetic landscape where, for example, hypomethylated regions become increasingly methylated, while hypermethylated regions become increasingly demethylated, leading to eventual loss of cellular identity. In support of the RCM hypothesis of ageing, a tamoxifen-inducible Cre system was use to introduce "non-mutational" double stranded DNA breaks in mice, *in vivo* (J.-H. Yang et al., 2023a). These so-called 'ICE-mice' harbour an inducible expression cassette for I-*Ppo*I, an endonuclease from *Physarum polycephalum*, that introduces double-stranded DNA breaks with sticky overhangs in 20 known locations in the mouse genome which could be monitored for mutational burden. Brief *in vivo* induction of I-*Ppo*I resulted in accelerated ageing by several measures including frailty phenotypes, multi-omics analysis and DNA methylation clocks with no increase in mutational burden (J.-H. Yang et al., 2023a). In the same study, artificially aged cells from these ICE-mice were then subjected to partial reprogramming using Yamanaka factors and many of the molecular phenotypes of ageing such as DNA methylation and transcriptional output were restored to youthful levels (J.-H. Yang et al., 2023a).

1.3.2 Age "reversal" using Yamanaka factors

Adult cells can be reprogrammed to a pluripotent state resembling that of an embryo by overexpression of the embryonic transcription factors Oct4, Sox2, Klf4 and Myc (OSKM), otherwise known as the Yamanaka factors (Takahashi & Yamanaka, 2006). As mentioned

above, normal healthy animals can be generated using SCNT-based serial cloning (Wakayama et al., 2013); Wakayama et al., 2026), but also by the transfer of the nucleus of an adult cell that has undergone induced pluripotency induction by genetic overexpression of the Yamanaka factors (Kim et al., 2019; Zhao et al., 2010). This demonstrates not only that the average somatic mutational burden in many mammalian species is insufficient to impede the normal epigenetic and transcriptional patterns required for multiples rounds of development, but also that the age of the cloned cell can be reset to zero. Analysis of senescent fibroblast from centenarians that underwent full reprogramming to pluripotency showed that their telomere lengths were reset, senescent markers were removed and transcriptional programs restored (Lapasset et al., 2011). Furthermore, the epigenetic "age" of reprogrammed cells, as measured by DNA methylation clocks, is reset to zero (Gill et al., 2022; Petkovich et al., 2017).

Reprogramming cells to full pluripotency to achieve rejuvenation has limited *in vivo* applications because these pluripotent cells rapidly proliferate and can form a type of tumour called a teratoma (Abad et al., 2013). However, a single round of transient expression of these factors, sometimes called *partial* reprogramming, was performed in aged mice *in vivo*, and improved functional indicators such as muscle regeneration and pancreatic function without any sign of teratoma formation (Ocampo et al., 2016). Transient expression of the OSKM factors has, since then, been used *in vitro* to restore youthful gene expression to aged adipocytes and muscle derived mesenchymal stromal cells (Roux et al., 2022), and to reduce the epigenetic age of aged human fibroblasts, endothelial cells, chondrocytes and skeletal muscle stem cells (Sarkar et al., 2020). Additionally, OSKM factors have been expressed systemically *in vivo* to restore function to multiple organs (Browder et al., 2022) and in a cell type-specific manner to restore function in cardiomyocytes (Chen et al., 2021; Kisby et al., 2021), retinal ganglion cells (Y. Lu et al., 2020) and skin (Doeser et al., 2018). The Belmonte group examined 40 tissues and found a preponderance of what they term mesenchymal drift (MD), which was reversed with OSK (Lu et al., 2025). Finally, whole body transient expression of OSK in aged mice increases their remaining lifespan (Macip et al., 2024).

Other examples of OSK(M) reprogramming demonstrate the clinical potential. For example, in vivo treatment of mice with OSK in a mouse model of hypertension involving endothelial-to-mesenchymal transition (EndMT), also reversed the EndMT and promoted a

normotensive response (Pernomian et al., 2025). OSK packaged into adeno-associated virus (AAV) particles have been injected directly into knee joints of mice in a model of osteoarthritis and led to cartilage regeneration (Y. W. Liu et al., 2026). Finally, AAV delivery of OSK is currently being developed as a treatment for various age-related eye diseases (Karg et al., 2023; Y. Lu et al., 2020) and has completed early clinical testing in non-human primates (Ksander et al., 2023).

1.3.3 Epigenetic memory of a youthful state

The kinetics and mechanisms of partial reprogramming are an ongoing subject of study. For example, Olova et al. used OSKM to induce pluripotency in human dermal fibroblasts and used the original Horvath clock (Horvath, 2013) to show that epigenetic age decreases linearly between day 3 and 20 of OSKM expression, while pluripotency genes increase in a non-linear fashion (Olova et al., 2019). Furthermore, genes associated with fibroblast identity remained fairly stable until day 15, after which a sharp drop indicated a point of no return (Olova et al., 2019).

Similarly, Gill et al. (2022) also used time-course analysis of OSKM reprogrammed fibroblasts, but transiently expressed OSKM so the stability of the epigenetic rejuvenation could be measured (Gill et al., 2022). In this case, fibroblasts were subjected to OSKM expressed for 10, 13, 15, or 17 days, $SSEA4^{+}$ cells were isolated by FACS, then cultured without OSKM for a further 4-5 weeks. Results showed that day 13 was the "sweet spot" between reprogramming and loss of identity which reduced the DNA methylation age of aged human fibroblasts by 30 years without inducing a pluripotent state (Gill et al., 2022). Crucially, the Gill et al. (2022) study showed that a set of 2351 out of 4204 fibroblast specific enhancers, which usually become methylated during full reprogramming to pluripotency, remained unmethylated, so it was hypothesized that these unmethylated enhancers may act as an epigenetic memory that retains the cells' fibroblast identity. This is important since it has been demonstrated that reprogramming likely works by repression of cellular identity and cells must undergo a "secondary differentiation" process that allows them to restore their original identity (Roux et al., 2022). Therefore, TFs and non-coding RNAs likely play a major role in re-establishing cell identity. Furthermore, it was also demonstrated by Roux et al. (2022) that different cell types lose their cellular identity to different degrees during

reprogramming and that using only the factors Oct4 and Sox2 (OS) as a cocktail could give a similar reduction in the ageing score of mesenchymal cells, while suppressing their cell identity 54% less. This kind of analysis of reprogramming kinetics is an important component in determining the mechanism, dose and efficacy of each reprogramming strategy.

Reprogramming efficiency is also tissue specific and dosage of Yamanaka factor expression is related to the kind of expression cassette used, the regulatory elements that control its expression and how plastic the host cell type already is (Chondronasiou et al., 2022; Parras et al., 2023; Picó et al., 2025). For example, *in vivo* transient expression of a dox inducible OSKM cassette inserted into an intron of the Pparg gene demonstrated that pancreatic acinar cells are particularly susceptible to reprogramming, inducing loss of cell identity that is similar to oncogenic transformation (Chondronasiou et al., 2022). Similarly, long-term cyclical *in vivo* expression of OSKM results in hepatic and intestinal failure and death in strains where the cassette is in Pparg or Col1a1 (Parras et al., 2023). Subsequent strains in which the OSKM cassette is selectivity removed from liver and intestinal cells allowed for safe long-term cyclical induction of OSKM in aged mice resulting in a reduction of epigenetic age in the heart, spleen, brain and kidneys (Parras et al., 2023). Other attempts at expressing the OSKM cassette only in post-mitotic cells (Picó et al., 2025) or only in senescent or stressed cells that express cyclin-dependent kinase inhibitor 2a (Cdkn2a) (Sahu et al., 2024) have been successful in reducing the negative side effects of reprogramming.

1.3.4 Potential dangers of pluriopotency factors

The main concerns with reprogramming using pluripotency factors are the promotion of stemness, epigentic silencing of cell identity and the pushing of precancerous cells into a cancerous state. It has been shown, for example, that Oct4 and Sox2 are overexpressed in glioblastoma, enhancing stemness and immune evasion in stem-like glioblastoma propagating cells (Ma et al., 2021). Even partial reprogramming (transient expression of OSKM) can produce tumours through epigenetic dysregulation without requiring full iPSC formation (Ohnishi et al., 2014). Reprogramming and oncogenic transformation pass through overlapping early plasticity states before diverging, supporting the idea that reprogramming can expose or share transformation-prone intermediate states (Huyghe et al., 2022).

Before widespread clinical adoption of OSK(M)-based reprogramming, it will be necessary to examine the effect of transient OSKM or OSK expression in cells harbouring precancerous mutations. For example, some forms of pancreatic cancer develop after a 4-hit series of mutations, usually *KRAS*, *CDKN2A*, *TP53*, and *SMAD4*, where mutations in only *Kras* and *Tp53* were shown to be insufficent to drive ERK mediated hyperplasia (Shibata et al., 2018). However, a transient three-day expression of OSKM caused reversible acinar to ductal metaplasia (ADM), an early event of pancreatic cancer development, even in non-mutated cells, while cells harboring a single Kras mutatation developed ERK mediated hyperplasia, which was exacerbated even more with the presence of an additional Tp53 mutation (Shibata et al., 2018). Even without Myc, transient OSK expression produces a stable, heritable pro-metastatic epigenetic state in already malignant colon cancer cells (Singovski et al., 2016), suggesting it may worsen malignant behaviour in genetically abnormal cells.

Despite the evidence that pluripotency factors like OSKM, or even OSK, promote tumourogenesis, there is also some evidence that targeted reprogramming can actually inhibit tumour progression. For example, transient OSKM expression in lung cancer cells harbouring a Kras mutation promoted cancer cell apotosis and senescence after transplantation, with OCT4 and KLF4 contributing strongly to this effect (Pedrosa et al., 2024). A similar result was found in an earlier study in pancreatic ductal adenocarcinoma cells (Khoshchehreh et al., 2019) and in various cancer cell lines (Wang et al., 2019). However, the ability of OSKM reprogramming to reactivate apotosis or senescence pathways appears to be cell-type specific.

Clinical application of OSK(M)-based reprogramming will likely require targeted avoidance of delivery to cells that are prone to extreme dysplasia and oncogenic transformation (e.g. active healthy intestinal and pancreatic cells). Furthermore, the whole idea of *partial* reprogramming rests on the idea that, despite the erasure of some epigenetic marks through overexpression of the Yamanaka factors, there remains enough epigenetic information to allow the cell to complete a secondary round of differentiation and return to its original identity. Further analysis of transcription factor networks, the non-coding RNAs present and DNA regulatory elements accessible during reprogramming may reveal strategies that can uncouple the rejuvenating aspects of reprogramming from the cell identity

changes. These strategies may include, for example, the identification of alternate TFs that reaffirm youthful cellular identity with minimal step-change towards pluripotency.

1.4 3D genome organisation in GRN construction and analysis

Transcription factor inhibition and overexpression are the basis for most epigenetic reprogramming, although chemical reprogramming with small molecules is also an emerging field (Mitchell et al., 2024; Schoenfeldt et al., 2025; J.-H. Yang et al., 2023b). Identification of TFs that promote and establish cell identity is traditionally achieved through large screens of differentially expressed TFs in the target cell type. The discovery of the pluripotency factors, for example, was achieved by identifying the genes most differentially expressed in embryonic stem cells (ESCs) then eliminating them one by one until the final minimal set was found (Takahashi & Yamanaka, 2006; Yu et al., 2007). Additionally, by screening genes highly expressed in brain tissue, the cocktail of transcription factors Brn2, Ascl1 and Myt1l was discovered to transdifferentiate fibroblasts into neurons, bypassing the pluripotency phase altogether (Vierbuchen et al., 2010). Interestingly, transdifferentiation of fibroblasts to HSCs has proven to be more difficult. In this case, overexpressing a large pool of factors known to be highly upregulated in HSCs only made mature blood cells, whereas HSC-like cells could only be produced after going through an endothelial intermediate using the factors Gata2, Gfi1b, cFos, and Etv6 and culturing the cells in media containing HSC supporting cytokines (Pereira et al., 2013). These experimental results highlight the fact that not all differentially upregulated factors identified in the target cell were necessary for reprogramming and raises the question of how best to predict the factors that actually drive reprogramming. More recently, analysis of GRNs has been used to identify TFs for reprogramming and will be discussed next.

1.4.1 Gene regulatory networks (GRNs) for studying ageing

Construction of GRNs from multi-omic data and databases of motif binding or protein interactions is a relatively recent technique for exploring drivers of disease and ageing. GRNs give specialized information beyond principal component analysis and differential analysis. While principal component analysis applied to genomics tells you which features explain the major variance in the data, and differential analysis identifies statistically significant

differences in the data, network analysis attempts to infer the mechanistic interactions of regulatory proteins and DNA regulatory elements that explain patterns of gene expression (Jiang et al., 2025; Loers & Vermeirssen, 2024). Predicting causal TF drivers of gene expression and cell identity from the differential expression of the TFs themselves is prone to false negatives because it misses the regulatory flow and directionality that network analysis provides (Kamimoto et al., 2023). Indeed, TF activity has been demonstrated to be a better predictor of each TFs role in cell identification than expression level or motif enrichment within DEG promotors (Aibar et al., 2017; Wlodarczyk et al., 2025). Furthermore, comparison of GRNs from different conditions can help identify transcription factors that drive the changes in gene expression and, thus, which factors can be used to change cell state or identity (Morris, 2026; Xu et al., 2021).

Many different computational tools have been invented to construct and compare GRNs. Broadly speaking, GRNs can be inferred using databases of protein interaction data or databases of TF binding motifs. For example, by constructing a network prior from known protein-protein interactions (PPI) to obtain a starting network of all biologically known TF-gene relationships, the nodes and weights of this starting network can then be pruned based on measured gene expression data. GRN inference tools that use PPIs are tools like iDREM (B. Mishra et al., 2021), PANDA and LIONESS from the NetZoo suite (Ben Guebila et al., 2023) and the tool agingXAI (Li et al., 2025) which uses deep learning and explainable artificial intelligence (XAI). Alternatively, GRNs can be inferred by examining TF binding motifs in gene promotors of expressed genes and/or accessible chromatin regions that contain putative regulatory elements. GRN inference tools that use TF binding motif databases include SCENIC (Aibar et al., 2017), SCENIC+ (Bravo Gonzalez-Blas et al., 2023), several packages in the NetZoo suite (Ben Guebila et al., 2023), CellOracle (Kamimoto et al., 2023), DeepMAPS (Ma et al., 2023), ANANSE (Xu et al., 2021) and scANANSE (Smits et al., 2023), scREMOTE (Tran et al., 2022), scTFBridge (Wang et al., 2025), Dictys (Wang et al., 2023), Epiregulon (Wlodarczyk et al., 2025). Conversely, some tools such as weighted gene co-expression network analysis (WGCNA) (Zhang & Horvath, 2005), or sophisticated non-linear analysis tools like ANNI (Tong et al., 2014) and VIPER (Alvarez et al., 2016) use neither PPI nor TF binding motif data for GRN inference, using only co-expression patterns or hierarchical organization to infer GRN modules. Therefore, an important consideration in

GRN inference is that reliance on PPI databases and/or TF binding motif databases means the inferred GRNs are only as biologically complete as the databases used to construct them.

Some tools have already been used to study ageing (Brase et al., 2023; He et al., 2025; Lee et al., 2021; Ma et al., 2022; Macarie et al., 2026; Millet et al., 2024; Mishra et al., 2021; Saha et al., 2025; Sengstack et al., 2026; Tarum et al., 2024; Yucel et al., 2025). For example, SCENIC uses RNA-seq data to integrate co-expression analysis with motif enrichment then identify modules of TFs and their target genes, known as "regulons". This tool was used to identify multiple age-associated TFs, including EOMES, TBX21, RUNX3 and NFATC2, that govern the gene expression and signalling dynamics of aged and exhausted terminally differentiated effector memory T (Temra) cells (He et al., 2025). The SCENIC tool was also used in conjunction with CRISPR-based perturbations in senescent skin fibroblasts to identify the overexpression of E2F3 and EZH2, or the inhibition of STAT3 and ZFX as ways to reverse or inhibit cellular senescence (Sengstack et al., 2026).

Remarkably, cell-cell communication networks (CCNs) can be combined with GRNs to link cell surface signalling to downstream gene regulatory outcomes (Browaeys et al., 2020; Du et al., 2025; Jin et al., 2025; Kyaw et al., 2023; Ma et al., 2022; Raghavan et al., 2025). For example, NicheNet was used to identify SPP1 from human bone marrow MSCs and MMP9 from macrophages as ligands driving the upregulation of myeloid-bias inducing AP-1 factors in human HSCs (Feng et al., 2024). Additionally, Ma et al. (2022) used the CellPhoneDB ligand-receptor database and GRN analysis on aged HSPCs exposed to young blood during heterochronic parabiosis to show that cytokine networks dysregulated in the aged HSPCs are restored when exposed to young blood (Ma et al., 2022). However, the same group also showed that much of the TF activity was not restored in the aged HSPCs exposed to young blood and overexpression of some of these young-blood resistant TFs, including Yy1, could be used to rejuvenate the molecular signature and restore some function to the aged HSPCs (Ma et al., 2022).

There are also many GRN inference and comparison tools specifically designed to predict TFs for direct cell reprogramming (also known as transdifferentiation). For example, Mogrify uses RNA-seq data from source and target cell types to predict TFs that will transdifferentiate the source cell type into the target cell type (Rackham et al., 2016) and was recently used to discover novel TFs to reprogram fibroblasts into cardiomyocytes (Romero-

Tejeda et al., 2023). While Mogrify predicts TF cocktails for identity conversion, EpiMogrify identifies the specific signalling molecules and growth factors (external environment) required to maintain that identity or enhance differentiation efficiency (Kamaraj et al., 2020) and has been used to identify novel factors to maintain human astrocytes *in vitro*.

Another tool called NETISCE uses gene expression data and signal flow analysis to estimate TF activity attractor landscapes and predict TF reprogramming candidates (Marazzi et al., 2022). NETISCE was used to identify factors for inhibition to overcome resistance to MAPK inhibitor therapy in different cancers (Marazzi et al., 2022). On the other hand, ANANSE integrates gene expression and chromatin accessibility data to generate GRNs based on TF activity, then specifically compares two GRNs to identify key TFs governing cellular identity (Xu et al., 2021). ANANSE was used, for example, to identify transcription factors required for neuronal cell fate determination (Cirnaru et al., 2021). ANANSE was also adapted to work with cap analysis gene expression sequencing (CAGE-seq) (Heuts et al., 2022). Furthermore, another incarnation of ANANSE uses single-cell data (Smits et al., 2023) and was used to identify novel TF targets for differentiation of iPSCs into cardiomyocytes (Snabel et al., 2025) and corneal organoids (Arts et al., 2025).

If we assume that aged GRN cell states are distinct from young GRN cell states, then these tools normally used to identify TFs for transdifferentiation should be able to identify TFs that drive the aged state or restore the young state. A central question in this PhD project is: which TFs drive the aged or young states of HSCs?

1.4.2 Hi-C informed gene regulatory networks

Integration of Hi-C data into the construction of GRNs for the identification of state-defining TFs is an emerging concept being adopted by many tools. For example, the scMultiMap tool primarily uses paired scATAC-seq and scRNA-seq to map cell-type-specific enhancers to their target genes but still uses Hi-C data to validate enhancer-gene pairings (Su et al., 2025). So why not incorporate the Hi-C data directly into the enhancer-gene mappings and GRN construction? A recent preprint describes the development of a machine learning pipeline SCEG-HiC that uses Hi-C data as a prior to penalize the correlation matrix made from integration of scRNA-seq and scATAC-seq in order to prioritise enhancer-gene links that align with known physical interactions found in the bulk

Hi-C (Liang et al., 2025). Similarly, DeepMAPS is a GRN inference tool that uses a graph neural network (GNN) to integrate scRNA-seq and scATAC-seq while using Hi-C or promotor capture Hi-C as the graph's backbone by setting enhancer promotor spatial constraints (Ma et al., 2023).

For GRN inference, Hi-C chromatin interaction data has been used as a starting point to constrain the linkage of putative enhancers to their target genes. For example, scGRNom (Jin et al., 2021) starts with Hi-C interaction data and identifies potential enhancer-promotor interactions within TADs then maps TF motifs to these regions to create a large reference GRN. This reference GRN is then refined to a final GRN by selecting and weighting regions that show open chromatin in accompanying ATAC-seq data and associated gene expression from RNA-seq data. The scGRNom pipeline has been used to prioritize risk genes in Alzheimer's disease (Gupta et al., 2022) and risk SNPs in covid-19 severity (Khullar & Wang, 2023) that potentially interrupt TF binding sites. Similarly, scREMOTE uses databases of Hi-C data to simply remove or penalize regulatory elements that have a low probability of being able to physically interact with the target gene's promotor (Tran et al., 2022). GRaNIE (Kamal et al., 2023) which also builds GRNs by integrating ATAC-seq and RNA-seq data takes TAD domains as input so that only peak-gene pairs within a TAD are tested. The MAGICAL pipeline does a similar thing, selecting enhancer gene connections within user-supplied TAD domains, but this pipeline is specifically designed to compare conditions and uses differential accessibility and differential expression from single-cell data as the input to build the differential GRN (X. Chen et al., 2023).

In addition, Hi-C, DNAase-seq/ATAC-seq & ChIP-seq data have been previously integrated using a method known as activity-by-contact (ABC), in which an ABC score is calculated for each enhancer-gene pair by multiplying the candidate enhancer accessibility value by the Hi-C contact value, then normalizing this by dividing it by the sum of the ABC scores of other enhancers within 5 Mb distance (Fulco et al., 2019). This normalization step gives the relative fractional contribution of each enhancer to the regulation of the target gene to reflect the fact that each enhancer's regulatory power is modulated by competing enhancers. The enhancer-gene predictions from ABC scores performed better than distance-based co-accessibility predictions or Hi-C contacts alone (Fulco et al., 2019). A related method called IVEA (Kimura et al., 2024), combines ABC with a metric for transcriptional

bursting, i.e. the burst size (number of transcripts) multiplied by the burst frequency (frequency of transitions to the active state). The IVEA method claims to predict more eQTL-supported enhancer-gene pairs than ABC alone in some evaluations (Kimura et al., 2024).

The ABC method was further refined to a generalized ABC score (gABC), by also considering all competing target genes and all TSSs, and also allowing for single-cell ATAC-seq to be used as input (Hecker et al., 2023). Using single-cell cardiac cell data to validate the method, Hi-C informed gABC enhancer-gene pairings recovered more eQTL-linked gene pairs than ATAC-seq-based co-accessibility alone, and the gABC-derived TF affinity matrix showed better correlation with gene expression than regular ABC or co-accessibility (Hecker et al., 2023). This gABC method was recently used to identify TF-gene networks in 45 cell types related to coronary artery disease (CAD) and was combined with GWAS results to highlight specific transcription factors whose binding affinities are perturbed by the CAD-associated risk SNPs (Hecker et al., 2026).

All in all, incorporation of Hi-C chromatin contact data, even at relatively low resolution, consistently improves GRN inference by augmenting enhancer-gene network wiring confidence and is thus an important component of identifying TFs for cell reprogramming. As will be discussed in Chapter 4, I opted to use the gABC method in this PhD project because this method uses Hi-C interaction frequencies to modulate the enhancer activity value from the chromatin accessibility data rather than just using the Hi-C TAD boundaries as a distance constrainer. I then used the ANANSE method of GRN construction and TF scoring because it can take TF activity scores as input and is specifically designed for differential analysis of two GRNs to identify TF drivers of cell states.

1.5 Significance and scope of the PhD project

As discussed above, cellular ageing is predominantly caused by a loss of epigenetically controlled cell identity and gene regulatory states that results from the combination of:

1. Entropic (random) and programmed changes to the ECM (e.g. irreversible cross-linking, fibrosis, etc.);
2. Deleterious autocrine, paracrine and long-distance (often inflammatory) signalling from senescent cells, inflammation promoting cells reacting to increased damage signalling and stressed cells that harbour latent viral and bacterial infections; and

3. Cell intrinsic epigenetic changes due to deficiencies in the molecular machinery that copies and maintains epigenetic marks during cell division, telomere attrition and DNA repair (e.g. after double-stranded DNA breaks).

Cell reprogramming using Yamanaka factors or other identified factors presents an opportunity to restore the molecular and epigenetic aspects of aged LT-HSCs, including restoration of molecular cell identity, myeloid-lymphoid balance and differentiation capacity. However, this comes with the caveat that the other extrinsic and intrinsic aspects of ageing (loss of ECM structure, aberrant signalling, latent infections, etc.) would also need to be addressed for the restored LT-HSC function to persist.

1.6 Aims and Hypothesis of the PhD project

Aged murine bone marrow is characterised by an expansion of HSC clones that display increased self-renewal, reduced output and myeloid-bias. These features of ageing are largely epigenetically encoded, allowing for the ageing phenotypes to be retained in downstream progeny even after transplantation into young recipients, but crucially, can be restored after reprogramming via a pluripotent intermediate. Additionally, partial reprogramming can rejuvenate molecular and functional features of many aged cell types yet reprogramming of aged LT-HSCs using transient expression of Yamanaka factors has not been reported. However, even partial reprogramming comes with the risk of activation of oncogenic programs, or teratoma formation if some cells attain pluripotency, so alternate reprogramming strategies that either restore molecular and functional phenotypes without transition towards a pluripotent state, or reinforce cellular identity, are being explored by various groups.

The aims of this PhD project were to:

1) Assess the practicalities of exogenous delivery of Yamanaka factors for partial reprogramming of the relatively rare HSC population;

2) Explore the epigenetic differences in aged vs young murine HSCs compared to mature blood cell types using Hi-C, chromatin accessibility and gene expression data; and

3) Use Hi-C informed gene-regulatory networks to identify potential factors that could reprogram aged myeloid-biased LT-HSCs back to a high output, lineage-balanced (i.e. youthful) phenotype.

Since aged LT-HSCs have a clear phenotype that is carried into downstream progenitors (even after transplant into young recipients), I have hypothesised that there would be clear differences in the 3D genome organisation between aged and young LT-HSCs and that these differences could be aligned with gene expression and chromatin accessibility data to generate GRN maps. These GRN maps could then be compared and used to identify TFs that govern the aged and young states of LT-HSCs, TFs that could possibly be used in reprogramming experiments that reaffirm youthful cell identity without transition towards a pluripotent state.

Chapter 2: Reprogramming of murine HSCs with Yamanaka factors

2.1 Introduction

Blood progenitors, including HSCs that give rise to all the different blood cell types, can be manipulated *ex vivo* and transplanted back into various mouse models (wild-type, immunodeficient, etc) and so represent a promising testing ground for the reprogramming and rejuvenation of aged HSCs. In transplantation experiments, HSC ageing is characterised by myeloid bias and reduced reconstitution ability, which is not rescued by exposure to a young BM environment (Amoah et al., 2022; Gekas & Graf, 2013; Mann et al., 2018; Pang et al., 2011; Yamamoto et al., 2013). HSC ageing is also characterised by increases symmetrical division and decreased asymmetrical division (Florian et al., 2018; Kawahigashi et al., 2024). Molecularly, aged murine HSCs undergo transcriptional changes (Flohr Svendsen et al., 2021), DNA hypermethylation of PRC2 targets (Beerman et al., 2013; Taiwo et al., 2013), changes to chromatin accessibility (Itokawa et al., 2022), repositioning of heterochromatin leading to derepression of transposable elements (Hidaoui et al., 2024; Hong et al., 2023), loss of polarity of cytoskeletal proteins (e.g. tubulin) and histone marks, particularly H3K16ac (Amoah et al., 2022; Florian et al., 2018).

In 2006, the factors Oct4, Sox2, Klf4 and Myc (OSKM) were shown to reprogram fibroblasts into pluripotent stem cells (Takahashi & Yamanaka, 2006). Later, fibroblasts from human centenarians were shown to be transcriptionally rejuvenated with fully restored telomeres by reprogramming with an OSKM cocktail that included NANOG and LIN28A (Lapasset et al., 2011). Transient or cyclic expression of OSKM (also known as partial reprogramming), or just OSK factors, can epigenetically, transcriptionally and functionally rejuvenate cells without causing pluripotency (Berdugo-Vega et al., 2026; Gill et al., 2022; Y. W. Liu et al., 2026; Lu et al., 2025; Y. Lu et al., 2020; Pernomian et al., 2025; Sarkar et al., 2020). Moreover, whole body transient expression of OSK via an adeno-associated virus (AAV9) vector in already aged (124-week old) mice increases their remaining lifespan (Macip et al., 2024). However, *in vivo* expression of OSK(M) in mice is currently marred by problems with dose control and variability of reprogramming of different organs, with major

risks being organ-specific loss of cell identity and dysplasia in certain susceptible tissues (Chondronasiou et al., 2022; Parras et al., 2023; Picó et al., 2025), but also oncogenic transformation of cells harbouring key pre-cancerous somatic mutations (Huyghe et al., 2022; Ohnishi et al., 2014; Shibata et al., 2018; Singovski et al., 2016).

Considering the strong role of the aged immune system on ageing pathologies (Jang et al., 2026; Khan et al., 2026), it is surprising that there are currently no published reports of the effect of transient Yamanaka factor over-expression on the rejuvenation of blood and blood progenitors and only one report of an indirect effect (Sahu et al., 2024). For example, using an accelerated ageing mouse model characterized in the blood by an ageing-like myeloid bias, Sahu and colleagues observed that selective overexpression of OSK (no Myc) using AAV-DJ delivery and OSK under the control of the cyclin-dependent kinase inhibitor 2a (Cdkn2a) promoter, to specifically target stressed and senescent cells, led to a reduction of myeloid-biased HSCs in the bone marrow and restoration of mature blood cell ratios (Sahu et al., 2024). Crucially, this restoration of HSC function was likely the side-effect of pCdkn2a-OSK overexpression in non-bone marrow cells, due to the low tropism of AAV-DJ for bone-marrow, which resulted in a systemic reduction in proinflammatory cytokines, including Il-1α, Il-1β, and Il-6 (Sahu et al., 2024). Long-term reduction in inflammatory cytokine signalling, like Il-1β, using receptor knockout or inhibitors, has also shown some restoration of HSC function in aged mice (Mitchell et al., 2023).

Cyclic or transient reprogramming of aged HSCs or other early blood progenitors using OSKM factors has not yet been reported. However, Klf4 overexpression in HSCs induces monocyte differentiation away from granulocyte differentiation (Feinberg et al., 2007) and Klf4 is naturally upregulated in aged LT-HSCs (Itokawa et al., 2022), so it is an open question as to whether OSK(M) overexpression in aged HSCs would restore HSCs to a youthful phenotype or exacerbate Klf4-driven myeloid bias. To begin to address this question, different transduction/transfection strategies (PiggyBac, Lentiviral, mRNA and DNA nucleofection) were tested with the hope of examining how overexpression of the Yamanaka factors affects the expression of lineage defining markers of HSCs.

2.2 Results

2.2.1 OSKM PiggyBac vector does not provide sufficient transfection of HSCs

The PiggyBac system uses a hyperactive transposase to insert an expression cassette (Yusa et al., 2011) and has been used by others to generate transgene free induced pluripotent stem cells (iPSCs), although this involves re-expressing the transposase and selection of iPSC colonies (Yusa et al., 2009). To test the transfection efficiency of an inducible OSKM cassette, I constructed a PiggyBac compatible vector (which I called Q02) carrying OSKM separated by 2A self-cleaving peptides and followed by an IRES2 controlled mNeonGreen reporter then amplified it using NEB's high-fidelity DNA assembly (an enhanced Gibson assembly) cloning in competent *E. coli* (see Methods and Fig. 2.1).

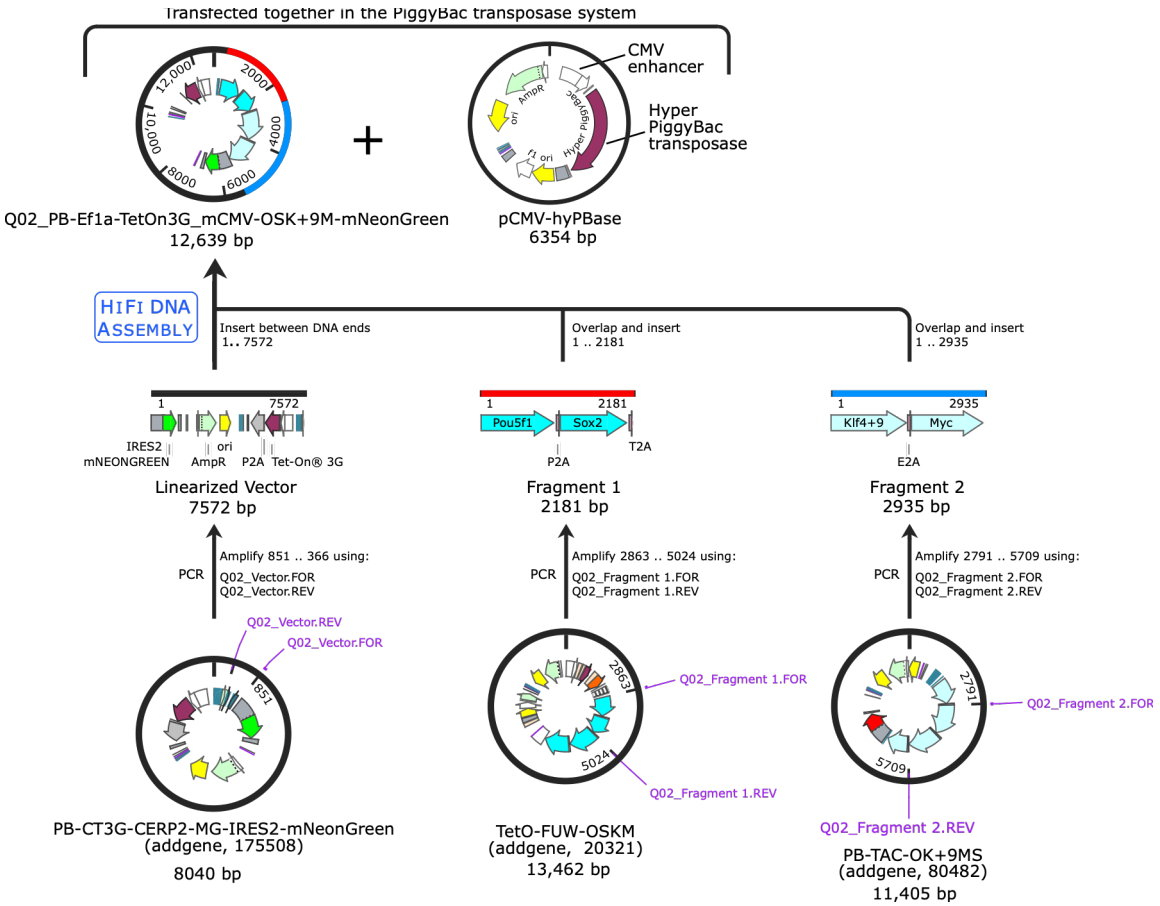


Figure 2.1. Construction of PiggyBac plasmid Q02_PB-Ef1a-TetOn3G_mCMV-OSK+9M-mNeonGreen (12,639 bp)

The Q02 plasmid was purified and sequenced confirmed using a diagnostic digest (Fig. 2.2) and subsequent nanopore longread sequencing (WEHI genomics), then colony 2 (Col2) was selected for further experiments. For integration of the Q02 expression cassette into HEK293T cells, the Q02 plasmid was combined with the hyperactive piggyBac (hyPBase) transposase plasmid, pCMV-hyPBase (a gift from Wellcome Trust Sanger Institute, Cambridge, UK) during nucleofection of HEK293T cells.

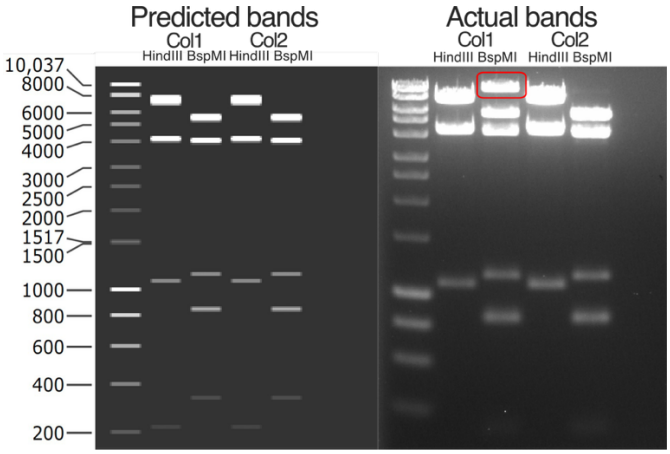


Figure 2.2. Diagnostic digest for Q02 DNA plasmids purified from two colonies, Col1 and Col2. Red rectangle shows a large unexpected large fragment indicating a possible mixed population of plasmids in the Col1 pellet.

Fig. 2.3 shows the general nucleofection protocol used and the nucleofection efficiency 48 hours post nucleofection (24 hours post-doxycycline induction of the OSKM cassette). Expression in HEK293T cells, read out by mNeonGreen expression and flow cytometry, only reached 5.39%, which for this cell line, is low. Transfection of rare, harder to transfect cell types such as primary hematopoietic stem and progenitor cells (HSPCs) would require higher transfection rates, therefore the low transfection efficiency in the HEK293T cells indicated that it would be unlikely to work in HSPCs.

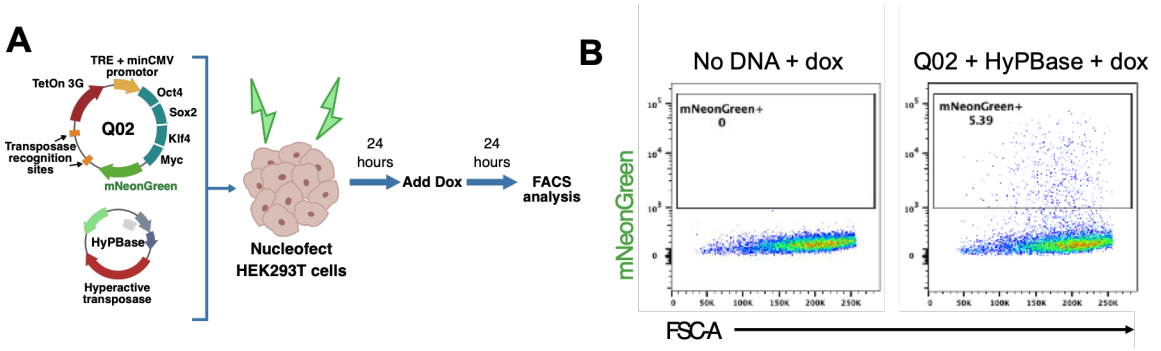


Figure 2.3. OSKM PiggyBac vector efficiency too low in HEK293T cells. A. Schematic of transfection of HEK293T cells with Q02 (Q02_PB-Ef1a-TetOn3G_mCMV-OSK+9M-mNeonGreen) PiggyBac vector harbouring a dox inducible OSKM expression cassette. B. FACS analysis results showing negative control (No DNA + dox) and treatment (Q02 + HyPBase + dox).

2.2.2 Dox-inducible lentiviral OSKM or OS2-17K vectors do not provide sufficient transduction of LT-HSCs

To test the transfection efficiency of a doxycycline inducible lentiviral OSKM vector in murine LSKs and HSCs, two lentiviruses were made: 1) the first called Q03-TRE-OSKM-mNeonGreen, or just Q03, containing the tetracycline response element (TRE) followed by a minimal CMV promoter and the OSKM genes separated by 2A peptide sequences and followed by an IRES2 controlled mNeonGreen reporter (see Fig. 2.4); and 2) Another lentivirus called pHAGE2_EF1a_TetOn_IRES_mCherry (addgene, 204155) containing the constitutively expressed Tet-On-3G transactivator protein (i.e. an enhanced rtTA protein) under the control of EF-1α promoter. Once expressed, the Tet-On-3G protein is activated by doxycycline causing it to bind to the TRE to activate transcription of the minCMV-OKSM-mNeonGreen cassette.

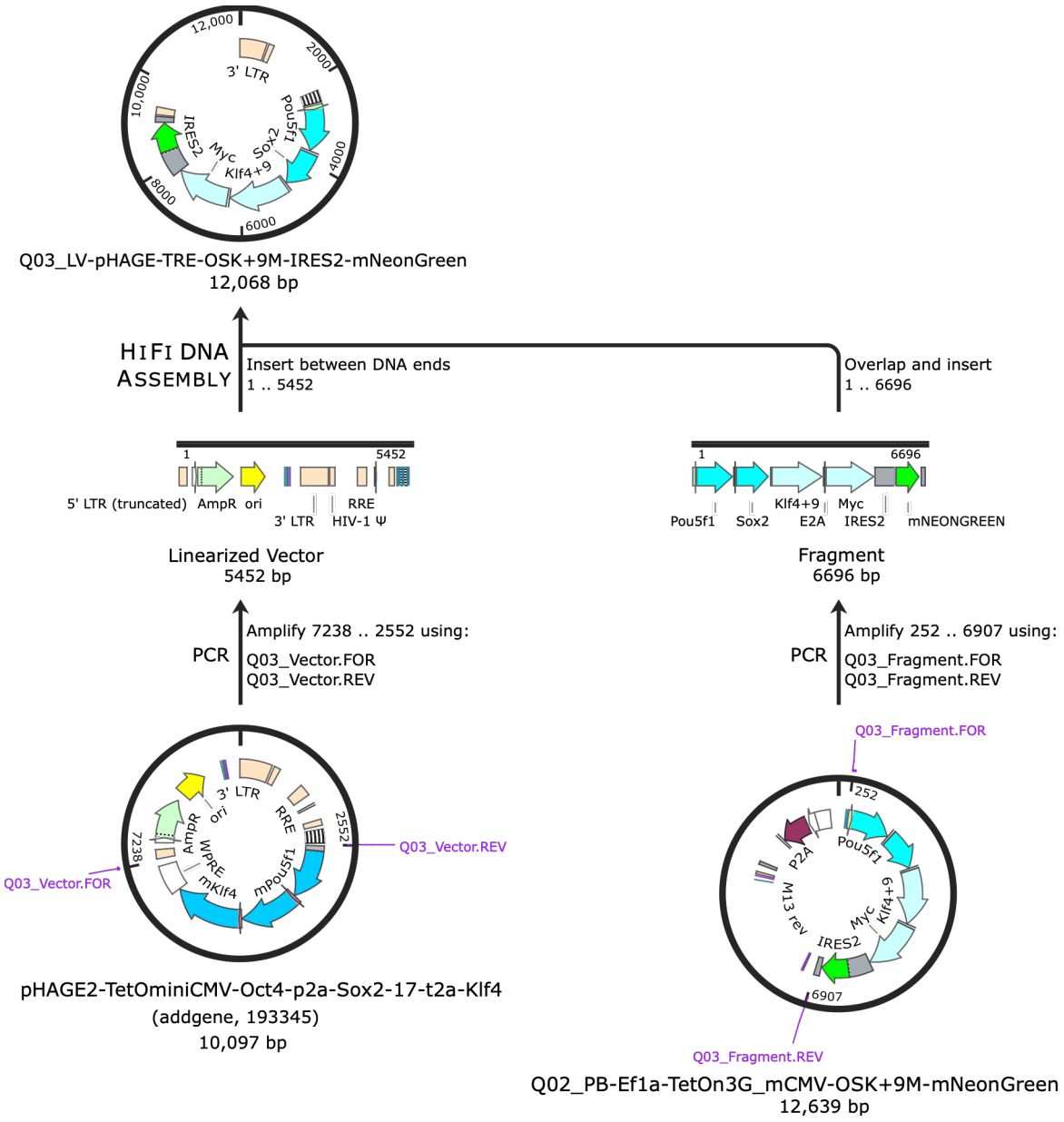


Figure 2.4. Construction of Q03 lentiviral vector with cassette for Oct4, Sox2, Klf4+9 and Myc (OSK+9M)

As this setup required a double transduction (see the Fig. 2.5B schematic below) it was anticipated that higher transduction efficiency of each individual vector would be required and so virus was concentrated from 20 mL to 2 mL using Amicon centrifugal filtration tubes (see Methods and Fig. 2.5A).

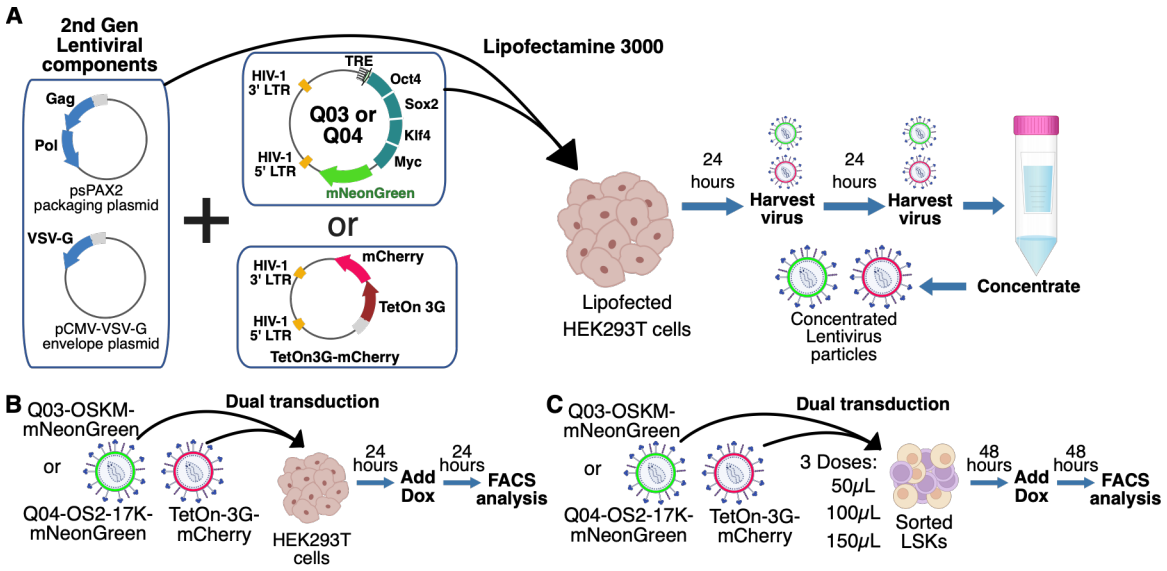


Figure 2.5. Lentiviral production and transduction of sorted LSKs blood progenitors. A. Lentivirus production schematic; B. Schematic of dual transduction of murine LSKs (bone marrow blood progenitors) with lentiviruses harbouring either OSKM or OS2-17K expression cassettes, plus simultaneous additional transduction with the lentivirus harbouring the TetOn-3G expression cassette.

Transduction of HEK293T cells with both Q03-TRE-OSKM-mNeonGreen and the Tet-On-3G-mCherry plasmids was achieved using 100 µL of both concentrated viruses (including polybrene) resulting in a 15.6% double transduction efficiency (Fig. 2.6A). For transduction of flow cytometry sorted primary murine LSKs, three doses of each concentrated virus were used: 50 µL, 100 µL and 150 µL. Transduction was achieved by adding both viruses to retronectin coated 12 well plates, then adding sorted LSKs followed by a 2 hour spinfection at 32°C. As shown in Fig. 2.6B, single transduction efficiency of the Tet-On-3G-mCherry vector (x-axis) did not increase substantially with increasing volume of virus added, and achieved a maximum of only 3.90% in LSKs and 3.47% in HSCs. Double transfection achieved near zero percent transduction (Fig. 2.6B).

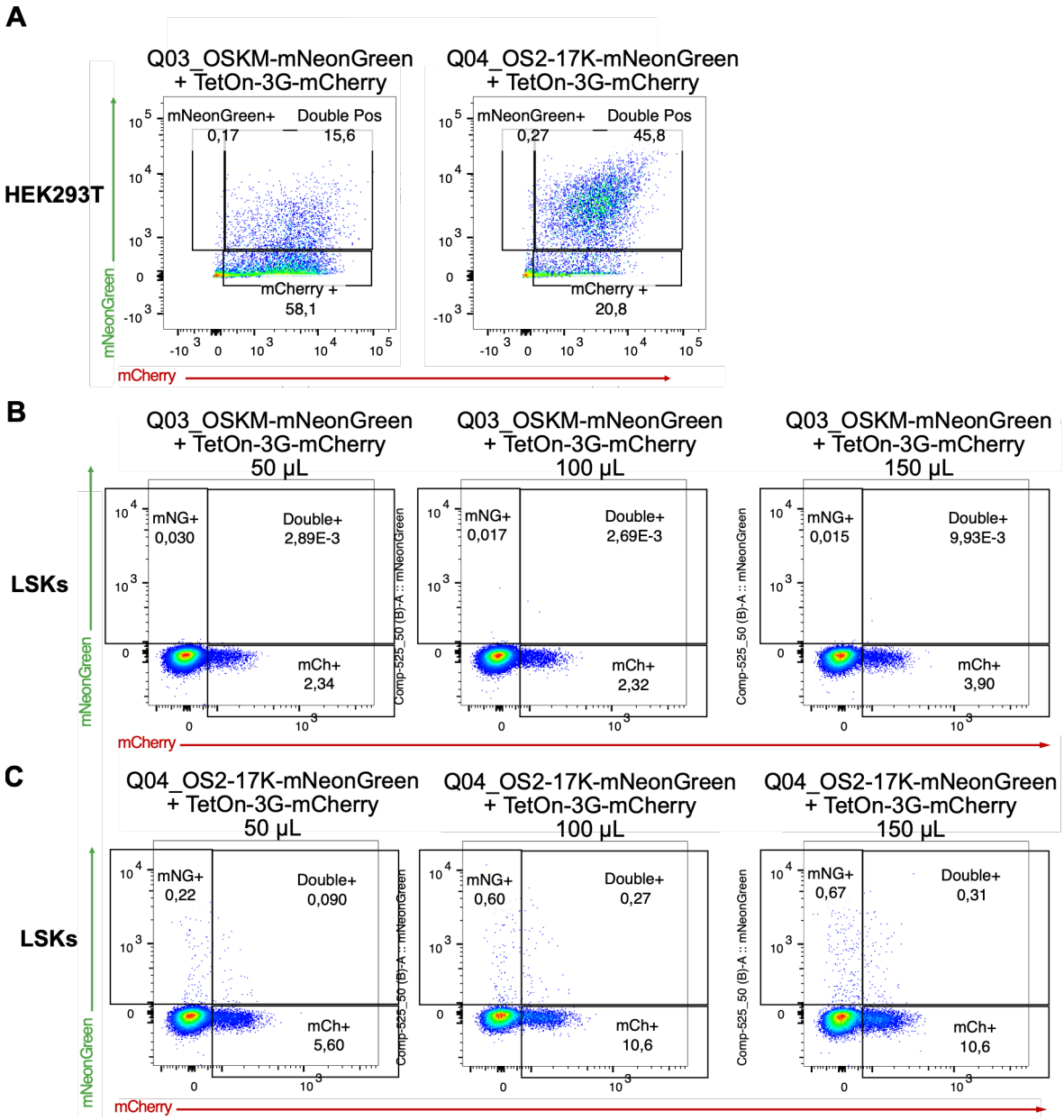


Figure 2.6. Lentiviral transduction of HEK293T cells then LSKs at 3 different doses. A. Lentiviral double transduction of HEK293T cells with Q03-TRE-OSKM-mNeonGreen + Tet-On-3G-mCherry and Q04-TRE-OS2-17K-mNeonGreen + Tet-On-3G-mCherry; B. Lentiviral double transduction of sorted lineage negative Sca-1^{+} cKit^{+} cells (LSKs) with Q03-TRE-OSKM-mNeonGreen + Tet-On-3G-mCherry lentiviruses; C. Double transduction of sorted LSKs with Q04-TRE-OS2-17K-mNeonGreen + Tet-On-3G-mCherry lentiviruses. Both yield insufficient transduction (double positive cells) at all 3 doses.

A cassette containing an engineered version of Sox2 called Sox2-17 that has been previously reported to enhance reprogramming to pluripotency (MacCarthy et al., 2024) was

also constructed with the same backbone as Q03 (Fig. 2.7). This vector (known as Q04-TRE-OS2-17K-mNeonGreen, or just Q04) was also used to produce concentrated virus and transduce first HEK293T cells, then LSKs on retronectin coated plates at doses of 50 µL, 100 µL and 150 µL (as in the schematic in Fig. 2.5A & B).

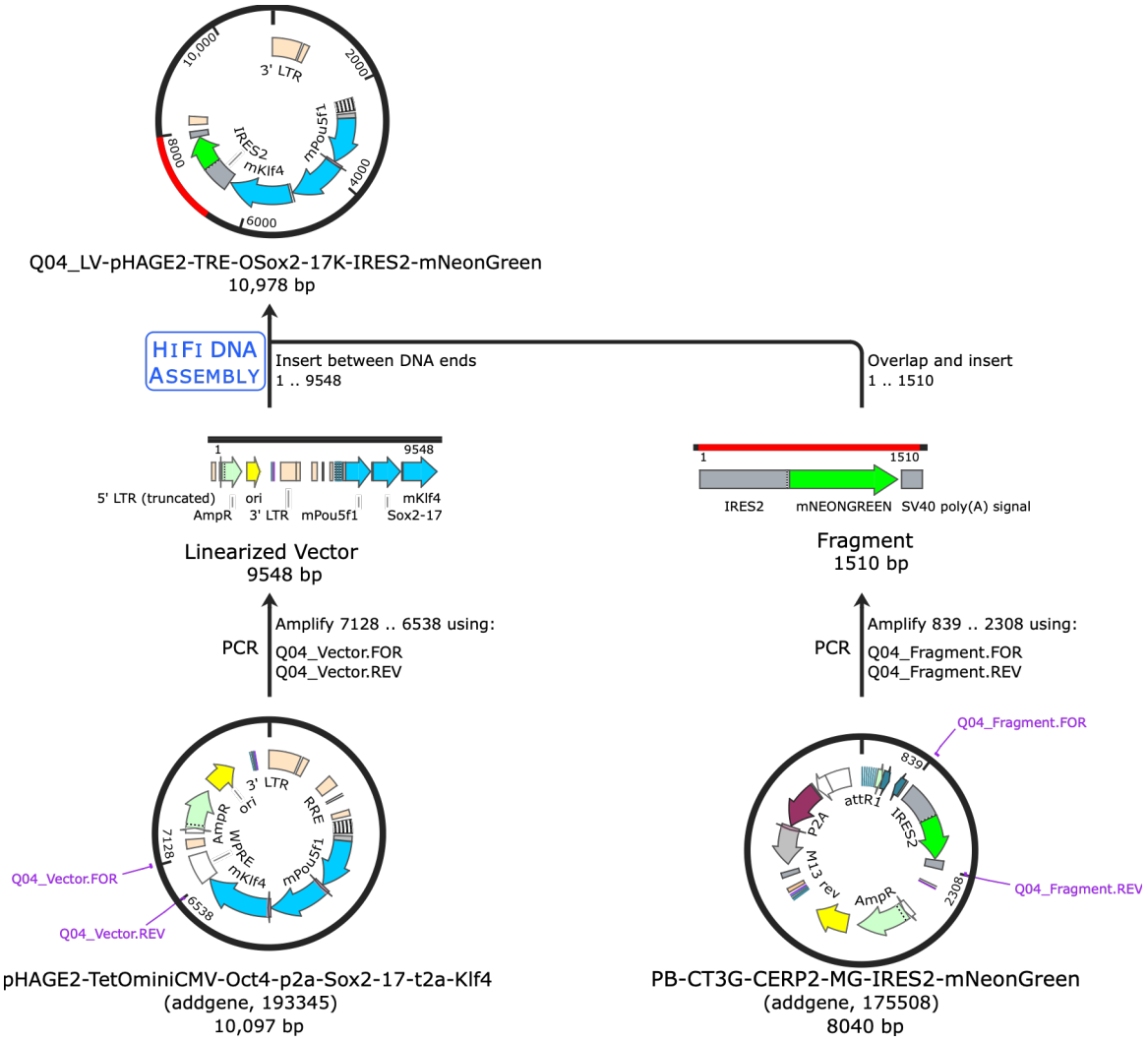


Figure 2.7. Construction of Q04 lentiviral vector with cassette for Oct4, Sox2-17 and Klf4 (OS2-17K).

As shown in Fig. 2.6A, double transduction of HEK293T cells with Q04-TRE-OS2-17K-mNeonGreen and Tet-On-3G-mCherry resulted in an encouraging 45.8% double transduction efficiency (Fig. 2.6A). However, in primary LSKs, even single transduction with the Tet-On-3G-mCherry vector (x-axis) only achieved a maximum efficiency of 10.6%

and 8.91% in HSCs at the 100 µL dose and did not increase at the 150 µL dose (Fig. 2.6C). Double-transduction with both Q04-TRE-OS2-17K-mNeonGreen and Tet-On-3G-mCherry vectors achieved a maximum of 0.31% at the 150 µL dose (Fig. 2.6C). However, there was also a substantial number of mNeonGreen positive mCherry negative cells (Fig. 2.6C, y-axis) which increased with increasing dose, indicating leaky expression of the Q04-TRE-OS2-17K-mNeonGreen cassette even without detectable Tet-On-3G-mCherry expression. Thus, transduction efficiency was deemed too low to proceed with lentiviral-based transduction.

2.2.3 In vitro transcription (IVT) and transfection with polycistronic Yamanaka factor mRNA depends on mRNA size and gene content

Nucleofection with mRNA is an attractive option for reprogramming because it is only transiently expressed (Warren et al., 2010), can yield equivalent or better transfection efficiencies than lentiviral systems (Dullaers et al., 2004), depending on the cell type; and has the added benefit of being less immunogenic than viral or DNA transgene delivery, especially when the modified bases 5-methyl cytidine and pseudouridine are used (Kariko et al., 2008; Papaioannou et al., 2023). High efficiencies of HSC transfection have also been achieved using nucleofection with mRNA (Papaioannou et al., 2023), but transfection with polycistronic mRNA for OSKM reprogramming has not been reported. To this end, I designed an OSKM plasmid that could be used as a template for *in vitro* transcription (IVT) called Q08_cleancap_pT7-OSKM-mNeonGreen_polyA_148 (Fig. 2.8).

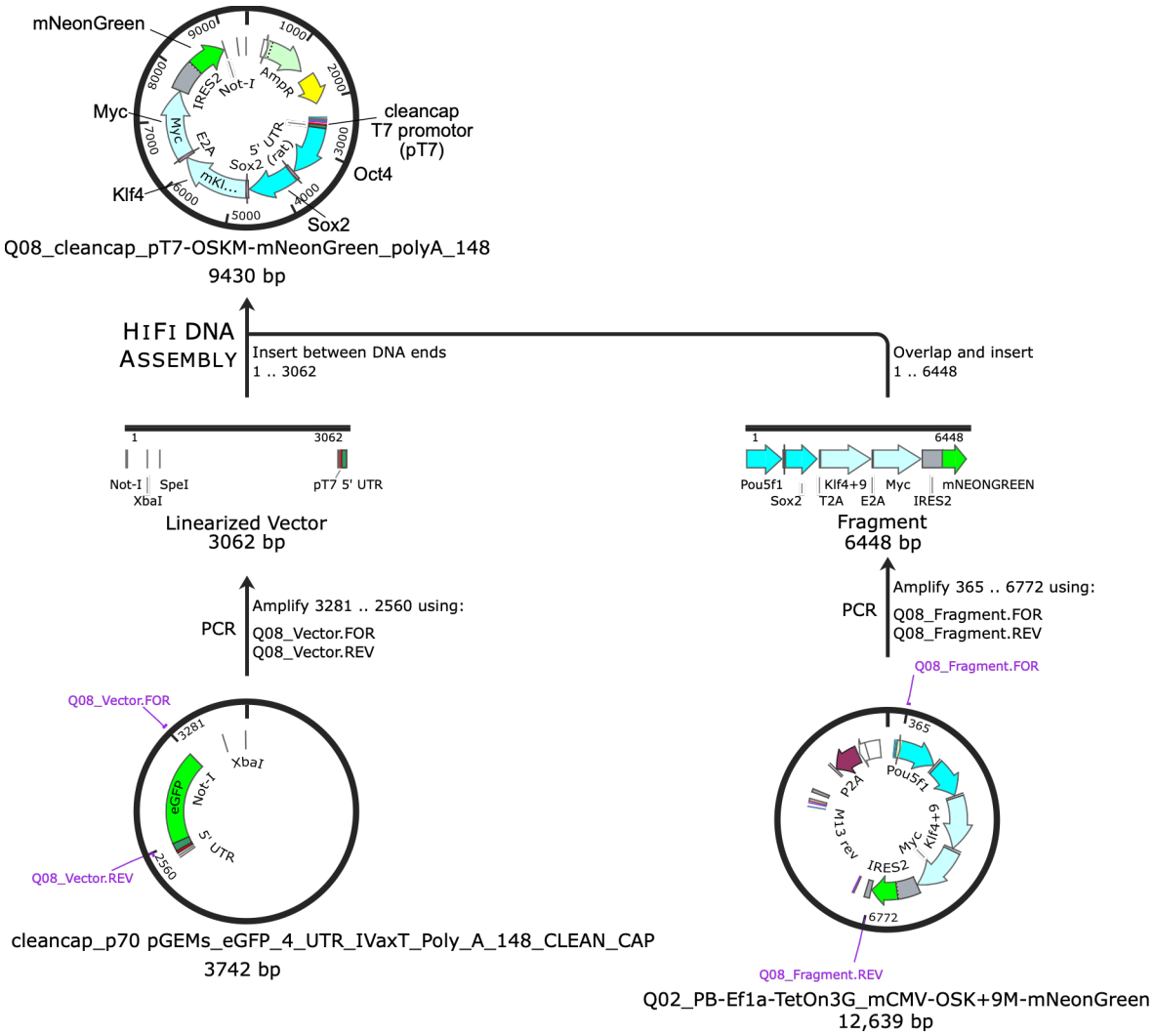


Figure 2.8. Construction of Q08 in vitro transcription template with cassette for Oct4-Sox2-Klf4-Myc-mNeonGreen (OSKM-mNeonGreen) under the control of a T7 promotor.

This template was designed to be used with the HiScribe T7 mRNA Kit with CleanCap Reagent AG (NEB #E2080) which utilizes linear templates containing a T7 promoter followed by an AG initiation sequence that incorporates a 5´-m7G Cap-1 structure to improve mRNA yield and stability (Henderson et al., 2021). The mRNA also contains modified cytidine and pseudouridine to improve stability and reduce immunogenicity. To test the transfection efficiency in a cell line, Q08 mRNA was used to transfect HEK293T cells at 3 different doses (see protocol schematic in Fig. 2.9).

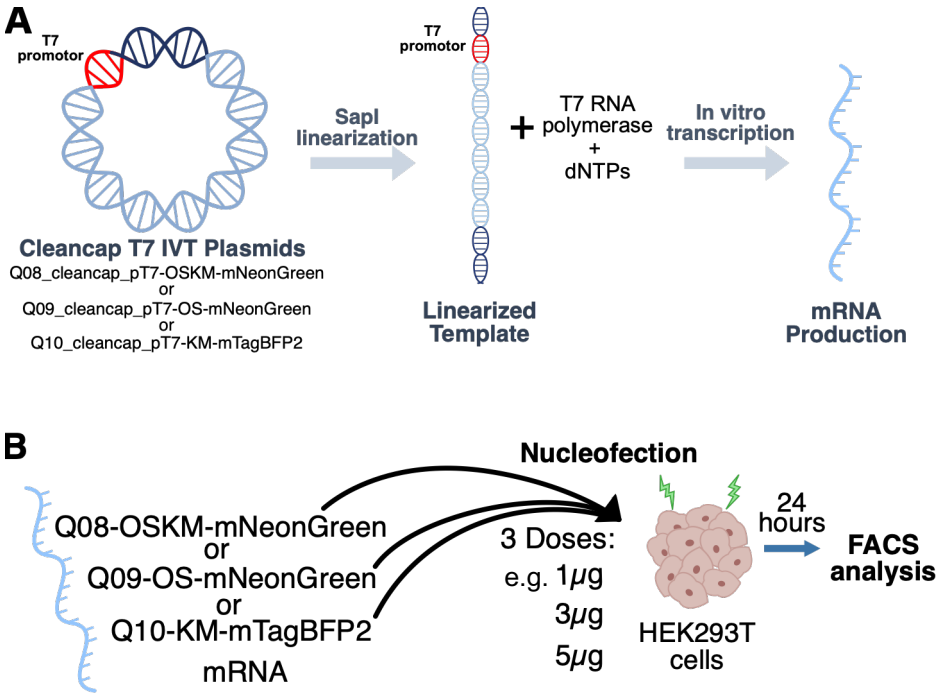


Figure 2.9. In vitro transcription mRNA production and nucleofection protocol. A. In vitro transcription of Q08, Q09 and Q10 involving linearization of the IVT plasmid using SapI, followed by transcription using the T7 polymerase and dNTPs (including modified dNTPs); B. Nucleofection of HEK293T cells with mRNA for Q08, Q09 and Q10 at different doses.

As shown in Fig. 2.10 below (first row), nucleofection of HEK293T cells with Q08 OSKM-mNeonGreen mRNA resulted in zero transfection compared to the GFP mRNA positive control (17% efficiency).

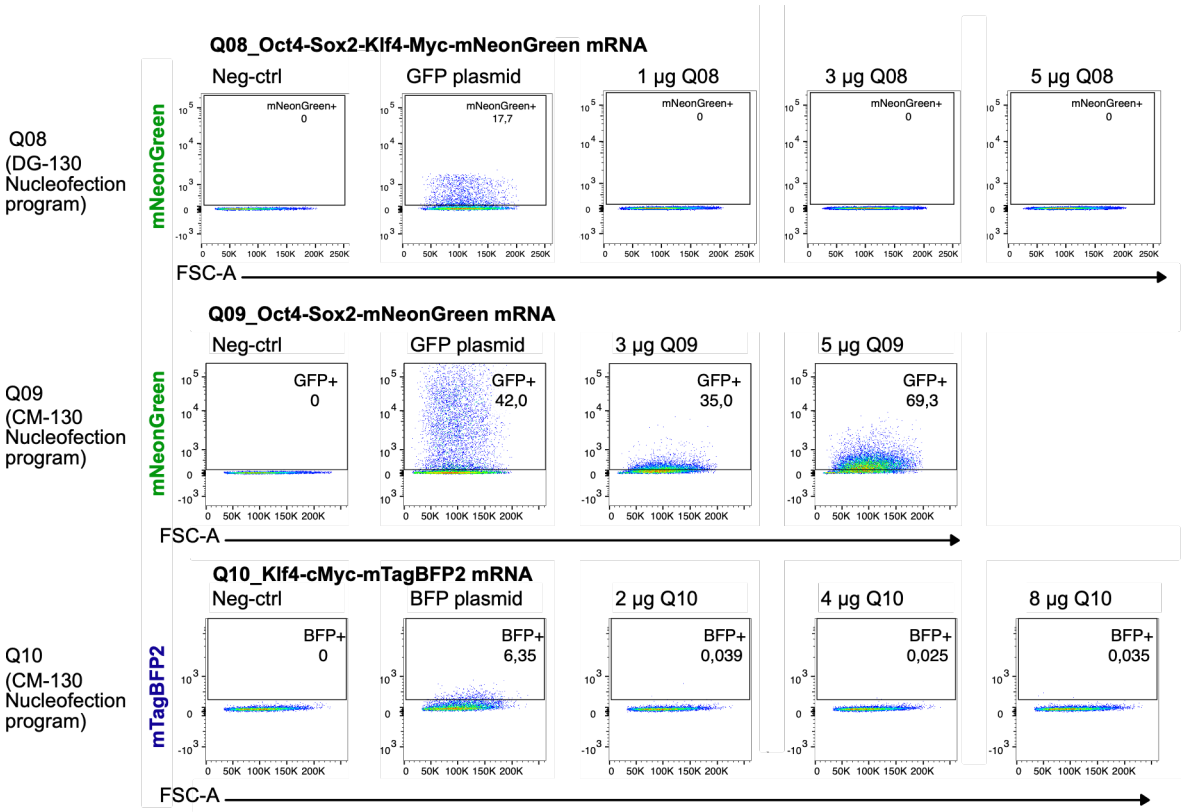


Figure 2.10. Transfection efficiencies in HEK293T cells of mRNA expression cassettes Q08_Oct4-Sox2-Klf4-Myc-mNeonGreen, Q09_Oct4-Sox2-mNeonGreen and Q10_ Klf4-Myc-mNeonGreen

Reasoning that Q08_cleancap_pT7-OSKM-mNeonGreen_polyA_148 mRNA was perhaps too large for efficient nucleofection, I split expression cassette into two smaller DNA templates each harbouring either Oct4 and Sox2 or Klf4 and Myc. These were called Q09_cleancap_pT7-OS-mNeonGreen_polyA_148 and Q10_cleancap_pT7-KM-mTagBFP2_polyA_148 (Figs. 11 & 12). As shown in Fig. 2.10, 2nd and 3rd rows, nucleofection of HEK293T cells with Q09 and Q10 mRNA in separate experiments yielded a maximum of 69.3% transfection efficiency for Q09 OS-mNeonGreen mRNA but effectively zero transfection with Q10 KM-mTagBFP2 mRNA.

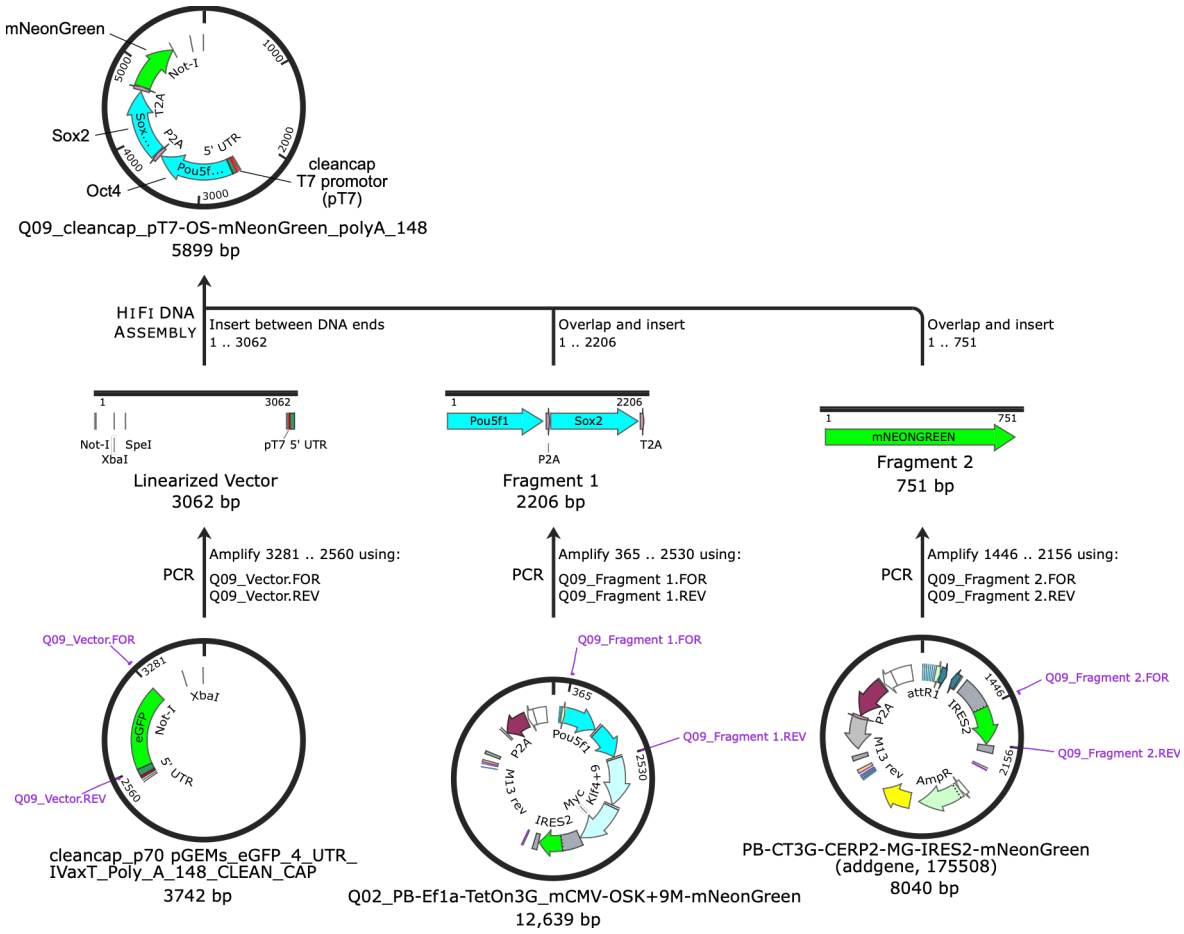


Figure 2.11. Construction of Q09 in vitro transcription template with cassette for Oct4-Sox2-mNeonGreen (OS-mNeonGreen) under the control of a T7 promotor.

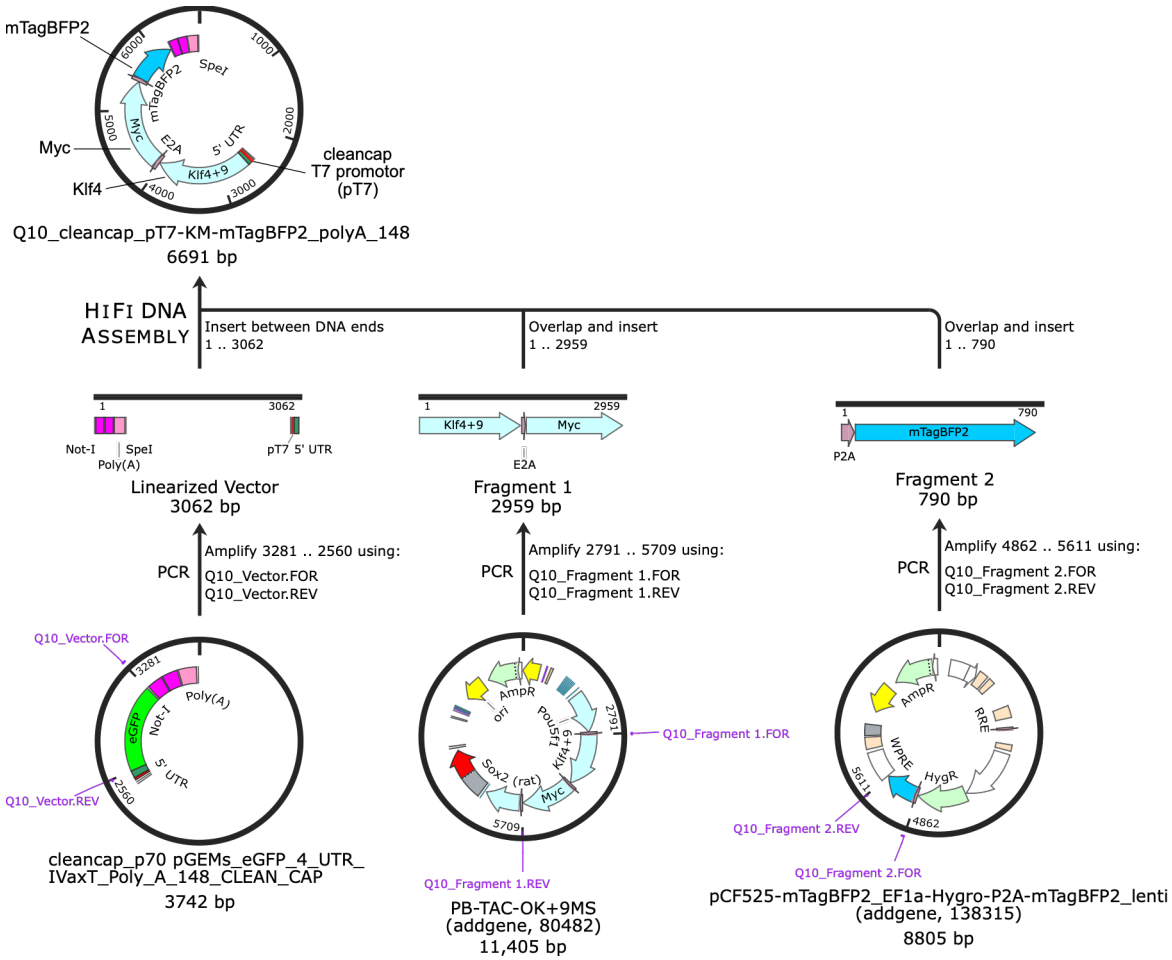


Figure 2.12. Construction of Q10 in vitro transcription template with cassette for Klf4-Myc-mTagBFP2 (KM-mTagBFP2) under the control of a T7 promotor.

2.2.4 Nucleofection with DNA plasmids bearing OSK fails to transfect primary murine blood stem cells

I also reasoned that perhaps the easiest way to demonstrate *ex-vivo* partial reprogramming of blood-progenitors would be one that did not require a lot of double handling and replating of cells, as is the case for lentiviral transduction, or one that requires expensive IVT reagents. Additionally, the ideal method would not require random integration of a cassette into the cell's genome as is the case for both PiggyBac and lentiviral systems, which risks upregulation of the DNA damage response or random mutations in the genome that might influence the results. Since DNA plasmids are non-integrating and degrade and dilute over time and cell divisions (thus ensuring only transient expression), I designed DNA plasmids

harbouring an expression cassette of OSK-mNeonGreen under the control of an EF-1α promotor to ensure robust yet transient expression of the reprogramming factors. In addition, Myc was excluded since recent papers have shown this might further prevent pluripotency without much loss of the rejuvenating aspects (Y. Lu et al., 2020; Macip et al., 2024; Nakagawa et al., 2008). This plasmid was called Q23-OSK-mNeonGreen and the positive control was Q25-mNeonGreen, the latter of which was made using the same backbone and promoter as Q23 (Fig. 2.13 & 2.14).

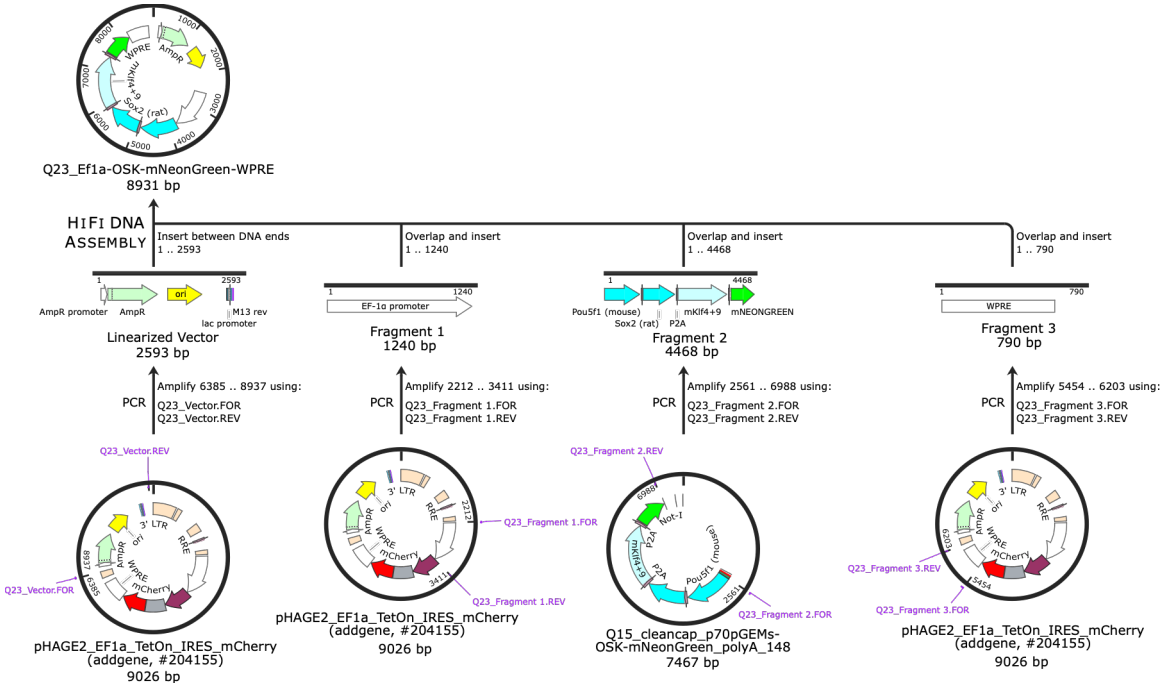


Figure 2.13. Construction of Q23 DNA plasmid harbouring the expression cassette for Oct4-Sox2-Klf4-mNeonGreen (OSK-mNeonGreen) under the control of the constitutive EF-1α promotor.

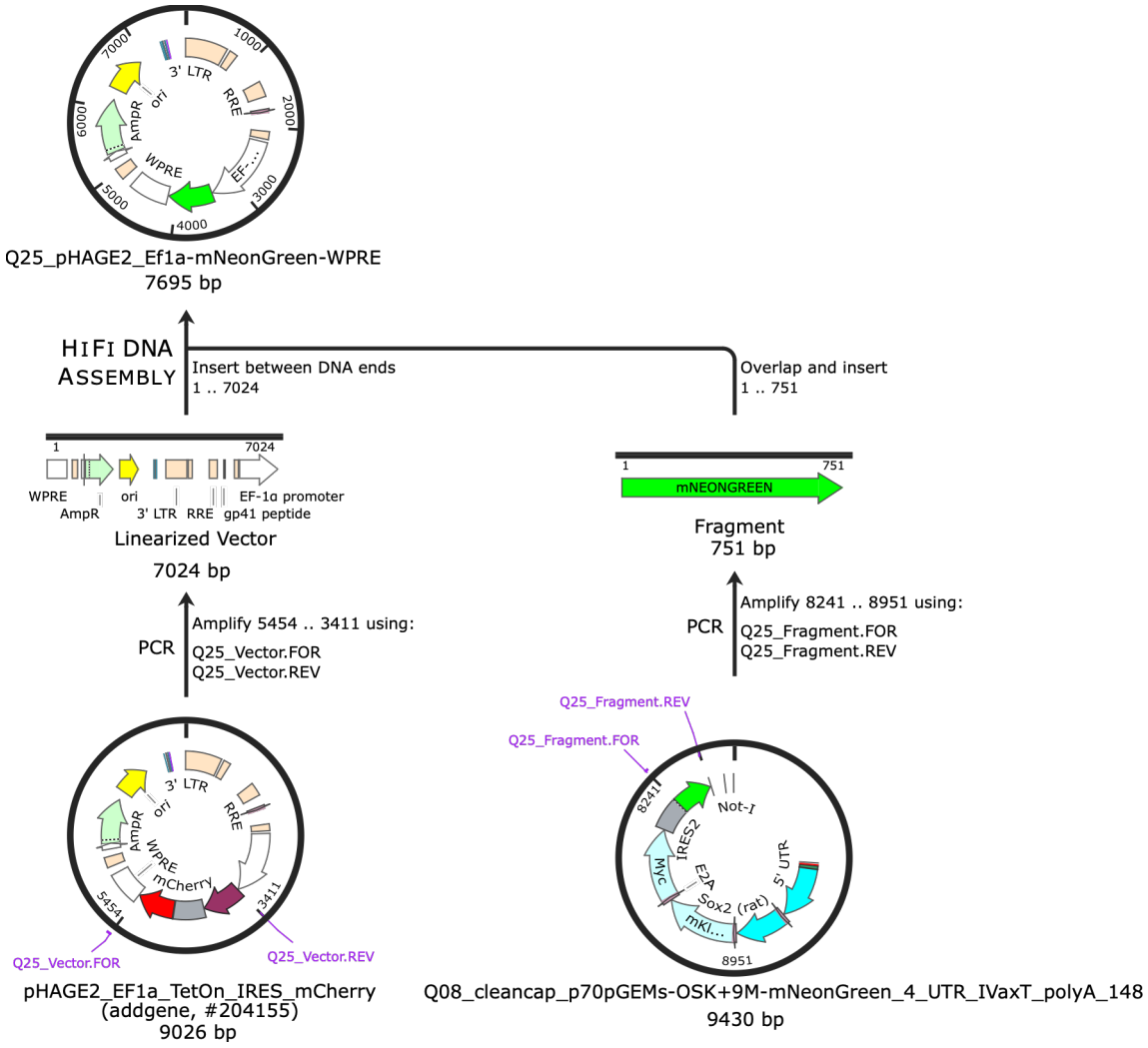


Figure 2.14. Construction of Q25 DNA positive control plasmid harbouring the expression cassette for mNeonGreen under the control of the constitutive EF-1α promotor.

Q23-OSK-mNeonGreen was able to nucleofect HEK293T cells with an efficiency of 40.3% (Fig. 2.15), thus demonstrating that the polycistronic cassette can be successfully translated.

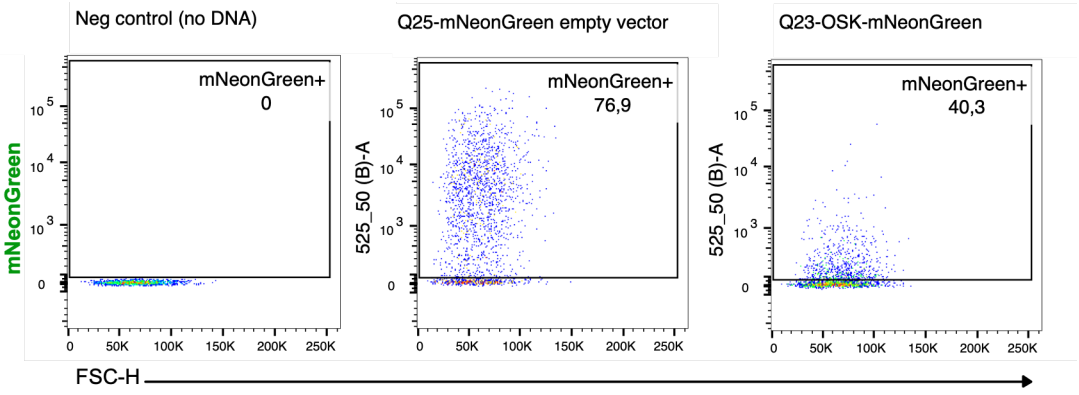


Figure 2.15. Transfection efficiencies in HEK293T cells using DNA plasmid vectors Q23_Oct4-Sox2-Klf4-mNeonGreen and the Q25_mNeonGreen empty vector positive control.

Nucleofection efficiency is cell type specific and depends on the nucleofector program used. A literature search for nucleofection programs ideal for primary murine HSCs revealed a small selection of programs (as well as those recommended by the Lonza company itself) as shown in Table 2.1. After some preliminary testing of different nucleofection programs for transfection of lineage marker depleted murine bone marrow cells (Lin^- BM cells) transfected with the Q25-mNeonGreen reporter (Fig. 2.16), I chose the 3 best programs which had a good balance of high cell viability and transfection of LT-HSCs, i.e. the programs EH-100, DN-107, and EO-100.

Table 2.1. Nucleofection programs for HSC and HSPCs from the literature

Program	Citation	Reported Efficiency (%)	Reported Viability (%)
DS-113	(Wang et al., 2021)	99	81.7
DS-112	(Wang et al., 2021)	86.4	89.1
CG-104	(Wang et al., 2021)	90.9	92.8
DN-107	(Wang et al., 2021)	99.2	22.9
EH-100	(Wang et al., 2021)	99.4	11.6
DN-100	(Wang et al., 2021)	99.6	30.4
EO-100	(Damhofer et al., 2021)	NA	NA

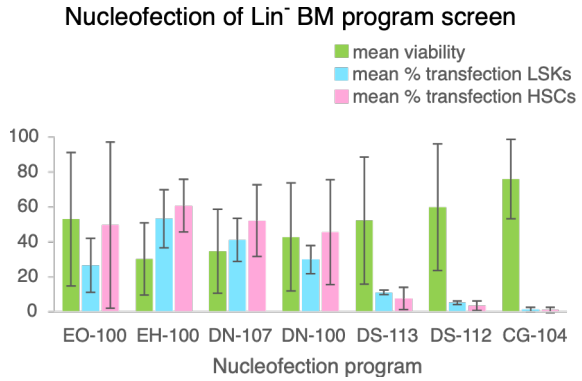


Figure 2.16. Screen of nucleofection programs for optimal LSK and LT-HSC transfection. Error bars are SD.

In addition, even though the CG-104 and DS-113 programs showed relatively poor ability to transfect LSKs and LT-HSCs in my preliminary experiment, they have been reported to give very high transfection efficiency in HSCs (Wang et al., 2021), so I included these in further tests and nucleofected flow cytometry sorted LSKs with Q23-OSK-mNeonGreen, using Q25-mNeonGreen as a positive control and nucleofection without DNA as a negative control. Unfortunately, in this experiment the sytox blue viability stain did not work, nor did the Flt3 (CD135) dye, so I was unable to distinguish MPP3s and MPP4s. However, this was moot because, although the Q25-mNeonGreen positive control was able to transfect LSKs with an efficiency of 29.3%, the polycistronic Q23-OSK-mNeonGreen showed zero transfection (Fig. 2.17), likely due to its larger size or effect on cell viability.

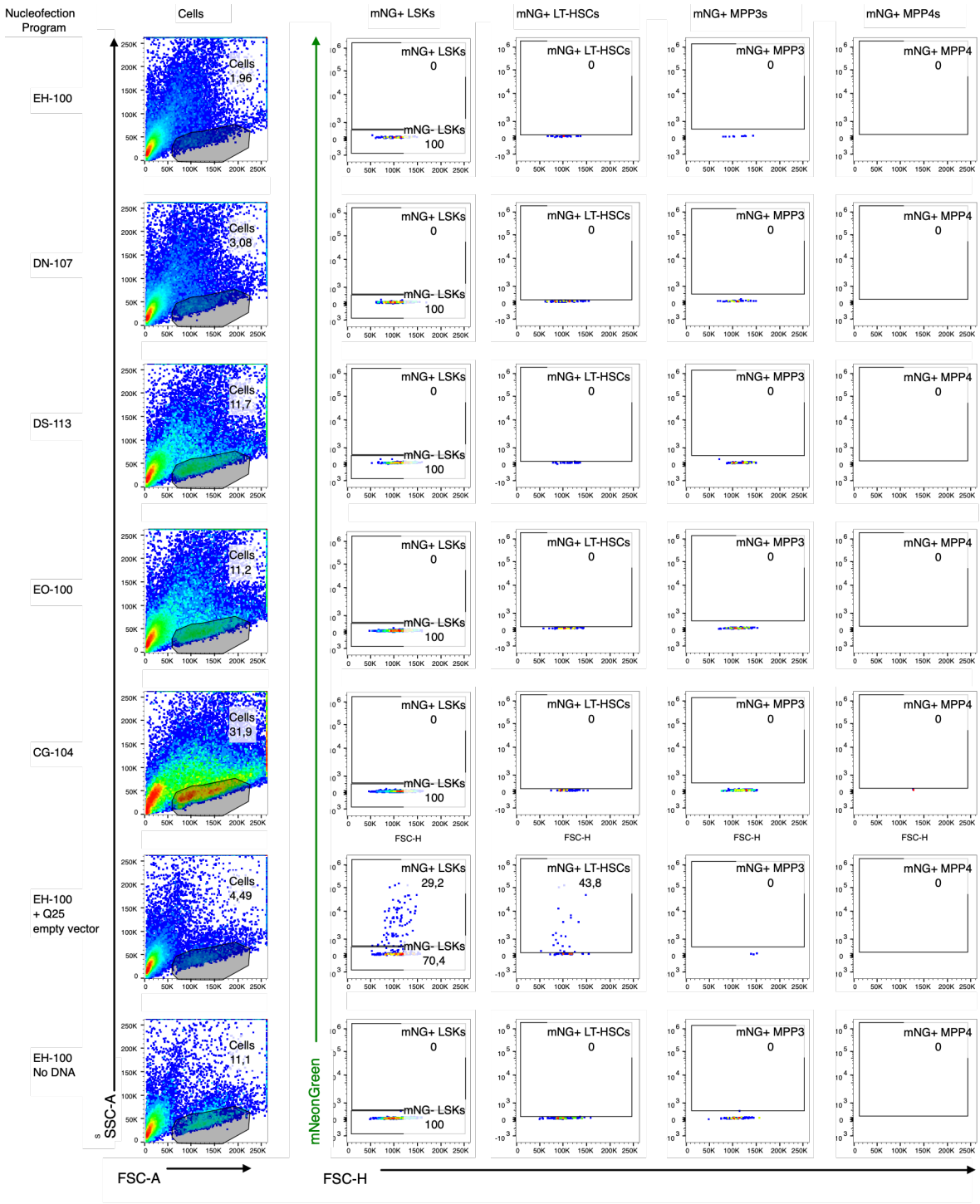


Figure 2.17. Screen for suitable nucleofection program for optimal transfection of lineage negative Sca-1+ cKit+ cells (LSKs) and long-term hematopoietic stem cells (LT-HSCs). First 5 rows show nucleofection with Q23-OSK-mNeonGreen DNA vector, last two row shows nucleofection with Q25-mNeonGreen empty vector as a positive control and nucleofection without a DNA vector (No DNA) as a negative control.

2.3 Discussion and conclusions

In this chapter, I have demonstrated that five-gene polysistronic expression cassettes harbouring Oct4, Sox2, Klf4, Myc plus a fluorescent reporter are likely too large for use in PiggyBac and lentiviral delivery systems. Both systems failed to sufficiently transfect or transduce even the HEK293T cell line. This was also the case for the long polysistronic OSKM-mNeonGreen mRNA which failed to sufficiently transfect HEK293T cells. Reducing the mRNA to two separate three-gene polycistronic cassettes rendered HEK293T cells capable of being transfected only in the case of Oct4-Sox2-mNeonGreen mRNA (Q09), while the Klf4-Myc-mTagBFP2 mRNA (Q10) failed. This difference of successful versus failed transfection could be due to different secondary structures that form in the single-stranded mRNA preventing its successful translation. Transfection with mRNA is thought to be less toxic to HSCs than DNA (Papaioannou et al., 2023), but transfection with polycistronic mRNA molecules containing three or more genes has not been well studied. Here, I have shown that transfection success appears to be sequence dependent, whereby the three gene mRNA Oct4-Sox2-mNeonGreen can transfect HEK293T cells while Klf4-Myc-mTagBFP2 cannot.

In addition, nucleofection with a DNA plasmid harbouring a reduced size four-gene polycistronic cassette containing only Oct4, Sox2, Klf4 and reporter (Q23-OSK-mNeonGreen) successfully transfected HEK293T cells, but failed to transfect primary murine LSKs. HEK293T cells have an innate immune defect that makes them less susceptible to foreign DNA (Reus et al., 2020; Warga et al., 2023), while primary murine hematopoietic progenitors are known to activate apoptosis more easily (Levetzow et al., 2006; Li et al., 2001). In addition, HSPCs are smaller with different membrane potentials and are more sensitive to standard electroporation buffers (C. P. Zhang et al., 2023) and so are generally more difficult to transfect. The inability of the Q23-OSK-mNeonGreen to transfect primary LSKs could be due to either the size of the plasmid or the effect of the Oct4, Sox2 or Klf4 transcription factors on the viability of the cells.

All in all, smaller single-gene-plus-reporter mRNA strands with modified nucleotides may be the best candidate going forward and warrant more thorough testing. However, obtaining

dose-controllable expression with a mixture of multiple different mRNA molecules is challenging. Furthermore, staining of LT-HSCs and other hematopoietic progenitors requires a minimal 8 colour antibody panel, so including an additional three or four colours for reporting of mRNA translation would require careful redesign of the flow cytometry panel, or upgrading to a high-parameter spectral flow cytometry panel. Despite these challenges, *in vivo* delivery of cocktails of mRNA for reprogramming factors is conceivable. For example, in mice, mRNA can be packaged into lipid nanoparticles and the nanoparticles covalently coated with anti-c-Kit (CD117) antibodies to specifically target hematopoietic progenitors, even *in vivo* (Breda et al., 2023; Shi et al., 2023). Finding the optimal delivery method and the most favourable reprogramming factors for restoration of aged HSCs (and LSKs) is an ongoing challenge.

2.4 Methods

2.4.1 Plasmids for reprogramming

Primers were designed with homologous 5′ overhangs for HiFi DNA assembly using the NEBuilder HiFi DNA Assembly Master Mix (NEB, #E2621).

Table 2.2. Primers used for plasmid DNA vector and fragment amplification.

Primer name	Sequence, 5' to 3'	Length (nt)	Target
Q02_Vector.FOR	tcgctccttgagatctcccctctccctcc	29	PB-CT3G-CERP2-MG-IRES2-mNeonGreen (addgene, #175508)
Q02_Vector.REV	ccatggtggcaggctggatcggtccc	26	PB-CT3G-CERP2-MG-IRES2-mNeonGreen (addgene, #175508)
Q02_Fragment 1.FOR	ccagcctgccaccatggctggacacc	26	TetO-FUW-OSKM (addgene, #20321)
Q02_Fragment 1.REV	tgcctcattgggccgggattttcct	25	TetO-FUW-OSKM (addgene, #20321)

Primer name	Sequence, 5' to 3'	Length (nt)	Target
Q02_Fragment 2.FOR	cggcccaatgaggcagccacct	22	PB-TAC-OK+9MS (addgene, #80482)
Q02_Fragment 2.REV	gagatctcaaggagcgacaattttgagatcccct	34	PB-TAC-OK+9MS (addgene, #80482)
Q03_Vector.FOR	taagctgcaataaacaagttcctgcaggacaggcgc	36	pHAGE2-TetOminiCMV-Oct4-p2a-Sox2-17-t2a-Klf4 (addgene, #193345)
Q03_Vector.REV	atataggcaagcttatacgtctcgacccgggtaccg	36	pHAGE2-TetOminiCMV-Oct4-p2a-Sox2-17-t2a-Klf4 (addgene, #193345)
Q03_Fragment.FOR	agctcggtacccgggtcgagacgtataagcttgcctatataagcagag	48	Q02_PB-Ef1a-TetOn3G_mCMV-OSK+9M-mNeonGreen
Q03_Fragment.REV	gggcgcgcctgtcctgcaggaacttgtttattgcagcttataatggttacaaataagg	58	Q02_PB-Ef1a-TetOn3G_mCMV-OSK+9M-mNeonGreen
Q04_Vector.FOR	taagctgcaataaacaagttctggtacctttaagaccaatgacttacaagg	51	pHAGE2-TetOminiCMV-Oct4-p2a-Sox2-17-t2a-Klf4 (addgene, #193345)
Q04_Vector.REV	agatctcattcatagttcttaggatctatcgatttaaaagtgccttcttcatg	52	pHAGE2-TetOminiCMV-Oct4-p2a-Sox2-17-t2a-Klf4 (addgene, #193345)
Q04_Fragment.FOR	cttttaaatcgatagatcctaagaactatgaatgagatctccctctctcc	49	PB-CT3G-CERP2-MG-IRES2-mNeonGreen (addgene, #175508)
Q04_Fragment.REV	attggtcttaaaggtaccagaacttgtttattgcagcttataatggttacaaataagg	58	PB-CT3G-CERP2-MG-IRES2-mNeonGreen (addgene, #175508)
Q08_Vector.FOR	taagcggccgctttctccgcgcggccgctcgaggc	35	cleancap_p70 pGEMs_eGFP_4_UTR_IVaxT_Poly_A_148_CLEAN_CAP
Q08_Vector.REV	aggtgtccagccatggtggcggtgtcgaatggacgcgttattttgc	46	cleancap_p70 pGEMs_eGFP_4_UTR_IVaxT_Poly_A_148_CLEAN_CAP

Primer name	Sequence, 5' to 3'	Length (nt)	Target
Q08_Fragment.FOR	taacgcgtccattcgacaccgccaccatggctggacacc	39	Q02_PB-Ef1a-TetOn3G_mCMV-OSK+9M-mNeonGreen
Q08_Fragment.REV	agcgagcctcgagcggccgcgcggagaaagcggcc	35	Q02_PB-Ef1a-TetOn3G_mCMV-OSK+9M-mNeonGreen
Q09_Vector.FOR	tggacgaactctataagtaagcggccgctcgagg	34	cleancap_p70 pGEMs_eGFP_4_UTR_IVaxT_Poly_A_148_CLEAN_CAP
Q09_Vector.REV	aggtgtccagccatggtggcggtgtcgaatggacgcg	37	cleancap_p70 pGEMs_eGFP_4_UTR_IVaxT_Poly_A_148_CLEAN_CAP
Q09_Fragment 1.FOR	taacgcgtccattcgacaccgccaccatggctggacac	38	Q02_PB-Ef1a-TetOn3G_mCMV-OSK+9M-mNeonGreen
Q09_Fragment 1.REV	tcttcgcctttgctgaccattgggccgggattttcctccacgt	43	Q02_PB-Ef1a-TetOn3G_mCMV-OSK+9M-mNeonGreen
Q09_Fragment 2.FOR	tggaggaaaatcccggcccaatggtcagcaaaggcgaagaagataacatgg	51	PB-CT3G-CERP2-MG-IRES2-mNeonGreen (addgene, #175508)
Q09_Fragment 2.REV	agcgagcctcgagcggccgcttacttatagagttc	35	PB-CT3G-CERP2-MG-IRES2-mNeonGreen (addgene, #175508)
Q10_Vector.FOR	tcgggcacaaattgaactaagcggccgctcgagg	34	cleancap_p70 pGEMs_eGFP_4_UTR_IVaxT_Poly_A_148_CLEAN_CAP
Q10_Vector.REV	tcgccaggtggctgcctcatggtgtcgaatggacgcg	37	cleancap_p70 pGEMs_eGFP_4_UTR_IVaxT_Poly_A_148_CLEAN_CAP
Q10_Fragment 1.FOR	taacgcgtccattcgacaccatgaggcagccacctgg	37	PB-TAC-OK+9MS (addgene, #80482)
Q10_Fragment 1.REV	agcagagagaagtttgttgcaggagcgacaattttgagatcccct	45	PB-TAC-OK+9MS (addgene, #80482)

Primer name	Sequence, 5' to 3'	Length (nt)	Target
Q10_Fragment 2.FOR	atctcaaaattgtcgctcctgcaacaaacttctctctgctgaaac	45	pCF525-mTagBFP2_Ef1a-Hygro-P2A-mTagBFP2_lenti (addgene, #138315)
Q10_Fragment 2.REV	agcgagcctcgagcggccgcttagttcaatttgtgcccgagcttactcg	49	pCF525-mTagBFP2_Ef1a-Hygro-P2A-mTagBFP2_lenti (addgene, #138315)
Q23_Vector.FOR	ccctgctttttgcttgtactcccgggcgattaaggaaagg	40	pHAGE2_EF1a_TetOn_IRES_mCherry (addgene, #204155)
Q23_Vector.REV	accggagcctcacgactagtccacaggtaattggcagtggtaatagggta	50	pHAGE2_EF1a_TetOn_IRES_mCherry (addgene, #204155)
Q23_Fragment 1.FOR	ccactgccaattacctgtggactagtcgtgaggctccg	38	pHAGE2_EF1a_TetOn_IRES_mCherry (addgene, #204155)
Q23_Fragment 1.REV	aggtgtccagccatggtggcggcggccgcttcac	34	pHAGE2_EF1a_TetOn_IRES_mCherry (addgene, #204155)
Q23_Fragment 2.FOR	ggtgtcgtgaagcggccgccgccaccatggctgg	34	Q15_cleancap_p70pGEMs-OSK-mNeonGreen_polyA_148
Q23_Fragment 2.REV	ttgattaggatctatcgattttacttatagagttcgtccatgcccat	47	Q15_cleancap_p70pGEMs-OSK-mNeonGreen_polyA_148
Q23_Fragment 3.FOR	tggacgaactctataagtaaaatcgatagatcctaatcaacctctggattacaaaa	56	pHAGE2_EF1a_TetOn_IRES_mCherry (addgene, #204155)
Q23_Fragment 3.REV	cctttccttaatcgcccgggagtacaagcaaaaagcagggc	41	pHAGE2_EF1a_TetOn_IRES_mCherry (addgene, #204155)
Q25_Vector.FOR	tggacgaactctataagtaaaatcgatagatcctaatcaacctctggattacaaaa	56	pHAGE2_EF1a_TetOn_IRES_mCherry (addgene, #204155)

Primer name	Sequence, 5' to 3'	Length (nt)	Target
Q25_Vector.REV	tcttcgcctttgctgaccatggcggccgcttcac	34	pHAGE2_EF1a_TetOn_IRES_mCherry (addgene, #204155)
Q25_Fragment.FOR	ggtgtcgtgaagcggccgccatggtcagcaaaggcgaagaag	42	Q08_cleancap_p70pGEMs-OSK+9M-mNeonGreen_4_UTR_IVaxT_polyA_148
Q25_Fragment.REV	ttgattaggatctatcgattttacttatagagttcgtccatgcccat	47	Q08_cleancap_p70pGEMs-OSK+9M-mNeonGreen_4_UTR_IVaxT_polyA_148

2.4.1.1 PiggyBac plasmid design construction & cloning

The Q02 PiggyBac plasmid, Q02_PB-Ef1a-TetOn3G_mCMV-OSK+9M-mNeonGreen (12,639 bp), was generated by NEBuilder HiFi DNA Assembly (an improved Gibson assembly) from a PCR-linearized vector backbone and two PCR-amplified inserts (Fig. 2.1). The linearized vector backbone, 7,572 bp, was amplified from PB-CT3G-CERP2-MG-IRES2-mNeonGreen (addgene, #175508) using primers Q02_Vector.FOR and Q02_Vector.REV. Fragment 1, 2,181 bp, was amplified from TetO-FUW-OSKM (addgene, # 20321) using primers Q02_Fragment 1.FOR and Q02_Fragment 1.REV. Fragment 2, 2,935 bp, was amplified from PB-TAC-OK+9MS (addgene, #80482), which contains the necessary full length Klf4 (Kim et al., 2015), using primers Q02_Fragment 2.FOR and Q02_Fragment 2.REV. Primer sequences are listed in Table 1.

PCR amplification was performed using NEBNext Ultra II Q5 Master Mix (NEB, #M0544) in 50 µL reactions containing 25 µL 2× master mix, 2.5 µL of 10 µM forward primer, 2.5 µL of 10 µM reverse primer, template DNA, and nuclease-free water to volume. Thermocycling consisted of an initial denaturation at 98°C for 30 s, followed by 35 cycles of 98°C for 10 s, primer-specific annealing at the temperature recommended by the NEB Tm Calculator for 30 s, and extension at 72°C for 30 s per kb, with a final extension at 72°C for 5 min and hold at 12°C.

Assembly was performed using the NEBuilder HiFi DNA Assembly Master Mix (NEB, #E2621). Vector and insert DNA were combined at a molar ratio of 1:2, with a total DNA input of approximately 0.1 pmol, in a final reaction volume of 20 µL, according to the manufacturer's recommendations. Reactions were incubated at 50°C for 15 min and then placed on ice prior to transformation.

Transformation was carried out using the chemically competent *E. coli* cells supplied with the NEBuilder kit. Briefly, 2 µL of assembly reaction was added to thawed competent cells, incubated on ice for 30 min, heat shocked at 42°C for 30 s, and returned to ice for 2 min. SOC medium (950 µL) was then added and cells were recovered at 37°C for 60 min with shaking at 250 rpm. A 100 µL aliquot was plated onto pre-warmed selective agar plates and incubated overnight at 37°C.

Colonies were picked and expanded in S broth. Plasmid DNA was purified using the QIAprep Spin Miniprep Kit (Qiagen, #27106), quantified by NanoDrop on a DeNovix instrument, and screened by diagnostic restriction digest using HindIII and BspMI (Fig. 2.2).

In addition to Q02, a plasmid encoding the hyperactive piggyBac (hyPBase) transposase pCMV-hyPBase (Yusa et al., 2011) was obtained (a gift from Allan Bradley of the Wellcome Trust Sanger Institute, Cambridge CB10 1SA, United Kingdom) and used in conjunction with Q02 to transfect cells (see later Methods section "Nucleofection of HEK293T cells with PiggyBac vector").

2.4.1.2 Lentiviral plasmid design & cloning

Two lentiviral expression constructs, Q03_LV-pHAGE-TRE-OSK+9M-IRES2-mNeonGreen and Q04_LV-pHAGE2-TRE-OSox2-17K-IRES2-mNeonGreen, the 2nd of which expresses a modified Sox2 protein called Sox2-17 (MacCarthy et al., 2024), were generated by NEBuilder HiFi DNA Assembly from PCR-amplified backbone and insert fragments.

For Q03_LV-pHAGE-TRE-OSK+9M-IRES2-mNeonGreen (12,068 bp), a 5,452 bp linearized backbone was amplified from pHAGE2-TetOminiCMV-Oct4-p2a-Sox2-17-t2a-Klf4 (Addgene, #193345) using primers Q03_Vector.FOR and Q03_Vector.REV. This backbone retained the lentiviral vector elements including the truncated 5′ LTR, bacterial origin of replication, ampicillin resistance cassette, 3′ LTR, RRE, and HIV-1 packaging

signal. A 6,696 bp insert fragment was amplified from Q02_PB-Ef1a-TetOn3G_mCMV-OSK+9M-mNeonGreen using primers Q03_Fragment.FOR and Q03_Fragment.REV. This insert contained the reprogramming cassette comprising mPou5f1, Sox2, Klf4+9, Myc, IRES2, and mNeonGreen. The backbone and insert were joined by overlap assembly to generate the final Q03 lentiviral construct.

For Q04_LV-pHAGE2-TRE-OSox2-17K-IRES2-mNeonGreen (10,978 bp), a 9,548 bp linearized backbone was amplified from pHAGE2-TetOminiCMV-Oct4-p2a-Sox2-17-t2a-Klf4 (Addgene, #193345) using primers Q04_Vector.FOR and Q04_Vector.REV. This backbone retained the lentiviral backbone elements including the truncated 5′ LTR, ampicillin resistance cassette, origin of replication, 3′ LTR, RRE, WPRE, and the coding sequences for mPou5f1, Sox2-17, and mKlf4. A 1,510 bp fragment was amplified from PB-CT3G-CERP2-MG-IRES2-mNeonGreen (Addgene, #175508) using primers Q04_Fragment.FOR and Q04_Fragment.REV. This insert contained IRES2, mNeonGreen, and the SV40 poly(A) signal. These PCR products were assembled by overlap cloning to generate the final Q04 lentiviral construct, in which the engineered Sox2-17 sequence was retained as part of the reprogramming cassette.

PCR amplification was performed using NEBNext Ultra II Q5 Master Mix (NEB, #M0544) in 50 µL reactions containing 25 µL 2× master mix, 2.5 µL of 10 µM forward primer, 2.5 µL of 10 µM reverse primer, template DNA, and nuclease-free water to volume. Thermocycling consisted of an initial denaturation at 98°C for 30 s, followed by 35 cycles of 98°C for 10 s, primer-specific annealing at the temperature recommended by the NEB Tm Calculator for 10 to 30 s, and extension at 72°C for 30 s per kb, with a final extension at 72°C for 2 min.

Assembly reactions were performed using NEBuilder HiFi DNA Assembly Master Mix (NEB, #E2621) according to the manufacturer's instructions. Vector and insert fragments were combined in a final reaction volume of 20 µL and incubated at 50°C for 15 min. Reactions were then placed on ice before transformation.

Transformation was performed using the chemically competent *E. coli* cells supplied with the NEBuilder kit. Briefly, 2 µL of assembly reaction was added to competent cells, incubated on ice for 30 min, heat shocked at 42°C for 30 s, and returned to ice for 2 min. SOC medium (950 µL) was then added and cells were recovered at 37°C for 60 min with

shaking at 250 rpm. Cells were plated onto selective agar plates and incubated overnight at 37°C.

Picked colonies were expanded in S broth, plasmid DNA was purified using the QIAprep Spin Miniprep Kit (Qiagen, #27106), and DNA concentration was measured on a DeNovix NanoDrop instrument. Sequences were confirmed by Nanopore longread sequencing.

2.4.1.3 pT7 mRNA plasmid design & cloning

Three plasmid DNA templates for in vitro transcription, Q08_cleancap_pT7-OSKM-mNeonGreen_polyA_148, Q09_cleancap_pT7-OS-mNeonGreen_polyA_148, and Q10_cleancap_pT7-KM-mTagBFP2_polyA_148, were assembled for use with the HiScribe T7 mRNA Kit with CleanCap Reagent AG (NEB #E2080). In all three constructs, a 3062 bp backbone was PCR amplified from cleancap_p70 pGEMs_eGFP_4_UTR_IVaxT_Poly_A_148_CLEAN_CAP. This backbone provided the CleanCap-compatible T7 promoter, the 5′ UTR, and the 148 bp poly(A) sequence, while the original eGFP coding region was replaced by the coding sequences of interest through NEBuilder HiFi DNA Assembly (Figs 8, 9 & 10).

For Q08 (Fig. 2.8), a single 6448 bp insert amplified from Q02_PB-Ef1a-TetOn3G_mCMV-OSK+9M-mNeonGreen was assembled into the backbone. This insert contained the coding sequence for Oct4, Sox2, Klf4+9, and Myc, together with the linked expression architecture present in the donor plasmid, followed by IRES2 and mNeonGreen, thereby generating an OSKM-mNeonGreen IVT template. For Q09 (Fig. 2.11), two inserts were assembled into the same backbone, a 2206 bp fragment from Q02_PB-Ef1a-TetOn3G_mCMV-OSK+9M-mNeonGreen containing Oct4 and Sox2 with the associated P2A and T2A junctions, and a 751 bp fragment from PB-CT3G-CERP2-MG-IRES2-mNeonGreen (addgene, #175508), containing mNeonGreen, generating an OS-mNeonGreen IVT template. For Q10 (Fig. 2.12), two inserts were assembled into the same backbone, a 2959 bp fragment from PB-TAC-OK+9MS (addgene, #80482), containing Klf4+9 and Myc with the E2A junction, and a 790 bp fragment from pCF525-mTagBFP2_Ef1a-Hygro-P2A-mTagBFP2_lenti, (addgene, #138315), containing P2A-mTagBFP2, generating a KM-mTagBFP2 IVT template.

PCR amplification of vector backbones and inserts was performed with NEBNext Ultra II Q5 Master Mix (NEB #M0544), in 50 µL reactions containing 25 µL master mix, 2.5 µL of 10 µM forward primer, 2.5 µL of 10 µM reverse primer, template DNA, and nuclease-free water to volume. Thermocycling conditions were 98°C for 30 s, followed by 35 cycles of 98°C for 10 s, primer-specific annealing at 50 to 72°C for 10 to 30 s, with annealing temperature selected using the NEB Tm Calculator, and extension at 72°C for 30 s per kb based on the longest expected amplicon, followed by 72°C for 5 min and hold at 12°C. Primer sequences are listed in Table 1.

HiFi assembly reactions were prepared using NEBuilder HiFi DNA Assembly Master Mix (NEB #E2621), with the recommended vector:insert molar ratios and a total vector plus insert amount of approximately 0.1 pmol. Reactions were incubated at 50°C for 15 min, then kept on ice before transformation. Chemically competent *E. coli* supplied with the NEBuilder kit were transformed with 2 µL of assembly reaction by heat shock, incubated on ice for 30 min, heat shocked at 42°C for 30 s, returned to ice for 2 min, recovered in 950 µL SOC medium at 37°C for 60 min with shaking at 250 rpm, and plated by spreading 100 µL of the culture onto selection plates followed by overnight incubation at 37°C. Colonies were picked, expanded in S broth, and plasmid DNA was purified using the QIAprep Spin Miniprep Kit (QIAGEN #27106). DNA concentration was measured on a DeNovix spectrophotometer, and final plasmid sequences were confirmed by Nanopore long-read sequencing.

2.4.1.4 DNA plasmid design & cloning

To test whether DNA plasmid delivery would result in robust but transient expression of Yamanaka factor cassettes, two plasmids were assembled by NEBuilder HiFi DNA Assembly. Firstly, Q23_Ef1a-OSK-mNeonGreen-WPRE was designed as an EF-1α-driven OSK reporter plasmid and was assembled from four PCR products. A 2593 bp vector backbone fragment amplified from pHAGE2_EF1a_TetOn_IRES_mCherry (addgene, #204155) provided the bacterial propagation elements, including the AmpR promoter, AmpR, origin of replication, lac promoter and M13 reverse priming region. A 1240 bp fragment from the same plasmid provided the EF-1α promoter. A 4468 bp insert amplified from Q15_cleancap_p70pGEMs-OSK-mNeonGreen_polyA_148 provided the coding cassette containing Oct4, Sox2, Klf4 and mNeonGreen genes separated by P2A sequences.

A 790 bp fragment from pHAGE2_EF1a_TetOn_IRES_mCherry provided the WPRE sequence. Together, these fragments generated a plasmid in which the EF-1α promoter drives OSK and mNeonGreen expression, with WPRE positioned downstream of the expression cassette.

Q25_Ef1a-mNeonGreen-WPRE was generated as an EF-1α-driven mNeonGreen positive control. This plasmid was assembled from a 7024 bp vector fragment amplified from pHAGE2_EF1a_TetOn_IRES_mCherry (addgene, #204155) and a 751 bp mNeonGreen fragment amplified from Q08_cleancap_p70pGEMs-OSK+9M-mNeonGreen_4_UTR_IVaxT_polyA_148.

Vector backbones and inserts were amplified using NEBNext Ultra II Q5 Master Mix (NEB #M0544) in 50 µL reactions containing 25 µL master mix, 2.5 µL of 10 µM forward primer, 2.5 µL of 10 µM reverse primer, template DNA, and nuclease-free water to volume. Thermocycling conditions were 98°C for 30 s, followed by 35 cycles of 98°C for 10 s, primer-specific annealing at 50 to 72°C for 10 to 30 s, with annealing temperature selected using the NEB Tm Calculator, and extension at 72°C for 30 s per kb based on the longest expected amplicon, followed by 72°C for 2 min and hold at 4 to 10°C. Primer sequences are listed in Table 1.

HiFi assembly reactions were prepared using NEBuilder HiFi DNA Assembly Master Mix (NEB #E2621) using the recommended vector:insert molar ratios a total vector plus insert amount of approximately 0.1 pmol. Reactions were incubated at 50°C for 15 min, then kept on ice or stored at −20°C before transformation. Chemically competent *E. coli* supplied with the NEBuilder kit were transformed with 2 µL of assembly reaction by heat shock, incubated on ice for 30 min, heat shocked at 42°C for 30 s, returned to ice for 2 min, recovered in 950 µL SOC medium at 37°C for 60 min with shaking at 250 rpm, and plated by spreading 100 µL of the culture onto selection plates followed by overnight incubation at 37°C. Colonies were picked, expanded in S broth, and plasmid DNA was purified using the QIAprep Spin Miniprep Kit (QIAGEN #27106). DNA concentration was measured on a DeNovix spectrophotometer, and final plasmid sequences were confirmed by Nanopore long-read sequencing.

2.4.2 Nucleofection of HEK293T cells and primary murine bone marrow cells

In all cases, nucleofection of HEK293T cells was performed using the 4D-Nucleofector system with 20 µL nucleocuvettes and SF Cell Line reagents for HEK293T cells. For each reaction, nucleofection solution was prepared by mixing 16.4 µL SF solution with 3.6 µL Supplement 1. Cells were counted, washed once in PBS, pelleted at 90 × g for 10 min at room temperature, and resuspended at 200,000 cells per 20 µL of nucleofection solution per well. HEK293T cells were nucleofected using program CM-130.

2.4.2.1 Nucleofection with PiggyBac vectors

For PiggyBac-based nucleofection of HEK293T cells, samples received pCMV-hyPBase together with either Q02_PB-Ef1a-TetOn3G_mCMV-OSK+9M-mNeonGreen or PB-CT3G-CERP2-MG-IRES2-mNeonGreen at a 1:5 HyPBase:vector mass ratio, with a total DNA input of 1.0 µg per well, comprising 0.20 µg HyPBase and 0.80 µg vector. A positive control received 0.4 µg pMaxGFP and a no-DNA control was included. Following nucleofection, 80 µL pre-warmed medium was added, cells were gently resuspended, incubated at 37°C for 10 min, and then transferred to 120 µL pre-warmed DMEM supplemented with 10% FCS for a final volume of 200 µL. Cells were cultured for 24 hours and then treated with doxycycline at a final concentration of 2 µg/mL by adding 2 µL of a 100× working solution to each well. Cells were analysed by flow cytometry 48 h after nucleofection (24 hours after addition of doxycycline).

2.4.2.2 Nucleofection with mRNA vectors

For mRNA nucleofection of HEK293T cells, 200,000 cells per well were nucleofected with *in vitro* transcribed mRNA products Q08_OSKM-mNeonGreen at 1, 3, or 5 µg, Q09_OS-mNeonGreen at 3 or 5 µg, or Q10_KM-mTagBFP2 at 2, 4, or 8 µg. Reporter expression was assessed by flow cytometry 24 h after nucleofection.

2.4.2.3 Nucleofection with DNA vectors

In separate DNA plasmid nucleofection experiments, HEK293T cells were nucleofected with 1 µg of either Q23_Ef1a-OSK-mNeonGreen-WPRE or Q25_Ef1a-mNeonGreen-WPRE. Lineage-depleted murine bone marrow cells were also nucleofected with DNA plasmids to assess delivery into primary LSKs and LT-HSCs. Q23_Ef1a-OSK-mNeonGreen-WPRE was tested at 1 µg per reaction using the programs DS-113, DS-112, CG-104, DN-107, EH-100, DN-100, and EO-100. Q25_Ef1a-mNeonGreen-WPRE was used as a positive

control and no-DNA samples were used as negative controls, both controls using the program EH-100. Cells were analysed by flow cytometry 24 h after nucleofection to assess reporter expression and viability.

The three best-performing programs from the lineage-depleted bone marrow experiment, based on a balance of cell viability and transfection of LT-HSCs, were EH-100, DN-107, and EO-100. These were subsequently tested in flow cytometry-sorted murine LSK cells together with CG-104 and DS-113, which were included because they had been reported among the best-performing programs in the literature for HSCs (Wang et al., 2021). Cells were analysed by flow cytometry 24 h after nucleofection.

2.4.3 Lentiviral production and transduction (spin infection) of sorted LSKs

Lentiviral particles encoding Q03_LV-pHAGE-TRE-OSK+9M-IRES2-mNeonGreen or Q04_LV-pHAGE2-TRE-OSox2-17K-IRES2-mNeonGreen were produced in HEK293T packaging cells using Lipofectamine 3000 transfection. HEK293T cells were seeded in 10 cm culture plates at 6×10^5 cells/ml, 10 mL per plate, in packaging medium consisting of Opti-MEM I with GlutaMAX, 1 mM sodium pyruvate, and 5% FBS. The following day, plasmid transfection complexes were prepared in two tubes. Tube 1 contained 1.25 mL Opti-MEM I and 35 µL Lipofectamine 3000. Tube 2 contained 1.25 mL Opti-MEM I, the transfer plasmids Q03-TRE-OSKM-mNeonGreen or Q04-TRE-OS2-17K-mNeonGreen, psPAX2 packaging plasmid, and pCMV-VSV-g envelope plasmid at a 1.35:1:1 molar ratio, plus 30 µL P3000 reagent. Tube 1 was added to Tube 2, mixed, and incubated for 20 min at room temperature. 5 mL of medium was removed from each plate and transfection mixture was added dropwise per well. Cells were incubated for 6 h at 37°C, 5% CO2, after which the medium was removed and replaced with 10 mL fresh packaging medium per well. Viral supernatant was collected at 24 h post-transfection, media replaced, then supernatant was collected again at 48 h, giving a total of 20 mL unconcentrated virus. Combined supernatant was centrifuged at 2,000 rpm for 10 min, filtered through a 0.45 µm filter, and then concentrated to 2 mL using Amicon Ultra centrifugal filters, 100 kDa MWCO, 15 mL capacity (Sigma-Aldrich, UFC9100). Virus was then aliquoted and stored at −80°C.

To assess lentiviral transduction efficiency in HEK293T cells, a spin infection assay was performed. Cells were seeded at 5×10^5 cells per well in 12-well plates and incubated

overnight. The following day, medium was removed and wells were supplemented with the indicated volume of viral supernatant together with 0.8 µL polybrene from a 10 mg/ml stock, corresponding to a final concentration of 8 µg/ml, and topped up to 1 mL total volume with culture medium. Plates were centrifuged at 2,500 rpm for 90 min at 32°C, then returned to 37°C. At 24 h post-infection, medium was replaced with 500 µL fresh culture medium lacking polybrene. At 48 h post-infection, cells were washed twice with 500 µL PBS, dissociated with 250 µL trypsin for 5 min at 37°C, quenched with 0.75 mL DMEM containing 10% FCS, and transferred to tubes. Residual cells were recovered with 1 mL PBS, pooled, pelleted, and resuspended in 250 µL FACS buffer. Propidium iodide was added and transduction efficiency was assessed by flow cytometry using non-transduced cells as the negative gating control.

For transduction of primary hematopoietic stem and progenitor cells, 2×10^5 murine LSK cells were used per sample. Retronectin-assisted spin infection was used to improve lentiviral delivery to sorted LSK cells as follows. Wells of a 12 well plate were first coated with 1 mL retronectin at 32 µg/ml and incubated for 2 h at 37°C. The retronectin solution was then removed, wells washed with PBS, then different volumes (50 µL, 100 µL or 150 µL) of Q03-TRE-OSKM-mNeonGreen & Tet-On-3G-mCherry or Q04-TRE-OS2-17K-mNeonGreen & Tet-On-3G-mCherry of concentrated lentiviruses (or controls) were combined, topped up to 500 µL with PVA-based F12 media (see the Cell culture section of Methods) then added to the appropriate retronectin coated wells. The plate was centrifuged at 2000 x g for 1 hour at 32℃ to adhere the viral particles to the retronectin. Next, for each well 2×10^5 murine LSK cells were pelleted and resuspended in 500 µL pre-warmed PVA-based F12 media which was then added directly to the coated wells containing viral particles for a total volume of 1 mL per well. The plate was then centrifuged at 1500 rpm for a further 1 hour at 32℃ then the plate was placed in 5% CO_2 at 37℃ overnight. The next day the media was replaced with fresh pre-warmed PVA-based F12 media. While the treatment samples received Q03 + Tet-On-3G or Q04 + Tet-On-3G lentiviruses, the negative control well received no virus, and the positive control well received GFP lentivirus that had been produced previously in the lab, which contained a GFP reporter under the control of an Ef1a promotor. To activate expression of the Q03 and Q04 cassettes, doxycycline (2µg/mL) was added 48 hours after

transduction in fresh pre-warmed PVA-based F12 media. Transduction efficiency was assesssed by FACs analysis 48 hours after doxycycline administration.

2.4.4 In vitro transcription

Plasmid DNA templates for in vitro transcription (Q08, Q09 and Q10) were first linearized with SapI (NEB #R0569), downstream of the transcription unit to generate run-off templates containing the CleanCap-compatible T7 promoter, the required AG initiation sequence, the coding region of interest, and the encoded 148 bp poly(A) tail. Linearized plasmids were then used as templates for co-transcriptional capping with the HiScribe T7 mRNA Kit with CleanCap Reagent AG (NEB #E2080), following the manufacturer's framework for 20 µL reactions, with modified nucleotide substitution. The kit is designed for linear templates containing a T7 promoter followed by an AG initiation sequence, and standard 20 µL reactions include 10X reaction buffer, ATP, GTP, CleanCap Reagent AG, template DNA and T7 RNA polymerase mix, with modified nucleotides optionally substituted for standard NTPs.

Each 20 µL transcription reaction contained 2 µL 10X T7 CleanCap Reagent AG Reaction Buffer, 2 µL ATP (60 mM), 2 µL GTP (50 mM), 1 µL Pseudo-UTP (100 mM, Jena Bioscience NU-1139S), 1 µL 5-Methyl-CTP (100 mM, Jena Bioscience NU-1138S), 2 µL CleanCap Reagent AG (40 mM), 2 µL T7 RNA Polymerase Mix, 1 µg linearized plasmid DNA template, and nuclease-free water to 20 µL total volume. These reagent volumes gave final concentrations of 6 mM ATP, 5 mM GTP, 5 mM Pseudo-UTP, 5 mM 5-Methyl-CTP, and 4 mM CleanCap Reagent AG. Reactions were assembled in nuclease-free tubes, mixed, pulse-spun, and incubated at 37°C for 2 h in a thermocycler with heated lid.

RNA was purified using the Monarch RNA Cleanup Kit (NEB #T2040). After transcription, 30 µL nuclease-free water was added to each 20 µL reaction to give a final volume of 50 µL. Then, 100 µL RNA Cleanup Binding Buffer was added followed by 150 µL ethanol and the sample was mixed by gentle pipetting. The mixture was applied to the cleanup column and centrifuged at 16,000 × g for 1 min at room temperature. The column was washed twice with 500 µL RNA Cleanup Wash Buffer, with centrifugation at 16,000 × g for 1 min after each wash. The column was then transferred to an RNase-free 1.5 mL tube

and RNA was eluted in 20 µL nuclease-free water. Purified RNA was stored at −80°C until use.

2.4.5 Cell culture

HEK293 T cells were cultured in DMEM with 10% FBS until confluent, then detached from T75 flasks by incubating with 0.5% w/v trypsin (Sigma Aldrich, # T4174) for 5 mins before washing and replating at the appropriate cell density for each experiment.

Primary lineage depleted murine bone marrow cells and sorted murine lineage negative, Sca-1 positive, c-Kit positive (LSK) cells were cultured in an the albumin-free polyvinyl alcohol (PVA)-based F12 media reported to maintain LT-HSC cells (Wilkinson et al., 2020). The protocol, as detailed by Wilkinson et al., involves dissolving the PVA in a 10% w/v stock before final formulation. The media consists of a base of Ham's F12 with 1 mg/mL (0.1% w/v) PVA (87–90% hydrolyzed), 10 mM HEPES (Thermofisher, #15630080), 1X ITS-X (Thermofisher, #51500056), 1X glutamax (Thermofisher, #35050061), 100 U/mL penicillin, 100 µg/mL streptomycin, 100 ng/mL mTPO (Peprotech) and 10 ng/mL mSCF (Peprotech). All cells were incubated in 5% CO_2 at 37°C.

2.4.6 Flow cytometry

Bone marrow (BM) was extracted from the femur, tibia and pelvic bones of adult female C57BL/6 mice, whereby bones were crushed with mortar and pestle in PBS with 2% FBS (FACS buffer) and BM cells filtered through a 45 µm filter. Filtered bone marrow cells were then incubated with RCRB for 1 minute to remove red blood cells, pelleted at 1500 rpm, washed with FACS buffer, then lineage positive cells were depleted using the EasySep™ Mouse Hematopoietic Progenitor Isolation Kit (Stem Cell Technologies #19856) according to the manufacturer's instructions. Thes lineage depleted BM cells were used in screens for optimal nucleofection programs (see Table 1 and Fig. 2.16).

For sorting of LSKs, the lineage-depleted BM cells cells were stained with:
Sca1-BUV395 (Ms Ly-6A/E BUV395 D7 Becton Dickinson #563990),
c-Kit-BV711 (Ms CD117 BV711 2B8 Becton Dickinson #563160),
Lineage-biotin (Miltenyi Biotec Australia Pty. Ltd. #130-092-613).

Cells were incubated with antibodies for 30mins on ice, before washing and staining with Streptavidin-BV650 (SAV BV650, Becton Dickinson #563855) for a further 15 mins. Cells were then washed and incubated with the sytox blue viability stain for 30 mins on ice. Finally, cells were washed then subjected to flow cytometry based analysis.

For assessing transduction/transfection efficiency, lentiviral transduced LSKs or nucelofected LSKs were pelletted, then resuspended in an antibody master mix which included:

CD34-BV421 (Brilliant Violet 421™ anti-mouse CD34, BioLegend #152208),

Flt3-APC (Ms CD135 APC A2F10.1, Becton Dickinson #560718),

Sca1-BUV395 (Ms Ly-6A/E BUV395 D7 Becton Dickinson #563990),

c-Kit-BV711 (Ms CD117 BV711 2B8 Becton Dickinson #563160),

CD150-PE-Cy7 (PE/Cyanine7 anti-mouse CD150, TC15-12F12.2, BioLegend #115914),

CD48-APC-Cy7 (APC/Cyanine7 anti-mouse CD150, HM48-1, BioLegend #103432),

Lineage-biotin (Miltenyi Biotec Australia Pty. Ltd. #130-092-613).

Cells were incubated with antibodies for 30mins on ice, before washing and staining with Streptavidin-BV650 (SAV BV650, Becton Dickinson #563855) for a further 15 mins. Cells were then washed and incubated with the Sytox blue (Thermo fisher #S34857) viability stain for 30 mins on ice. Finally, cells were washed then subjected to flow cytometry based analysis.

Chapter 3: *In Situ* Hi-C benefits from extended crosslinking with a double fixation method prior to DNA digestion

3.1 Introduction

Chromatin conformation capture experiments such as *in situ* Hi-C start with a fixation step to crosslink proteins and DNA, followed by cell lysis, DNA digestion with a restriction enzyme of choice, proximity ligation to covalently ligate together pieces of digested DNA that are in close proximity, crosslink reversal by heating, then purification and sequencing of the chimeric DNA fragments (Johanson & Allan, 2022). The fixation step during the *in situ* Hi-C protocol is traditionally achieved with formaldehyde (FA) (Diaz et al., 2018; Johanson & Allan, 2022; Rao et al., 2014), which forms a methylene bridge (-CH2-) between amino groups on protein amino acid residues, most often lysine residues (Lu et al., 2010), or between amino acid residues and amino groups on DNA bases (Hoffman et al., 2015; Lu et al., 2010). FA is small, can penetrate cell membranes and, due to its size and chemical nature, only links molecules that are in direct contact or in extremely close proximity (Hoffman et al., 2015). In addition, the propensity for positively charged lysine residues to be in close proximity to negatively charged DNA means that FA preferentially forms crosslinks between the proteins and DNA, primarily the nucleotide deoxyguanisine (Lu et al., 2010). Importantly, FA mediated crosslinks are also reversible upon heating to 65 ℃ so that DNA can be sheared and sequenced (Hoffman et al., 2015).

Disuccinimidyl glutarate (DSG) is another fixation chemical sometimes used in ChIP-seq (Bao et al., 2025; Tian et al., 2012) and chromatin conformation capture experiments such as Hi-C 3.0 (Akgol Oksuz et al., 2021; Lafontaine et al., 2021), micro-C (Ahmed et al., 2024; Hsieh et al., 2016; D. Li et al., 2023) and Omni-C (Ahmed et al., 2024). Unlike FA, which preferentially crosslinks protein residues to DNA bases, DSG is almost exclusively a protein-protein crosslinker and is irreversible (Bao et al., 2025; Tian et al., 2012). DSG is larger and forms two amide bonds separated by a large 5 carbon linker (Bao et al., 2025; Tian et al., 2012). It has previously been shown that double fixation with FA then DSG reduces genomic-mitochondrial contacts (i.e. mitochondrial contamination) and spurious trans-chromosomal

interactions and improves resolution of finer detail contacts (Akgol Oksuz et al., 2021; Lafontaine et al., 2021).

The choice of DNA digestion enzyme after fixation also affects Hi-C resolution. For example, the restriction enzyme HindIII, which recognizes AAGCTT and gives an average fragment length of ~4 kbp (Lieberman-Aiden et al., 2009), while MboI & DpnII, both of which recognize the same GATC sequence, gives an average length of ~500 bp (Rao et al., 2014). DdeI, which recognizes the sequence CTNAG also gives an average length of ~500 bp and has been used in conjunction with DpnII for dual cutting (Akgol Oksuz et al., 2021). Micrococcal nuclease, which is sequence independent but is sterically hindered by nucleosomes generally cuts DNA into smaller fragments depending on the incubation time (Hsieh et al., 2016). Notably, the Hi-C 2.0 protocol published in 2017 stated that they "prefer the use of DpnII for eukaryotes, because unlike MboI it is insensitive to CpG methylation" (Belaghzal et al., 2017). However, there is no reference given for MboI sensitivity to CpG methylation and the preference for DpnII over MboI has been carried over into the Hi-C 3.0 protocol despite this lack of evidence. MboI is 280 amino acids long while DpnII is 288 amino acids and each have slightly different structures and active sites. Despite recognizing the same site, DpnII and MboI could conceivably be differently affected by the endogenous protein network and 3 dimensional mesh created by crosslinking. The Allan lab at WEHI uses MboI for *in situ* Hi-C (Johanson & Allan, 2022; Johanson et al., 2018; Keenan et al., 2020) as have many other labs (Feng et al., 2022; Rao et al., 2014; Tomas-Daza et al., 2023) leading to many published findings. However, the question of whether differences in sensitivity between MboI and DpnII results in major differences in contact mapping remains to be answered.

This chapter describes the optimization of the *in situ* Hi-C protocol and is inspired by the experimental results by Akgol Oksuz et al. (2021) in which DSG is applied as a 2nd fixation step (Akgol Oksuz et al., 2021), but also by the open question regarding the choice of DpnII over MboI. The experiments described here seek to explore whether FA followed by DSG double fixation would improve results in a low-input setting (< 500 k cells) and whether there is a difference between using DpnII versus MboI.

3.2 Results

3.2.1 Double fixation shifts library composition toward shorter-range cis contacts and reduces trans-associated signal

To examine whether FA followed by DSG double fixation would improve results in a low-input setting and whether the choice of DpnII or MboI would affect the resulting contact maps, we performed *in situ* Hi-C on ~200,000 murine $B220^{+}$ splenocytes (B cells) using four different Hi-C experimental protocols, as follows:

Group 1: FA + MboI

Group 2: FA + DSG + MboI

Group 3: FA + DpnII

Group 4: FA + DSG + DpnII

Valid reads were calculated as mapped reads minus dangling ends and self-circles. Unfortunately, the number and proportion of valid reads was quite variable and the proportion unmapped reads was quite high (Fig. 3.1A), the latter likely due to either problems during the size selection step leading to sequencing adapter/short fragment contamination, or low quality base calling during sequencing. As is shown in the dot plot of the median length of duplicate free reads (Fig. 3.1B), double fixation with FA followed by DSG consistently gave smaller median fragment length, regardless of restriction enzyme used, indicating either that more efficient DNA digestion could be occurring after double fixation, or that the smaller library size (and lower library complexity) of both Rep 2 FA + DSG samples (Fig. 3.1A) led to biased PCR amplification of shorter fragments.

To determine whether the differences between Hi-C protocols resulted in differences in overall interaction frequencies, interaction distance decay curves of the deduplicated mapped reads were plotted. Comparison of the interaction distance decay plots by replicate revealed that most libraries showed broadly similar profiles (Fig. 3.1C), although replicate 1 of FA + DpnII seems to be an outlier having less interactions across all distances (Fig. 3.1D), likely due to the large amount of dangling end reads (see Fig. 3.1A). Despite this, double fixation

with FA followed by DSG, particularly if we compare replicate 2 decay curves, shows a consistently higher proportion of interactions across spans of 10^3 - 10^5 bp (Fig. 3.1E).

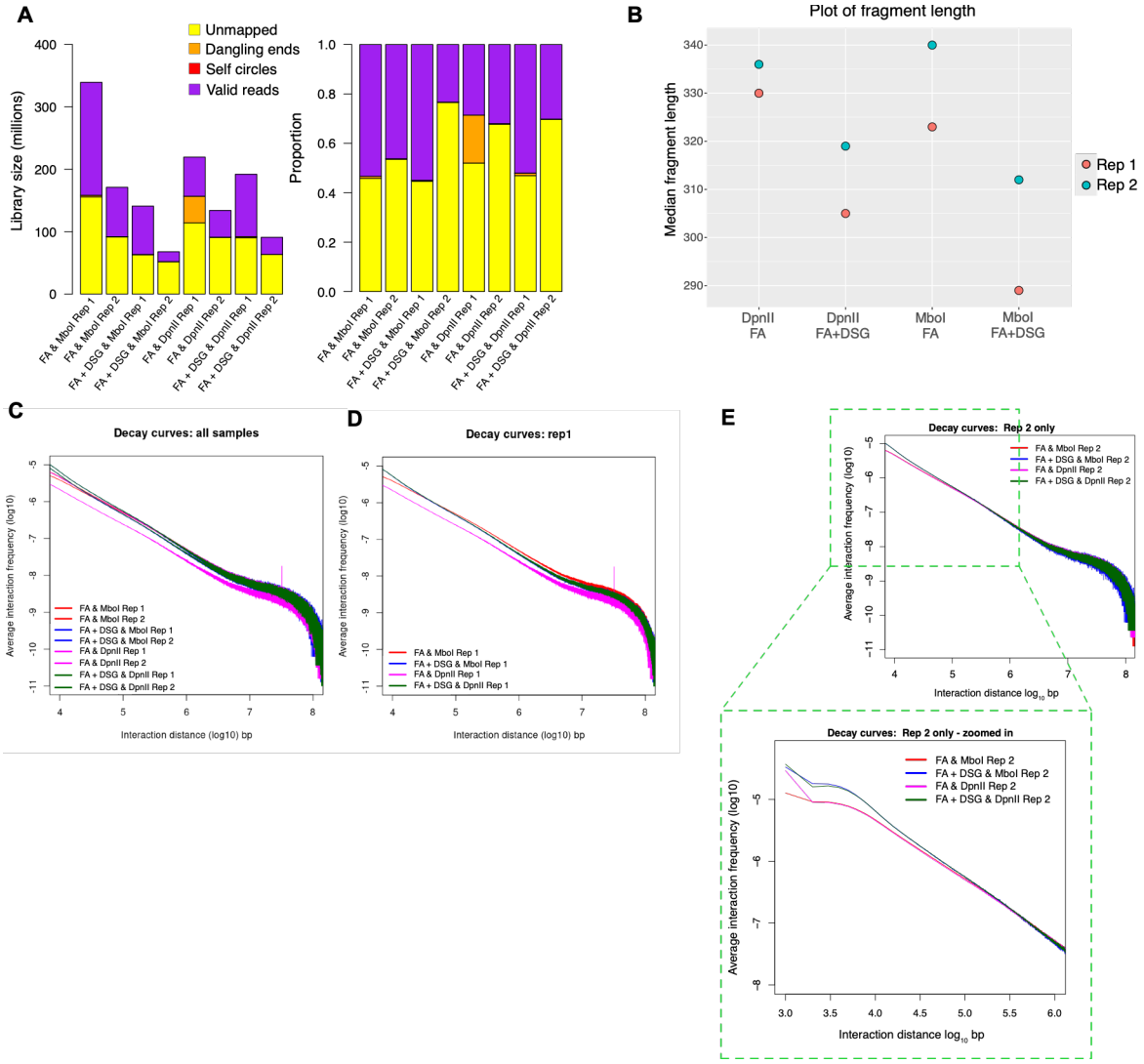


Figure 3.1. Library yield, detection of short-range interactions and trans-chromosomal interactions differ across fixation and enzyme conditions. A, Library size and proportion showing unmapped reads, dangling ends and valid reads obtained for each library; B, Median raw fragment length for the replicates of each library; C, Interaction distance decay plots of the deduplicated mapped reads for all libraries; D, Interaction distance decay plots of the deduplicated mapped reads for replicate 1 (Rep 1) libraries showing the FA + DpnII Rep 1 library outlier (pink curve) which has a broad-range drop in the average interaction frequency detected; E, Interaction distance decay plots for replicate 2 (Rep 2) with pop-out zoomed in view showing that addition of DSG (blue and green curves) leads to consistently higher proportions of interactions across spans of 10^3 - 10^5 bp.

Looking at the median proportion of cis-interactions spanning either 0-1 kbp (Fig. 3.2A), 1-10 kbps (Fig. 3.2B), >10 kbp (Fig. 3.2C), or the proportion of trans-chromosomal interactions (Fig. 3.2D) shows that addition of DSG to FA fixation was associated with a higher proportion of cis interactions in the 1-10 kbp range (Fig. 3.2B) and perhaps a lower proportion of trans interactions for both enzyme backgrounds (Fig. 3.2D), although this is more variable. While trans-chromosomal interactions are biologically real, a high proportion can indicate increased non-biologically relevant proximity ligation events due to excess crosslinking. Furthermore, there is no evidence that genomic nuclear DNA normally interacts with mitochondrial DNA, but contamination of nuclear DNA with mitochondrial DNA can occur during the fixation and proximity ligation steps of Hi-C. In our results, the ratio of trans-mitochondrial reads (reads that map to nuclear DNA and mitochondrial DNA) to cis-mitochondrial reads is consistently reduced with FA + DSG fixation regardless of which restriction enzyme was used, suggesting double fixation also reduces mitochondrial contamination (Fig. 3.2E).

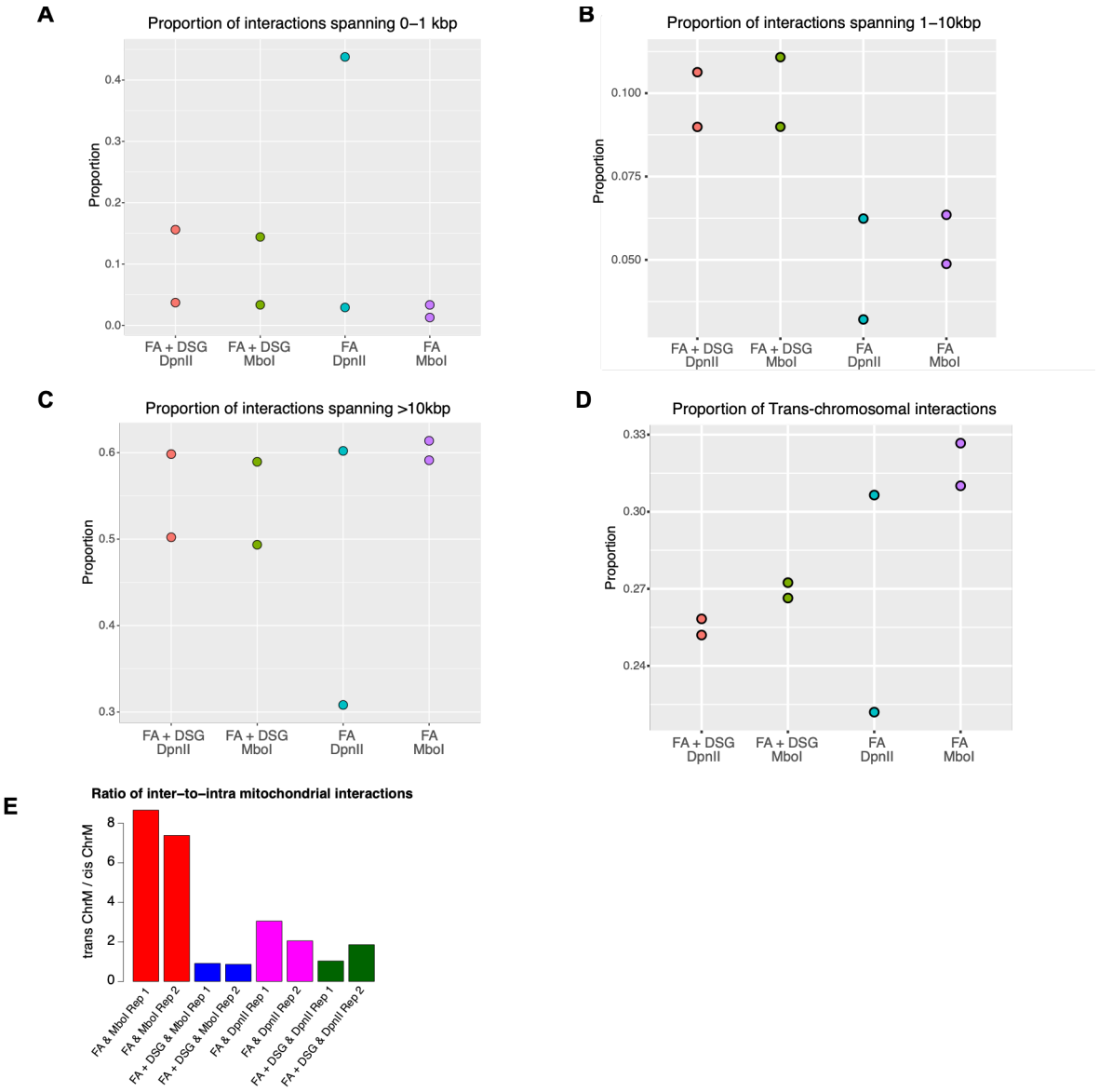


Figure 3.2. Double fixation reduces trans-associated signal and enriches short-range cis contacts. A, Scatter plot summarizing the proportions of cis interactions in the 0-1 kb range; B, Scatter plot summarizing the proportion cis interactions in the 1-10 kb rang; C, Scatter plot summarizing the proportion cis interactions in the >10 kb range; D, Scatter plot summarizing the proportion trans-chromosomal interactions; E, Bar plot showing the ratio of inter- to intra-mitochondrial interactions for each library, used as an additional library-quality metric. Collectively, the panels show that additional DSG crosslinking reduced trans-associated signal, increased the proportion of 1-10 kb cis interactions and reduced mitochondrial contamination, particularly in the cases where MboI digestion was used.

3.2.2 Differential contact analysis reveals scale-dependent protocol effects

To test whether the different protocols altered the resulting chromatin contact maps beyond library-level quality metrics, differential interactions (DIs) were quantified at 100 kb and 2 Mb resolution on quality filtered. At 100 kb resolution there were minimal differences between the libraries; however, the largest local differences were observed in the comparison FA + DpnII vs FA + MboI (Fig. 3.3A), suggesting the two restriction enzymes do likely cut the DNA differently resulting in differences in the detected interactions. Additionally, use of FA + DpnII vs FA + MboI comparison shows more trans-chromosomal interactions being detected when DpnII is used (Fig. 3.3A). Interestingly, the addition of DSG may equalize the ability of the two enzymes to digest the DNA since comparison of the two enzymes in the context of double fixation (FA + DSG + DpnII vs FA + DSG + MboI) showed no significant differences in interactions (Fig. 3.3A).

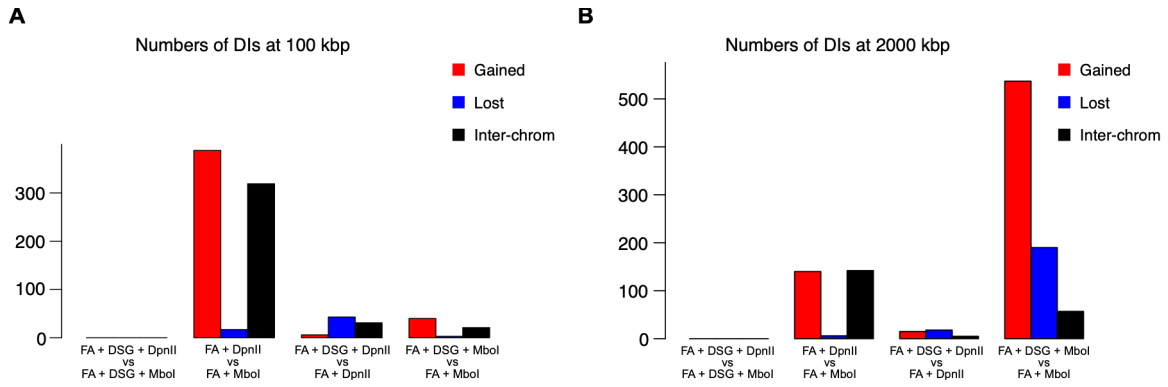


Figure 3.3. Differential interaction analysis identifies protocol-dependent differences in interaction detection at local and large genomic scales. A, Numbers of significant differential interactions detected at 100 kb resolution for each protocol comparison showing that the use of DpnII compared to MboI in the FA fixation setting (FA + DpnII vs FA + MboI) predominantly increases the frequency of interactions detected but also likely increases the number of spurious trans-chromosomal interactions detected; B, Numbers of significant differential interactions detected at 2 Mbp (2000 kbp) resolution showing that the addition of DSG in the context of MboI digestion (FA + DSG MboI vs FA + MboI) increases the frequency of interactions detected without much increase in trans-interactions detected. Overall, these results suggest that detection of interactions is slightly sensitive to enzyme choice under FA fixation and this sensitivity is reduced by the addition of DSG, and addition of DSG results in an increase in the long-range interactions that can be detected when MboI is used.

Comparisons that differed only by addition of DSG but used the same enzyme (FA + DSG + DpnII vs FA + DpnII, or FA + DSG + MboI vs FA + MboI) produced a few DIs at the 100 kbp scale (Fig. 3.2A), but the FA + DSG + MboI vs FA + MboI comparison showed a sudden jump in differences at the 2 Mbp scale (Fig. 3.2B). Overall, these results suggest that detection of interactions is mildly sensitive to enzyme choice (MboI use reduces potentially spurious trans-chromosomal interactions) under FA fixation and this sensitivity is reduced by the addition of DSG. When keeping the enzyme the same and comparing only what happens with the addition of DSG, the differences were smaller when DpnII was used but use of MboI with double fixation resulted in an increase in the long-range interactions that could be detected without much increase in the trans-chromosomal interactions detected, suggesting MboI might be superior.

3.3 Discussion and conclusions

Overall, this chapter demonstrates that addition of DSG as a second fixation step had the most consistent beneficial effect on library behaviour, chiefly by reducing potentially spurious trans-chromosomal interaction signals, reducing mitochondrial contamination of the library and increasing the number of short range cis-interactions detected, particularly in the MboI condition. The double fixation method used in this experiment was inspired by the papers describing the Hi-C 3.0 protocol, which also showed a reduction in trans-interactions and increased detection of cis-interactions across all enzymes tested (Akgol Oksuz et al., 2021; Lafontaine et al., 2021), although they did not compare MboI vs DpnII and claim MboI is inferior due to being sensitive to CpG methylation. Although our DI results suggest small differences in the cutting ability of DpnII and MboI, our results do not justify switching from MboI to DpnII and future experiments in this project will continue to use MboI for single-restriction enzyme *in situ* Hi-C. The library comparisons were also based on two replicate B cell libraries per condition, prepared in batches six days apart. Limited replication and variable library quality constrain confidence in our resulting library protocol differences and their generalisation from B cells to LT-HSCs.

The Hi-C 3.0 protocol also stipulates FA crosslinking should occur first, although no reason is given. Interestingly, many ChIP-seq protocols recommend a DSG + FA double fixation process, but stipulate that DSG crosslinking should be performed first in order to

first stabilize protein complexes that have short-lived binding to DNA or have other binding partners, then perform FA crosslinking second to crosslink the protein complexes to the DNA (Bao et al., 2025; Nowak et al., 2005). However, there are some reports of Hi-C or Micro-C experiments using DSG as a first crosslinking step, followed by FA as a second crosslinking step (Ahmed et al., 2024; D. Li et al., 2023). Although there are no published reports of a comparison of the crosslinking order, there are arguments for applying DSG first. For example, one could argue that better Hi-C results may be obtained by applying DSG first because you are stabilizing native protein structures first and then applying the much smaller FA molecule second to allow for reversible linking of these crosslinked proteins to the proximal DNA. Further, by applying FA first this creates a crosslinked proteinaceous mesh that could sterically hinder the DSG from diffusing properly, thus creating cell-specific biases in the results. Future work could benefit from experiments comparing other restriction enzyme combinations for higher resolution DNA digestion and comparing the order of crosslinking with FA then DSG or DSG then FA.

3.4 Methods

3.4.1 Low-input Hi-C library preparation

A low-input *in situ* Hi-C experiment was performed to compare fixation chemistry and restriction enzyme choice in murine splenic B cells. The four Hi-C groups consisted of either single fixation with formaldehyde (FA), double fixation with FA and disuccinimidyl glutamate (DSG) and then those two groups with either DNA digestion with DpnII or MboI. For each treatment group, 2 x 10^5 $B220^+$ splenocytes were isolated from female C57BL/6 mouse spleens by mechanical dissociation in ice-cold PBS, filtration through a 45 µm nylon mesh, incubation in 500 µL RCRB for 45 s to remove red blood cells, and two washes in ice-cold PBS. Centrifugation steps during red blood cell lysis and washing were performed at 1500 rpm at 4°C. Cell pellets were then processed in four groups: 1. FA + MboI, 2. FA + DSG + MboI, 3. FA + DpnII, and 4. FA + DSG + DpnII.

For single fixation, cell pellets were resuspended in 500 µL of 1% formaldehyde in FCS-free cell culture medium and incubated for 10 min at room temperature with rotation, then quenched with 300 µL of 1 M Tris-HCl, pH 7.5, to a final concentration of 375 mM for 5

min. Cells were pelleted and washed twice in cold 1× PBS. For double fixation, formaldehyde-fixed cells were additionally resuspended in 500 µL of 3 mM disuccinimidyl glutamate, DSG, in PBS, prepared from a 300 mM stock in DMSO, incubated for 45 min at room temperature with rotation, quenched with 300 µL of 1 M Tris-HCl, pH 7.5, and washed once in cold 1× PBS. Crosslinked pellets were then collected for Hi-C processing.

Pellets were lysed in 300 µL ice-cold Hi-C lysis buffer, consisting of 10 mM Tris-HCl pH 8.0, 10 mM NaCl and 0.2% Igepal CA-630, supplemented with 50 µL protease inhibitor cocktail, Sigma P8340, and incubated on ice for 20 min. Nuclei were pelleted at 2500 × g for 5 min, washed once in 500 µL lysis buffer, then permeabilized in 50 µL 0.5% SDS at 62°C for 5 to 10 min. SDS was quenched by adding 145 µL water and 25 µL 10% Triton X-100, followed by incubation at 37°C for 15 min. Chromatin was digested overnight at 37°C with slow rotation on an Intellimixer at 6 rpm in 1× NEBuffer 2, using either 100 U MboI, New England Biolabs, R0147, or 100 U DpnII, substituted at the same step for the corresponding treatment groups. After digestion, restriction enzymes were heat-inactivated at 62°C for 20 min.

DNA ends were filled in and biotinylated by adding 18.75 µL biotin-14-dATP, 0.4 mM stock, 0.75 µL each of 10 mM dCTP, dGTP and dTTP, and 8 µL DNA Polymerase I Klenow, 5 U/µL, New England Biolabs, M0210, followed by incubation at 37°C for 45 to 90 min with rotation. Proximity ligation was performed by adding 900 µL ligation mix containing 669 µL water, 120 µL 10× T4 DNA ligase buffer, New England Biolabs, B0202, 100 µL 10% Triton X-100, 6 µL 20 mg/mL bovine serum albumin and 5 µL T4 DNA ligase, 400 U/µL, New England Biolabs, M0202, giving a final ligation reaction in 1× ligase buffer. Samples were incubated for 4 h at room temperature with slow rotation. Nuclei were then pelleted and resuspended in 984 µL water, 120 µL 10× ligase buffer, 100 µL 10% Triton X-100 and 6 µL 20 mg/mL bovine serum albumin. Crosslinks were reversed by adding 50 µL proteinase K, 20 mg/mL, New England Biolabs, P8102 or P8107, and 120 µL 10% SDS, incubating at 55°C for 30 min, then adding 130 µL 5 M NaCl and incubating at 68°C overnight.

DNA was precipitated by splitting each sample into three 500 µL aliquots and adding 800 µL absolute ethanol and 130 µL 3 M sodium acetate, pH 5.2, to each tube, followed by incubation at -80°C for 15 min and centrifugation at maximum speed for 15 min at 4°C. Pellets were combined, washed twice in 70% ethanol, and dissolved in 130 µL 10 mM Tris-

HCl, pH 8.0. DNA was sheared to 300 to 500 bp in Covaris microTUBEs using a Covaris S220 instrument with fill level 10, duty cycle 10, peak incident power 175, 200 cycles per burst, and 58 s treatment time. Sheared DNA was transferred to a fresh tube, the Covaris tube was rinsed with 70 µL water, and the sample volume was adjusted to 300 µL.

Biotinylated DNA was captured using 150 µL Dynabeads MyOne Streptavidin C1 beads, 10 mg/mL, Thermo Fisher, after washing in 400 µL 1× Tween wash buffer, 5 mM Tris-HCl pH 7.5, 0.5 mM EDTA, 1 M NaCl, 0.05% Tween 20. Beads were resuspended in 300 µL 2× binding buffer, 10 mM Tris-HCl pH 7.5, 1 mM EDTA, 2 M NaCl, mixed with the DNA sample and incubated for 15 min at room temperature with rotation. Beads were washed twice in 600 µL 1× Tween wash buffer at 55℃ for 2 min with mixing at 1200 rpm, washed in 10 mM Tris-HCl pH 8.0, and resuspended in 50 µL 10 mM Tris-HCl pH 8.0.

Sequencing libraries were prepared on-bead using the NEBNext Ultra DNA Library Prep Kit for Illumina, New England Biolabs, E7645. End repair was performed by adding 3 µL Ultra II End Prep Enzyme Mix, E7646, and 6.5 µL End Prep Reaction Buffer, E7647, followed by incubation at 20℃ for 30 min and 65℃ for 30 min. Adapter ligation was performed with 15 µL Blunt/TA Ligase Master Mix, E7648, 2.5 µL barcoded Illumina adaptor, and 1 µL ligation enhancer, E7374, at 20℃ for 15 min, followed by treatment with 3 µL USER enzyme, M5505, at 37℃ for 15 min. After washing, DNA was released from the beads by heating at 98℃ for 10 min and recovering the supernatant on a magnetic rack. Libraries were amplified with 4 to 12 PCR cycles using Phusion polymerase and Illumina P5/P7 primers in a 50 µL reaction containing 34.1 µL DNA, 10 µL 5× Phusion HF buffer, 0.4 µL 25 mM dNTPs, 2.5 µL primer mix, 0.5 µL polymerase and 2.5 µL water. PCR cycling comprised 98℃ for 30 s, followed by cycles of 98℃ for 10 s, 60℃ for 30 s and 72℃ for 30 s, with a final extension at 72℃ for 5 min.

Amplified libraries were purified by AMPure XP bead size selection, Beckman Coulter, A63881, using 0.7× beads, followed by a second cleanup after elution in 100 µL Tris buffer with an additional 70 µL beads. Final libraries were eluted in 25 µL water and assessed on a TapeStation D1000 using 1 µL library and 3 µL D1000 sample buffer. Each condition was prepared in duplicate, with replicate batches prepared six days apart. Libraries were sequenced on an Illumina NextSeq 2000 as 66 bp paired-end reads.

3.4.2 Hi-C analysis

Read quality was assessed with FastQC v0.11.x (Andrews, 2010). FASTQ files were mapped to the mm39 genome with Bowtie2 v2.5.0 (Langmead & Salzberg, 2012) using the diffHic v1.42.0 presplit_map.py tool (A. T. Lun & G. K. Smyth, 2015) and the ligation signature GATCGATC. BAM files were processed with Picard v3.30 (Broad Institute, 2023) FixMateInformation and MarkDuplicates commands, retaining duplicate-marked reads, and name-sorted with SAMtools v1.21 (Li et al., 2009).

Restriction fragments were generated from the mm39 reference genome using diffHic cutGenome with the shared MboI and DpnII recognition motif GATC, then converted to a pairParam object. Aligned reads were assigned to restriction fragments with diffHic preparePairs, using duplicate removal, dedup = TRUE, minimum mapping quality minq = 10, and chim.dist = 1000. This produced HDF5 interaction files and diagnostic summaries including total pairs, duplicate-marked pairs, filtered pairs, mapped pairs, dangling ends, self-circles and invalid chimeras. Hi-C artefacts were removed with diffHic prunePairs. Fragment length and strand-orientation profiles were inspected for each library, and reads were filtered using max.frag = 800, min.inward = 1000 and min.outward = 1000, removing short fragments, dangling ends and self-circularised products. Cis and trans interaction proportions, short-range interaction frequency bins, interaction decay curves and mitochondrial interaction ratios were calculated from the HDF5 files with custom R scripts.

For differential interaction analysis, trimmed read pairs were counted into genomic bins using diffHic squareCounts, restricted to chromosomes chr1 to chr19, chrX and chrY. Interaction matrices were generated at 2 Mbp and 100 kbp resolution. For 100 kb analysis, interactions containing zero counts in any library were removed. Low-abundance interactions were filtered with filterDirect using a 2 Mb background reference and a threshold of direct$threshold + log2(4). Diagonal bin pairs were removed with filterDiag(data, by.diag = 1L). For the 2 Mb analysis, low-abundance interactions were filtered using direct$threshold + log2(2).

Filtered interaction counts were normalised using nonlinear loess offsets calculated with csaw v1.44.0 (Lun & Smyth, 2016) normOffsets. Near-diagonal and off-diagonal interactions were normalised separately, using filterDiag(data, by.dist = 400e3) for 100 kb matrices and filterDiag(data, by.dist = 4000e3) for 2 Mb matrices. Offset matrices were added to the

interaction object and converted to edgeR (Robinson et al., 2010) v4.8.0 DGEList objects. Differential interactions were modelled with edgeR quasi-likelihood negative binomial generalized linear models. The design matrix included group and replicate batch, ~0 + group + batch. Dispersion was estimated with estimateDisp(..., robust = TRUE), and quasi-likelihood models were fitted with glmQLFit(..., robust = TRUE). Contrasts tested the effects of restriction enzyme within fixation condition, fixation within restriction enzyme condition, and combined fixation and enzyme comparisons. Differential interactions were identified with glmQLFTest, adjusted using edgeR topTags, and retained at FDR < 0.1.

Chapter 4: Publication in review: “Multi-omic gene regulatory networks informed by 3D chromatin architecture reveal insights into hematopoietic stem cell ageing”

Multi-omic gene regulatory networks informed by 3D chromatin architecture reveal insights into hematopoietic stem cell ageing

Quinn Stacpoole[1,2*], Nadia Iannarella[1,2], Timothy M Johanson[1,2,3], Hannah D Coughlan[1,2,3] and Rhys S Allan[1,2,3*]

[1]The Walter and Eliza Hall Institute of Medical Research, Parkville, Victoria, 3052, Australia. [2]Department of Medical Biology, The University of Melbourne, Parkville, Victoria, 3010, Australia.

[3]These authors contributed equally.

***Corresponding authors:**
Quinn Stacpoole (stacpoole.q@wehi.edu.au) and Rhys S. Allan (rallan@wehi.edu.au)

Running title: 3D genome remodelling underlies haematopoietic stem cell aging.

Keywords: 3D genome, haematopoietic stem cells, aging, epigenetics.

4.1 Abstract

During ageing, hematopoietic stem cells (HSCs) have reduced regenerative potential, skewed differentiation toward the myeloid lineage, and heightened susceptibility to clonal expansion and malignancy. While epigenetic alterations are well documented, the impact of aging on higher-order 3D chromatin architecture remains poorly understood. Here, we examined the 3D genome organisation of aged murine HSCs using in-situ Hi-C then integrated this with gene expression and chromatin accessibility data to build HiC-informed gene regulatory networks (GRNs). Aged HSCs display erosion of topologically associating domain (TAD) boundaries, A/B compartment switching, and reorganised enhancer-promoter loops associated with lineage-inappropriate gene expression. Our GRN analysis identifies a hierarchy of transcription factors, including a c-Maf-Lyl1-Mnt axis that orchestrates the transition from a youthful to aged state and a Gfi1-Sox4 axis in young HSCs that regulates Bach1. This study provides a structural blueprint for aging HSCs and defines specific regulatory targets for potential reprogramming interventions to restore hematopoietic youthfulness.

4.2 Introduction

Hematopoietic stem cells (HSCs) are responsible for continually replenishing the blood system with mature cells, ensuring immune competence and tissue homeostasis (Osawa et al., 1996; Spangrude et al., 1988; Thomas et al., 1957). However, during the ageing process in mice and humans, HSCs expand due to increased self-renewal (Sun et al., 2014), decline in regenerative potential (Kuribayashi et al., 2021), shift toward myeloid-biased differentiation (Dykstra et al., 2011; Pang et al., 2011) and display increased genomic instability (Rossi et al., 2007; Rube et al., 2011), all of which contribute to reduced immune function and a higher risk of hematological malignancies in the elderly.

Studies have found that transplantation of aged murine HSCs into young mice can restore some function (Ergen et al., 2012; Montecino-Rodriguez et al., 2019; Yamamoto et al., 2018), especially after secondary transplantation (Yamamoto et al., 2018), but in many experiments transplantation of old HSCs into young mice does not correct the repopulating abilities of the stem cells (Dykstra et al., 2011; Liang et al., 2005; Rossi et al., 2005), suggesting an intrinsic dysfunction. HSCs accumulate epigenetic alterations with age, such as changes to chromatin accessibility (Itokawa et al., 2022) and DNA methylation (Bogeska et al., 2022) both of which alter gene expression in ways that reflect myeloid bias and a cellular reaction to an inflammatory bone marrow environment. However, whether these alterations in epigenetics and gene expression are primarily due to downstream effects of somatic mutations (Kapadia et al., 2025) or an independent reversable process of epigenetic alteration is still unclear since iPSCs derived from aged HSCs that are then redifferentiated to HSCs are functionally indistinguishable from young HSCs (Wahlestedt et al., 2017). Additionally, recent clonal tracing reveals that aged HSCs are likely an expanded population of epigenetically altered clones (Scherer et al., 2025).

A key driving factor in cell identity and gene regulation are the interactions between enhancers and promoters that are mediated via transcription factor (TF) binding (Martin et al., 2023), this is more broadly described as the 3 dimensional (3D) folding of the genome (Lafontaine et al., 2021; Tomas-Daza et al., 2023) and few studies have examined how the 3D genome of stem cells changes with age. Hi-C, a genome-wide chromatin conformation capture technique, has provided critical insights into the spatial organization of chromatin in mature immune cells (Bediaga et al., 2021; Chan et al., 2021; Johanson et al., 2018) and

blood stem cells (Chen et al., 2019; Zhang et al., 2020). In addition to high resolution enhancer promoter interactions, Hi-C data allow for the identification of the large-scale hierarchical features of the 3D genome such as chromatin compartments (active A and inactive B compartments), topologically associating domains (TADs). Differential style analysis allows us to identity differences in the 3D genomes of conditions i.e. young and aged, and determine which regulatory elements and TFs are involved in the ageing of chromatin organisation (Lafontaine et al., 2021; Tomas-Daza et al., 2023). Studies in other cell types have revealed significant age-associated changes in chromatin organization. Age-related chromatin changes are often cell type-specific but share common features such as loss of TAD integrity, altered enhancer-promoter interactions, and redistribution of chromatin between A and B compartments (Kriukov et al., 2024; Ma et al., 2024). In muscle stem cells, ageing is accompanied by a gain in long-range chromatin contacts and a loss of short-range interactions, impairing the transcription of regeneration-associated genes (B. A. Yang et al., 2023; Zhao et al., 2023). Neuronal ageing, on the other hand, is characterized by the decay of heterochromatin domains, activation of transposable elements, and nuclear expansion (Kriukov et al., 2024; Zhang et al., 2022). Furthermore, Liu et al. demonstrated increased Shannon entropy in the B compartments of late-passage mesenchymal stromal cells (MSCs), indicating an increase in disorder with replicative age (Liu et al., 2022b). Importantly, environmental and genetic interventions such as exercise and epigenetic reprogramming have been shown to mitigate some of these chromatin changes, emphasizing their potential reversibility (J.-H. Yang et al., 2023a).

Often gene regulation is examined by correlating gene expression with the closest open chromatin region to infer gene regulatory elements. However, Hi-C allows us to directly link gene regulatory elements (often distal) to target genes (Javierre et al., 2016; Milevskiy et al., 2023). TF activity (i.e. the extent to which it is exerting its regulatory potential on its target genes through motif binding) has been shown to be a better predictor of cell-defining gene regulation than expression alone (Wlodarczyk et al., 2025). Even at low resolution, Hi-C data can add an additional layer during multi-omic integration for mapping gene regulatory mechanisms and identifying TFs that govern gene regulatory networks (GRNs) (Fulco et al., 2019; Hecker et al., 2023). For example, integration of Hi-C, ATAC-seq and RNA-seq is one method of constructing GRNs, where TFs and genes are nodes and the strength of their

interaction and activity are the edges (Fulco et al., 2019; Hecker et al., 2023). Furthermore, the differential analysis of network weights between conditions (e.g. cell type 1 vs cell type 2, or young vs aged) can provide additional information beyond differential expression or differential chromatin accessibility alone, since genes may change their connectivity through the 3D genome in the network with little change in their expression, allowing for the identification of TFs that drive network state changes (Hecker et al., 2023; Wlodarczyk et al., 2025; Xu et al., 2021). While the use of differential network analysis to identify TFs that drive trans-differentiation of one cell type to another is relatively common, its use to identify TFs that define aged states in the same cell type is a growing area of research (Lee et al., 2021; Randhawa & Kumar, 2021; Wang et al., 2023). However, none have yet used Hi-C derived genome organisation to inform the construction of TF-gene networks.

Investigations into the chromatin architecture of HSCs, let alone aged HSCs, are scarce, but in blood progenitors such as aged pro-B cells, alterations in enhancer-promoter interactions and shifts in chromatin compartmentalization have been linked to impaired B cell development (Ma et al., 2024). These findings imply that changes in chromatin architecture could play a role in HSC ageing, yet the specific changes occurring in HSCs remain to be elucidated. Here, we examine the 3D genome organisation of young and aged murine long-term (LT-) HSCs using Hi-C to gain further insights into the molecular drivers of their functional decline and potentially identify novel strategies to reprogram aged HSCs back to a more youthful state. We find that ageing appears to cause a loss of TAD boundary strength and an increase in disorder in the 3D chromatin contacts of murine LT-HSCs. Additionally, differentially expressed genes (DEGs) are enriched in the differentially interacting (DI) regions (i.e. regions that gain or lose chromatin interactions with age) and a small set of upregulated genes appear to be lineage inappropriate, as they are not normally expressed in any young blood progenitors, but are expressed in aged LT-HSCs and are particularly enriched in the DI regions. Furthermore, while differential TF-gene networks are often used to identify TFs for direct cell reprogramming (Xu et al., 2021), we used similar methods to identify TFs that govern the TF-gene regulatory network states of aged and young LT-HSCs and our analysis predicts a potential role for c-Maf, Cebpd and Atf3 as top drivers of the aged state, while Gfi1, Hif3a, Sox4 and Hes1 are top TFs predicted to govern the youthful state.

4.3 Results

4.3.1 Mitochondrial membrane potential status does not confer differences in 3D genome architecture, but age does

To tackle potential heterogeneity of the aged LT-HSC pool we leveraged knowledge from a previous study that demonstrated that mitochondrial membrane potential (MMPot) status could discriminate between young-like LT-HSCs in old mouse bone marrow (Mansell et al., 2021). To this end, aged and young LT-HSCs ($CD34^-$ $CD48^-$ $Flt3^-$ $CD150^+$ LSKs) were sorted based on MMPot status (low and high) (see Methods and Fig. 4.1A) and subjected to Hi-C. We processed the data and performed differential analysis using diffHic (A. T. Lun & G. K. Smyth, 2015) between old and young then high and low MMPot groups. While aged mice had a higher proportion of MMPot low LT-HSCs than young mice, as previously reported (Mansell et al., 2021) (Supplementary Fig. 4.1B-C), there were no significant differential interactions (DIs) between MMPot High and MMPot Low LT-HSCs from either young or aged mice (Supplementary Fig. 4.1D). However, when contrasted according to age, both MMPot high and low LT-HSCs groups each displayed differences in chromatin contacts (Supplementary Fig. 4.1D), suggesting ageing has a much stronger effect on chromatin structure than MMPot status. Therefore, all further analysis was performed on LT-HSCs in which MMPot high and low groups were pooled to compare LT-HSCs by age only.

4.3.2 Changes in higher order chromatin structures indicate an age-associated increase in disorder

To understand the higher order genomic structures, we assessed the number and strength of TADs using HiCExplorer (Ramirez et al., 2018) in which TAD boundary "separation scores" are calculated to call TADs. In our data, TAD separation scores are increased in aged LT-HSCs (Fig. 4.1B & C; Supplementary Table 1), indicating that there are more interactions across TAD boundaries, i.e. a loss of TAD boundary strength. Segments of the genome can also be classified into A or B compartments depending on how the large-scale interactions segregate within principal component analysis. Calculation of A/B compartments in our LT-HSCs using HiCDOC (Kurylo et al., 2023) reveals an age-associated increase in the

proportion of B compartments and decrease in the proportion of A compartments (Fig. 4.1D; Supplementary Table 1).

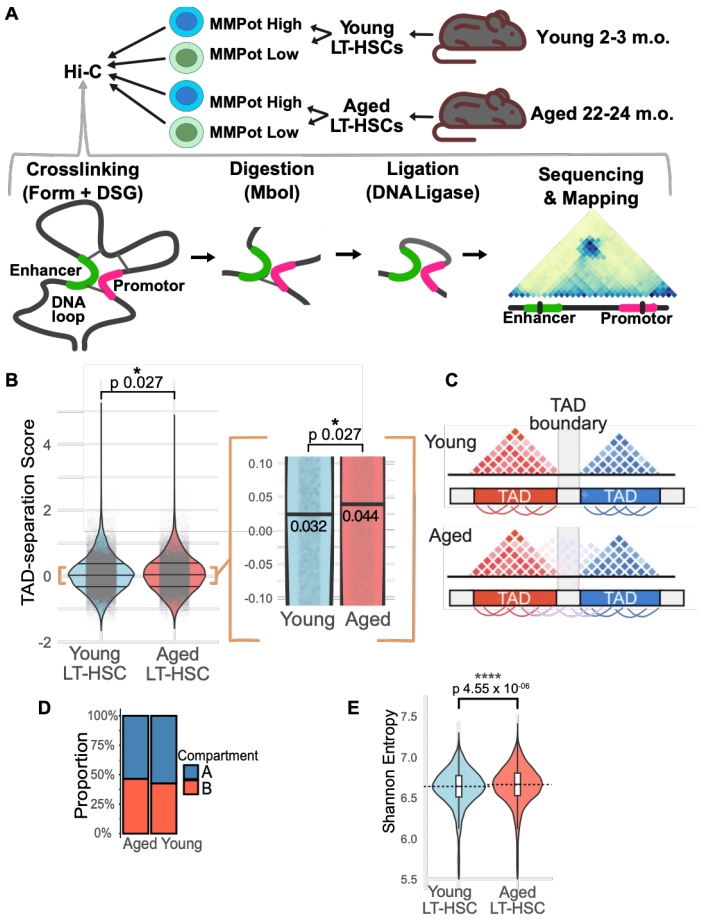


Figure 4.1. Age-associated changes in 3D chromatin architecture in LT-HSCs reveals increased disorder and a preponderance of gained interactions. A. Schematic of Hi-C experiment on LT-HSCs from young and aged C57Bl6 mice (MMPot = mitochondrial membrane potential, HSC = hematopoietic stem cell, Form = formaldehyde, DSG = disuccinimidyl glutarate); B. Violin plots of TAD separation scores in Young vs Aged LT-HSCs (difference assessed by Mann-Whitney U-test); C. Diagram depicting how an increase in TAD-separation score translates to overall reduced TAD boundary strength with more interactions occurring across TAD boundaries; D. A/B compartment proportions for Aged & Young LT-HSCs; E. Violin plots of Shannon entropy values for all 2 Mbp genomic spans in Young vs Aged LT-HSCs (difference assessed by Mann-Whitney U-test).

We wondered if the age-associated loss of TAD boundary strength reflects a general increase in disorder in the LT-HSC chromatin structure. To address this, we calculated

Shannon entropy for young and aged LT-HSCs by calculating the probability distribution of contact frequencies for every 2 Mbp genomic span tiled along the mm39 genome, a method previously used in other models of ageing (Jenkinson et al., 2017; Liu et al., 2022b). Aged LT-HSCs have a higher median Shannon entropy across all 2Mbp spans than young LT-HSCs (Fig. 4.1E; Supplementary Table 1), indicating a subtle erosion of the contact frequency landscape with ageing. Altogether, the changes in TAD boundary strength, changes to compartments and the overall increase in Shannon entropy suggest an increase in the disorder of the chromatin architecture in aged LT-HSCs.

4.3.3 Aged LT-HSCs develop chromatin interactions associated with differentially expressed genes

DI analysis was performed on aged versus young LT-HSCs using, which revealed that 1353 cis-interactions decrease in interactivity and 3448 increase in interactivity during ageing in murine LT-HSCs (Fig. 4.2B, Supplementary Table 2). The highest ranked region (by false discovery rate (FDR)) in the analysis, was a gain in interactions on chromosome 5 between a 100 kbp region near *Gabra2* and a 100 kbp region upstream near *Guf1* (Fig. 4.2A & C, left panel). Interestingly, many chromosomes 5 regions near other GABA receptor ion-channel components *Gabrb1* and *Gabra4* also gained interactions (Fig. 4.2G, middle panel). The highest ranked lost interaction was on chromosome 15 near *Nipbl* and *Wdr70*, respectively (Fig. 4.2C, right panel). To compliment this analysis, we reanalysed previously published RNA-seq data from Itokawa et al 2022 data (see Methods) to determine differentially expressed genes (DEGs) between young and old HSCs. We observed that DEGs are significantly enriched in the DI regions (Fig. 4.2E). Furthermore, the DEGs *B3galt1*, *Gabra4*, *Gabra1* and *Terf1* all overlap with the top 20 DI regions that alter interaction frequency with age (Fig. 4.2G and Supplementary Fig. 4.2A). Interestingly, comparison of aged versus young murine monocytes or natural killer (NK) cells showed a negligible number of DIs at 100 kbp resolution (Supplementary Fig. 4.1F), suggesting that either mature blood cells correct their 3D genome as they differentiate, or that the myeloid and lymphoid progenitors that go on to differentiate to maturity already have chromatin architecture similar to that of young progenitors.

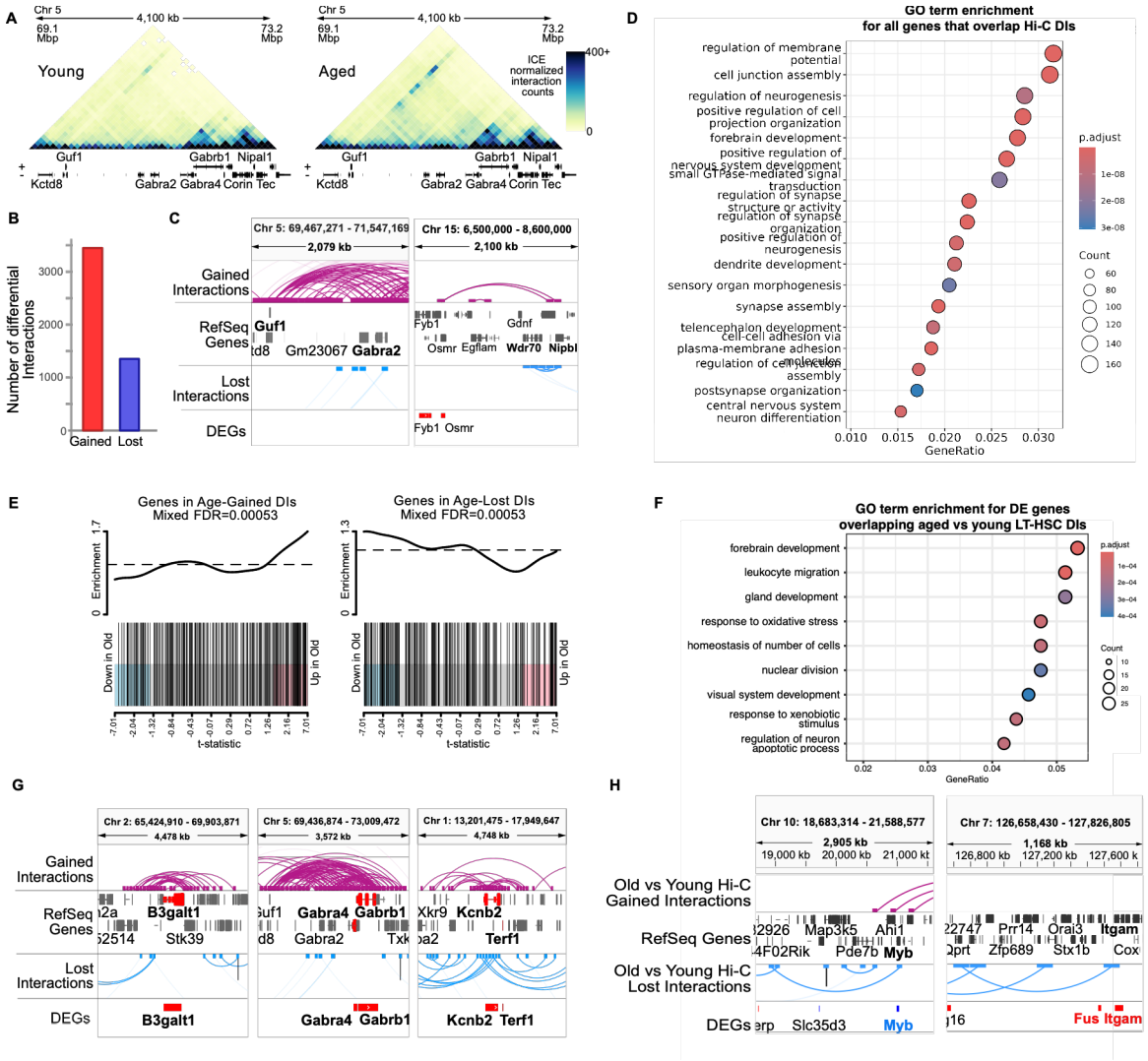


Figure 4.2. Genes overlapping regions which alter their interactions with age in murine LT-HSCs reveals biological processes associated with signalling, activation, migration and differentiation. A. Hi-C Contact maps (bin size = 100 kbp) of the region 69.1 – 73.2 Mbp on chromosome 5 for Young and Aged LT-HSCs, which includes the most significant differential interaction (DI) that occurs between regions around Guf1 and Gabra2; B. The number of differential intra-chromosomal (cis) interactions in Aged/Young LT-HSCs (red bar = interactions gained with age, blue bar = interactions lost with age); C. Arc plots of the most significant (FDR < 0.1) gained (left panel) and lost (right panel) DIs at 100 kbp resolution; D. GO term enrichment for all genes that overlap Hi-C aged vs young LT-HSC DIs; E. Enrichment of differentially expressed genes (DEGs) in aged vs young DIs using the fry test where "mixed" false discovery rate (FDR) is the FDR value for enrichment in the combined gained and lost DIs; F. GO term enrichment for DEGs overlapping aged vs young LT-HSC DIs; G. Arc plots of the most significant gained and lost DIs at 100 kbp resolution and the upregulated DEGs they overlap (upregulated DEGs shown in red). H. Age-associated loss of interactions between a region near myeloid-associated gene *Myb* and a region ~2 Mbp downstream of Myb's promotor (1st panel) and age-

associated loss of interactions between a region overlapping myeloid-associated gene *Itgam* and a region over 800 kbp upstream (2nd panel).

Gene Ontology (GO) term enrichment analysis of genes near regions that change chromatin architecture with age in LT-HSCs revealed an enrichment of genes involved in the regulation of membrane potential, cell junction assembly and many genes involved in neurogenesis (Fig. 4.2D; Supplementary Table 3), likely reflecting share processes. Kyoto Encyclopedia of Genes and Genomes (KEGG) pathway enrichment analysis revealed many genes involved in cancer (especially miRNAs), as well as glutamatergic and serotonergic synapses (Supplementary Fig. 4.2B; Supplementary Table 3). When GO term analysis is restricted to only genes that are both differentially expressed (from the Itokawa et al 2022 dataset) and that also overlap with regions of differential interactions, many genes appear to be involved in leukocyte migration (especially myeloid cell migration) and neuron-related processes (Fig. 4.2F; Supplementary Table 3), while efferocytosis pathway genes were the most significantly enriched in Kyoto Encyclopedia of Genes and Genomes (KEGG) analysis (Supplementary Fig. 4.2C; Supplementary Table 3). As expected, many prominent genes involved in LT-HSC activation and myeloid differentiation appear in the GO term enrichment and show both age-associated chromatin contact changes and changes in gene expression (Supplementary Table 3). For example, *Myb* (aka *c-Myb*) and *Itgam* (among others) appears in GO terms such as "myeloid cell homeostasis", "myeloid leukocyte migration" and "negative regulation of myeloid cell differentiation" to name a few (Supplementary Table 3). The expression of *Myb* decreases with age in LT-HSCs as does the frequency of interactions between a region near *Myb* and a region ~2 Mbp upstream of *Myb*'s promotor (Fig. 4.2H, 1st panel). Similarly, *Itgam* (*Cd11b*) is upregulated in aged LT-HSCs and a region overlapping its promotor shows a decreased frequency of interactions with a region over 800 kbp upstream (Fig. 4.2H, 2nd panel).

4.3.4 Genes that have age-related inappropriate lineage expression overlap with changes in genome organisation

We reasoned that the observed increase in disorder within the chromatin contacts might result in the expression of genes that are not usually expressed in the blood-cell progenitor

lineage. To test this, we used the raw counts from the Itokawa et al. (2022) RNA-seq data, which contains expression data for young (8 week old) and aged (20 month old) blood progenitors, including LT-HSCs, multipotent progenitors 1-4 (MPP1-4s), megakaryocyte-erythroid progenitors (MEPs), granulocyte-monocyte progenitors (GMPs) and common lymphoid progenitors (CLPs). We defined a set of genes that have low or negligible expression in young LT-HSCs, MPP1-4s, GMPs, MEPs or CLP and significantly higher expression in aged LT-HSCs (Supplementary Fig. 4.3B), which resulted in a list of 85 genes (Supplementary Fig. 4.3A). GO term enrichment of these DEGs that are very lowly or absent in young progenitors highlighted groups of genes such as *Tmem215*, *Kdr*, *Bmp4*, *Myo6*, *Ror2*, *Tbx1* and *Rorb* being involved in sensory organ morphogenesis and *Kdr, Bmpr1a, Bmp4 and Tbx1* involved regulation of mesenchymal cell proliferation (Supplementary Fig. 4.3D and E). Restricting our definition again to genes that have very low expression in young blood progenitors (Supplementary Fig. 4.3C) defined a list of genes we term "lineage inappropriate genes" (LIGs) which refined our list to 8 genes: *Rcvrn*, *Ntf3*, *Syt15*, *Mab21l2*, *Rorb*, *Aldh3a1*, *Chrm3* and *Tdrd9* (Fig. 4.3A & C). Interestingly, 7 out of 8 strict LIGs (which are also DEGs) also overlap with and are significantly enriched within regions of differential interactions in our Hi-C data compared to other randomly selected sets of upregulated DEGs (Fig. 4.3B), likely indicating that age-related 3D chromatin changes lead to expression of these lineage inappropriate genes.

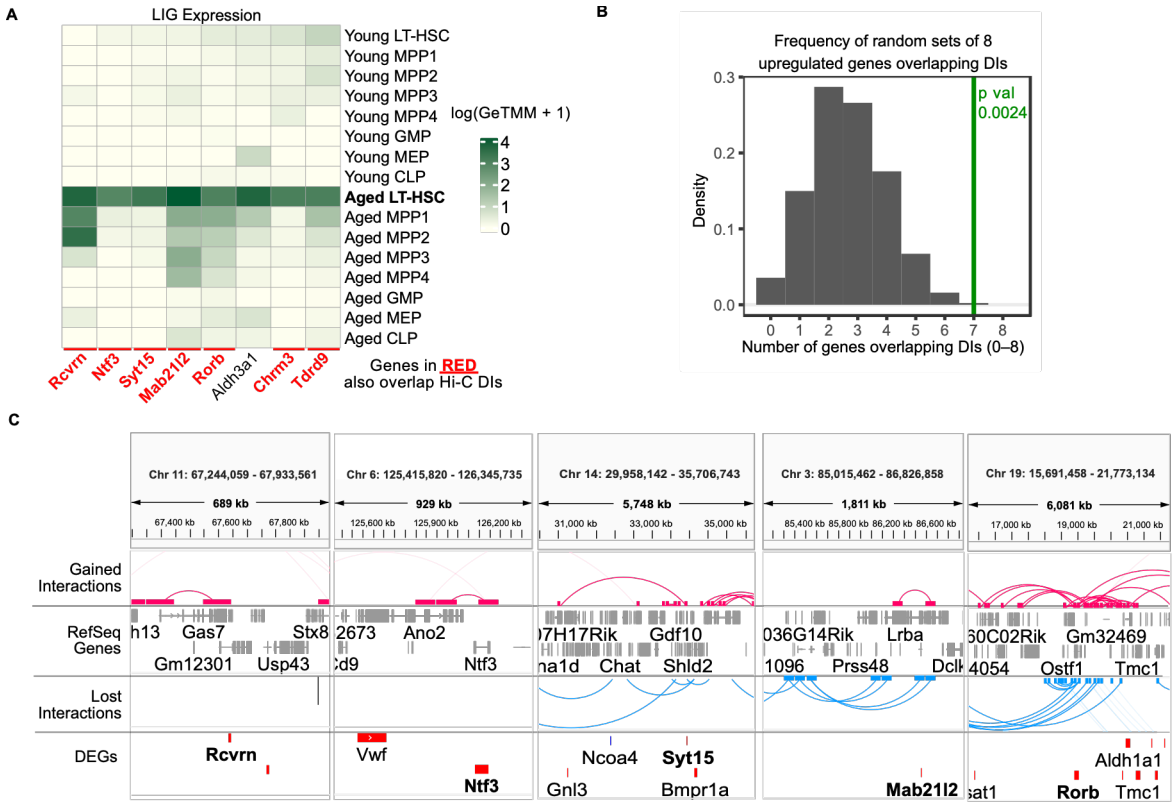


Figure 4.3. Genes not normally expressed in any young murine blood progenitors are upregulated with age, especially in LT-HSCs, and 7/8 overlap aged vs young LT-HSC Hi-C DIs (genes in red). A. Heatmap of expression (logGeTMM+1) across all blood progenitors for the 8 strictly defined lineage inappropriate genes (LIGs) identified in the Itokawa et al 2022 dataset (genes in green and columns marked with a green bar also overlap aged vs young LT-HSC differential interactions (DIs); B. Density plot of how often genes within sets of 8 randomly chosen upregulated genes (testing 10000 sets of 8 genes) overlap DI regions as determined by a random sampling Monte Carlo permutation test (the p value of the likelihood of 7 upregulated genes overlapping DIs is 0.0024 as determined by the Monte Carlo empirical test); C. Interaction arc plots for gained and lost interactions for aged vs young LT-HSC DIs (100 kbp resolution) that overlap 5 of the LIGs: *Rcvrn*, *Ntf3*, *Syt15*, *Mab21l2* and *Rorb*.

4.3.5 AP-1 factor binding motifs are enriched in chromatin that opens and gain interactions during ageing

We wondered if regions that change in interaction frequency are enriched for particular TF motifs. To answer this question, we used ATAC-seq data to determine differentially accessible regions (DARs) between young and aged LT-HSCs using the Itokawa et al 2022 data, then performed motif enrichment analysis within DARs that overlap our Hi-C DI

regions (Fig. 4.4A). Strikingly, motifs for AP-1 factors Jun, Jund and Fosl2, as well as the common AP-1 binding partner Ets1, are enriched in age-opening peaks that overlap regions that gain interactions (Fig. 4.4B, age-opening/age-gained columns). There is also a mild enrichment of PPARG and NR1H3 motifs in age-closing peaks that overlap regions that lose interactions with age (Fig. 4.4B, age-closing columns).

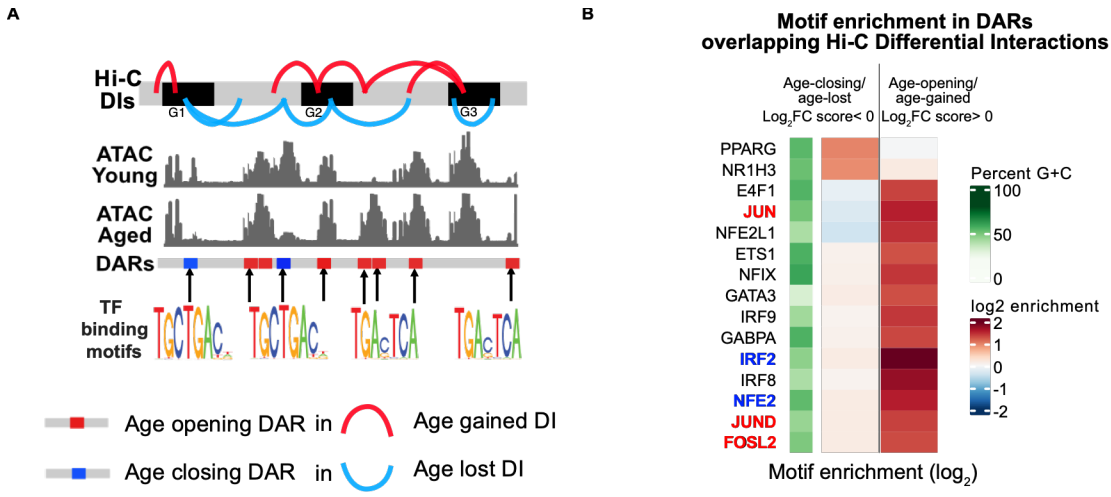


Figure 4.4. Differentially accessible regions (DARs) overlapping DIs with the same logFC direction show strong enrichment for AP-1 factor motifs. A. Schematic of motif enrichment analysis whereby transcription factor (TF) binding motif enrichment was assessed in age-opening and age-closing DARs that overlap Hi-C differential interactions with the same log fold change sign (e.g. logFC > 0 means age-opening DARs in gained DIs, logFC < 0 means age-closing DARs in lost DIs); B. MonaLisa TF motif enrichment results showing the top HOCOMOCO v13 motifs enriched in age-closing DARs that overlap age-lost differential interactions (Log_2FC score < 0) and in age-opening DARs that overlap age-gained differential interactions (Log_2FC score > 0) – red highlighted TFs are upregulated in aged LT-HSCs, blue highlighted TFs are downregulated.

4.3.6 Integrated multi-omic analysis predicts TFs that drive the aged and youthful states of LT-HSCs

To further explore how transcription factor binding influences age-related changes in epigenetics and gene regulation we used differential GRN analysis. While our motif enrichment analysis highlighted the DEGs Jun, Jund and Fosl2, TFs regulate genes in a network and can change network connectivity with little change in expression (Wlodarczyk

et al., 2025). As such, changes in network connectivity can reveal TF drivers of network state change. Moreover, analysis of differential GRNs can rank TFs based on the strength of the change in connectivity to predict which TFs to use for cell reprogramming (Kamaraj et al., 2020; Rackham et al., 2016; Xu et al., 2021). Therefore, we constructed GRNs using our Hi-C data and publicly available ATAC-seq and RNA-seq data using a combined workflow of STARE (Hecker et al., 2023) and a modified pipeline similar to ANANSE (Xu et al., 2021) (Fig. 4.5A).

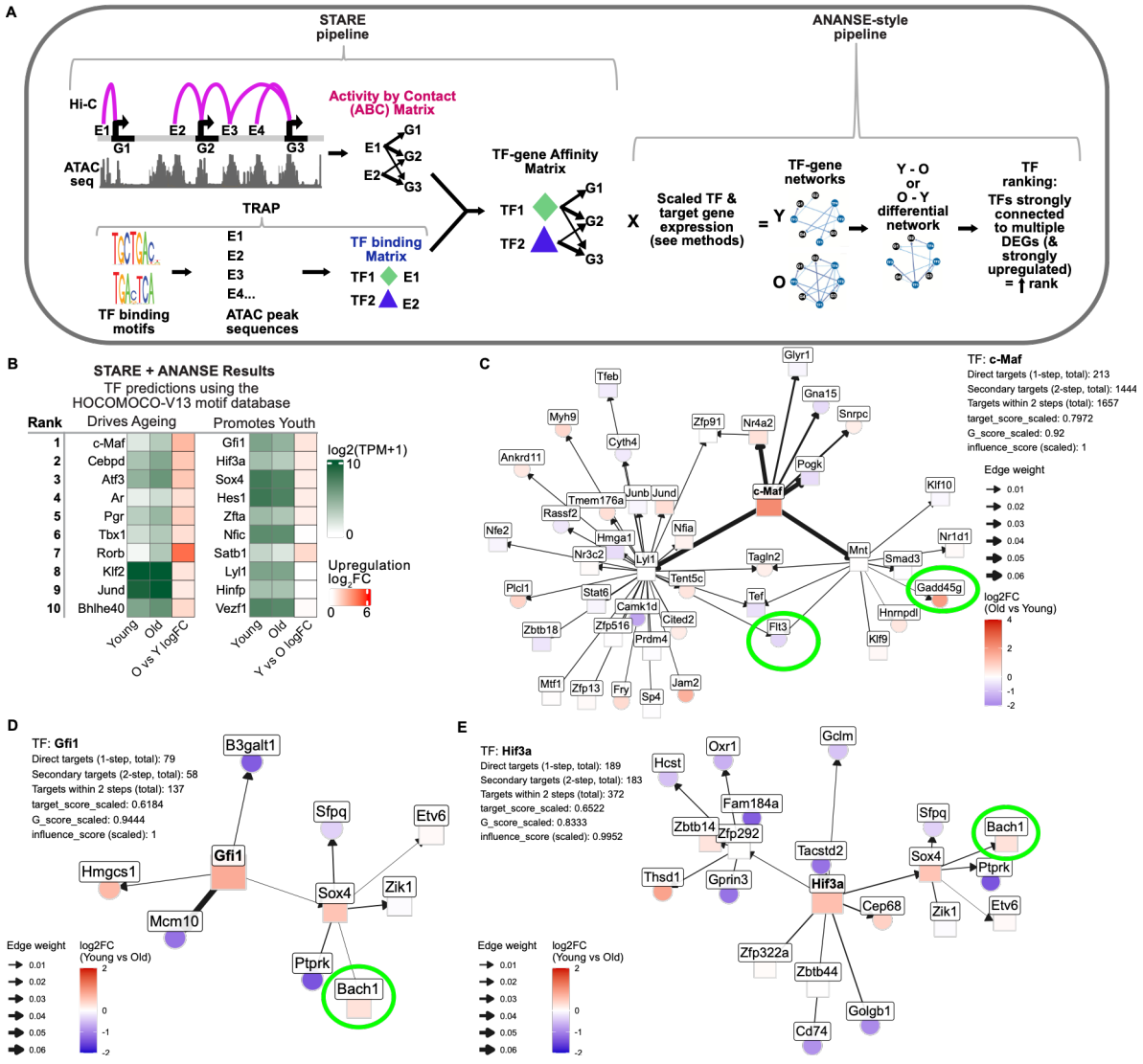


Figure 4.5. Integrated differential network analysis predicts transcription factors (TFs) that drive the aged and young states of murine LT-HSCs. A. Schematic of the combined STARE and ANANSE-style pipeline that integrates Hi-C, ATAC-seq and RNA-seq data: purple arcs represent ICE-normalized Hi-C interaction frequencies that overlap candidate enhancers (E1-E4), and genes (G1-G3) 2.5 kbp either side of the

gene's TSS, which are combined with ATAC-seq loess offset normalized peak values to generate an activity by contact (ABC) matrix, which is combined with a TF binding matrix to generate a TF-gene affinity matrix, which is then used by the ANANSE-style pipeline to generate differential gene regulatory networks (GRNs) and rank the TFs that drive the GRN changes; B. TF ranking results using the HOCOMOCO v13 TF motif database showing the expression (log2 TPM+1) and fold-change (log2FC) heatmaps of the top 10 ranked TFs predicted to either (i) drive the gene regulatory network towards the aged state (left 3 "Drive Ageing" columns) or (ii) drive the network towards the young state (right 3 "Promotes Youth" columns); C. Simplified network diagram of the top ranked age driving TF, c-Maf, which is predicted to regulate 213 direct targets in this GRN; D. Simplified network diagram of the top ranked youth promoting TF, Gfi1, which is predicted to regulate 79 direct targets, including Sox4; E. Simplified network diagram of the 2nd top ranked youth promoting TF, Hif3a, which is predicted to regulate 189 direct targets, including Sox4

The top 10 ranked TFs predicted to drive each condition are shown in Fig. 4.5B and Supplementary Table 4; c-Maf (aka Maf), Cebpd, Atf3, Ar, Pgr, Tbx1, Rorb, Klf2, Jund and Bhlhe40 are predicted to drive the gene regulatory network changes during LT-HSC ageing, while Gfi1, Hif3a, Sox4, Hes1, Zfta, Nfic, Satb1, Lyl1, Hinfp and Vesf1 are predicted to be candidates to restore the youthful LT-HSC gene regulatory network state.

Inspection of these Hi-C informed differential GRNs (Supplementary Table 4) predicts that c-Maf regulates the TFs Lyl1 and Mnt to influence Flt3 downregulation in aged LT-HSCs (Fig. 4.5 C) as does Cebpd via Myc (Supplementary Fig. 4.4A). Both c-Maf1 via Mnt (Fig. 4.5C) and Cebpd via Myc (Supplementary Fig. 4.4A) are also predicted to drive the upregulation of Gadd45g, a driver of differentiation (Thalheimer et al., 2014). Furthermore, both Cebpd and Atf3 are predicted in our differential GRN to directly downregulate the TF Bach1 (Supplementary Figs. 4A and B), a known suppressor of myelopoiesis (Itoh-Nakadai et al., 2014; Kato et al., 2018). The LIG Rorb is ranked 7th as a driver of LT-HSC ageing (Fig. 4.5B) and is predicted in the ageing-specific differential GRN to drive the downregulation of the TFs Dbp & Nr4a1 (Supplementary Fig. 4.4C).

Inspection of the Hi-C informed differential GRNs driving the youthful LT-HSC state predicts that Gfi1 & Hif3a both target Sox4 to upregulate Bach1 (Fig. 4.5D & E; Supplementary Fig. 4.4D), previously mentioned as a suppressor of myelopoiesis, and therefore Gfi1 & Hif3a have the opposite role of Cebpd and Atf3, which were predicted to downregulate Bach1. The 4th ranked TF predicted to drive the young LT-HSC GRN is Hes1

(Fig. 4.5B) and inspection of its immediate targets shows it is predicted to suppress the expression of the sphingosine-1-phosphate transporter gene, *Mfsd2b*, and upregulate the suppressor of cholesterol synthesis gene, *Insig1* (Supplementary Fig. 4.4E).

It is expected that many DEGs in the networks would overlap our Hi-C DIs and inspection of the target DEGs of the top ranked age-driving TF, c-Maf (Fig. 4.5A), show that many do, including the DEGs Glyr, Plcl1, Tent5c, Zbtb18, Jam2 and Fry (Supplementary Fig. 4.4F).

4.4 Discussion

Our results are, to our knowledge, the first to show that the 3D chromatin architecture of aged murine LT-HSCs is altered and demonstrates that aged LT-HSCs display a loss, albeit subtle, of overall TAD boundary strength and an increase in chromatin interaction Shannon entropy, which indicates that there is a general increase in disorder within the 3D chromatin structures. This increase in chromatin interaction Shannon entropy is in line with *in vitro* studies looking at late passage mesenchymal stem cells which show an increase in Shannon entropy in B compartments (Liu et al., 2022b). We found negligible differences in chromatin architecture in aged vs young monocytes and NK cells. Since myeloid-biased LT-HSCs with low differentiation capacity are clonally expanded from a small set of original stem cells (Scherer et al., 2025), we hypothesise that LT-HSC fate is epigenetically set early in the mouse lifespan and that the aged monocytes and NK cells mostly derive from the remaining young-like LT-HSCs with youthful genome architecture.

Obtaining sufficient numbers of LT-HSCs is difficult and a limitation of our Hi-C data is the low resolution due to low cell input. Although we did not find any differences in chromatin architecture between LT-HSCs with high and low mitochondrial membrane potential, this does not exclude this possibility. Increased cell input, and thus higher resolution, may reveal more subtle differences in chromatin architecture between MMPot high and low LT-HSCs and other LT-HSC sub-populations such as CD150 high and low LT-HSCs which have been shown to be functionally distinct (Wang et al., 2025). Despite these caveats, our analysis was able to detect clear age-related 3D genome changes suggesting that MPPot status does not correlate with overt epigenetic alterations.

Since aged phenotypic LT-HSCs ($CD34^-$ $CD48^-$ $Flt3^-$ $CD150^+$ LSKs) contain a higher proportion of myeloid-primed LT-HSCs, locus-specific differences in chromatin are likely

to reflect this myeloid priming. For example, our results show a region near the gene *Nipbl* has a strong loss of interactions with a region near *Wdr70* and a gain in interactions with a region near *Osmr* (Fig. 4.2C). *Nipbl* encodes a protein, Nipped B-like, a cohesin complex chromatin loading protein that is more abundant in aged LT-HSCs (Zaro et al., 2020) and likely upregulates *Runx1* and increases myeloid cell differentiation (Mazzola et al., 2020), thus supporting the observed increase in myeloid-biased LT-HSCs. *Osmr*, encodes a subunit of the oncostatin M (OSM) receptor and that is significantly upregulated in aged murine HSCs (Flohr Svendsen et al., 2021; Itokawa et al., 2022) and promotes inflammatory signalling (Jakob et al., 2021) and HSC mobilization (Bisht et al., 2022). The observed downregulation of *Myb* and upregulation of *Itgam* (*Cd11b*) are also known to be important for myeloid differentiation and these DEGs overlap differentially interacting regions in our aged vs young LT-HSCs (Fig. 4.2H). *Myb* is likely a target of the Runx1 transcription factor during differentiation of megakaryocyte-biased LT-HSCs (C. Wang et al., 2023) and its downregulation is important for differentiation of LT-HSCs into downstream lineages (Bianchi et al., 2010; Garcia et al., 2009; Sakamoto et al., 2012). *Itgam* upregulation in LT-HSCs is associated with both enhanced regenerative potential and myeloid cell differentiation (Rydstrom et al., 2023; Trento et al., 2017).

It is also interesting to note that regions near GABA receptor ion-channel genes *Gabra2*, *Gabrb1* and *Gabra4* show many gained interactions and *Gabrb1* and *Gabra4* are both upregulated. In addition, the top two terms in our DI GO term enrichment analysis were “regulation of membrane potential” and “cell junction assembly” and there were many other gene sets associated with ion transport and neurogenesis (Fig. 4.2 and Supplementary Fig. 4.2). A recent proposed model of ageing proposes ageing as a loss of the collective goal of cells mediated by changes in the bioelectric network, which is governed primarily by regulation of ion-channels (Pio-Lopez & Levin, 2024). A promising avenue of further research would be to determine if there is a difference in bioelectric patterns in young vs old bone marrow and whether the manipulation of ion-channels could restore old bioelectrical patterns in the bone-marrow to a younger state.

We determined so-called lineage inappropriate genes (LIGs) which are not expressed in young blood lineages but are upregulated in aged LT-HSCs, genes which are normally expressed in other lineages. For example, *Rcvrn* (coding for Recoverin) is normally

expressed in retinal cells and yet is expressed in aged LT-HSCs but not in any young blood progenitors (Fig. 4.3A and 4.3C panel 1). Our finding that LIGs (which are also DEGs) show a disproportionate overlap with DI regions in the Hi-C data compared to other upregulated DEGs, suggests that the regions of chromatin around the LIGs are susceptible to age-associated 3D chromatin changes that lead to expression of these genes. We speculate that the expression of lineage inappropriate genes is a consequence of an overall increase in disorder of the chromatin interactions (TF mediated low-frequency enhancer-promoter interactions), which could allow for the selection of LT-HSCs in which these changes are advantageous for survival and proliferation. Examination of the mutational burden of aged murine LT-HSCs would be required to assess whether mutations linked to clonal hematopoiesis are also involved.

We also report a strong enrichment of AP-1 binding motifs in the DARs that overlap regions of age-gained interactions, in line with a recent paper demonstrating in 22 different murine cell types that regions that increase in chromatin accessibility during ageing show enrichment for AP-1 binding motifs (Patrick et al., 2024). Our novel multi-omic integration pipeline uniquely integrates Hi-C interaction data with ATAC-seq and RNA-seq using a hybrid workflow of STARE (Hecker et al., 2023) and the TF prediction tool ANANSE (Xu et al., 2021). ANASE is normally used to predict TFs for direct cell reprogramming of one cell type to another, but which we have adapted to predict TFs that govern different states of LT-HSCs ageing. Wahlestedt and colleagues demonstrated that aged myeloid-biased LT-HSCs can be epigenetically reset to have a balanced output via reprogramming to a pluripotent state (Wahlestedt et al., 2017). However, there is a growing use of direct reprogramming factors to reinforce the cell identity lost with age (Roux et al., 2022) or other factors that promote youthful gene expression (Sengstack et al., 2026) or epigenetic patterns (de Lima Camillo et al., 2025) without any transition through a pluripotent state. From our Hi-C informed GRN analysis in LT-HSCs, the TFs most strongly predicted to drive the aged state are c-Maf, Cebpd & Atf3 and thus would be candidates for inhibition. On the other hand, Gfi1, Hif3a, Sox4 and Hes1 overexpression are predicted to be candidates to restore the youthful LT-HSC gene regulatory network state.

The results of our differential GRN analysis are strongly supported by the literature. For example, c-Maf family proteins have known roles in LT-HSC proliferation and maintenance

(Asano et al., 2025; Hurt et al., 2004). As shown by us and others (Itokawa et al., 2022; Mooney et al., 2017), Flt3 mRNA expression is detectable in LT-HSCs (even though the protein is not present on the surface of during sorting) and is downregulated in aged LT-HSCs. Interestingly, our Hi-C informed differential GRN predicts that c-Maf regulates the TFs Lyl1 and Mnt which both induce Flt3 downregulation in aged LT-HSCs (Fig. 4.4 C), although the role of Flt3 in LT-HSCs, where it is lowly expressed and not present on the cell surface, is still relatively unexplored. Meanwhile, the 2nd most highly ranked age-driving TF, Cebpd, is known to promote myeloid differentiation (Pawar et al., 2014) and both c-Maf1 and Cebpd are predicted to drive the upregulation of Gadd45g (Fig. 4.4C and Supplementary Fig. 4.4C), which has known roles in driving HSCs out of quiescence toward differentiation (Thalheimer et al., 2014). Furthermore, Atf3 (next in the ranked list) is known to prevent stem cell exhaustion (Liu et al., 2020), promote myeloid cell differentiation (Perrone et al., 2023) and both Cebpd and Atf3 are predicted in our differential GRN to directly downregulate the TF Bach1 (Supplementary Fig. 4.4A and B), which is known to suppress myelopoiesis (Itoh-Nakadai et al., 2014; Kato et al., 2018). Thus, inhibition of one or more of these TFs could potentially prevent the myeloid-biased output of aged murine LT-HSCs. It is also worth noting that the most highly ageing-upregulated TF is Rorb (which is also a LIG) and is predicted in the ageing-specific differential GRN to drive the downregulation of the TFs Dbp & Nr4a1 (Supplementary Fig. 4.4C), which have known roles associated with neuronal excitability, connectivity, and circadian rhythms in the brain (Kunst et al., 2015). Thus, our results predict a role for these neuron related TFs in LT-HSC ageing.

The TFs predicted to reprogram cells back to a youthful state in our analysis also have good evidence from the literature linking them to LT-HSC maintenance. For example, Gfi1 has roles in regulating differentiation and proliferation of LT-HSCs (Hock et al., 2004; Khandanpour et al., 2011), Hes1 is required to prevent stem cell exhaustion (Ma et al., 2020), while the role of Hif3a is less understood. In addition, Sox4 downregulation is thought to enable myeloid differentiation (Aue et al., 2011) and has known pioneer factor abilities (Katsuda et al., 2024). Our young LT-HSC-specific differential GRN predicts that Gfi1 & Hif3a both target Sox4 which upregulates the TF, Bach1 (Fig. 4.5D & E), which is known to supress myelopoiesis (Itoh-Nakadai et al., 2014; Kato et al., 2018). This appears to be the opposite role of Cebpd and Atf3, which are predicted to downregulate it, suggesting an

antagonistic role of Gfi1 & Hif3a via Sox4 in combating age-associated gene expression changes driven by Cebpd and Atf3.

In summary, we have described epigenetic changes in aged murine LT-HSCs associated with the degradation of cell identity and expansion of myeloid-primed LT-HSCs. AP-1 factors and factors such as c-Maf, Cebpd and Atf3 are top age-driving factors, while Gfi1, Hif3a, Sox4 and Hes1 are strong candidates for restoring the youthful LT-HSC state. While the roles of these individual factors have been previously studied, often in the context of oncogenesis and blood cancers (Binod et al., 2024; Foronda et al., 2014; Hönes et al., 2017; Tian et al., 2013), TFs for cellular reprogramming are usually described as collections or cocktails of TFs due to their combined effect on the overall GRN, effects that are generally difficult to predict with single knockout or overexpression experiments. Future reprogramming experiments would likely benefit from assessing knockdown or overexpression of various combinations of our top ranked TFs to see if balanced and robust differentiation can be restored to aged murine LT-HSCs.

4.5 Methods

4.5.1 HSC, monocyte and NK cell isolation

For isolation of LT-HSCs, bone marrow from young (8-12 weeks old) and aged (100-130 weeks old) C57BL/6 female mice was harvested by extracting femur, tibia and pelvic bones, crushing with mortar and pestle in PBS with 2% FBS (FACS buffer) and filtering through 45 µm filter. Filtered bone marrow cells were then incubated with red cell removal buffer [RCRB; 156 mM NH4Cl (Sigma Aldrich), 11.9 mM, NaHCO3 (Sigma Aldrich) and 0.097 mM, EDTA, made in-house at WEHI] for 1 minute at room temperature (RT), pelleted at 1500 rpm, washed with FACS buffer, then lineage positive cells were depleted using the EasySep™ Mouse Hematopoietic Progenitor Isolation Kit (Stem Cell Technologies #19856) according to the manufacturer's instructions. The bone marrow of approximately 12 young mice and 6 aged mice was pooled per experiment with 3 experimental (biological) replicates performed.

For isolation of monocytes and NK cells, spleens from young (8-13 weeks old) and aged (100-104 weeks) C57BL/6 female mice were harvested, placed in ice-cold PBS,

mechanically dissociated using a 3 mL syringe plunger end, filtered through a 45 μm nylon mesh filter, incubated in 500 μL RCRB for 1 min at RT to remove red blood cells, then washed twice in ice-cold PBS. Centrifugation steps during red blood cell lysis and washing were performed at 1500 rpm at 4°C.

4.5.2 LT-HSCs antibody staining and FACS

Lineage depleted cells were incubated with the following antibodies on ice for 30 mins:

CD34-BV421 (Brilliant Violet 421™ anti-mouse CD34, BioLegend #152208)

Flt3-APC (Ms CD135 APC A2F10.1, Becton Dickinson #560718)

Sca1-BUV395 (Ms Ly-6A/E BUV395 D7 Becton Dickinson #563990)

c-Kit-BV711 (Ms CD117 BV711 2B8 Becton Dickinson #563160)

CD150-PE-Cy7 (PE/Cyanine7 anti-mouse CD150, TC15-12F12.2, BioLegend #115914)

CD48-APC-Cy7 (APC/Cyanine7 anti-mouse CD150, HM48-1, BioLegend #103432)

Lineage-biotin (Miltenyi Biotec Australia Pty. Ltd. #130-092-613)

Cells were then washed and incubated with Streptavidin-BV650 (SAV BV650, Becton Dickinson #563855) on ice for a further 15 mins. For staining of mitochrondrial membrane potential (MMPot), the lineage depleted cells were then incubated with TMRM (Image-iT TMRM Reagent, ThermoFisher #I34361) and 50 mM Verapamil hydrochloride (99%, Merck, #V4629-1G) for 30 mins at 37°C before staining with SYTOX Blue (Thermo fisher #S34857) on ice for 20 mins. MMPot High LT-HSCs ($CD34^-$ $CD48^-$ $Flt3^-$ $CD150^+$ $TMRM^{High}$ LSKs) and MMPot Low LT-HSCs ($CD34^-$ $CD48^-$ $Flt3^-$ $CD150^+$ $TMRM^{Low}$ LSKs) were FACS sorted (Supplementary Fig. 4.1A, B and C), yielding approximately 400,000 aged and 60,000 young LT-HSCs per experiment.

4.5.3 Monocyte & NK cell antibody staining and FACS

Splenocyte cell suspensions were incubated for 30 minutes on ice with the following antibodies:

CD44-FITC (IM7.81, in-house, WEHI, Vic, Australia)

B220-BUV395 (RA3-6B2, Becton Dickinson #563793)

TCRβ-APC-eFluor 780 (H57-597, eBioscience #47-5961-82)

Ly6C-eFluor 450 (HK1.4, eBioscience #48-5932-82)
CD115-BV605 (T38-320, Becton Dickinson #743640)
Ly6G-PE (1A8, Becton Dickinson #551461)
CD4-APC (GK1.5-7, in-house, WEHI, Vic, Australia)
NK1.1-PE-Cy7 (PK136, Becton Dickinson #552878)
CD62L-biotin (MEL-14, Becton Dickinson # 553149)

Cells were washed and stained for a further 15 mins with Streptavidin-Alexa594 (Thermo fisher #S32356), washed again and stained with Sytox blue (Thermo fisher #S34857) for 30 mins on ice. Monocytes ($B220^-$ $TCR\beta^-$ $CD115^+$ $Ly6C^+$) and NK cells ($B220^-$ $TCR\beta^-$ $NK1.1^+$) were FACS sorted (Supplementary Fig. 4.1E) yielding approximately 320,000-540,000 aged and 200,000 young monocytes per experiment; and yielding approximately 360,000-640000 aged and 770,000 young NK cells per experiment with 2 experimental (biological) replicates in total.

4.5.4 In situ Hi-C

Immediately following FACS, sorted MMPot High and Low LT-HSCs, or sorted monocytes and NK cells, were double fixed with 1% formaldhyde (10 mins) & 3mM disuccinimidyl glutarate (45 mins), pelleted at 850 × g at 4 °C, then snap frozen and stored at -80°C. Cells were then lysed in lysis buffer (10mM Tris-HCl pH8.0, 10mM NaCl, 0.2% Igepal CA630) with 50µl of protease inhibitors (Sigma, #P8340), washed with lysis buffer without protease inhibitors, then nuclei were placed in 0.5% sodium dodecyl sulfate (SDS) and incubated at 62°C for 10 minutes. The SDS was then quenched with 10% Triton X-100 (Sigma, #93443) for 15 mins at 37°C, then 100U of MboI restriction enzyme (NEB, #R0147) was added and the mixture incubated at 37°C overnight. The MboI enzyme was inactivated by heating to 62°C for 20 minutes, DNA fragment ends were biotinylated by incubating nuclei with biotin-14-ATP, dCTP, dGTP and dTTP and 5 U/µL DNA polymerase I Klenow (NEB, #M0210), then incubating at 37°C for 90 minutes with rotation. Proximity ligation was performed using 2000 U of T4 DNA Ligase (NEB, #M0202), incubating at room temperature for 4 hours with slow mixing on a rotator. Nuclei were lysed and crosslinked proteins were degraded by adding 50µl of 20mg/ml proteinase K (NEB, #P8107) and 120µl

of 10% SDS, incubating at 55°C for 30 minutes, then 130µl of 5M sodium chloride was added and the mixture incubated at 68°C overnight with rotation.

4.5.5 Hi-C DNA library preparation and sequencing

Hi-C DNA libraries were prepared by first purifying the biotinylated DNA: 1.6X volumes of pure ethanol and 0.1X volumes of 3M sodium acetate, pH 5.2, was added to each tube, mixed by inverting and incubated at -80°C for 15 minutes. DNA solutions were centrifuged at maximum speed for 15 minutes at 4°C, supernatant discarded, then precipitated DNA pellets washed twice with 70% ethanol, then resuspended in Tris buffer (10 mM Tris-HCl, pH 8) and incubated at 37°C for 15 minutes to fully dissolve the DNA. The purified biotinylated DNA was placed in 130µl Covaris microTUBEs (TrendBio, #520045) and sheared using the Covaris S220 (fill level: 10, duty cycle: 10, PIP: 175, cycles/burst: 200, time: 58 s). Sheared biotinylated DNA was purified using Dynabeads MyOne Streptavidin C1 beads (10mg/ml, ThermoFisher #65002) in Tween washing buffer (5mM Tris-HCl pH 7.5; 0.5mM EDTA; 1M NaCl; 0.05% Tween 20), DNA separated using a magnet, washed twice with buffer, then resuspended in 10 mM Tris-Cl pH 8.0. DNA libraries were end-repaired and Illumina sequencing barcodes added using the NEBNext Ultra DNA Library Prep Kit for Illumina (NEB, #E7645). The Hi-C libraries were then PCR amplified using the Phusion Taq polymerase (NEB, #M0530S) with P5+P7 primer cocktail (in-house, WEHI) and 9 cycles of PCR. Amplified DNA was then size-selected and purified using AMPure XP beads (Beckman Coulter, #A63881) and magnetic separation, then final libraries resuspended in 10mM TrisHCl pH 8. Libraries were prepared for 3 separate Hi-C experiments for LT-HSCs and 2 separate Hi-C experiments for monocytes and NK cells, then barcoded libraries were pooled. Pooled Hi-C libraries for LT-HSCs, or pooled monocytes and NK cells, were sequenced using the Illumina NextSeq 2000 sequencer on a P3 100 flow cell, using 66 bp paired-end reads.

4.5.6 Hi-C analysis

Reads were aligned using Bowtie2 v.2.5.3 (Langmead & Salzberg, 2012), duplicates were marked using Picard tools v.3.3.0 (Broad Institute, 2023), files sorted using Samtools v. 1.21 (Li et al., 2009). Differential analysis was performed on three replicates per condition for

LT-HSC (combined low and high MMpot) and two replicates per condition for monocytes and NK cells, in two separate analysis using diffHic v.1.36.1 (A. T. Lun & G. K. Smyth, 2015). In brief, pairwise interactions were quantified at 100 kbp resolution using the squareCounts function. Genomic fragments were defined using an mm39 reference, and analyses were restricted to canonical chromosomes. Low-abundance and artifactual interactions were removed by applying filterDirect, which estimated non-specific ligation rates from inter-chromosomal pairs, and filterDiag to eliminate short-range (diagonal) contacts. For differential interaction analysis, systematic non-linear biases (including distance-dependent trends) were corrected by calculating offsets using the normOffsets function with method="loess" from the csaw (Lun & Smyth, 2016) package. These offsets were calculated separately for near-diagonal (<500 kbp) and far-diagonal/inter-chromosomal interactions to account for distinct noise profiles. Differential interactions were then identified using the edgeR v.4.2.2 (Chen et al., 2025; Robinson et al., 2010) quasi-likelihood (QL) framework. Interaction data were converted into a DGEList, and biological variability was modelled through dispersion estimation with estimateDisp and glmQLFit. Differential interaction analysis between aged and young samples was then performed using glmQLFTest with subsequent multiple testing correction (FDR < 0.1), and significant interactions were annotated with genomic coordinates using GenomicRanges (Lawrence et al., 2013) and visualized using custom ggplot2 v.4.0.1 (Wickham, 2016) plots and using Integrative Genomics Viewer (IGV) v3.0.0 (Thorvaldsdóttir et al., 2013). Additional Hi-C heatmap and multitrack plots were made using the plotgardener v1.14.0 R package (Kramer et al., 2022), but for this the Hi-C data had blacklisted sites removed, replicate merged and counts normalized using Iterative Correction and Eigenvector decomposition (see the Methods section “Topologically associated domains (TAD) analysis” for details).

4.5.7 Gene biological pathway enrichment analysis

Genes or DEGs that overlap regions of age-increased and age-decreased interactions were analysed using the R package clusterProfiler (Yu et al., 2012) by running the goenrich and enrichPathway functions with the default settings recommended in the documentation (p value 0.05, q value 0.2, with BH correction for the adjusted p value), and the results plotted using the dotplot and heatplot functions from the enrichplot v1.28.4 (Yu, 2025) package.

4.5.8 Topologically associated domains (TAD) analysis

Hi-C data were processed using HiCExplorer v3.6 (Ramirez et al., 2018) for TAD analysis. Initially, mm39 aligned BAM files were coordinate-sorted using SAMtools v1.22.1 (Li et al., 2009) and reads overlapping mm39 blacklisted regions were removed via bedtools intersect. The filtered BAMs were then name-sorted and converted to pairs format using pairtools v1.1.3 (Open2C et al., 2024) with a minimum mapping quality of 30, a unique walks-policy, and a maximum inter-align gap of 20 bp. Subsequent steps included sorting, deduplication (allowing up to three mismatches), and filtering to retain valid intra- and inter-chromosomal interactions (with a minimum distance of 1 kb), thereby generating high-confidence interaction pairs. These pairs were converted into contact matrices in the .cool format, and replicates were merged using cooler merge. Finally, the merged .cool files were transformed into the HDF5 (.h5) format with hicConvertFormat.

The resulting Hi-C contact matrices were normalized using hicNormalize with the 'smallest' normalization method across multiple resolutions (ranging from 10 kb to 2 Mb) to ensure data comparability. Diagnostic plots were generated using hicCorrectMatrix, and matrices were further corrected using Iterative Correction and Eigenvector decomposition (ICE) normalization, with threshold values determined from the diagnostic plots. These ICE normalized, merged Hi-C files were for all Hi-C heatmap plots using the plotgardener v1.14.0 R package (Kramer et al., 2022). TADs were subsequently identified at 100kbp resolution using hicFindTADs, where the step size was set to the resolution and the minimum and maximum depths were defined as three- and ten-fold the resolution, respectively. TAD separation scores from hicFindTADs were then plotted for each condition (aged and young) and the significance of the difference in distribution determined using a Mann Whitney U test.

4.5.9 Compartment analysis

Compartment analysis was performed using HiCDOC v.1.6.0 (Kurylo et al., 2023). Raw data stored in .cool files were first organized into HiCDOCDataSet objects by extracting resolution-specific replicates and conditions (aged vs. young) via the function HiCDOCDataSetFromCool. To ensure data quality, matrices were filtered using a series of

functions: filterSmallChromosomes removed chromosomes below a set length threshold, filterSparseReplicates excluded replicates with fewer than 5% non-zero interactions, and filterWeakPositions eliminated bins with average interactions below 1/6th of the overall signal.

Normalization was performed in three sequential steps to correct for technical, biological, and distance-dependent biases. Technical biases were normalized using normalizeTechnicalBiases (employing cyclic loess normalization), followed by normalizeBiologicalBiases to adjust for sample-specific effects, and finally, normalizeDistanceEffect was applied with resolution-specific loess sample sizes to correct for the decay of interaction frequency with genomic distance. A/B compartments were then detected using detectCompartments and compartment differences between conditions were identified using the differences function (threshold = 0.05). For the final analyses, only the 200 kbp resolution data were used to generate compartment assignments, differential calls, and corresponding visualizations with plotCompartmentChanges.

4.5.10 Shannon entropy analysis

Shannon entropy was calculated using a method similar to Jenkinson et al. (Jenkinson et al., 2017) by calculating the probability distribution of interactions of all 100 kbp bins within each 2 Mbp span. Entropy value distributions in young vs aged were then compared using a Mann Whitney U-test. In brief, MMPot high and low merged Hi-C BAM files (3 aged, 3 young) were initially processed using custom bash scripts to downsample the coordinate-sorted BAM files to a common depth: Unique read counts for each sample were determined and the minimum unique read count was used as a reference to calculate a downsampling fraction. BAM files were then subsampled using the SAMtools v1.22.1 (Li et al., 2009) view command with a fixed random seed (42) to ensure reproducibility, then a name-sorting step was performed to prepare the files for downstream analysis.

Downsampled Hi-C interaction matrices were imported into R as InteractionSet (Lun et al., 2016) objects. Bins were first filtered based on their size (e.g., retaining those within 90–110 kb) to maintain a consistent resolution. Genomic spans of 2 Mbp were then generated using the GenomicRanges tileGenome function (Lawrence et al., 2013), and bins were mapped to these spans via findOverlaps. Within each span, the interaction counts for each

sample in each condition were aggregated by unique bin-pair identifiers so only aged and young samples were compared. Probabilities were computed from these counts, and Shannon entropy was calculated as the negative sum of the probability multiplied by the $\log_2$ of the probability. This step was adapted from established protocols (Jenkinson et al., 2017; Liu et al., 2022) to capture the local interaction variability within defined genomic spans. Distribution of entropy values were compared between aged and young LT-HSCs using a non-parametric Mann Whitney U-test.

4.5.11 RNA-seq analysis

RNA-seq data for aged and young LT-HSCs from Itokawa et al., 2022 (GSE162607) were analysed for differential expression as follows: Raw sequencing reads were subjected to quality control and adapter trimming. Adapters were removed and reads were filtered for a minimum length of 20 bp and a quality score of 20 using Cutadapt 4.9 (Martin, 2011). The quality of trimmed reads was further assessed using FastQC v0.11.x (Andrews, 2010). Cleaned reads were then aligned to the GRCm39 reference genome (Ensembl release 113) using STAR 2.7.11b (Dobin et al., 2013). Alignment was performed in two-pass mode, and output was sorted by coordinate into BAM format.

Gene-level read counts were quantified from the aligned BAM files using featureCounts from Subread v2.0.6 (Liao et al., 2013), with annotations provided by the _Mus musculus_ GRCm39.113 GTF file. Downstream differential expression analysis was conducted in R using the edgeR package 4.2.2 (Chen et al., 2025; Robinson et al., 2010). Gene annotation information, including Entrez Gene IDs and MGI symbols, was retrieved from Ensembl (mmusculus_gene_ensembl dataset) using the biomaRt R package (Durinck et al., 2009). A design matrix was constructed using the model.matrix function so that groups of the same age and cell type were compared (aged vs young LT-HSCs), then lowly expressed genes were filtered using filterByExpr, followed by Trimmed Mean of M-values (TMM) normalization to account for library size and compositional biases. A Quasi-Likelihood Negative Binomial Generalized Linear Model (GLM) was fitted, and differential expression was determined using Quasi-Likelihood F-tests. Genes with a false discovery rate (FDR) adjusted p-value of less than 0.05 were considered statistically significant. Genomic ranges for differentially expressed genes were subsequently incorporated using the rtracklayer

v.1.68.0 R package (Lawrence et al., 2009), based on the same Ensembl GTF annotation. Importantly, LT-HSCs surface markers used for sorting cells in the GSE162607 dataset, i.e. Il-7^{-} CD34^{-} CD48^{-} Flt3^{-} CD150^{+} LSKs, are similar to those used for our Hi-C experiments, where Itokawa et al. use IL-7 to also isolate Il-7$^{-/+}$ later progenitors CLPs, MEPs and GMPs (See (Itokawa et al., 2022)).

The differential expression values used to build gene regulatory networks were generated in R using DESeq2 v.1.48.2 (Love et al., 2014) on the STAR count matrices for LT-HSCs only. DESeqDataSet objects were constructed using DESeqDataSetFromMatrix, library size normalization was performed by estimating size factors with estimateSizeFactors and differential expression testing was then carried out using DESeq using alt_hypothesis = 'greaterAbs', independent_filtering = TRUE, p_adjust_method = 'BH' and minmu = 0.5. Pairwise contrasts were performed for aged/young or young/aged depending on whether the target condition was aged LT-HSCs or young LT-HSCs, respectively.

4.5.12 Determination of lineage inappropriate expression

Raw RNA-seq expression counts for LT-HSCs, MPP1-4s, MEPs, GMPs and CLPs from the Itokawa et al. 2022 data (GSE162607) were normalized by a recently described technique called gene length corrected trimmed mean of M-values (GeTMM) (Smid et al., 2018), which uses edgeR's TMM normalization on read counts that have been adjusted by gene length. By filtering for only genes that were significantly differentially expressed and setting upper and lower log2GeTMM expression thresholds we defined a set of genes lowly expressed or absent in young blood progenitors, which have low or negligible expression [$\log_2$(GeTMM) < 2.71] in young LT-HSCs, MPP1-4s, GMPs, MEPs or CLP and significantly higher expression [$\log_2$(GeTMM) > 2.88] in aged LT-HSCs. Restricting our definition again to genes that have near zero expression [$\log_2$(GeTMM) < 1] in young blood progenitors further defined genes we term "lineage inappropriate genes" (LIGs).

4.5.13 ATAC-seq analysis

ATAC-seq FASTQ files from the Itokawa et al (2022) dataset (GSE162551) were quality-checked with FastQC v0.11.x (Andrews, 2010) and reads aligned to the GRCm39 mouse reference genome using Bowtie2 v2.5.3 (Langmead & Salzberg, 2012) and converted to

BAM with SAMtools v1.22.1 (Li et al., 2009); alignments were coordinate-sorted and PCR duplicates were removed with Picard v3.1.1 (Broad Institute, 2023) using MarkDuplicates (REMOVE_DUPLICATES=true). Deduplicated alignments were filtered to retain mapped reads with mapping quality ≥10, and mitochondrial reads were excluded; filtered BAMs were then indexed. To remove artefactual signal, reads overlapping genomic exclusion regions from mm39.excluderanges (Ogata et al., 2023) were removed with BEDTools v2.31.1 (Quinlan & Hall, 2010) and the remaining reads were re-sorted and indexed. Peaks were called per sample using MACS3 v3.0.1 (Y. Zhang et al., 2008) with an effective genome size of 2,654,621,783 using the arguments --nomodel --shift -100 --extsize 200 with a significance threshold of q≤0.05.

Differential chromatin accessibility analysis was performed in R using DiffBind v3.18.0 (Stark & Brown, 2011) on blacklist-filtered ATAC-seq BAM files and MACS3 narrowPeak calls and analyses were restricted to primary autosomes (1–19) and chromosome X. A DiffBind sample sheet was constructed from the study metadata, and a consensus peakset was generated with minOverlap=2 to harmonize peak coordinates across samples. Read counts over consensus peaks were obtained with SummarizeOverlaps (bUseSummarizeOverlaps=TRUE) and, to reduce between-lineage variability, differential accessibility was performed separately for each hematopoietic cell type (LT-HSC, MPP1–4, GMP, MEP, CLP). For each cell type, an offset-based loess normalization was performed and differential testing was run as aged versus young using edgeR within DiffBind. Differentially accessible regions (DARs) were defined at FDR < 0.05.

4.5.14 Motif enrichment analysis

Transcription factor (TF) binding motif enrichment analysis was performed on regions of differential interactions (DIs) identified in Hi-C data from aged versus young LT-HSCs at 100 kbp resolution. Briefly, DI regions were intersected with differentially accessible regions (DARs) determined from analysis of the Itokawa et al (2022) ATAC-seq dataset. Mouse TF binding motifs were retrieved from the HOCOMOCO v13 (Vorontsov et al., 2024) and database and filtered to only include TFs with a TPM > 0.1 in the Itokawa et al (2022) RNA-seq dataset, then converted to position weight matrices lists using the universalmotif v1.26.2 (Tremblay, 2024) and TFBSTools v1.46.0 (Tan & Lenhard, 2016) R packages. Enrichment

of filtered TF motifs in DARs overlapping DIs was then performed using the monaLisa R package (Machlab et al., 2022). For enrichment of TF motifs in DARs overlapping DIs, only DARs and DIs that change in the same direction (age-opening DARs with gained DIs, or age-closing DARs with lost DIs) were analysed. To enable binning, a combined DAR-DI "logFC score" was calculated by multiplying together the log_2FoldChange values for the DARs and the DIs they overlap, then making the age-closing/lost interaction scores negative by multiplying it by -1. The logFC scores were then binned into 4 bins and the DARs were analysed using the monaLisa calcBinnedMotifEnrR function. Results were filtered for motifs that were significantly enriched (enrichment adj.p < 0.05) then plotted using the plotMotifHeatmaps function.

4.5.15 Network analysis and transcription factor ranking

In summary, TF-gene affinities were calculated using the STARE pipeline (Hecker et al., 2023) in gABC mode by combining Hi-C data and ATAC-seq data then mapping TF motifs to the ATAC-seq peaks and aggregating TF binding scores from different peaks assigned to the same gene. TF-gene affinities were then combined with RNA-seq expression values to generate GRNs. Differential GRNs were generated by subtracting the network weights of one condition from another and TFs were ranked, following the ANANSE pipeline (Xu et al., 2021), according to their strength of influence on the overall changes in network weights.

Firstly, Hi-C contact matrices that had previously been blacklist-filtered and ICE normalized were converted to STARE-compatible contact files. For each condition (young and aged LT-HSCs), Hi-C contact matrices at 100 kb in .h5 format were converted to a genome-wide GInteractions-style TSV using hicConvertFormat from HiCExplorer v3.6 (Ramirez et al., 2018) and then split by chromosome. For each chromosome, intra-chromosomal contacts were kept and written as a three-column STARE contact files (bin1, bin2, contact) at the chosen bin size (100 kb). ATAC-seq peak summits from all young and aged LT-HSC replicates were mereged, reduced to 1 bp summit positions, and expanded symmetrically by ±250 bp using the BEDTools v2.31.1 (Quinlan & Hall, 2010) slop command with mm39 chrom sizes to create a union set of fixed 500 bp windows. Windows overlapping mm39 blacklist regions were removed (bedtools subtract). Per-peak activity was quantified by counting overlaps of each union window with filtered ATAC-seq BAM files

using bedtools coverage -counts. The resulting peak-by-sample count matrix was imported into R and normalized with the csaw v1.42.0 (Aaron TL Lun & Gordon K Smyth, 2015) normOffsets function. Condition-specific chromatin accessibility was then summarized as offset normalized counts per million (CPM) for each replicate and as the mean CPM per condition, and written back to a BED-like table (chr, start, end, peak_id, per-replicate CPMs and Young/Old mean CPM).

These accessibility peak windows, together with the normalized Hi-C contacts and genome annotations, were then used as input to STARE in ABC mode to compute enhancer-gene ABC scores and TF-gene affinities. STARE was run via the provided STARE.sh driver script with the union ATAC-seq peak windows as -b, the Ensembl GRCm39 (mm39) primary assembly FASTA as -g, and the corresponding Ensembl GTF annotation as -a. For the ABC model we supplied the per-chromosome Hi-C contact files (-f), the Hi-C bin size (-k 100000), the column number for the mean ATAC-seq CPM value for each condition from per-peak activity table (-n), a gene-centred window of 5 Mb around TSSs (-w 5000000), an enhancer window of 5 Mb for the adapted ABC adjustment (-m 5000000), an ABC score cutoff of 0.02 (-t 0.02), and enabled both pseudocounts and the adapted ABC scoring (-d True, -q True) with tss_mode set to all_tss. Position-specific energy matrices (PSEMs) were generated from transfac-format PSCMs using the built-in PSCM-to-PSEM conversion. STARE was run using the HOCOMOCO-derived H13 CORE (Vorontsov et al., 2024) TF motif set. STARE first extracted open-chromatin sequences from the reference genome (bedtools getfasta), cleaned non-canonical bases, and then computed TF-DNA affinities for each peak using TRAP, which sums the per-position binding probabilities for each peak region, followed by integration of TRAP scores, ABC enhancer-gene scores and TSS annotations to produce TF-gene affinity matrices for each condition (young and old LT-HSCs). To make the STARE output compatible with ANANSE influence, the TF-gene affinity matrix values were scaled to a value of between 0 and 1. Mean TPM expression for target genes and TFs was then computed, rescaled to between 0 and 1, then these scaled expression values were used to modulate the scaled TF-gene affinity matrix scores ($affinity_{[0,1]}$) such that each TF-gene edge weight becomes $prob_{TF,gene}$ using the following:

$$\text{prob}_{TF,gene} = affinity_{[0,1]}\left(0.5 + 0.5 \cdot TF_expr_{[0,1]}\right)\left(0.5 + 0.5 \cdot target_expr_{[0,1]}\right)$$

These expression-weighted affinity (prob) values were then used by the ANANSE influence command to rank the TFs in several steps using the DEG logFC values. First a differential network (Old - Young or Young - Old) was built by subtracting the source GRN from the target GRN (i.e. the modified STARE networks with the "prob" values as network edges), where only edges with positive differences (higher values in the target condition) were kept. For each TF, a Target score was then computed by summing, over all DEGs reachable within two steps in this differential network, the product of each TF's target gene connection weights and the target gene expression-change score (i.e. the $|\log_2 FC|$):

$$Target\ score\ = \sum network\ weight\ x\ |target\ gene\ logFC|$$
$$(for\ all\ DEGs\ within\ 2\ steps\ of\ the\ TF)$$

A G_score equal to the TF's own expression-change score ($|\log_2 FC|$ if upregulated and padj < 0.05) was also assigned:

$$G\ score\ = |logFC\ of\ TF\ itself|$$

Finally, ANANSE influence ranked TFs by an Influence score, whereby the rank is equivalent to:

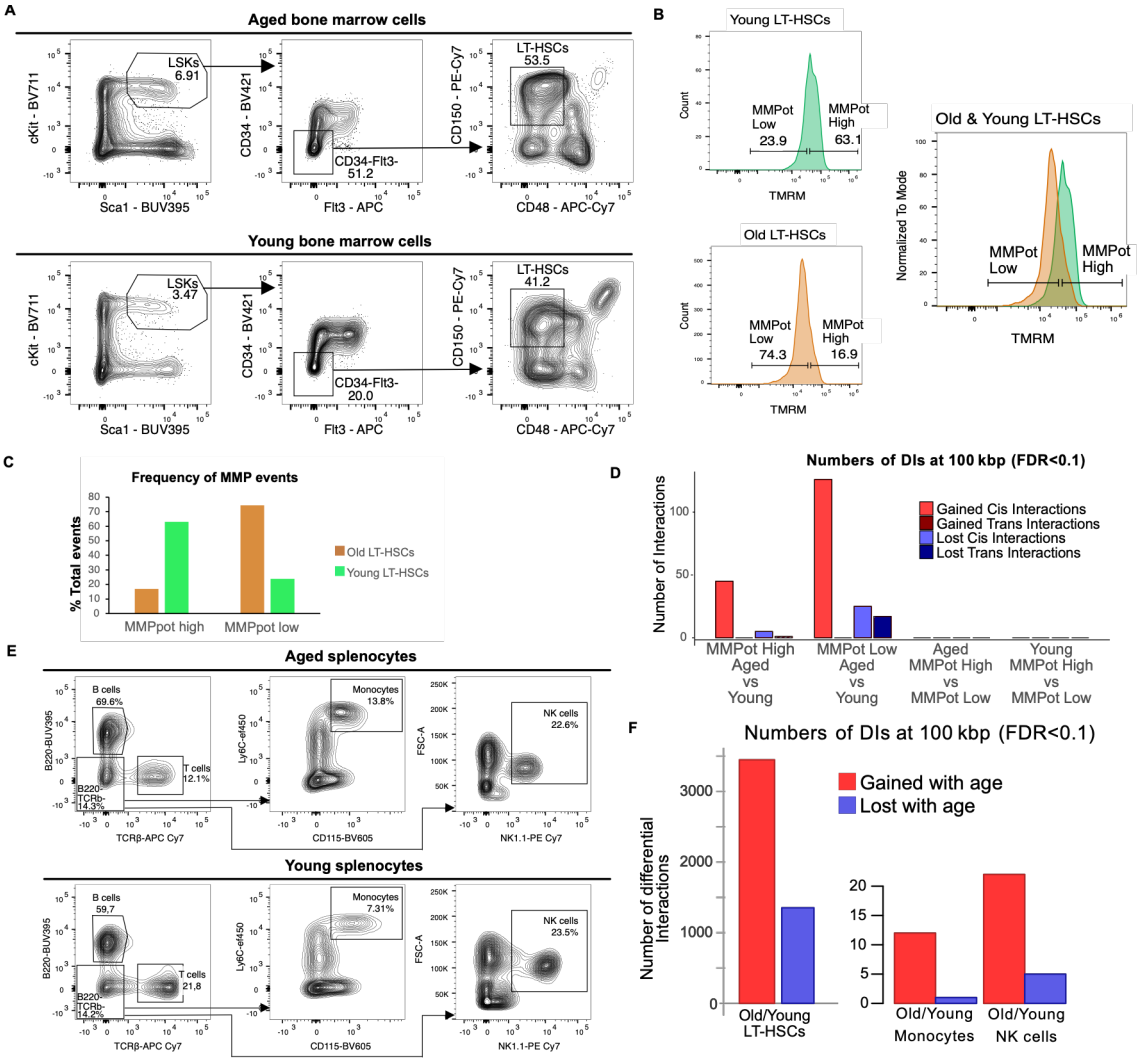
$$Rank\ (Influence)\ = Target\ score\ + G\ score$$

The TF Rank (Influence score) is derived by summing the Target score and G score then scaling to a value between 0 and 1. A TF is thus highly ranked if it is strongly connected to multiple target DEGs (1 or 2 steps away in the network) that have high changes in expression and if the TF itself is strongly upregulated, but whereby the connectivity to multiple DEGs generally has more influence in the final ranking.

Differential GRN plots were generated in R by importing the TF influence table and differential network (source, target, weight) with readr v 2.1.5 (Wickham et al., 2024) and dplyr v 1.1.4 (Wickham et al., 2023), constructing directed graphs with igraph v 2.2.1 (Csardi & Nepusz, 2006), then visualising them with ggraph v 2.2.2 (Pedersen, 2025) and ggplot2 v4.0.1 (Wickham, 2016). For each TF of interest, a TF-centered network was extracted to a maximum path length of two steps (max_steps = 2) to reflect ANANSE's influence

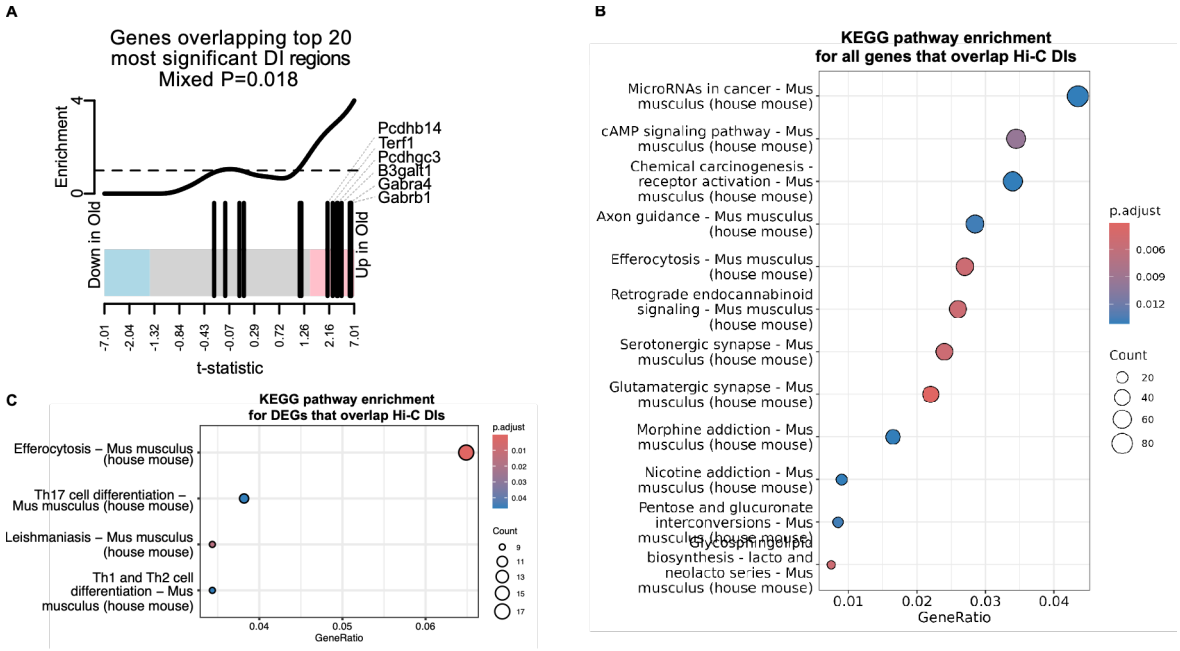
neighbourhood, and edges were restricted to outward connections only to emphasise TF→TF→gene cascades. To limit visual complexity, the differential network was filtered to the strongest edges (weight $\geq 1\times10^{-4}$) and plotted subnetworks retained TF nodes plus differentially expressed target genes defined from DESeq2 results (padj ≤ 0.05 and $|\log2FoldChange| \geq 0.2$). The networks weights are shown in Supplementary Table 4.

4.6 Supplementary Figures for the paper in review "Multi-omic gene regulatory networks informed by 3D chromatin architecture reveal insights into hematopoietic stem cell ageing"

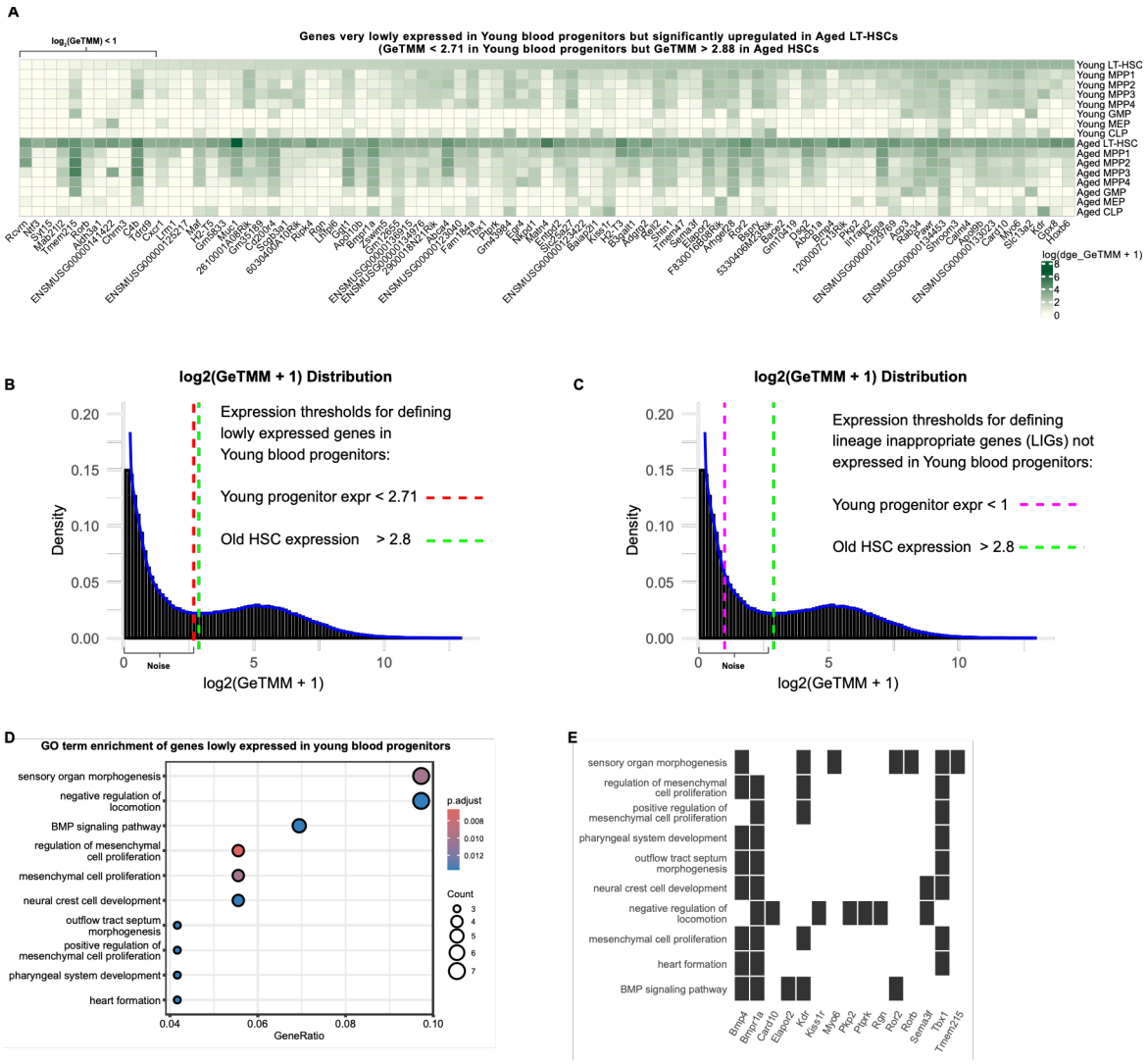


Supplementary figure 4.1. Sorting strategy and differential interaction results for murine (C57Bl/6) aged and young mitochondrial membrane potential (MMPot) high and low long-term hematopoietic stem cells (LT-HSCs), monocytes and NK cells. A. Fluoresence associtated cell sorting (FACS) plots for the isolation of aged and young LT-HSCs; B. FACS plots for isolation of aged (old) and young MMPot high and low LT-HSCs; C. Bar plot of the typical frequency (%) of MMPot high and MMPot low LT-HSCs obtained from each age condition; D. Differential interaction (DI) numbers for the four different contrasts tested, comparing either age or MMPot status, showing that ageing has a stronger effect than MMPot status; E. FACS plots for the isolation of murine (C57Bl/6) aged and young monocytes and NK cells; F. DI numbers for aggregated aged (old) versus young MMPot combined LT-HSCs (left) compared to old versus young

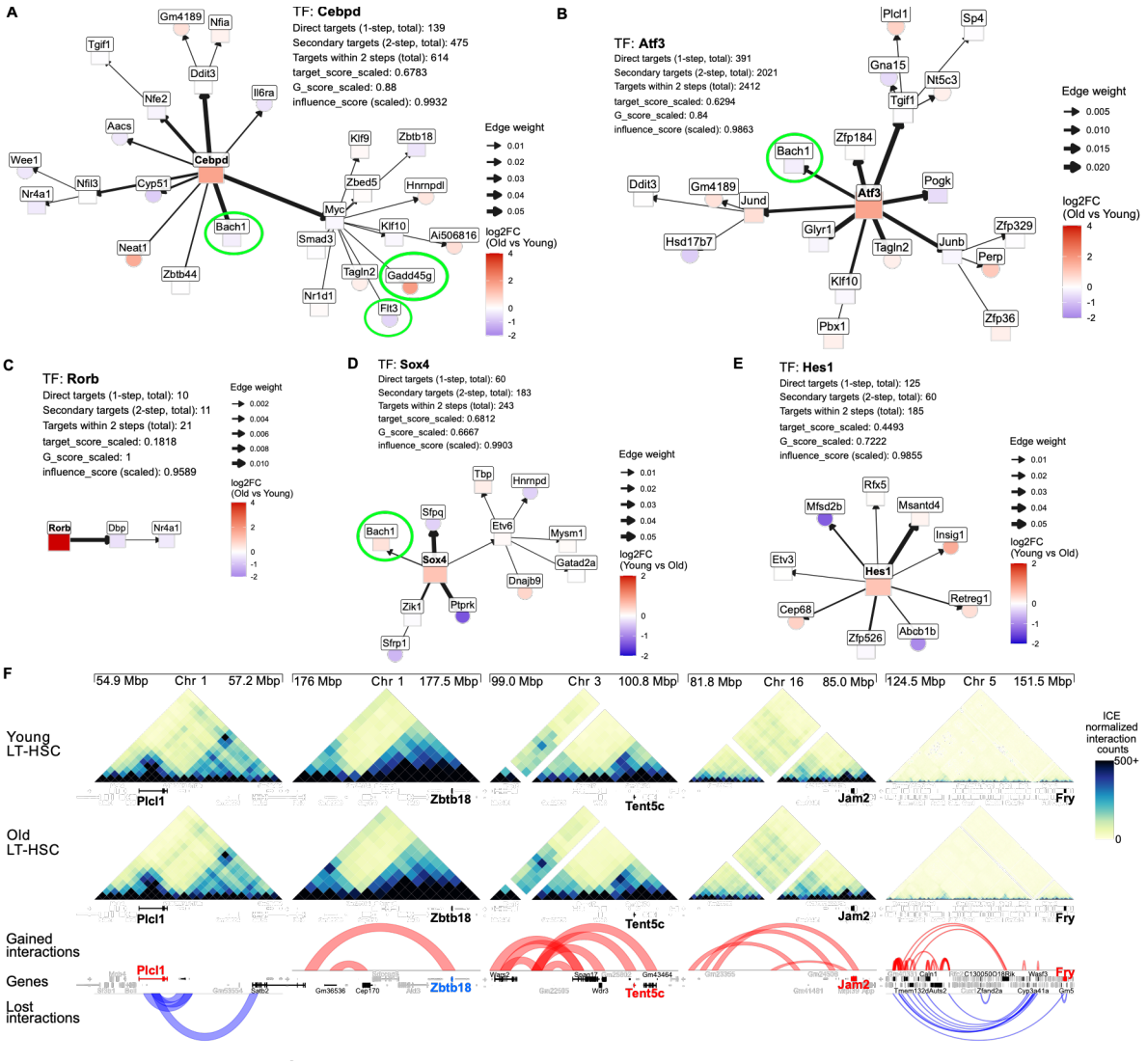
monocytes or NK cells, showing that these mature cell types acquire far less chromatin architecteral differences than LT-HSCs during ageing.



Supplementary figure 4.2. Fry test and KEGG pathway enrichment analysis results. A. Fry test showing that differentially expressed genes (DEGs) are enriched in the top 20 differentially interacting (DI) regions that alter interaction frequency with age and that the upregulated DEGs B3galt1, Gabra4, Gabra1 and Terf1 are particularly enriched in these top DI regions; B. Kyoto Encyclopedia of Genes and Genomes (KEGG) pathway enrichment analysis results for all genes that overlap HI-C DI regions that change with age in long-term hematopoietic stem cells (LT-HSCs); C. KEGG pathway enrichment analysis results for all DEGs that overlap HI-C DI regions that change with age in long-term hematopoietic stem cells (LT-HSCs).



Supplementary figure 4.3. Significantly upregulated genes in aged long-term hematopoietic stem cells (LT-HSCs) that are absent or lowly expressed in young blood progenitors. A. Heatmap of $\log_2$ transformed gene-length corrected trimmed mean of M-values (GeTMM) expression values for 85 genes that appear to be lowly expressed or not-expressed in young blood progenitors (GeTMM expression value < 2.71) but that are significantly upregulated in aged LT-HSCs (GeTMM expression value > 2.88); B. Distribution of $\log_2$ transformed GeTMM expression values to determine express value thresholds that define actual expression versus noise where genes defined as "expressed" were above the 2.88 threshold (green dashed line) and genes defined as "not expressed" or "very lowly expressed" were below the 2.71 threshold (red dashed line); C. Distribution of $\log_2$ transformed GeTMM expression thresholds for lineage inapproriate genes (LIGs) whereby the upper threshold of 2.88 remained the same (green dashed line) but the lower threshold for the "not expressed" genes was lowered to the $\log_2$ GeTMM value of 1 (pink dashed line); D. Gene ontology (GO) term enrichment results for the genes shown in panel A; E. GO terms and the gene sets that that are enriched in each term.



Supplementary figure 4.4. A. Simplified network diagram of the 2nd ranked age-driving TF, Cebpd, which is predicted to regulate 139 direct targets in this differential gene regulatory network (GRN), including the downregulation of the myeloid supressing TF Bach1 and regulation of Myc which in turn regulates Flt3 downregulation and Gadd45g upregulation (shown in green circles); B. Simplified network diagram of the 3rd ranked age-driving TF, Atf3, which is predicted to regulate 391 direct targets in this differential GRN, including the downregulation of Bach1 (shown in green circles) and upregulation of AP-1 factors such as Jund; C. Simplified network diagram of the 7th ranked age-driving TF, Rorb, which is predicted to regulate 10 direct targets in this differential GRN, including the downregulation of the TFs Dbp and Nr4a1; D. Simplified network diagram of the 3rd ranked youth-promoting TF, Sox4, which is predicted to regulate 60 direct targets in the young vs aged differential GRN, including the upregulation of the myeloid supressing TF Bach1 (shown in green circle); E. Simplified network diagram of the 4rd ranked youth-promoting TF, Hes1, which is predicted to regulate 125 direct targets in the young vs aged differential GRN, including the

downregulation of the sphingosine-1-phosphate transporter gene, *Mfsd2b*, and upregulation of the suppressor of cholesterol synthesis gene, *Insig1*; F. Hi-C heatmaps and arc-plots for Young and Aged LT-HSCs showing region interactivity that changes with age near the differentially expressed genes (DEGs) targeted by highest ranked age-driving TF, c-Maf, including the DEGs *Plcl1*, *Zbtb18*, *Tent5c*, *Jam2* and *Fry* (DEGs in red are upregulated, DEGs in blue are downregulated).

Chapter 5: Overall discussion, conclusions and future perspectives

As previously discussed, partial reprogramming with transient expression of the Yamanaka factors may be a viable way to restore some function to aged cells; yet partial reprogramming of aged HSCs using Yamanaka factors has not yet been reported. In chapter 2, I presented my attempts to optimise the expression of Yamanaka factors in HSCs and more broadly LSKs. My attempts to transfect LSKs with polycistronic expression cassettes harbouring OSKM, then later OSK, all failed to reach sufficient levels, despite successful expression in the hardier HEK293T cell line. For example, transfection of HEK293T cells with OSK-mNeonGreen DNA plasmid led to ~40% transfection efficiency. While transfection of LSKs with OSK-mNeonGreen DNA plasmids failed (0% transfection), transfection with the single gene positive control (Q25-mNeonGreen) DNA plasmid resulted in ~30% transfected LSKs (and 43% of the LT-HSC subpopulation) using the EH-100 nucleofection program, indicating that smaller plasmids are likely required. However, exogenous DNA is known to activate c-gas sting pathways (Langereis et al., 2015) making DNA plasmids imperfect for sensitive cell-types (e.g. HSCs).

There is evidence that modified mRNA containing 5-methyl cytidine and pseudouridine is less immunogenic (Alessio et al., 2017; Andries et al., 2015; Kariko et al., 2005; Papaioannou et al., 2023) and transfection of HEK293T cells with OS-mNeonGreen mRNA led to an impressive 69% transfection efficiency. Unfortunately, transfection of LSKs with modified mRNA such as OS-mNeonGreen was not attempted due to time constraints and the high cost of IVT reagents. However, transfection of LSKs with mRNA seems like a promising avenue and it is likely that splitting the cassettes into separate smaller cassettes made up of one transcription factor and one reporter could be the best option going forward. In addition, encasing each mRNA molecule within lipid nanoparticles (LNPs) may further increase transfection efficiency with reduced immunogenicity. For example, it has already been demonstrated by others that LNPs coated with CD117 (c-Kit) antibodies can be targeted to HSPCs with very high efficiency to deliver Cre recombinase mRNA (Shi et al., 2023) and Cas9 adenine base editor mRNA (Breda et al., 2023). In human HSPCs, virus like particles targeted to CD133 were able to specifically target and edit the genomes of $CD34^{+}$ human

HSCs in a humanized mouse model (Botchkarev et al., 2025). Furthermore, antibody-free LNPs made from certain ionizable lipids were demonstrated to specifically target human bone marrow progenitors in vivo (Xu et al., 2026). These examples demonstrate the high potential of targeting reprogramming factor encoding mRNA to aged HSCs.

Epigenetic reprogramming may be particularly necessary for cells that do not show restoration of function when transplanted into younger recipients, which is an intrinsic ageing phenotype of LT-HSCs. To circumvent the practical and translational difficulties of transcription factor-based reprogramming, chemical reprogramming is being explored, using molecules that either interact with cell surface receptors or permeate the cell membrane to activate or inhibit gene regulatory programs. For example, a screen of chemicals identified compounds such as valproic acid, CHIR-99021, E-616452 (RepSox), tranylcypromine and forskolin as able to reduce age-associated and senescence-associated leakage of nuclear proteins into the cytoplasm and transcriptomic signatures (J.-H. Yang et al., 2023b). Similarly, aged human fibroblasts treated with a cocktail of RepSox, trans-2-phenylcyclopropylamine (tranylcypromine), DZNep, TTNPB, CHIR99021, forskolin, and valproic acid displayed reduced DNA methylation clock age and transcriptomic clock age (Mitchell et al., 2024). A dual molecule reprogramming cocktail also restored molecular signatures of aged human cells *in vitro* and extended the lifespan of nematode worms (Schoenfeldt et al., 2025). Furthermore, a recent preprint showed that both overexpression of OSKM or chemical reprogramming with a cocktail consisting of tranylcypromine + RepSox ameliorates cellular senescence (Núñez-Quintela et al., 2026).

While individual -omics have been used to assess the effects of chemical reprogramming, multi-omic GRN analysis is also being used. For example, GRN analysis has been used to identify novel compounds that change cell fate (Xiao et al., 2025) and identify molecular targets to rejuvenate aged cells (Lee et al., 2021). GRN analysis to identify novel compounds that change the aged GRN state, or to molecularly confirm the rejuvenating effects of known or newly devised chemical reprogramming cocktails is a promising area of future research.

Reprogramming aged cells to a more youthful state using transcription factors that do not push cells towards a pluripotent state has also begun to be explored. Reinforcing cell identity with TFs whose activity is more dominant in the young cell GRN could represent an alternative approach to using pluripotency factors. Determining these TFs can be achieved

through multi-omic integration and comparison of GRNs. Furthermore, construction of GRNs using Hi-C data provides additional information regarding the way genes are regulated, particularly by distal regulatory elements. Here, Hi-C-informed GRNs were used to investigate the hypothesis that TFs associated with a youthful LT-HSC state may be candidate rejuvenation factors. These predictions require functional validation.

In chapter 3, I presented results of an experiment to optimise the Hi-C protocol in a low-input setting such as is the case when dealing with LT-HSCs. Double fixation with FA and DSG resulted in an increased detection of short range (1-10 kbp) interactions and a reduction in potentially spurious trans-chromosomal interactions and mitochondrial contamination, so this was incorporated into subsequent *in situ* Hi-C experiments. Furthermore, choice of restriction enzyme digestion with MboI or DpnII (which have the same recognition site but possibly different kinetics due to size and active site differences) did not significantly affect the median length of digested DNA fragments or the proportion of interactions in each category of interaction distance. However, as was shown by differential interaction analysis, choice of restriction enzyme did seem to result in small differences in which interactions were detected, but likely not enough to justify switching from MboI to DpnII.

Ultimately, it was decided that addition of DSG to the *in situ* Hi-C protocol was justified, while switching from MboI to DpnII was not. However, the Hi-C 3.0 paper (Lafontaine et al., 2021) recommends using a cocktail of two restriction enzymes (DpnII + DdeI), which purportedly further increased the ability to detect more short range 1-10 kbp interactions without loss of long range interactions (Akgol Oksuz et al., 2021; Lafontaine et al., 2021). The use of restriction enzyme cocktails is also one of the claimed benefits of commercial Hi-C kits such as the Arima kit (Kadota et al., 2020), although this complicates computational analysis somewhat because it no longer uses a single ligation site sequence to split reads and align to the genome and instead uses restriction site independent alignment (Akgol Oksuz et al., 2021).

LT-HSCs are known to consist of lineage-biased subpopulations. For these rare cell types, specialized low-input Hi-C may be the best option for mapping their 3D genomes and building GRNs. For example, tagHi-C, which uses Tn5-based tagmentation to insert sequencing adapters post-ligation, claims to achieve 100 kbp resolution with only 1000 cells (Zhang et al., 2020), although there are still many washing and resuspending steps where

cells can be lost. Easy Hi-C (eHi-C) claims to achieve the same resolution as *in situ* Hi-C with 100 times less input (L. Lu et al., 2020). The eHi-C protocol uses biotin-free enzymatic digestion after proximity ligation, followed by circularization of chimeric fragments, then exonuclease digestion of non-chimeric fragments and finally relinearization of circular chimeric fragments, so that only chimeric fragments are retained and sequenced (L. Lu et al., 2020). Alternatively, the small-scale *in situ* Hi-C (sis-Hi-C) method attempts to reduce material loss by fixing cells in droplets on plastic culture dishes and later uses AluI digestion instead of sonication, claiming good results at 40 kbp resolution (Song et al., 2025; Zhang et al., 2025). Plate-C and Easy Dip-C use dual restriction digestion of DNA after fixation and Tn5 transposase insertion of sequencing adaptors (Parasar et al., 2026). For extremely low input cases, Easy Dip-C performs DNA digestion and proximity ligation on bulk cell populations prior to nuclear staining and sorting into 384 well plates where the remainder of the Hi-C library prep can be performed on single nuclei or minibulk quantities of nuclei (Parasar et al., 2026). Finally, HiChew (Chen et al., 2026) allows for deeper sequencing by enriching the chimeric fragment library using dam methyltransferases to mark the GATC (MboI) or AGCT (AluI) ligation sites, then uses an anti-N6-methyladenosine antibody or anti-5-methylcytosine antibody to enrich for the labelled chimeric fragments.

While all these alternative options would require extensive testing to replicate published results, it seems likely that aspects of these low-input/single-cell Hi-C methods could be combined to further improve Hi-C coverage and resolution for rare subpopulations of LT-HSCs and other rare supporting cells in the bone marrow compartment. This Hi-C data could then be used to construct and compare Hi-C informed GRNs from these subpopulations.

In chapter 4, I presented a published bioRxiv preprint describing my extensive investigation into the epigenetic comparison of aged versus young LT-HSCs. Prediction of reprogramming factors from GRNs is a growing trend, and Hi-C-informed GRNs can incorporate measured chromatin contacts when linking distal regulatory elements to genes. However, Hi-C is only valuable when it is sufficiently cell-type and condition matched and Hi-C informed GRNs become biologically informative only when Hi-C contact information is properly integrated with chromatin accessibility and gene expression. It is expected that as Hi-C methods become further optimized for low-input rare cell types, for example using the methods discussed in this chapter, that predictions from Hi-C informed GRNs will become

more reflective of real biology. Furthermore, these predictions should be validated with TF binding evidence and enhancer perturbations.

Two aspects not discussed in the preprint are the construction of GRNs using chromatin accessibility with higher coverage and using expression data that includes expression of non-coding RNAs not captured by conventional RNA-seq protocols. For example, DAF-seq and single-cell DAF-seq (scDAF-seq) uses a double-stranded cytidine deaminase toxin A (DddA) to convert cytidines to uridines only within regions accessible to the enzyme, and the uridines are then converted to thymidine during PCR amplification (Swanson et al., 2025). Due to the specific chemistry of the DddA enzyme, DAF-seq is reported to give higher resolution and more coverage allowing TF footprinting to be accomplished on less cell input and less sequencing (Swanson et al., 2025). Furthermore, building GRNs with non-coding RNA expression data is an extremely interesting avenue. For example, Razavi-Mohseni & Beer (2024) used machine learning to build a GRN model using miRNA expression data, chromatin accessibility and regular gene expression data, demonstrating that miRNAs inactivate cell lineage determining TFs during embryonic stem cell to definitive endoderm (ESC-DE) transition (Razavi-Mohseni & Beer, 2024). Altogether, integration of higher quality Hi-C, chromatin accessibility and total RNA expression (including non-coding RNAs) represents a future goal for generating better and more biologically informative GRNs.

A large component of the functional and molecular aspects of HSC ageing is due to the changes in structure within the bone marrow, chronic inflammation and changes to signalling from HSC supporting cells (Peters et al., 2025) such as bone cells (H. Zhang et al., 2023), macrophages (Feng et al., 2024; Frisch et al., 2019), vascular cells (Maryanovich et al., 2019; Poulos et al., 2017), plasma cells (Pioli et al., 2019) and MSCs (Massaro et al., 2023; Peters et al., 2025). For example, while young MSCs maintain high proliferative capacity and clear lineage commitment, old MSCs display senescence markers and shift toward a pro-inflammatory state losing their niche-supporting abilities (Gao et al., 2023; Massaro et al., 2023; Peters et al., 2025; Yamada et al., 2022; W. Zhang et al., 2008; Zhou et al., 2008). In addition, multilineage-differentiating stress-enduring (MUSE) cells, which can differentiate into many lineages in the bone marrow, including bone, neural, endothelial and stromal cells (Dezawa, 2025; Kuroda et al., 2010), likely support HSCs in times of stress (Alessio et al.,

2017; Jeong et al., 2018), but the effect of ageing on MUSE cell numbers and function has yet to be explored (Rudnitsky et al., 2025). Co-culture and co-transplant of HSCs with MSCs has been shown to improve survival and reconstitution ability of gene-edited HSCs (Crippa et al., 2023), so future experiments with reprogrammed HSCs may benefit from co-culture and co-transplant with MSCs or the more potent MUSE cells. Bone-marrow organoids, such as the combined bone and bone-marrow organoids (Shen et al., 2026) and bone-marrow-on-a-chip technologies (Chou et al., 2020; Rosalem et al., 2026), may also facilitate the study of the reprogramming of aged human HSCs and MSCs.

Reversal of organismal ageing is a formidable goal that will almost certainly require multiple interventions. Even if epigenetic patterns could be restored, telomeres lengthened, chronic inflammation prevented, senescent cells removed or reprogrammed, stem cells replenished, etc., there is still the problem of the accumulation of somatic mutations, irreversible extracellular matrix crosslinks (i.e. AGEs) and tissue fibrosis. Therefore, technologies that prevent or repair somatic mutations, or simply eliminate mutated cells, will be required. In addition, engineered enzymes that reverse AGEs and persistent fibrosis will also be required. Furthermore, organisms that show remarkable rejuvenation and undetectable ageing exhibit massive reductions in morphological mass and size then extensive regeneration. This is the case for the seemingly ageless *Turritopsis dohrnii* jellyfish which can revert to a polyp then regenerate (Piraino et al., 1996; Velasco-Muñoz et al., 2025) and certain species of planaria flat worms, which physically tear themselves into smaller pieces in order to regenerate afresh (Dai et al., 2025). Whether humans and other mammals need to somehow replicate this cycle of reduction and regeneration remains to be determined. Periodic removal of senescent cells, mutated cells, chronically infected cells, AGEs and fibrosis may prove to be sufficient to provide a suitable environment for the homeostatic replenishment of lost cells. Moreover, periodic epigenetic reprogramming of aged cells will likely be required to resolve the problem of intrinsic epigenetic drift and loss of cell identity. Experimental efforts should address exactly which and how many interventions are required to significantly reverse or halt ageing in mammalian species.

Bibliography

Abad, M., Mosteiro, L., Pantoja, C., Cañamero, M., Rayon, T., Ors, I., Graña, O., Megías, D., Domínguez, O., & Martínez, D. (2013). Reprogramming in vivo produces teratomas and iPS cells with totipotency features. *Nature*, *502*(7471), 340-345.

Adelman, E. R., Huang, H.-T., Roisman, A., Olsson, A., Colaprico, A., Qin, T., Lindsley, R. C., Bejar, R., Salomonis, N., & Grimes, H. L. (2019). Aging human hematopoietic stem cells manifest profound epigenetic reprogramming of enhancers that may predispose to leukemia. *Cancer discovery*, *9*(8), 1080-1101.

Ahmed, N., Cavattoni, I., Villiers, W., Cugno, C., Deola, S., & Mifsud, B. (2024). Multi-omic analysis of longitudinal acute myeloid leukemia patient samples reveals potential prognostic markers linked to disease progression. *Front Genet*, *15*, 1442539. https://doi.org/10.3389/fgene.2024.1442539

Aibar, S., Gonzalez-Blas, C. B., Moerman, T., Huynh-Thu, V. A., Imrichova, H., Hulselmans, G., Rambow, F., Marine, J. C., Geurts, P., Aerts, J., van den Oord, J., Atak, Z. K., Wouters, J., & Aerts, S. (2017). SCENIC: single-cell regulatory network inference and clustering. *Nat Methods*, *14*(11), 1083-1086. https://doi.org/10.1038/nmeth.4463

Akgol Oksuz, B., Yang, L., Abraham, S., Venev, S. V., Krietenstein, N., Parsi, K. M., Ozadam, H., Oomen, M. E., Nand, A., & Mao, H. (2021). Systematic evaluation of chromosome conformation capture assays. *Nature methods*, *18*(9), 1046-1055.

Alessio, N., Ozcan, S., Tatsumi, K., Murat, A., Peluso, G., Dezawa, M., & Galderisi, U. (2017). The secretome of MUSE cells contains factors that may play a role in regulation of stemness, apoptosis and immunomodulation. *Cell Cycle*, *16*(1), 33-44. https://doi.org/10.1080/15384101.2016.1211215

Alvarez, M. J., Shen, Y., Giorgi, F. M., Lachmann, A., Ding, B. B., Ye, B. H., & Califano, A. (2016). Network-based inference of protein activity helps functionalize the genetic landscape of cancer. *Nature genetics*, *48*(8), 838.

Amoah, A., Keller, A., Emini, R., Hoenicka, M., Liebold, A., Vollmer, A., Eiwen, K., Soller, K., Sakk, V., Zheng, Y., Florian, M. C., & Geiger, H. (2022). Aging of human hematopoietic stem cells is linked to changes in Cdc42 activity. *haematologica*, *107*(2), 393-402. https://doi.org/10.3324/haematol.2020.269670

Anandakrishnan, R., Varghese, R. T., Kinney, N. A., & Garner, H. R. (2019). Estimating the number of genetic mutations (hits) required for carcinogenesis based on the distribution of somatic mutations. *PLoS Comput Biol*, *15*(3), e1006881. https://doi.org/10.1371/journal.pcbi.1006881

Andrews, S. (2010). FastQC: a quality control tool for high throughput sequence data. (Version 0.11.x) Babraham Bioinformatics. https://www.bioinformatics.babraham.ac.uk/projects/fastqc/

Andries, O., Mc Cafferty, S., De Smedt, S. C., Weiss, R., Sanders, N. N., & Kitada, T. (2015). N1-methylpseudouridine-incorporated mRNA outperforms pseudouridine-incorporated mRNA by providing enhanced protein expression and reduced immunogenicity in mammalian cell lines and mice. *Journal of Controlled Release*, *217*, 337-344.

Aoyagi, Y., Hayashi, Y., Harada, Y., Choi, K., Matsunuma, N., Sadato, D., Maemoto, Y., Ito, A., Yanagi, S., & Starczynowski, D. T. (2022). Mitochondrial Fragmentation Triggers Ineffective Hematopoiesis in Myelodysplastic SyndromesDysregulated Mitochondrial Dynamics Induces MDS Pathogenesis. *Cancer discovery*, *12*(1), 250-269.

Arakawa, S., Suzuki, R., Kurosaka, D., Ikeda, R., Hayashi, H., Kayama, T., Ohno, R. I., Nagai, R., Marumo, K., & Saito, M. (2020). Mass spectrometric quantitation of AGEs and enzymatic crosslinks in human cancellous bone. *Sci Rep*, *10*(1), 18774. https://doi.org/10.1038/s41598-020-75923-8

Arts, J. A., Fallo, S., Florencio, M. S., Smits, J. G. A., Lima Cunha, D., Roubroeks, J. A. Y., Dickman, M. M., LaPointe, V. L. S., Yu, R., & Zhou, H. (2025). Prediction of cell states and key transcription factors of the human cornea through integrated single-cell omics analyses. *PNAS Nexus*, *4*(8), pgaf235. https://doi.org/10.1093/pnasnexus/pgaf235

Asano, S., Liao, C. W., Matsunaga, Y., Jeon, H., Sawaguchi, K., Asano, K., Kusakabe, M., Shahri, Z. J., Gogoleva, N., Yokomizo, T., Takahashi, S., & Hamada, M. (2025). MAFB regulates hematopoietic stem cell proliferation and maintenance. *Sci Rep*, *15*(1), 40592. https://doi.org/10.1038/s41598-025-24389-7

Aue, G., Du, Y., Cleveland, S. M., Smith, S. B., Dave, U. P., Liu, D., Weniger, M. A., Metais, J. Y., Jenkins, N. A., Copeland, N. G., & Dunbar, C. E. (2011). Sox4 cooperates with PU.1 haploinsufficiency in murine myeloid leukemia. *Blood*, *118*(17), 4674-4681. https://doi.org/10.1182/blood-2011-04-351528

Bao, Y., Cacioppo, R., Crisp, A., Shlamovitz, I., Sale, J. E., Tufegdzic Vidakovic, A., Vervoort, S. J., & Zeller, A. (2025). Protocol for double-crosslinking ChIP-seq to improve data quality and enhance detection of challenging chromatin targets. *STAR Protoc*, *6*(4), 104171. https://doi.org/10.1016/j.xpro.2025.104171

Barnes, R. P., de Rosa, M., Thosar, S. A., Detwiler, A. C., Roginskaya, V., Van Houten, B., Bruchez, M. P., Stewart-Ornstein, J., & Opresko, P. L. (2022). Telomeric 8-oxo-guanine drives rapid premature senescence in the absence of telomere shortening. *Nat Struct Mol Biol*, *29*(7), 639-652. https://doi.org/10.1038/s41594-022-00790-y

Baumgartner, C., Toifl, S., Farlik, M., Halbritter, F., Scheicher, R., Fischer, I., Sexl, V., Bock, C., & Baccarini, M. (2018). An ERK-Dependent Feedback Mechanism Prevents Hematopoietic Stem Cell Exhaustion. *Cell stem cell*, *22*(6), 879-892 e876. https://doi.org/10.1016/j.stem.2018.05.003

Bediaga, N. G., Coughlan, H. D., Johanson, T. M., Garnham, A. L., Naselli, G., Schroder, J., Fearnley, L. G., Bandala-Sanchez, E., Allan, R. S., Smyth, G. K., & Harrison, L. C. (2021). Multi-level remodelling of chromatin underlying activation of human T cells. *Sci Rep*, *11*(1), 528. https://doi.org/10.1038/s41598-020-80165-9

Beerman, I., Bock, C., Garrison, B. S., Smith, Z. D., Gu, H., Meissner, A., & Rossi, D. J. (2013). Proliferation-dependent alterations of the DNA methylation landscape underlie hematopoietic stem cell aging. *Cell stem cell*, *12*(4), 413-425. https://doi.org/10.1016/j.stem.2013.01.017

Belaghzal, H., Dekker, J., & Gibcus, J. H. (2017). Hi-C 2.0: An optimized Hi-C procedure for high-resolution genome-wide mapping of chromosome conformation. *Methods*, *123*, 56-65. https://doi.org/10.1016/j.ymeth.2017.04.004

Berdugo-Vega, G., Sierra, C., Astori, S., Calati, V., Orsat, J., Scoglio, M. J., Sandi, C., & Graff, J. (2026). Cognitive rejuvenation through partial reprogramming of engram cells. *Neuron*, *114*(6), 1102-1116 e1107. https://doi.org/10.1016/j.neuron.2025.11.028

Bernitz, J. M., Kim, H. S., MacArthur, B., Sieburg, H., & Moore, K. (2016). Hematopoietic Stem Cells Count and Remember Self-Renewal Divisions. *Cell*, *167*(5), 1296-1309 e1210. https://doi.org/10.1016/j.cell.2016.10.022

Bernitz, J. M., Rapp, K., Daniel, M. G., Shcherbinin, D., Yuan, Y., Gomes, A., Waghray, A., Brosh, R., Lachmann, A., Ma'ayan, A., Papatsenko, D., & Moore, K. A. (2020). Memory of Divisional History Directs the Continuous Process of Primitive Hematopoietic Lineage Commitment. *Stem cell reports*, *14*(4), 561-574. https://doi.org/10.1016/j.stemcr.2020.03.005

Bernstein, N., Spencer Chapman, M., Nyamondo, K., Chen, Z., Williams, N., Mitchell, E., Campbell, P. J., Cohen, R. L., & Nangalia, J. (2024). Analysis of somatic mutations in whole blood from 200,618 individuals identifies pervasive positive selection and novel drivers of clonal hematopoiesis. *Nat Genet*, *56*(6), 1147-1155. https://doi.org/10.1038/s41588-024-01755-1

Bhattacharya, R., Zekavat, S. M., Haessler, J., Fornage, M., Raffield, L., Uddin, M. M., Bick, A. G., Niroula, A., Yu, B., Gibson, C., Griffin, G., Morrison, A. C., Psaty, B. M., Longstreth, W. T., Bis, J. C., Rich, S. S., Rotter, J. I., Tracy, R. P., Correa, A.,…Reiner, A. P. (2022). Clonal Hematopoiesis Is Associated With Higher Risk of Stroke. *Stroke*, *53*(3), 788-797. https://doi.org/10.1161/STROKEAHA.121.037388

Biechonski, S., Olender, L., Zipin-Roitman, A., Yassin, M., Aqaqe, N., Marcu-Malina, V., Rall-Scharpf, M., Trottier, M., Meyn, M. S., Wiesmuller, L., Beider, K., Raz, Y., Grisaru, D., Nagler, A., & Milyavsky, M. (2018). Attenuated DNA damage responses and increased apoptosis characterize human hematopoietic stem cells exposed to irradiation. *Sci Rep*, *8*(1), 6071. https://doi.org/10.1038/s41598-018-24440-w

Binod, G., Hoyt, L. J., Dovat, S., & Dong, F. (2024). Upregulation of nuclear protein Hemgn by transcriptional repressor Gfi1 through repressing PU. 1 contributes to the anti-apoptotic activity of Gfi1. *Journal of Biological Chemistry*, *300*(11), 107860.

Bisht, K., McGirr, C., Lee, S. Y., Tseng, H. W., Fleming, W., Alexander, K. A., Matsumoto, T., Barbier, V., Sims, N. A., Muller-Newen, G., Winkler, I. G., Bonig, H., & Levesque, J. P. (2022). Oncostatin M regulates hematopoietic stem cell (HSC) niches in the bone marrow to restrict HSC mobilization. *Leukemia*, *36*(2), 333-347. https://doi.org/10.1038/s41375-021-01413-z

Bogeska, R., Mikecin, A. M., Kaschutnig, P., Fawaz, M., Buchler-Schaff, M., Le, D., Ganuza, M., Vollmer, A., Paffenholz, S. V., Asada, N., Rodriguez-Correa, E., Frauhammer, F., Buettner, F., Ball, M., Knoch, J., Stable, S., Walter, D., Petri, A., Carreno-Gonzalez, M. J.,…Milsom, M. D. (2022). Inflammatory exposure drives long-lived impairment of hematopoietic stem cell self-renewal activity and accelerated aging. *Cell stem cell*, *29*(8), 1273-1284 e1278. https://doi.org/10.1016/j.stem.2022.06.012

Botchkarev, V. V., Jr., Harrington, S., Stoppato, M., Justen, A., Kimber, C., Kapuria, A., Gibson, K. M., Chu, C. S., Xu, Y., Haugh, K., Ankala, R., Kipniss, N., DeGroot, A., Moore, E., de Jesus, R., Adewale, F., Daniels, K., Crocker, S., Liang, A.,…Biasco,

L. (2025). In vivo gene editing of human hematopoietic stem and progenitor cells using envelope-engineered virus-like particles. *Nat Biotechnol*. https://doi.org/10.1038/s41587-025-02915-2

Boutzen, H., Murison, A., Oriecuia, A., Bansal, S., Arlidge, C., Wang, J. C. Y., Lupien, M., Kaufmann, K. B., & Dick, J. E. (2024). Identification of leukemia stem cell subsets with distinct transcriptional, epigenetic and functional properties. *Leukemia*, *38*(10), 2090-2101. https://doi.org/10.1038/s41375-024-02358-9

Boyle, C., Lansdorp, P. M., & Edelstein-Keshet, L. (2023). Predicting the number of lifetime divisions for hematopoietic stem cells from telomere length measurements. *iScience*, *26*(7), 107053. https://doi.org/10.1016/j.isci.2023.107053

Brase, L., You, S. F., D'Oliveira Albanus, R., Del-Aguila, J. L., Dai, Y., Novotny, B. C., Soriano-Tarraga, C., Dykstra, T., Fernandez, M. V., Budde, J. P., Bergmann, K., Morris, J. C., Bateman, R. J., Perrin, R. J., McDade, E., Xiong, C., Goate, A. M., Farlow, M., Dominantly Inherited Alzheimer, N.,…Harari, O. (2023). Single-nucleus RNA-sequencing of autosomal dominant Alzheimer disease and risk variant carriers. *Nat Commun*, *14*(1), 2314. https://doi.org/10.1038/s41467-023-37437-5

Breda, L., Papp, T. E., Triebwasser, M. P., Yadegari, A., Fedorky, M. T., Tanaka, N., Abdulmalik, O., Pavani, G., Wang, Y., & Grupp, S. A. (2023). In vivo hematopoietic stem cell modification by mRNA delivery. *Science*, *381*(6656), 436-443.

Broad Institute. (2023). Picard Toolkit. (Version 3.30 or 3.1.1) [GitHub repository]. Broad Institute. https://broadinstitute.github.io/picard/

Browaeys, R., Saelens, W., & Saeys, Y. (2020). NicheNet: modeling intercellular communication by linking ligands to target genes. *Nat Methods*, *17*(2), 159-162. https://doi.org/10.1038/s41592-019-0667-5

Browder, K. C., Reddy, P., Yamamoto, M., Haghani, A., Guillen, I. G., Sahu, S., Wang, C., Luque, Y., Prieto, J., & Shi, L. (2022). In vivo partial reprogramming alters age-associated molecular changes during physiological aging in mice. *Nature Aging*, *2*(3), 243-253.

Cagan, A., Baez-Ortega, A., Brzozowska, N., Abascal, F., Coorens, T. H. H., Sanders, M. A., Lawson, A. R. J., Harvey, L. M. R., Bhosle, S., Jones, D., Alcantara, R. E., Butler, T. M., Hooks, Y., Roberts, K., Anderson, E., Lunn, S., Flach, E., Spiro, S., Januszczak, I.,…Martincorena, I. (2022). Somatic mutation rates scale with lifespan across mammals. *Nature*, *604*(7906), 517-524. https://doi.org/10.1038/s41586-022-04618-z

Chacón-Martínez, C. A., Koester, J., & Wickström, S. A. (2018). Signaling in the stem cell niche: regulating cell fate, function and plasticity. *Development*, *145*(15), dev165399.

Chan, W. F., Coughlan, H. D., Zhou, J. H. S., Keenan, C. R., Bediaga, N. G., Hodgkin, P. D., Smyth, G. K., Johanson, T. M., & Allan, R. S. (2021). Pre-mitotic genome re-organisation bookends the B cell differentiation process. *Nat Commun*, *12*(1), 1344. https://doi.org/10.1038/s41467-021-21536-2

Chen, C., Yu, W., Tober, J., Gao, P., He, B., Lee, K., Trieu, T., Blobel, G. A., Speck, N. A., & Tan, K. (2019). Spatial Genome Re-organization between Fetal and Adult Hematopoietic Stem Cells. *Cell Rep*, *29*(12), 4200-4211 e4207. https://doi.org/10.1016/j.celrep.2019.11.065

Chen, X., Wang, Y., Cappuccio, A., Cheng, W. S., Zamojski, F. R., Nair, V. D., Miller, C. M., Rubenstein, A. B., Nudelman, G., Tadych, A., Theesfeld, C. L., Vornholt, A., George, M. C., Ruffin, F., Dagher, M., Chawla, D. G., Soares-Schanoski, A., Spurbeck, R. R., Ndhlovu, L. C.,…Sealfon, S. C. (2023). Mapping disease regulatory circuits at cell-type resolution from single-cell multiomics data. *Nat Comput Sci*, *3*(7), 644-657. https://doi.org/10.1038/s43588-023-00476-5

Chen, Y., Chen, L., Lun, A. T., Baldoni, P. L., & Smyth, G. K. (2025). edgeR v4: powerful differential analysis of sequencing data with expanded functionality and improved support for small counts and larger datasets. *Nucleic acids research*, *53*(2), gkaf018.

Chen, Y., Luttmann, F. F., Schoger, E., Scholer, H. R., Zelarayan, L. C., Kim, K. P., Haigh, J. J., Kim, J., & Braun, T. (2021). Reversible reprogramming of cardiomyocytes to a fetal state drives heart regeneration in mice. *Science*, *373*(6562), 1537-1540. https://doi.org/10.1126/science.abg5159

Chen, Y. H., Yeung, F., Lacey, K. A., Zaldana, K., Lin, J. D., Bee, G. C. W., McCauley, C., Barre, R. S., Liang, S. H., Hansen, C. B., Downie, A. E., Tio, K., Weiser, J. N., Torres, V. J., Bennett, R. J., Loke, P., Graham, A. L., & Cadwell, K. (2023). Rewilding of laboratory mice enhances granulopoiesis and immunity through intestinal fungal colonization. *Sci Immunol*, *8*(84), eadd6910. https://doi.org/10.1126/sciimmunol.add6910

Chen, Z., Xie, Y., Zhang, C., Tan, C., Ruan, F., Chen, W., Luo, M., Guo, M., Xie, Z., Cao, H., Tang, M., Zhang, X., Zhang, Y., & Tang, C. (2026). Highly efficient chromatin conformation capture with post-enrichment in single cells by HiChew. *Genome Biol*, *27*(1). https://doi.org/10.1186/s13059-026-04059-1

Cheng, P., Eksioglu, E. A., Chen, X., Kandell, W., Le Trinh, T., Cen, L., Qi, J., Sallman, D. A., Zhang, Y., Tu, N., Adams, W. A., Zhang, C., Liu, J., Cleveland, J. L., List, A. F., & Wei, S. (2019). S100A9-induced overexpression of PD-1/PD-L1 contributes to ineffective hematopoiesis in myelodysplastic syndromes. *Leukemia*, *33*(8), 2034-2046. https://doi.org/10.1038/s41375-019-0397-9

Chin, D. W. L., Yoshizato, T., Virding Culleton, S., Grasso, F., Barbachowska, M., Ogawa, S., Jacobsen, S. E. W., & Woll, P. S. (2022). Aged healthy mice acquire clonal hematopoiesis mutations. *Blood*, *139*(4), 629-634.

Chiu, C. P., Dragowska, W., Kim, N. W., Vaziri, H., Yui, J., Thomas, T. E., Harley, C. B., & Lansdorp, P. M. (1996). Differential expression of telomerase activity in hematopoietic progenitors from adult human bone marrow. *Stem Cells*, *14*(2), 239-248. https://doi.org/10.1002/stem.140239

Chondronasiou, D., Martinez de Villarreal, J., Melendez, E., Lynch, C. J., Pozo, N. D., Kovatcheva, M., Aguilera, M., Prats, N., Real, F. X., & Serrano, M. (2022). Deciphering the roadmap of in vivo reprogramming toward pluripotency. *Stem cell reports*, *17*(11), 2501-2517. https://doi.org/10.1016/j.stemcr.2022.09.009

Chou, D. B., Frismantas, V., Milton, Y., David, R., Pop-Damkov, P., Ferguson, D., MacDonald, A., Vargel Bolukbasi, O., Joyce, C. E., Moreira Teixeira, L. S., Rech, A., Jiang, A., Calamari, E., Jalili-Firoozinezhad, S., Furlong, B. A., O'Sullivan, L. R., Ng, C. F., Choe, Y., Marquez, S.,…Ingber, D. E. (2020). On-chip recapitulation of clinical bone marrow toxicities and patient-specific pathophysiology. *Nat Biomed Eng*, *4*(4), 394-406. https://doi.org/10.1038/s41551-019-0495-z

Cianfruglia, L., Badillo Pazmay, G. V., Fortunato, C., Spezia, P. G., Novazzi, F., Piacenza, F., Malavolta, M., Marchegiani, F., Recchioni, R., Matacchione, G., Giordani, C., Cardelli, M., Casoli, T., Di Rosa, M., Cherubini, A., Pelliccioni, G., Sarzani, R., Spannella, F., Lattanzio, F.,…Giacconi, R. (2026). High Torque teno virus viremia predicts long-term mortality and reflects chronic low-grade inflammation (inflammaging) in geriatric inpatients. *Exp Gerontol*, *213*, 112978. https://doi.org/10.1016/j.exger.2025.112978

Ciccarone, F., Zampieri, M., & Caiafa, P. (2017). PARP1 orchestrates epigenetic events setting up chromatin domains. Seminars in cell & developmental biology,

Cirnaru, M. D., Song, S., Tshilenge, K. T., Corwin, C., Mleczko, J., Galicia Aguirre, C., Benlhabib, H., Bendl, J., Apontes, P., Fullard, J., Creus-Muncunill, J., Reyahi, A., Nik, A. M., Carlsson, P., Roussos, P., Mooney, S. D., Ellerby, L. M., & Ehrlich, M. E. (2021). Unbiased identification of novel transcription factors in striatal compartmentation and striosome maturation. *elife*, *10*. https://doi.org/10.7554/eLife.65979

Corona, M., Hughes, K. A., Weaver, D. B., & Robinson, G. E. (2005). Gene expression patterns associated with queen honey bee longevity. *Mechanisms of ageing and development*, *126*(11), 1230-1238.

Crippa, S., Conti, A., Vavassori, V., Ferrari, S., Beretta, S., Rivis, S., Bosotti, R., Scala, S., Pirroni, S., Jofra-Hernandez, R., Santi, L., Basso-Ricci, L., Merelli, I., Genovese, P., Aiuti, A., Naldini, L., Di Micco, R., & Bernardo, M. E. (2023). Mesenchymal stromal cells improve the transplantation outcome of CRISPR-Cas9 gene-edited human HSPCs. *Mol Ther*, *31*(1), 230-248. https://doi.org/10.1016/j.ymthe.2022.08.011

Csardi, G., & Nepusz, T. (2006). The igraph software. *Complex syst*, *1695*, 1-9.

Dai, X., Li, X., Tyshkovskiy, A., Zuckerman, C., Cheng, N., Lin, P., Paris, D., Qureshi, S., Kruglyak, L., Mao, X., Nandakumar, J., Gladyshev, V. N., Pletcher, S., Sobota, J., & Guo, L. (2025). Regeneration leads to global tissue rejuvenation in aging sexual planarians. *Nat Aging*, *5*(5), 780-798. https://doi.org/10.1038/s43587-025-00847-9

Damania, B., Kenney, S. C., & Raab-Traub, N. (2022). Epstein-Barr virus: Biology and clinical disease. *Cell*, *185*(20), 3652-3670. https://doi.org/10.1016/j.cell.2022.08.026

Damhofer, H., Radzisheuskaya, A., & Helin, K. (2021). Generation of locus-specific degradable tag knock-ins in mouse and human cell lines. *STAR Protoc*, *2*(2), 100575. https://doi.org/10.1016/j.xpro.2021.100575

de la Rica, L., Rodríguez-Ubreva, J., García, M., Islam, A. B., Urquiza, J. M., Hernando, H., Christensen, J., Helin, K., Gómez-Vaquero, C., & Ballestar, E. (2013). PU. 1 target genes undergo Tet2-coupled demethylation and DNMT3b-mediated methylation in monocyte-to-osteoclast differentiation. *Genome biology*, *14*(9), 1-21.

de Lima Camillo, L. P., Gam, R., Maskalenka, K., LeBlanc, F. J., Urrutia, G. A., Mejia, G. M., Miller, H. E., Wardlaw, C. P., Pickles, A., & Everton, L. (2025). A single factor for safer cellular rejuvenation. *bioRxiv*, 2025.2006. 2005.657370.

Desterke, C., Bennaceur-Griscelli, A., & Turhan, A. G. (2021). EGR1 dysregulation defines an inflammatory and leukemic program in cell trajectory of human-aged hematopoietic stem cells (HSC). *Stem Cell Res Ther*, *12*(1), 419. https://doi.org/10.1186/s13287-021-02498-0

Dezawa, M. (2025). Macrophage- and pluripotent-like reparative Muse cells are unique endogenous stem cells distinct from other somatic stem cells. *Front Bioeng Biotechnol*, *13*, 1553382. https://doi.org/10.3389/fbioe.2025.1553382

Diaz, N., Kruse, K., Erdmann, T., Staiger, A. M., Ott, G., Lenz, G., & Vaquerizas, J. M. (2018). Chromatin conformation analysis of primary patient tissue using a low input Hi-C method. *Nat Commun*, *9*(1), 4938. https://doi.org/10.1038/s41467-018-06961-0

Djeghloul, D., Kuranda, K., Kuzniak, I., Barbieri, D., Naguibneva, I., Choisy, C., Bories, J. C., Dosquet, C., Pla, M., Vanneaux, V., Socie, G., Porteu, F., Garrick, D., & Goodhardt, M. (2016). Age-Associated Decrease of the Histone Methyltransferase SUV39H1 in HSC Perturbs Heterochromatin and B Lymphoid Differentiation. *Stem cell reports*, *6*(6), 970-984. https://doi.org/10.1016/j.stemcr.2016.05.007

Dobbin, M. M., Madabhushi, R., Pan, L., Chen, Y., Kim, D., Gao, J., Ahanonu, B., Pao, P.-C., Qiu, Y., & Zhao, Y. (2013). SIRT1 collaborates with ATM and HDAC1 to maintain genomic stability in neurons. *Nature neuroscience*, *16*(8), 1008-1015.

Dobin, A., Davis, C. A., Schlesinger, F., Drenkow, J., Zaleski, C., Jha, S., Batut, P., Chaisson, M., & Gingeras, T. R. (2013). STAR: ultrafast universal RNA-seq aligner. *Bioinformatics*, *29*(1), 15-21.

Doeser, M. C., Scholer, H. R., & Wu, G. (2018). Reduction of Fibrosis and Scar Formation by Partial Reprogramming In Vivo. *Stem Cells*, *36*(8), 1216-1225. https://doi.org/10.1002/stem.2842

Dozmorov, M. G. (2015). Polycomb repressive complex 2 epigenomic signature defines age-associated hypermethylation and gene expression changes. *Epigenetics*, *10*(6), 484-495. https://doi.org/10.1080/15592294.2015.1040619

Du, Y., Xu, K., Zhang, S., Chen, L., Liu, Z., & Xie, L. (2025). Construction of Gene Regulatory Networks Based on Spatial Multi-Omics Data and Application in Tumor-Boundary Analysis. *Genes (Basel)*, *16*(7). https://doi.org/10.3390/genes16070821

Dullaers, M., Breckpot, K., Van Meirvenne, S., Bonehill, A., Tuyaerts, S., Michiels, A., Straetman, L., Heirman, C., De Greef, C., & Van Der Bruggen, P. (2004). Side-by-side comparison of lentivirally transduced and mRNA-electroporated dendritic cells: implications for cancer immunotherapy protocols. *Molecular Therapy*, *10*(4), 768-779.

Durinck, S., Spellman, P. T., Birney, E., & Huber, W. (2009). Mapping identifiers for the integration of genomic datasets with the R/Bioconductor package biomaRt. *Nature protocols*, *4*(8), 1184-1191.

Dykstra, B., Olthof, S., Schreuder, J., Ritsema, M., & de Haan, G. (2011). Clonal analysis reveals multiple functional defects of aged murine hematopoietic stem cells. *J Exp Med*, *208*(13), 2691-2703. https://doi.org/10.1084/jem.20111490

Elias, H. K., Mitra, S., da Silva, M. B., Rajagopalan, A., Gipson, B., Lee, N., Kousa, A. I., Ali, M. A. E., Grassmann, S., Raghuraman, R., Zhang, X. C., DeWolf, S., Smith, M., Andrlova, H., Argyropoulos, K. V., Sharma, R., Fei, T., Sun, J. C., Dunbar, C. E.,…van den Brink, M. R. M. (2025). Kit(lo) hematopoietic stem cells exhibit distinct lymphoid-primed chromatin landscapes that enhance thymic reconstitution. *Nat Commun*, *16*(1), 6170. https://doi.org/10.1038/s41467-025-61125-1

Ergen, A. V., Boles, N. C., & Goodell, M. A. (2012). Rantes/Ccl5 influences hematopoietic stem cell subtypes and causes myeloid skewing. *Blood*, *119*(11), 2500-2509. https://doi.org/10.1182/blood-2011-11-391730

Fali, T., Fabre-Mersseman, V., Yamamoto, T., Bayard, C., Papagno, L., Fastenackels, S., Zoorab, R., Koup, R. A., Boddaert, J., & Sauce, D. (2018). Elderly human hematopoietic progenitor cells express cellular senescence markers and are more susceptible to pyroptosis. *JCI insight*, *3*(13).

Fard, M. B., Atashi, A., Amiri, S., Kaviani, S., Gholampour, M. A., & Ajami, M. (2021). Parvovirus B19 affects thrombopoietin and IL-11 gene expression in human bone marrow mesenchymal stem cells. *Future Virology*, *16*(8), 519-526.

Feinberg, M. W., Wara, A. K., Cao, Z., Lebedeva, M. A., Rosenbauer, F., Iwasaki, H., Hirai, H., Katz, J. P., Haspel, R. L., Gray, S., Akashi, K., Segre, J., Kaestner, K. H., Tenen, D. G., & Jain, M. K. (2007). The Kruppel-like factor KLF4 is a critical regulator of monocyte differentiation. *EMBO J*, *26*(18), 4138-4148. https://doi.org/10.1038/sj.emboj.7601824

Feng, C., Fan, H., Tie, R., Xin, S., & Chen, M. (2024). Deciphering the evolving niche interactome of human hematopoietic stem cells from ontogeny to aging. *Front Mol Biosci*, *11*, 1479605. https://doi.org/10.3389/fmolb.2024.1479605

Feng, D., Chen, Y., Dai, R., Bian, S., Xue, W., Zhu, Y., Li, Z., Yang, Y., Zhang, Y., Zhang, J., Bai, J., Qin, L., Kohwi, Y., Shi, W., Kohwi-Shigematsu, T., Ma, J., Liao, S., & Hao, B. (2022). Chromatin organizer SATB1 controls the cell identity of CD4(+) CD8(+) double-positive thymocytes by regulating the activity of super-enhancers. *Nat Commun*, *13*(1), 5554. https://doi.org/10.1038/s41467-022-33333-6

Flohr Svendsen, A., Yang, D., Kim, K., Lazare, S., Skinder, N., Zwart, E., Mura-Meszaros, A., Ausema, A., von Eyss, B., de Haan, G., & Bystrykh, L. (2021). A comprehensive transcriptome signature of murine hematopoietic stem cell aging. *Blood*, *138*(6), 439-451. https://doi.org/10.1182/blood.2020009729

Florian, M. C., Dorr, K., Niebel, A., Daria, D., Schrezenmeier, H., Rojewski, M., Filippi, M. D., Hasenberg, A., Gunzer, M., Scharffetter-Kochanek, K., Zheng, Y., & Geiger, H. (2012). Cdc42 activity regulates hematopoietic stem cell aging and rejuvenation. *Cell stem cell*, *10*(5), 520-530. https://doi.org/10.1016/j.stem.2012.04.007

Florian, M. C., Klose, M., Sacma, M., Jablanovic, J., Knudson, L., Nattamai, K. J., Marka, G., Vollmer, A., Soller, K., Sakk, V., Cabezas-Wallscheid, N., Zheng, Y., Mulaw, M. A., Glauche, I., & Geiger, H. (2018). Aging alters the epigenetic asymmetry of HSC division. *PLoS Biol*, *16*(9), e2003389. https://doi.org/10.1371/journal.pbio.2003389

Florian, M. C., Leins, H., Gobs, M., Han, Y., Marka, G., Soller, K., Vollmer, A., Sakk, V., Nattamai, K. J., Rayes, A., Zhao, X., Setchell, K., Mulaw, M., Wagner, W., Zheng, Y., & Geiger, H. (2020). Inhibition of Cdc42 activity extends lifespan and decreases circulating inflammatory cytokines in aged female C57BL/6 mice. *Aging cell*, *19*(9), e13208. https://doi.org/10.1111/acel.13208

Foronda, M., Martinez, P., Schoeftner, S., Gomez-Lopez, G., Schneider, R., Flores, J. M., Pisano, D. G., & Blasco, M. A. (2014). Sox4 links tumor suppression to accelerated aging in mice by modulating stem cell activation. *Cell Rep*, *8*(2), 487-500. https://doi.org/10.1016/j.celrep.2014.06.031

Frisch, B. J., Hoffman, C. M., Latchney, S. E., LaMere, M. W., Myers, J., Ashton, J., Li, A. J., Jerry Saunders, I., Palis, J., & Perkins, A. S. (2019). Aged marrow macrophages expand platelet-biased hematopoietic stem cells via interleukin-1B. *JCI insight*, *4*(10).

Fuchs, E., & Chen, T. (2013). A matter of life and death: self-renewal in stem cells. *EMBO reports*, *14*(1), 39-48.

Fujino, T., Goyama, S., Sugiura, Y., Inoue, D., Asada, S., Yamasaki, S., Matsumoto, A., Yamaguchi, K., Isobe, Y., Tsuchiya, A., Shikata, S., Sato, N., Morinaga, H., Fukuyama, T., Tanaka, Y., Fukushima, T., Takeda, R., Yamamoto, K., Honda, H.,…Kitamura, T. (2021). Mutant ASXL1 induces age-related expansion of phenotypic hematopoietic stem cells through activation of Akt/mTOR pathway. *Nature communications*, *12*(1), 1-20. https://doi.org/10.1038/s41467-021-22053-y

Fulco, C. P., Nasser, J., Jones, T. R., Munson, G., Bergman, D. T., Subramanian, V., Grossman, S. R., Anyoha, R., Doughty, B. R., Patwardhan, T. A., Nguyen, T. H., Kane, M., Perez, E. M., Durand, N. C., Lareau, C. A., Stamenova, E. K., Aiden, E. L., Lander, E. S., & Engreitz, J. M. (2019). Activity-by-contact model of enhancer-promoter regulation from thousands of CRISPR perturbations. *Nat Genet*, *51*(12), 1664-1669. https://doi.org/10.1038/s41588-019-0538-0

Fulton, T. L., Macartney, E. L., & Senior, A. M. (2026). No evidence for squaring the survival curve: lifespan-extending treatments increase variation in age- at-death. *Biol Lett*, *22*(2). https://doi.org/10.1098/rsbl.2025.0651

Gao, Y., Chi, Y., Chen, Y., Wang, W., Li, H., Zheng, W., Zhu, P., An, J., Duan, Y., Sun, T., Liu, X., Xue, F., Liu, W., Fu, R., Han, Z., Zhang, Y., Yang, R., Cheng, T., Wei, J.,…Zhang, X. (2023). Multi-omics analysis of human mesenchymal stem cells shows cell aging that alters immunomodulatory activity through the downregulation of PD-L1. *Nat Commun*, *14*(1), 4373. https://doi.org/10.1038/s41467-023-39958-5

Gekas, C., & Graf, T. (2013). CD41 expression marks myeloid-biased adult hematopoietic stem cells and increases with age. *Blood, The Journal of the American Society of Hematology*, *121*(22), 4463-4472.

Genovese, G., Kähler, A. K., Handsaker, R. E., Lindberg, J., Rose, S. A., Bakhoum, S. F., Chambert, K., Mick, E., Neale, B. M., & Fromer, M. (2014). Clonal hematopoiesis and blood-cancer risk inferred from blood DNA sequence. *New England Journal of Medicine*, *371*(26), 2477-2487.

Ghosh, S., Liu, B. H., Wang, Y., Hao, Q., & Zhou, Z. J. (2015). Lamin A Is an Endogenous SIRT6 Activator and Promotes SIRT6-Mediated DNA Repair. *Cell reports*, *13*(7), 1396-1406. https://doi.org/10.1016/j.celrep.2015.10.006

Giansanti, C., Manzini, V., Dickmanns, A., Dickmanns, A., Palumbieri, M. D., Sanchi, A., Kienle, S. M., Rieth, S., Scheffner, M., & Lopes, M. (2022). MDM2 binds and ubiquitinates PARP1 to enhance DNA replication fork progression. *Cell reports*, *39*(9).

Gill, D., Parry, A., Santos, F., Okkenhaug, H., Todd, C. D., Hernando-Herraez, I., Stubbs, T. M., Milagre, I., & Reik, W. (2022). Multi-omic rejuvenation of human cells by maturation phase transient reprogramming. *elife*, *11*, e71624. https://doi.org/10.7554/eLife.71624

Grants, J. M., Wegrzyn, J., Hui, T., O'Neill, K., Shadbolt, M., Knapp, D., Parker, J., Deng, Y., Gopal, A., Docking, T. R., Fuller, M., Li, J., Boldin, M., Eaves, C. J., Hirst, M.,

& Karsan, A. (2020). Altered microRNA expression links IL6 and TNF-induced inflammaging with myeloid malignancy in humans and mice. *Blood*, *135*(25), 2235-2251. https://doi.org/10.1182/blood.2019003105

Grigoryan, A., Guidi, N., Senger, K., Liehr, T., Soller, K., Marka, G., Vollmer, A., Markaki, Y., Leonhardt, H., Buske, C., Lipka, D. B., Plass, C., Zheng, Y., Mulaw, M. A., Geiger, H., & Florian, M. C. (2018). LaminA/C regulates epigenetic and chromatin architecture changes upon aging of hematopoietic stem cells. *Genome biology*, *19*(1), 1-21. https://doi.org/10.1186/s13059-018-1557-3

Grigoryan, A., Pospiech, J., Kramer, S., Lipka, D., Liehr, T., Geiger, H., Kimura, H., Mulaw, M. A., & Florian, M. C. (2021). Attrition of X Chromosome Inactivation in Aged Hematopoietic Stem Cells. *Stem cell reports*, *16*(4), 708-716. https://doi.org/10.1016/j.stemcr.2021.03.007

Gu, M., Kovilakam, S. C., Dunn, W. G., Marando, L., Barcena, C., Mohorianu, I., Smith, A., Kar, S. P., Fabre, M. A., Gerstung, M., Cargo, C. A., Malcovati, L., Quiros, P. M., & Vassiliou, G. S. (2023). Multiparameter prediction of myeloid neoplasia risk. *Nat Genet*, *55*(9), 1523-1530. https://doi.org/10.1038/s41588-023-01472-1

Guidi, N., Sacma, M., Ständker, L., Soller, K., Marka, G., Eiwen, K., Weiss, J. M., Kirchhoff, F., Weil, T., & Cancelas, J. A. (2017). Osteopontin attenuates aging-associated phenotypes of hematopoietic stem cells. *The EMBO journal*, *36*(7), 840-853.

Gulati, G. S., Zukowska, M., Noh, J. J., Zhang, A., Wesche, D. J., Sinha, R., George, B. M., Weissman, I. L., & Szade, K. (2019). Neogenin-1 distinguishes between myeloid-biased and balanced Hoxb5(+) mouse long-term hematopoietic stem cells. *Proc Natl Acad Sci U S A*, *116*(50), 25115-25125. https://doi.org/10.1073/pnas.1911024116

Gupta, C., Xu, J., Jin, T., Khullar, S., Liu, X., Alatkar, S., Cheng, F., & Wang, D. (2022). Single-cell network biology characterizes cell type gene regulation for drug repurposing and phenotype prediction in Alzheimer's disease. *PLoS Comput Biol*, *18*(7), e1010287. https://doi.org/10.1371/journal.pcbi.1010287

He, R., Xiao, C., Lei, W., Chen, G., Li, Y., & Luo, O. J. (2025). Aging-associated transcriptional programs in T cells signify constituents of TGF-beta signaling for immunosenescence. *BMC Biol*, *24*(1), 17. https://doi.org/10.1186/s12915-025-02484-5

Hecker, D., Behjati Ardakani, F., Karollus, A., Gagneur, J., & Schulz, M. H. (2023). The adapted Activity-By-Contact model for enhancer-gene assignment and its application to single-cell data. *Bioinformatics*, *39*(2). https://doi.org/10.1093/bioinformatics/btad062

Hecker, D., Song, X., Baumgarten, N., Diagel, A., Katsaouni, N., Li, L., Li, S., Kumar Maji, R., Behjati Ardakani, F., & Ma, L. (2026). Cell type-specific epigenetic regulatory circuitry of coronary artery disease loci. *Nature communications*, *17*(2367). https://doi.org/10.1038/s41467-026-70216-6

Henderson, J. M., Ujita, A., Hill, E., Yousif-Rosales, S., Smith, C., Ko, N., McReynolds, T., Cabral, C. R., Escamilla-Powers, J. R., & Houston, M. E. (2021). Cap 1 Messenger RNA Synthesis with Co-transcriptional CleanCap((R)) Analog by In Vitro Transcription. *Curr Protoc*, *1*(2), e39. https://doi.org/10.1002/cpz1.39

Hérault, L., Poplineau, M., Mazuel, A., Platet, N., Remy, É., & Duprez, E. (2021). Single-cell RNA-seq reveals a concomitant delay in differentiation and cell cycle of aged hematopoietic stem cells. *BMC biology*, *19*(1), 1-20.

Heuts, B. M. H., Arza-Apalategi, S., Frolich, S., Bergevoet, S. M., van den Oever, S. N., van Heeringen, S. J., van der Reijden, B. A., & Martens, J. H. A. (2022). Identification of transcription factors dictating blood cell development using a bidirectional transcription network-based computational framework. *Sci Rep*, *12*(1), 18656. https://doi.org/10.1038/s41598-022-21148-w

Hidaoui, D., Porquet, A., Chelbi, R., Bohm, M., Polyzou, A., Alcazer, V., Depil, S., Imanci, A., Morabito, M., Renneville, A., Selimoglu-Buet, D., Thepot, S., Itzykson, R., Laplane, L., Droin, N., Trompouki, E., Elvira-Matelot, E., Solary, E., & Porteu, F. (2024). Targeting heterochromatin eliminates chronic myelomonocytic leukemia malignant stem cells through reactivation of retroelements and immune pathways. *Commun Biol*, *7*(1), 1555. https://doi.org/10.1038/s42003-024-07214-1

Hinge, A., He, J., Bartram, J., Javier, J., Xu, J., Fjellman, E., Sesaki, H., Li, T., Yu, J., Wunderlich, M., Mulloy, J., Kofron, M., Salomonis, N., Grimes, H. L., & Filippi, M. D. (2020). Asymmetrically Segregated Mitochondria Provide Cellular Memory of Hematopoietic Stem Cell Replicative History and Drive HSC Attrition. *Cell stem cell*, *26*(3), 420-430 e426. https://doi.org/10.1016/j.stem.2020.01.016

Hirche, C., Frenz, T., Haas, S. F., Doring, M., Borst, K., Tegtmeyer, P. K., Brizic, I., Jordan, S., Keyser, K., Chhatbar, C., Pronk, E., Lin, S., Messerle, M., Jonjic, S., Falk, C. S., Trumpp, A., Essers, M. A. G., & Kalinke, U. (2017). Systemic Virus Infections Differentially Modulate Cell Cycle State and Functionality of Long-Term Hematopoietic Stem Cells In Vivo. *Cell Rep*, *19*(11), 2345-2356. https://doi.org/10.1016/j.celrep.2017.05.063

Ho, T. T., Dellorusso, P. V., Verovskaya, E. V., Bakker, S. T., Flach, J., Smith, L. K., Ventura, P. B., Lansinger, O. M., Herault, A., Zhang, S. Y., Kang, Y. A., Mitchell, C. A., Villeda, S. A., & Passegue, E. (2021). Aged hematopoietic stem cells are refractory to bloodborne systemic rejuvenation interventions. *J Exp Med*, *218*(7). https://doi.org/10.1084/jem.20210223

Ho, T. T., Warr, M. R., Adelman, E. R., Lansinger, O. M., Flach, J., Verovskaya, E. V., Figueroa, M. E., & Passegue, E. (2017). Autophagy maintains the metabolism and function of young and old stem cells. *Nature*, *543*(7644), 205-210. https://doi.org/10.1038/nature21388

Hock, H., Hamblen, M. J., Rooke, H. M., Schindler, J. W., Saleque, S., Fujiwara, Y., & Orkin, S. H. (2004). Gfi-1 restricts proliferation and preserves functional integrity of haematopoietic stem cells. *Nature*, *431*(7011), 1002-1007. https://doi.org/10.1038/nature02994

Hoffman, E. A., Frey, B. L., Smith, L. M., & Auble, D. T. (2015). Formaldehyde crosslinking: a tool for the study of chromatin complexes. *J Biol Chem*, *290*(44), 26404-26411. https://doi.org/10.1074/jbc.R115.651679

Hofmann, M. A., Drury, S., Fu, C., Qu, W., Taguchi, A., Lu, Y., Avila, C., Kambham, N., Bierhaus, A., Nawroth, P., Neurath, M. F., Slattery, T., Beach, D., McClary, J., Nagashima, M., Morser, J., Stern, D., & Schmidt, A. M. (1999). RAGE mediates a novel proinflammatory axis: a central cell surface receptor for S100/calgranulin polypeptides. *Cell*, *97*(7), 889-901. https://doi.org/10.1016/s0092-8674(00)80801-6

Hohaus, S., Voso, M. T., Orta-La Barbera, E., Cavallo, S., Bellacosa, A., Rutella, S., Rumi, C., Genuardi, M., Neri, G., & Leone, G. (1997). Telomerase activity in human hematopoietic progenitor cells. *haematologica*, *82*(3), 262-268. https://www.ncbi.nlm.nih.gov/pubmed/9234570

Hönes, J. M., Thivakaran, A., Botezatu, L., Patnana, P., Castro, S. V. d. C., Al-Matary, Y. S., Schütte, J., Fischer, K. B., Vassen, L., & Görgens, A. (2017). Enforced GFI1 expression impedes human and murine leukemic cell growth. *Scientific reports*, *7*(1), 15720.

Hong, T., Li, J., Guo, L., Cavalier, M., Wang, T., Dou, Y., DeLaFuente, A., Fang, S., Guzman, A., Wohlan, K., Kapadia, C., Rosas, C., Yang, Y., Yin, C. C., Li, S., You, M. J., Cheng, X., Goodell, M. A., Zhou, Y., & Huang, Y. (2023). TET2 modulates spatial relocalization of heterochromatin in aged hematopoietic stem and progenitor cells. *Nat Aging*, *3*(11), 1387-1400. https://doi.org/10.1038/s43587-023-00505-y

Horvath, S. (2013). DNA methylation age of human tissues and cell types. *Genome Biol*, *14*(10), R115. https://doi.org/10.1186/gb-2013-14-10-r115

Hosokawa, K., MacArthur, B. D., Ikushima, Y. M., Toyama, H., Masuhiro, Y., Hanazawa, S., Suda, T., & Arai, F. (2017). The telomere binding protein Pot1 maintains haematopoietic stem cell activity with age. *Nat Commun*, *8*(1), 804. https://doi.org/10.1038/s41467-017-00935-4

Hsieh, T. S., Fudenberg, G., Goloborodko, A., & Rando, O. J. (2016). Micro-C XL: assaying chromosome conformation from the nucleosome to the entire genome. *Nat Methods*, *13*(12), 1009-1011. https://doi.org/10.1038/nmeth.4025

Huh, D., & Paulsson, J. (2011). Non-genetic heterogeneity from stochastic partitioning at cell division. *Nature genetics*, *43*(2), 95-100.

Hurt, E. M., Wiestner, A., Rosenwald, A., Shaffer, A. L., Campo, E., Grogan, T., Bergsagel, P. L., Kuehl, W. M., & Staudt, L. M. (2004). Overexpression of c-maf is a frequent oncogenic event in multiple myeloma that promotes proliferation and pathological interactions with bone marrow stroma. *Cancer Cell*, *5*(2), 191-199. https://doi.org/10.1016/s1535-6108(04)00019-4

Huyghe, A., Furlan, G., Schroeder, J., Cascales, E., Trajkova, A., Ruel, M., Studer, F., Larcombe, M., Yang Sun, Y. B., Mugnier, F., De Matteo, L., Baygin, A., Wang, J., Yu, Y., Rama, N., Gibert, B., Kielbassa, J., Tonon, L., Wajda, P.,…Lavial, F. (2022). Comparative roadmaps of reprogramming and oncogenic transformation identify Bcl11b and Atoh8 as broad regulators of cellular plasticity. *Nat Cell Biol*, *24*(9), 1350-1363. https://doi.org/10.1038/s41556-022-00986-w

Itoh-Nakadai, A., Hikota, R., Muto, A., Kometani, K., Watanabe-Matsui, M., Sato, Y., Kobayashi, M., Nakamura, A., Miura, Y., & Yano, Y. (2014). The transcription repressors Bach2 and Bach1 promote B cell development by repressing the myeloid program. *Nature immunology*, *15*(12), 1171-1180.

Itokawa, N., Oshima, M., Koide, S., Takayama, N., Kuribayashi, W., Nakajima-Takagi, Y., Aoyama, K., Yamazaki, S., Yamaguchi, K., Furukawa, Y., Eto, K., & Iwama, A. (2022). Epigenetic traits inscribed in chromatin accessibility in aged hematopoietic stem cells. *Nat Commun*, *13*(1), 2691. https://doi.org/10.1038/s41467-022-30440-2

Jaiswal, S., Fontanillas, P., Flannick, J., Manning, A., Grauman, P. V., Mar, B. G., Lindsley, R. C., Mermel, C. H., Burtt, N., Chavez, A., Higgins, J. M., Moltchanov, V., Kuo, F. C., Kluk, M. J., Henderson, B., Kinnunen, L., Koistinen, H. A.,

Ladenvall, C., Getz, G.,…Ebert, B. L. (2014). Age-related clonal hematopoiesis associated with adverse outcomes. *N Engl J Med*, *371*(26), 2488-2498. https://doi.org/10.1056/NEJMoa1408617

Jaiswal, S., Natarajan, P., Silver, A. J., Gibson, C. J., Bick, A. G., Shvartz, E., McConkey, M., Gupta, N., Gabriel, S., Ardissino, D., Baber, U., Mehran, R., Fuster, V., Danesh, J., Frossard, P., Saleheen, D., Melander, O., Sukhova, G. K., Neuberg, D.,…Ebert, B. L. (2017). Clonal Hematopoiesis and Risk of Atherosclerotic Cardiovascular Disease. *N Engl J Med*, *377*(2), 111-121. https://doi.org/10.1056/NEJMoa1701719

Jakob, L., Muller, T. A., Rassner, M., Kleinfelder, H., Veratti, P., Mitschke, J., Miething, C., Oostendorp, R. A. J., Pfeifer, D., Waterhouse, M., & Duyster, J. (2021). Murine Oncostatin M Has Opposing Effects on the Proliferation of OP9 Bone Marrow Stromal Cells and NIH/3T3 Fibroblasts Signaling through the OSMR. *Int J Mol Sci*, *22*(21). https://doi.org/10.3390/ijms222111649

Jang, I. H., Niedernhofer, L. J., Robbins, P. D., & Camell, C. D. (2026). The ageing immune system as a driver of systemic ageing. *Nat Rev Immunol*. https://doi.org/10.1038/s41577-026-01269-3

Javierre, B. M., Burren, O. S., Wilder, S. P., Kreuzhuber, R., Hill, S. M., Sewitz, S., Cairns, J., Wingett, S. W., Varnai, C., Thiecke, M. J., Burden, F., Farrow, S., Cutler, A. J., Rehnstrom, K., Downes, K., Grassi, L., Kostadima, M., Freire-Pritchett, P., Wang, F.,…Fraser, P. (2016). Lineage-Specific Genome Architecture Links Enhancers and Non-coding Disease Variants to Target Gene Promoters. *Cell*, *167*(5), 1369-1384 e1319. https://doi.org/10.1016/j.cell.2016.09.037

Jenkinson, G., Pujadas, E., Goutsias, J., & Feinberg, A. P. (2017). Potential energy landscapes identify the information-theoretic nature of the epigenome. *Nat Genet*, *49*(5), 719-729. https://doi.org/10.1038/ng.3811

Jeong, S. Y., Kim, J. A., & Oh, I. H. (2018). The Adaptive Remodeling of Stem Cell Niche in Stimulated Bone Marrow Counteracts the Leukemic Niche. *Stem Cells*, *36*(10), 1617-1629. https://doi.org/10.1002/stem.2870

Jiang, W., Ye, W., Tan, X., & Bao, Y. J. (2025). Network-based multi-omics integrative analysis methods in drug discovery: a systematic review. *BioData Min*, *18*(1), 27. https://doi.org/10.1186/s13040-025-00442-z

Jin, S., Plikus, M. V., & Nie, Q. (2025). CellChat for systematic analysis of cell-cell communication from single-cell transcriptomics. *Nat Protoc*, *20*(1), 180-219. https://doi.org/10.1038/s41596-024-01045-4

Jin, T., Rehani, P., Ying, M., Huang, J., Liu, S., Roussos, P., & Wang, D. (2021). scGRNom: a computational pipeline of integrative multi-omics analyses for predicting cell-type disease genes and regulatory networks. *Genome Med*, *13*(1), 95. https://doi.org/10.1186/s13073-021-00908-9

Johanson, T. M., & Allan, R. S. (2022). In Situ HiC. In *Chromatin: Methods and Protocols* (pp. 333-343). Springer.

Johanson, T. M., Lun, A. T. L., Coughlan, H. D., Tan, T., Smyth, G. K., Nutt, S. L., & Allan, R. S. (2018). Transcription-factor-mediated supervision of global genome architecture maintains B cell identity. *Nat Immunol*, *19*(11), 1257-1264. https://doi.org/10.1038/s41590-018-0234-8

Jurkowska, R. Z., Jurkowski, T. P., & Jeltsch, A. (2011). Structure and function of mammalian DNA methyltransferases. *Chembiochem*, *12*(2), 206-222.
Kadota, M., Nishimura, O., Miura, H., Tanaka, K., Hiratani, I., & Kuraku, S. (2020). Multifaceted Hi-C benchmarking: what makes a difference in chromosome-scale genome scaffolding? *Gigascience*, *9*(1). https://doi.org/10.1093/gigascience/giz158
Kamal, A., Arnold, C., Claringbould, A., Moussa, R., Servaas, N. H., Kholmatov, M., Daga, N., Nogina, D., Mueller-Dott, S., Reyes-Palomares, A., Palla, G., Sigalova, O., Bunina, D., Pabst, C., & Zaugg, J. B. (2023). GRaNIE and GRaNPA: inference and evaluation of enhancer-mediated gene regulatory networks. *Mol Syst Biol*, *19*(6), e11627. https://doi.org/10.15252/msb.202311627
Kamaraj, U. S., Chen, J., Katwadi, K., Ouyang, J. F., Sun, Y. B. Y., Lim, Y. M., Liu, X. D., Handoko, L., Polo, J. M., Petretto, E., & Rackham, O. J. L. (2020). EpiMogrify Models H3K4me3 Data to Identify Signaling Molecules that Improve Cell Fate Control and Maintenance. *Cell Systems*, *11*(5), 509-+. https://doi.org/10.1016/j.cels.2020.09.004
Kamimoto, K., Stringa, B., Hoffmann, C. M., Jindal, K., Solnica-Krezel, L., & Morris, S. A. (2023). Dissecting cell identity via network inference and in silico gene perturbation. *Nature*, *614*(7949), 742-751.
Kapadia, C. D., Williams, N., Dawson, K. J., Watson, C., Yousefzadeh, M. J., Le, D., Nyamondo, K., Kodavali, S., Cagan, A., Waldvogel, S., Zhang, X., De La Fuente, J., Leongamornlert, D., Mitchell, E., Florez, M. A., Sosnowski, K., Aguilar, R., Martell, A., Guzman, A.,…Nangalia, J. (2025). Clonal dynamics and somatic evolution of haematopoiesis in mouse. *Nature*, *641*(8063), 681-689. https://doi.org/10.1038/s41586-025-08625-8
Karagiannis, T. T., Dowrey, T. W., Villacorta-Martin, C., Montano, M., Reed, E., Belkina, A. C., Andersen, S. L., Perls, T. T., Monti, S., & Murphy, G. J. (2023). Multi-modal profiling of peripheral blood cells across the human lifespan reveals distinct immune cell signatures of aging and longevity. *EBioMedicine*, *90*.
Karg, M. M., Lu, Y. R., Refaian, N., Cameron, J., Hoffmann, E., Hoppe, C., Shirahama, S., Shah, M., Krasniqi, D., Krishnan, A., Shrestha, M., Guo, Y., Cermak, J. M., Walthier, M., Broniowska, K., Rosenzweig-Lipson, S., Gregory-Ksander, M., Sinclair, D. A., & Ksander, B. R. (2023). Sustained Vision Recovery by OSK Gene Therapy in a Mouse Model of Glaucoma. *Cell Reprogram*, *25*(6), 288-299. https://doi.org/10.1089/cell.2023.0074
Kariko, K., Buckstein, M., Ni, H., & Weissman, D. (2005). Suppression of RNA recognition by Toll-like receptors: the impact of nucleoside modification and the evolutionary origin of RNA. *Immunity*, *23*(2), 165-175. https://doi.org/10.1016/j.immuni.2005.06.008
Kariko, K., Muramatsu, H., Welsh, F. A., Ludwig, J., Kato, H., Akira, S., & Weissman, D. (2008). Incorporation of pseudouridine into mRNA yields superior nonimmunogenic vector with increased translational capacity and biological stability. *Mol Ther*, *16*(11), 1833-1840. https://doi.org/10.1038/mt.2008.200
Katahira, Y., Higuchi, H., Matsushita, H., Yahata, T., Yamamoto, Y., Koike, R., Ando, K., Sato, K., Imadome, K. I., & Kotani, A. (2019). Increased Granulopoiesis in the Bone Marrow following Epstein-Barr Virus Infection. *Sci Rep*, *9*(1), 13445. https://doi.org/10.1038/s41598-019-49937-w

Kato, H., Itoh-Nakadai, A., Matsumoto, M., Ishii, Y., Watanabe-Matsui, M., Ikeda, M., Ebina-Shibuya, R., Sato, Y., Kobayashi, M., & Nishizawa, H. (2018). Infection perturbs Bach2-and Bach1-dependent erythroid lineage 'choice'to cause anemia. *Nature immunology*, *19*(10), 1059-1070.

Katsuda, T., Sussman, J. H., Ito, K., Katznelson, A., Yuan, S., Takenaka, N., Li, J., Merrell, A. J., Cure, H., Li, Q., Rasool, R. U., Asangani, I. A., Zaret, K. S., & Stanger, B. Z. (2024). Cellular reprogramming in vivo initiated by SOX4 pioneer factor activity. *Nat Commun*, *15*(1), 1761. https://doi.org/10.1038/s41467-024-45939-z

Kaufmann, K. B., Zeng, A. G. X., Coyaud, E., Garcia-Prat, L., Papalexi, E., Murison, A., Laurent, E. M. N., Chan-Seng-Yue, M., Gan, O. I., Pan, K., McLeod, J., Boutzen, H., Zandi, S., Takayanagi, S. I., Satija, R., Raught, B., Xie, S. Z., & Dick, J. E. (2021). A latent subset of human hematopoietic stem cells resists regenerative stress to preserve stemness. *Nat Immunol*, *22*(6), 723-734. https://doi.org/10.1038/s41590-021-00925-1

Kawahigashi, T., Iwanami, S., Takahashi, M., Bhadury, J., Iwami, S., & Yamazaki, S. (2024). Age-related changes in the hematopoietic stem cell pool revealed via quantifying the balance of symmetric and asymmetric divisions. *Plos one*, *19*(1), e0292575. https://doi.org/10.1371/journal.pone.0292575

Keenan, C. R., Iannarella, N., Naselli, G., Bediaga, N. G., Johanson, T. M., Harrison, L. C., & Allan, R. S. (2020). Extreme disruption of heterochromatin is required for accelerated hematopoietic aging. *Blood*, *135*(23), 2049-2058. https://doi.org/10.1182/blood.2019002990

Khan, S., Chakraborty, M., Wu, F., Chen, N., Wang, T., Chan, Y. T., Sayad, A., Kotlyar, M., Alibhai, F. J., Woo, M., Li, R. K., Husain, M., Jurisica, I., Gehring, A. J., Ohashi, P. S., Furman, D., Tsai, S., Winer, S., & Winer, D. A. (2026). B cells drive CD4 T cell immunosenescence and age-associated health decline. *Sci Immunol*, *11*(115), eadv7615. https://doi.org/10.1126/sciimmunol.adv7615

Khandanpour, C., Kosan, C., Gaudreau, M. C., Duhrsen, U., Hebert, J., Zeng, H., & Moroy, T. (2011). Growth factor independence 1 protects hematopoietic stem cells against apoptosis but also prevents the development of a myeloproliferative-like disease. *Stem Cells*, *29*(2), 376-385. https://doi.org/10.1002/stem.575

Khetarpal, S. A., Qamar, A., Bick, A. G., Fuster, J. J., Kathiresan, S., Jaiswal, S., & Natarajan, P. (2019). Clonal Hematopoiesis of Indeterminate Potential Reshapes Age-Related CVD: JACC Review Topic of the Week. *J Am Coll Cardiol*, *74*(4), 578-586. https://doi.org/10.1016/j.jacc.2019.05.045

Khokhar, E. S., Borikar, S., Eudy, E., Stearns, T., Young, K., & Trowbridge, J. J. (2020). Aging-associated decrease in the histone acetyltransferase KAT6B is linked to altered hematopoietic stem cell differentiation. *Exp Hematol*, *82*, 43-52 e44. https://doi.org/10.1016/j.exphem.2020.01.014

Khoshchehreh, R., Totonchi, M., Carlos Ramirez, J., Torres, R., Baharvand, H., Aicher, A., Ebrahimi, M., & Heeschen, C. (2019). Epigenetic reprogramming of primary pancreatic cancer cells counteracts their in vivo tumourigenicity. *Oncogene*, *38*(34), 6226-6239. https://doi.org/10.1038/s41388-019-0871-x

Khullar, S., & Wang, D. (2023). Predicting brain-regional gene regulatory networks from multi-omics for Alzheimer's disease phenotypes and Covid-19 severity. *Hum Mol Genet*, *32*(11), 1797-1813. https://doi.org/10.1093/hmg/ddad009

Kim, K. M., Mura-Meszaros, A., Tollot, M., Krishnan, M. S., Grundl, M., Neubert, L., Groth, M., Rodriguez-Fraticelli, A., Svendsen, A. F., Campaner, S., Andreas, N., Kamradt, T., Hoffmann, S., Camargo, F. D., Heidel, F. H., Bystrykh, L. V., de Haan, G., & von Eyss, B. (2022). Taz protects hematopoietic stem cells from an aging-dependent decrease in PU.1 activity. *Nat Commun*, *13*(1), 5187. https://doi.org/10.1038/s41467-022-32970-1

Kim, S.-J., Kwon, H.-S., Kwon, D.-k., Koo, O.-J., Moon, J.-H., Park, E.-J., Yum, S.-Y., Lee, B.-C., & Jang, G. (2019). Production of transgenic porcine embryos reconstructed with induced pluripotent stem-like cells derived from porcine endogenous factors using piggyBac system. *Cellular reprogramming*, *21*(1), 26-36.

Kim, S. I., Oceguera-Yanez, F., Hirohata, R., Linker, S., Okita, K., Yamada, Y., Yamamoto, T., Yamanaka, S., & Woltjen, K. (2015). KLF4 N-terminal variance modulates induced reprogramming to pluripotency. *Stem cell reports*, *4*(4), 727-743. https://doi.org/10.1016/j.stemcr.2015.02.004

Kimura, Y., Ono, Y., Katayama, K., & Imoto, S. (2024). IVEA: an integrative variational Bayesian inference method for predicting enhancer-gene regulatory interactions. *Bioinform Adv*, *4*(1), vbae118. https://doi.org/10.1093/bioadv/vbae118

Kisby, T., de Lázaro, I., Fisch, S., Cartwright, E. J., Cossu, G., & Kostarelos, K. (2021). Adenoviral Mediated Delivery of OSKM Factors Induces Partial Reprogramming of Mouse Cardiac Cells In Vivo. *Advanced Therapeutics*, *4*(2), 2000141.

Koide, S., Oshima, M., Nishiyama, A., Murakami, K., Yamada, Y., Itokawa, N., Nakajima-Takagi, Y., Zheng, Z. Q., Tomohiko, T., & Iwama, A. (2021). Unraveling Heterogeneity of Aged Hematopoietic Stem Cells By Single-Cell RNA Sequence Analysis. *Blood*, *138*, 4299. https://doi.org/10.1182/blood-2021-149876

Konturek-Ciesla, A., Dhapola, P., Zhang, Q., Säwén, P., Wan, H., Karlsson, G., & Bryder, D. (2023). Temporal multimodal single-cell profiling of native hematopoiesis illuminates altered differentiation trajectories with age. *Cell reports*, *42*(4), 112304.

Koohy, H., Bolland, D. J., Matheson, L. S., Schoenfelder, S., Stellato, C., Dimond, A., Varnai, C., Chovanec, P., Chessa, T., Denizot, J., Garcia, R. M., Wingett, S. W., Freire-Pritchett, P., Nagano, T., Hawkins, P., Stephens, L., Elderkin, S., Spivakov, M., Fraser, P.,…Varga-Weisz, P. D. (2018). Genome organization and chromatin analysis identify transcriptional downregulation of insulin-like growth factor signaling as a hallmark of aging in developing B cells. *Genome biology*, *19*(1), 1-24. https://doi.org/10.1186/s13059-018-1489-y

Kovtonyuk, L. V., Caiado, F., Garcia-Martin, S., Manz, E. M., Helbling, P., Takizawa, H., Boettcher, S., Al-Shahrour, F., Nombela-Arrieta, C., Slack, E., & Manz, M. G. (2022). IL-1 mediates microbiome-induced inflammaging of hematopoietic stem cells in mice. *Blood*, *139*(1), 44-58. https://doi.org/10.1182/blood.2021011570

Kramer, N. E., Davis, E. S., Wenger, C. D., Deoudes, E. M., Parker, S. M., Love, M. I., & Phanstiel, D. H. (2022). Plotgardener: cultivating precise multi-panel figures in R. *Bioinformatics*, *38*(7), 2042-2045.

Kriukov, D., Eremenko, E., Smirnov, D., Stein, D., Tsitrina, A., Golova, A., Einav, M., Khrameeva, E., & Toiber, D. (2024). Nuclear expansion and chromatin structure remodeling in mouse aging neurons. *NAR Molecular Medicine*, *1*(3), ugae011.

Ksander, B., Shah, M., Krasniqi, D., Gregory-Ksander, M. S., Rosenzweig-Lipson, S., Broniowska, K., Wathier, M., Mannick, J., Cermak, J., & Karg, M. (2023).

Epigenetic reprogramming-A novel gene therapy that restores vision loss in a nonhuman primate model of NAION. *Investigative Ophthalmology & Visual Science*, *64*(8), 474-474.

Kulkarni, R., Bajaj, M., Ghode, S., Jalnapurkar, S., Limaye, L., & Kale, V. P. (2018). Intercellular Transfer of Microvesicles from Young Mesenchymal Stromal Cells Rejuvenates Aged Murine Hematopoietic Stem Cells. *Stem Cells*, *36*(3), 420-433. https://doi.org/10.1002/stem.2756

Kunst, S., Wolloscheck, T., Kelleher, D. K., Wolfrum, U., Sargsyan, S. A., Iuvone, P. M., Baba, K., Tosini, G., & Spessert, R. (2015). Pgc-1alpha and Nr4a1 Are Target Genes of Circadian Melatonin and Dopamine Release in Murine Retina. *Invest Ophthalmol Vis Sci*, *56*(10), 6084-6094. https://doi.org/10.1167/iovs.15-17503

Kuranda, K., Vargaftig, J., de la Rochere, P., Dosquet, C., Charron, D., Bardin, F., Tonnelle, C., Bonnet, D., & Goodhardt, M. (2011). Age-related changes in human hematopoietic stem/progenitor cells. *Aging cell*, *10*(3), 542-546. https://doi.org/10.1111/j.1474-9726.2011.00675.x

Kuribayashi, W., Oshima, M., Itokawa, N., Koide, S., Nakajima-Takagi, Y., Yamashita, M., Yamazaki, S., Rahmutulla, B., Miura, F., Ito, T., Kaneda, A., & Iwama, A. (2021). Limited rejuvenation of aged hematopoietic stem cells in young bone marrow niche. *J Exp Med*, *218*(3). https://doi.org/10.1084/jem.20192283

Kuroda, Y., Kitada, M., Wakao, S., Nishikawa, K., Tanimura, Y., Makinoshima, H., Goda, M., Akashi, H., Inutsuka, A., Niwa, A., Shigemoto, T., Nabeshima, Y., Nakahata, T., Nabeshima, Y., Fujiyoshi, Y., & Dezawa, M. (2010). Unique multipotent cells in adult human mesenchymal cell populations. *Proc Natl Acad Sci U S A*, *107*(19), 8639-8643. https://doi.org/10.1073/pnas.0911647107

Kurylo, C., Zytnicki, M., Foissac, S., & Maigné, É. (2023). HiCDOC: A/B compartment detection and differential analysis. (Version 1.6.0) [R package]. https://bioconductor.org/packages/HiCDOC

Kyaw, W., Chai, R. C., Khoo, W. H., Goldstein, L. D., Croucher, P. I., Murray, J. M., & Phan, T. G. (2023). ENTRAIN: integrating trajectory inference and gene regulatory networks with spatial data to co-localize the receptor–ligand interactions that specify cell fate. *Bioinformatics*, *39*(12), btad765.

Lafontaine, D. L., Yang, L., Dekker, J., & Gibcus, J. H. (2021). Hi-C 3.0: Improved Protocol for Genome-Wide Chromosome Conformation Capture. *Curr Protoc*, *1*(7), e198. https://doi.org/10.1002/cpz1.198

Langereis, M. A., Rabouw, H. H., Holwerda, M., Visser, L. J., & van Kuppeveld, F. J. (2015). Knockout of cGAS and STING Rescues Virus Infection of Plasmid DNA-Transfected Cells. *J Virol*, *89*(21), 11169-11173. https://doi.org/10.1128/JVI.01781-15

Langmead, B., & Salzberg, S. L. (2012). Fast gapped-read alignment with Bowtie 2. *Nat Methods*, *9*(4), 357-359. https://doi.org/10.1038/nmeth.1923

Lanna, A., Vaz, B., D'Ambra, C., Valvo, S., Vuotto, C., Chiurchiu, V., Devine, O., Sanchez, M., Borsellino, G., Akbar, A. N., De Bardi, M., Gilroy, D. W., Dustin, M. L., Blumer, B., & Karin, M. (2022). An intercellular transfer of telomeres rescues T cells from senescence and promotes long-term immunological memory. *Nat Cell Biol*, *24*(10), 1461-1474. https://doi.org/10.1038/s41556-022-00991-z

Lapasset, L., Milhavet, O., Prieur, A., Besnard, E., Babled, A., Aït-Hamou, N., Leschik, J., Pellestor, F., Ramirez, J.-M., & De Vos, J. (2011). Rejuvenating senescent and centenarian human cells by reprogramming through the pluripotent state. *Genes & development*, *25*(21), 2248-2253.

Lawrence, M., Gentleman, R., & Carey, V. (2009). rtracklayer: an R package for interfacing with genome browsers. *Bioinformatics*, *25*(14), 1841.

Lawrence, M., Huber, W., Pages, H., Aboyoun, P., Carlson, M., Gentleman, R., Morgan, M. T., & Carey, V. J. (2013). Software for computing and annotating genomic ranges. *PLoS Comput Biol*, *9*(8), e1003118. https://doi.org/10.1371/journal.pcbi.1003118

Lawson, A. R. J., Abascal, F., Nicola, P. A., Lensing, S. V., Roberts, A. L., Kalantzis, G., Baez-Ortega, A., Brzozowska, N., El-Sayed Moustafa, J. S., Vaitkute, D., Jakupovic, B., Nessa, A., Wadge, S., Osterdahl, M. F., Paterson, A. L., Rassl, D. M., Alcantara, R. E., O'Neill, L., Widaa, S.,…Martincorena, I. (2025). Somatic mutation and selection at population scale. *Nature*, *647*(8089), 411-420. https://doi.org/10.1038/s41586-025-09584-w

Lee, H. Y., Jeon, Y., Kim, Y. K., Jang, J. Y., Cho, Y. S., Bhak, J., & Cho, K. H. (2021). Identifying molecular targets for reverse aging using integrated network analysis of transcriptomic and epigenomic changes during aging. *Sci Rep*, *11*(1), 12317. https://doi.org/10.1038/s41598-021-91811-1

Lee, J.-H., Demarest, T. G., Babbar, M., Kim, E. W., Okur, M. N., De, S., Croteau, D. L., & Bohr, V. A. (2019). Cockayne syndrome group B deficiency reduces H3K9me3 chromatin remodeler SETDB1 and exacerbates cellular aging. *Nucleic acids research*, *47*(16), 8548-8562.

Lettera, E., Basso-Ricci, L., Carsana, E., Giannetti, K., Tavella, T., Seffin, L., Farina, G., Gualandi, N., Quaranta, P., Lo Furno, E., Pacini, G., Della Volpe, L., Kaufmann, K. B., Garcia-Prat, L., Hernandez, R. J., Murison, A., Aguilar-Navarro, A. G., Beretta, S., Conti, A.,…Di Micco, R. (2026). Molecular and phenotypic blueprint of human hematopoiesis links proliferation stress to stem cell aging. *J Exp Med*, *223*(2). https://doi.org/10.1084/jem.20251805

Levetzow, G. V., Spanholtz, J., Beckmann, J., Fischer, J., Kögler, G., Wernet, P., Punzel, M., & Giebel, B. (2006). Nucleofection, an efficient nonviral method to transfer genes into human hematopoietic stem and progenitor cells. *Stem cells and development*, *15*(2), 278-285.

Li, D., Zhao, X. Y., Zhou, S., Hu, Q., Wu, F., & Lee, H. Y. (2023). Multidimensional profiling reveals GATA1-modulated stage-specific chromatin states and functional associations during human erythropoiesis. *Nucleic Acids Res*, *51*(13), 6634-6653. https://doi.org/10.1093/nar/gkad468

Li, H., Handsaker, B., Wysoker, A., Fennell, T., Ruan, J., Homer, N., Marth, G., Abecasis, G., Durbin, R., & Genome Project Data Processing, S. (2009). The Sequence Alignment/Map format and SAMtools. *Bioinformatics*, *25*(16), 2078-2079. https://doi.org/10.1093/bioinformatics/btp352

Li, L. H., McCarthy, P., & Hui, S. W. (2001). High-efficiency electrotransfection of human primary hematopoietic stem cells. *FASEB J*, *15*(3), 586-588. https://doi.org/10.1096/fj.00-0447fje

Li, R., Cheng, X., Yang, Y., Schwebel, D. C., Ning, P., Li, L., Rao, Z., Cheng, P., Zhao, M., & Hu, G. (2023). Global deaths associated with population aging—1990–2019. *China CDC weekly*, *5*(51), 1150.

Li, Z. P., Du, Z., Huang, D. S., & Teschendorff, A. E. (2025). Interpretable deep learning of single-cell and epigenetic data reveals novel molecular insights in aging. *Sci Rep*, *15*(1), 5048. https://doi.org/10.1038/s41598-025-89646-1

Liang, R., Arif, T., Kalmykova, S., Kasianov, A., Lin, M., Menon, V., Qiu, J., Bernitz, J. M., Moore, K., & Lin, F. (2020). Restraining lysosomal activity preserves hematopoietic stem cell quiescence and potency. *Cell stem cell*, *26*(3), 359-376. e357.

Liang, X., Miao, Y., Han, D., Li, Y., Zhang, W., & Wang, Z. (2025). Predicting enhancer-gene links from single-cell multi-omics data by integrating prior Hi-C information. *bioRxiv*, 2025.2010. 2009.681330.

Liang, Y., Van Zant, G., & Szilvassy, S. J. (2005). Effects of aging on the homing and engraftment of murine hematopoietic stem and progenitor cells. *Blood*, *106*(4), 1479-1487.

Liao, Y., Smyth, G. K., & Shi, W. (2013). The Subread aligner: fast, accurate and scalable read mapping by seed-and-vote. *Nucleic acids research*, *41*(10), e108-e108.

Lieberman-Aiden, E., Van Berkum, N. L., Williams, L., Imakaev, M., Ragoczy, T., Telling, A., Amit, I., Lajoie, B. R., Sabo, P. J., & Dorschner, M. O. (2009). Comprehensive mapping of long-range interactions reveals folding principles of the human genome. *Science*, *326*(5950), 289-293.

Liotti, A., Ferrara, A. L., Loffredo, S., Galdiero, M. R., Varricchi, G., Di Rella, F., Maniscalco, G. T., Belardo, M., Vastano, R., & Prencipe, R. (2022). Epigenetics: an opportunity to shape innate and adaptive immune responses. *Immunology*, *167*(4), 451-470.

Liu, B., Ghosh, S., Yang, X., Zheng, H., Liu, X., Wang, Z., Jin, G., Zheng, B., Kennedy, B. K., & Suh, Y. (2012). Resveratrol rescues SIRT1-dependent adult stem cell decline and alleviates progeroid features in laminopathy-based progeria. *Cell Metabolism*, *16*(6), 738-750.

Liu, Q., Fang, F., Xue, H., Wasterlid, T., Smedby, K. E., & Liu, X. (2026). Clonal hematopoiesis may precede the diagnosis of aplastic anemia by several years. *Blood Adv*, *10*(4), 1293-1300. https://doi.org/10.1182/bloodadvances.2024015776

Liu, Y., Chen, Y., Deng, X., & Zhou, J. (2020). ATF3 Prevents Stress-Induced Hematopoietic Stem Cell Exhaustion. *Front Cell Dev Biol*, *8*, 585771. https://doi.org/10.3389/fcell.2020.585771

Liu, Y. W., Zou, J. T., Gong, J. S., Jin, L., Cao, J., He, Z. H., Qian, Y. X., Wang, X., Wan, M. D., Hu, X. Y., Hong, C. G., Du, W., Chen, C. Y., Liu, H. J., Xie, H., & Wang, Z. X. (2026). Local delivery of OSK factors enables partial cellular reprogramming to mitigate osteoarthritis and cartilage fibrosis. *Exp Mol Med*, *58*, 782–797. https://doi.org/10.1038/s12276-026-01662-x

Liu, Z., Belmonte, J. C. I., Zhang, W., Qu, J., & Liu, G.-H. (2022a). Deciphering aging at three-dimensional genomic resolution. *Cell Insight*, *1*(3), 100034.

Liu, Z., Ji, Q., Ren, J., Yan, P., Wu, Z., Wang, S., Sun, L., Wang, Z., Li, J., & Sun, G. (2022b). Large-scale chromatin reorganization reactivates placenta-specific genes

that drive cellular aging. *Developmental cell*, *57*(11), 1347-1368.e1312. https://doi.org/10.1016/j.devcel.2022.05.004

Loeffler, D., Schneiter, F., Wang, W., Wehling, A., Kull, T., Lengerke, C., Manz, M. G., & Schroeder, T. (2022). Asymmetric organelle inheritance predicts human blood stem cell fate. *Blood, The Journal of the American Society of Hematology*, *139*(13), 2011-2023.

Loers, J. U., & Vermeirssen, V. (2024). A single-cell multimodal view on gene regulatory network inference from transcriptomics and chromatin accessibility data. *Brief Bioinform*, *25*(5). https://doi.org/10.1093/bib/bbae382

Love, M. I., Huber, W., & Anders, S. (2014). Moderated estimation of fold change and dispersion for RNA-seq data with DESeq2. *Genome biology*, *15*(12), 550.

Lu, A. T., Fei, Z., Haghani, A., Robeck, T. R., Zoller, J. A., Li, C. Z., Lowe, R., Yan, Q., Zhang, J., Vu, H., Ablaeva, J., Acosta-Rodriguez, V. A., Adams, D. M., Almunia, J., Aloysius, A., Ardehali, R., Arneson, A., Baker, C. S., Banks, G.,…Horvath, S. (2023). Universal DNA methylation age across mammalian tissues. *Nat Aging*, *3*(9), 1144-1166. https://doi.org/10.1038/s43587-023-00462-6

Lu, J. Y., Tu, W. B., Li, R., Weng, M., Sanketi, B. D., Yuan, B., Reddy, P., Rodriguez Esteban, C., & Izpisua Belmonte, J. C. (2025). Prevalent mesenchymal drift in aging and disease is reversed by partial reprogramming. *Cell*, *188*(21), 5895-5911 e5817. https://doi.org/10.1016/j.cell.2025.07.031

Lu, K., Ye, W., Zhou, L., Collins, L. B., Chen, X., Gold, A., Ball, L. M., & Swenberg, J. A. (2010). Structural characterization of formaldehyde-induced cross-links between amino acids and deoxynucleosides and their oligomers. *J Am Chem Soc*, *132*(10), 3388-3399. https://doi.org/10.1021/ja908282f

Lu, L., Liu, X., Huang, W. K., Giusti-Rodriguez, P., Cui, J., Zhang, S., Xu, W., Wen, Z., Ma, S., Rosen, J. D., Xu, Z., Bartels, C. F., Kawaguchi, R., Hu, M., Scacheri, P. C., Rong, Z., Li, Y., Sullivan, P. F., Song, H.,…Jin, F. (2020). Robust Hi-C Maps of Enhancer-Promoter Interactions Reveal the Function of Non-coding Genome in Neural Development and Diseases. *Mol Cell*, *79*(3), 521-534 e515. https://doi.org/10.1016/j.molcel.2020.06.007

Lu, Y., Brommer, B., Tian, X., Krishnan, A., Meer, M., Wang, C., Vera, D. L., Zeng, Q., Yu, D., Bonkowski, M. S., Yang, J. H., Zhou, S., Hoffmann, E. M., Karg, M. M., Schultz, M. B., Kane, A. E., Davidsohn, N., Korobkina, E., Chwalek, K.,…Sinclair, D. A. (2020). Reprogramming to recover youthful epigenetic information and restore vision. *Nature*, *588*(7836), 124-129. https://doi.org/10.1038/s41586-020-2975-4

Lun, A. T., Perry, M., & Ing-Simmons, E. (2016). Infrastructure for genomic interactions: Bioconductor classes for Hi-C, ChIA-PET and related experiments. *F1000Res*, *5*, 950. https://doi.org/10.12688/f1000research.8759.2

Lun, A. T., & Smyth, G. K. (2015). csaw: a Bioconductor package for differential binding analysis of ChIP-seq data using sliding windows. *Nucleic acids research*, *44*(5), e45.

Lun, A. T., & Smyth, G. K. (2015). diffHic: a Bioconductor package to detect differential genomic interactions in Hi-C data. *BMC Bioinformatics*, *16*, 258. https://doi.org/10.1186/s12859-015-0683-0

Lun, A. T., & Smyth, G. K. (2016). csaw: a Bioconductor package for differential binding analysis of ChIP-seq data using sliding windows. *Nucleic Acids Res*, *44*(5), e45. https://doi.org/10.1093/nar/gkv1191

Ma, F., Cao, Y., Du, H., Braikia, F. Z., Zong, L., Ollikainen, N., Bayer, M., Qiu, X., Park, B., Roy, R., Nandi, S., Sarantopoulou, D., Ziman, A., Bianchi, A. H., Beerman, I., Zhao, K., Grosschedl, R., & Sen, R. (2024). Three-dimensional chromatin reorganization regulates B cell development during ageing. *Nat Cell Biol*, *26*(6), 991-1002. https://doi.org/10.1038/s41556-024-01424-9

Ma, S., Wang, S., Ye, Y., Ren, J., Chen, R., Li, W., Li, J., Zhao, L., Zhao, Q., Sun, G., Jing, Y., Zuo, Y., Xiong, M., Yang, Y., Wang, Q., Lei, J., Sun, S., Long, X., Song, M.,…Liu, G. H. (2022). Heterochronic parabiosis induces stem cell revitalization and systemic rejuvenation across aged tissues. *Cell stem cell*, *29*(6), 990-1005 e1010. https://doi.org/10.1016/j.stem.2022.04.017

Ma, T., Hu, C., Lal, B., Zhou, W., Ma, Y., Ying, M., Prinos, P., Quinones-Hinojosa, A., Lim, M., & Laterra, J. (2021). Reprogramming transcription factors Oct4 and Sox2 induce a BRD-dependent immunosuppressive transcriptome in GBM-propagating cells. *Cancer research*, *81*(9), 2457-2469.

Ma, Z., Xu, J., Wu, L., Wang, J., Lin, Q., Chowdhury, F. A., Mazumder, M. H. H., Hu, G., Li, X., & Du, W. (2020). Hes1 deficiency causes hematopoietic stem cell exhaustion. *Stem Cells*, *38*(6), 756-768. https://doi.org/10.1002/stem.3169

Macarie, R. D., Tucureanu, M. M., Ciortan, L., Preda, M. B., Manduteanu, I., & Butoi, E. (2026). Osteopontin-expressing valvular interstitial cell subpopulation as a driver of extracellular matrix remodeling in aortic valve disease. *Front Cardiovasc Med*, *13*, 1755830. https://doi.org/10.3389/fcvm.2026.1755830

MacCarthy, C. M., Wu, G., Malik, V., Menuchin-Lasowski, Y., Velychko, T., Keshet, G., Fan, R., Bedzhov, I., Church, G. M., & Jauch, R. (2024). Highly cooperative chimeric super-SOX induces naive pluripotency across species. *Cell stem cell*, *31*(1), 127-147. e129.

Machlab, D., Burger, L., Soneson, C., Rijli, F. M., Schubeler, D., & Stadler, M. B. (2022). monaLisa: an R/Bioconductor package for identifying regulatory motifs. *Bioinformatics*, *38*(9), 2624-2625. https://doi.org/10.1093/bioinformatics/btac102

Macip, C. C., Hasan, R., Hoznek, V., Kim, J., Lu, Y. R., Metzger, L. E. t., Sethna, S., & Davidsohn, N. (2024). Gene Therapy-Mediated Partial Reprogramming Extends Lifespan and Reverses Age-Related Changes in Aged Mice. *Cell Reprogram*, *26*(1), 24-32. https://doi.org/10.1089/cell.2023.0072

Malin, K., Witkowska-Piłaszewicz, O., & Papis, K. (2022). The many problems of somatic cell nuclear transfer in reproductive cloning of mammals. *Theriogenology*, *189*, 246-254.

Mann, M., Mehta, A., de Boer, C. G., Kowalczyk, M. S., Lee, K., Haldeman, P., Rogel, N., Knecht, A. R., Farouq, D., Regev, A., & Baltimore, D. (2018). Heterogeneous Responses of Hematopoietic Stem Cells to Inflammatory Stimuli Are Altered with Age. *Cell Rep*, *25*(11), 2992-3005 e2995. https://doi.org/10.1016/j.celrep.2018.11.056

Mannino, G., Russo, C., Maugeri, G., Musumeci, G., Vicario, N., Tibullo, D., Giuffrida, R., Parenti, R., & Lo Furno, D. (2022). Adult stem cell niches for tissue homeostasis. *Journal of Cellular Physiology*, *237*(1), 239-257.

Mansell, E., Sigurdsson, V., Deltcheva, E., Brown, J., James, C., Miharada, K., Soneji, S., Larsson, J., & Enver, T. (2021). Mitochondrial Potentiation Ameliorates Age-Related Heterogeneity in Hematopoietic Stem Cell Function. *Cell stem cell*, *28*(2), 241-256 e246. https://doi.org/10.1016/j.stem.2020.09.018

Mao, Z., Hine, C., Tian, X., Van Meter, M., Au, M., Vaidya, A., Seluanov, A., & Gorbunova, V. (2011). SIRT6 promotes DNA repair under stress by activating PARP1. *Science*, *332*(6036), 1443-1446.

Marazzi, L., Shah, M., Balakrishnan, S., Patil, A., & Vera-Licona, P. (2022). NETISCE: a network-based tool for cell fate reprogramming. *NPJ Syst Biol Appl*, *8*(1), 21. https://doi.org/10.1038/s41540-022-00231-y

Martens, U. M., Brass, V., Sedlacek, L., Pantic, M., Exner, C., Guo, Y., Engelhardt, M., Lansdorp, P. M., Waller, C. F., & Lange, W. (2002). Telomere maintenance in human B lymphocytes. *Br J Haematol*, *119*(3), 810-818. https://doi.org/10.1046/j.1365-2141.2002.03910.x

Martin, E. W., Rodriguez, Y. B. A., Reggiardo, R. E., Worthington, A. K., Mattingly, C. S., Poscablo, D. M., Krietsch, J., McManus, M. T., Carpenter, S., Kim, D. H., & Forsberg, E. C. (2023). Dynamics of Chromatin Accessibility During Hematopoietic Stem Cell Differentiation Into Progressively Lineage-Committed Progeny. *Stem Cells*, *41*(5), 520-539. https://doi.org/10.1093/stmcls/sxad022

Martin, M. (2011). Cutadapt removes adapter sequences from high-throughput sequencing reads. *EMBnet. journal*, *17*(1), 10-12.

Martincorena, I., Raine, K. M., Gerstung, M., Dawson, K. J., Haase, K., Van Loo, P., Davies, H., Stratton, M. R., & Campbell, P. J. (2017). Universal Patterns of Selection in Cancer and Somatic Tissues. *Cell*, *171*(5), 1029-1041 e1021. https://doi.org/10.1016/j.cell.2017.09.042

Maryanovich, M., Zahalka, A. H., Pierce, H., Pinho, S., Nakahara, F., Asada, N., Wei, Q., Wang, X., Ciero, P., Xu, J., Leftin, A., & Frenette, P. S. (2019). Author Correction: Adrenergic nerve degeneration in bone marrow drives aging of the hematopoietic stem cell niche. *Nat Med*, *25*(4), 701. https://doi.org/10.1038/s41591-019-0425-3

Massaro, F., Corrillon, F., Stamatopoulos, B., Dubois, N., Ruer, A., Meuleman, N., Bron, D., & Lagneaux, L. (2023). Age-related changes in human bone marrow mesenchymal stromal cells: morphology, gene expression profile, immunomodulatory activity and miRNA expression. *Front Immunol*, *14*, 1267550. https://doi.org/10.3389/fimmu.2023.1267550

Matatall, K. A., Jeong, M., Chen, S., Sun, D., Chen, F., Mo, Q., Kimmel, M., & King, K. Y. (2016). Chronic infection depletes hematopoietic stem cells through stress-induced terminal differentiation. *Cell reports*, *17*(10), 2584-2595.

Maya-Mendoza, A., Moudry, P., Merchut-Maya, J. M., Lee, M., Strauss, R., & Bartek, J. (2018). High speed of fork progression induces DNA replication stress and genomic instability. *Nature*, *559*(7713), 279-284.

Mayer, I. M., Hoelbl-Kovacic, A., Sexl, V., & Doma, E. (2022). Isolation, Maintenance and Expansion of Adult Hematopoietic Stem/Progenitor Cells and Leukemic Stem Cells. *Cancers (Basel)*, *14*(7), 1723. https://doi.org/10.3390/cancers14071723

Mayne, B., Berry, O., Davies, C., Farley, J., & Jarman, S. (2019). A genomic predictor of lifespan in vertebrates. *Scientific reports*, *9*(1), 1-10.

Mazzola, M., Pezzotta, A., Fazio, G., Rigamonti, A., Bresciani, E., Gaudenzi, G., Pelleri, M. C., Saitta, C., Ferrari, L., Parma, M., Fumagalli, M., Biondi, A., Cazzaniga, G., Marozzi, A., & Pistocchi, A. (2020). Dysregulation of NIPBL leads to impaired RUNX1 expression and haematopoietic defects. *J Cell Mol Med*, *24*(11), 6272-6282. https://doi.org/10.1111/jcmm.15269

McCauley, B. S., Sun, L., Yu, R., Lee, M., Liu, H., Leeman, D. S., Huang, Y., Webb, A. E., & Dang, W. (2021). Altered Chromatin States Drive Cryptic Transcription in Aging Mammalian Stem Cells. *Nat Aging*, *1*(8), 684-697. https://doi.org/10.1038/s43587-021-00091-x

Mehta, A., Zhao, J. L., Sinha, N., Marinov, G. K., Mann, M., Kowalczyk, M. S., Galimidi, R. P., Du, X., Erikci, E., Regev, A., Chowdhury, K., & Baltimore, D. (2015). The MicroRNA-132 and MicroRNA-212 Cluster Regulates Hematopoietic Stem Cell Maintenance and Survival with Age by Buffering FOXO3 Expression. *Immunity*, *42*(6), 1021-1032. https://doi.org/10.1016/j.immuni.2015.05.017

Meng, F., Qian, M., Peng, B., Peng, L., Wang, X., Zheng, K., Liu, Z., Tang, X., Zhang, S., & Sun, S. (2020). Synergy between SIRT1 and SIRT6 helps recognize DNA breaks and potentiates the DNA damage response and repair in humans and mice. *elife*, *9*, e55828.

Michishita, E., McCord, R. A., Berber, E., Kioi, M., Padilla-Nash, H., Damian, M., Cheung, P., Kusumoto, R., Kawahara, T. L., & Barrett, J. C. (2008). SIRT6 is a histone H3 lysine 9 deacetylase that modulates telomeric chromatin. *Nature*, *452*(7186), 492-496.

Milevskiy, M. J. G., Coughlan, H. D., Kane, S. R., Johanson, T. M., Kordafshari, S., Chan, W. F., Tsai, M., Surgenor, E., Wilcox, S., Allan, R. S., Chen, Y., Lindeman, G. J., Smyth, G. K., & Visvader, J. E. (2023). Three-dimensional genome architecture coordinates key regulators of lineage specification in mammary epithelial cells. *Cell Genom*, *3*(11), 100424. https://doi.org/10.1016/j.xgen.2023.100424

Miller, K. M., Tjeertes, J. V., Coates, J., Legube, G., Polo, S. E., Britton, S., & Jackson, S. P. (2010). Human HDAC1 and HDAC2 function in the DNA-damage response to promote DNA nonhomologous end-joining. *Nature structural & molecular biology*, *17*(9), 1144-1151.

Millet, A., Ledo, J. H., & Tavazoie, S. F. (2024). An exhausted-like microglial population accumulates in aged and APOE4 genotype Alzheimer's brains. *Immunity*, *57*(1), 153-170 e156. https://doi.org/10.1016/j.immuni.2023.12.001

Milon, B. C., Cheng, H., Tselebrovsky, M. V., Lavrov, S. A., Nenasheva, V. V., Mikhaleva, E. A., Shevelyov, Y. Y., & Nurminsky, D. I. (2012). Role of histone deacetylases in gene regulation at nuclear lamina. *Plos one*, *7*(11), e49692.

Mishra, S., Srivastava, D., & Kumar, V. (2021). Improving gene network inference with graph wavelets and making insights about ageing-associated regulatory changes in lungs. *Brief Bioinform*, *22*(4). https://doi.org/10.1093/bib/bbaa360

Mitchell, C. A., Verovskaya, E. V., Calero-Nieto, F. J., Olson, O. C., Swann, J. W., Wang, X., Hérault, A., Dellorusso, P. V., Zhang, S. Y., & Svendsen, A. F. (2023). Stromal niche inflammation mediated by IL-1 signalling is a targetable driver of haematopoietic ageing. *Nature cell biology*, *25*(1), 30-41.

Mitchell, W., Goeminne, L. J. E., Tyshkovskiy, A., Zhang, S., Chen, J. Y., Paulo, J. A., Pierce, K. A., Choy, A. H., Clish, C. B., Gygi, S. P., & Gladyshev, V. N. (2024).

Multi-omics characterization of partial chemical reprogramming reveals evidence of cell rejuvenation. *elife*, *12*. https://doi.org/10.7554/eLife.90579

Miyata, T., Kawai, R., Taketomi, S., & Sprague, S. M. (1996). Possible involvement of advanced glycation end-products in bone resorption. *Nephrol Dial Transplant*, *11 Suppl 5*, 54-57. https://doi.org/10.1093/ndt/11.supp5.54

Moehrle, B. M., Nattamai, K., Brown, A., Florian, M. C., Ryan, M., Vogel, M., Bliederhaeuser, C., Soller, K., Prows, D. R., Abdollahi, A., Schleimer, D., Walter, D., Milsom, M. D., Stambrook, P., Porteus, M., & Geiger, H. (2015). Stem Cell-Specific Mechanisms Ensure Genomic Fidelity within HSCs and upon Aging of HSCs. *Cell Rep*, *13*(11), 2412-2424. https://doi.org/10.1016/j.celrep.2015.11.030

Montecino-Rodriguez, E., Kong, Y., Casero, D., Rouault, A., Dorshkind, K., & Pioli, P. D. (2019). Lymphoid-Biased Hematopoietic Stem Cells Are Maintained with Age and Efficiently Generate Lymphoid Progeny. *Stem cell reports*, *12*(3), 584-596. https://doi.org/10.1016/j.stemcr.2019.01.016

Montserrat-Vazquez, S., Ali, N. J., Matteini, F., Lozano, J., Zhaowei, T., Mejia-Ramirez, E., Marka, G., Vollmer, A., Soller, K., Sacma, M., Sakk, V., Mularoni, L., Mallm, J. P., Plass, M., Zheng, Y., Geiger, H., & Florian, M. C. (2022). Transplanting rejuvenated blood stem cells extends lifespan of aged immunocompromised mice. *NPJ Regen Med*, *7*(1), 78. https://doi.org/10.1038/s41536-022-00275-y

Mooney, C. J., Cunningham, A., Tsapogas, P., Toellner, K. M., & Brown, G. (2017). Selective Expression of Flt3 within the Mouse Hematopoietic Stem Cell Compartment. *Int J Mol Sci*, *18*(5). https://doi.org/10.3390/ijms18051037

Moqri, M., Cipriano, A., Simpson, D. J., Rasouli, S., Murty, T., de Jong, T. A., Nachun, D., de Sena Brandine, G., Ying, K., Tarkhov, A., Aberg, K. A., van den Oord, E., Zhou, W., Smith, A., Mackall, C., Gladyshev, V. N., Horvath, S., Snyder, M. P., & Sebastiano, V. (2024). PRC2-AgeIndex as a universal biomarker of aging and rejuvenation. *Nat Commun*, *15*(1), 5956. https://doi.org/10.1038/s41467-024-50098-2

Morris, S. A. (2026). Redefining cellular reprogramming with advanced genomic technologies. *Nat Rev Genet*, *27*(3), 193-211. https://doi.org/10.1038/s41576-025-00899-y

Muir, A., Bennett, A., Smith, H., Logunova, L., Wolfenden, A., Fenn, J., Lowe, A. E., Brass, A., Grainger, J. R., Konkel, J. E., Bradley, J. E., Mair, I., & Else, K. J. (2023). The wild mouse bone marrow has a unique myeloid and lymphoid composition and phenotype. *Discov Immunol*, *2*(1), kyad005. https://doi.org/10.1093/discim/kyad005

Munz, C. M., Dressel, N., Chen, M., Grinenko, T., Roers, A., & Gerbaulet, A. (2023). Regeneration after blood loss and acute inflammation proceeds without contribution of primitive HSCs. *Blood*, *141*(20), 2483-2492. https://doi.org/10.1182/blood.2022018996

Nachun, D., Lu, A. T., Bick, A. G., Natarajan, P., Weinstock, J., Szeto, M. D., Kathiresan, S., Abecasis, G., Taylor, K. D., Guo, X., Tracy, R., Durda, P., Liu, Y., Johnson, C., Rich, S. S., Van Den Berg, D., Laurie, C., Blackwell, T., Papanicolaou, G. J.,…Consortium, N. T.-O. f. P. M. (2021). Clonal hematopoiesis associated with epigenetic aging and clinical outcomes. *Aging cell*, *20*(6), e13366. https://doi.org/10.1111/acel.13366

Naghavi, M., Kyu, H. H., Aalipour, M. A., Aalruz, H., Ababneh, H. S., Abafita, B. J., Abaraogu, U. O., Abbafati, C., Abbasi, M., & Abbaspour, F. (2025). Global burden of 292 causes of death in 204 countries and territories and 660 subnational locations, 1990–2023: a systematic analysis for the Global Burden of Disease Study 2023. *The Lancet*, *406*(10513), 1811-1872.

Nagpal, N., & Agarwal, S. (2025). Extension of replicative lifespan by synthetic engineered telomerase RNA in patient induced pluripotent stem cells. *Nat Biomed Eng*, *9*(12), 2083-2097. https://doi.org/10.1038/s41551-025-01429-1

Nagpal, N., Wang, J., Zeng, J., Lo, E., Moon, D. H., Luk, K., Braun, R. O., Burroughs, L. M., Keel, S. B., Reilly, C., Lindsley, R. C., Wolfe, S. A., Tai, A. K., Cahan, P., Bauer, D. E., Fong, Y. W., & Agarwal, S. (2020). Small-Molecule PAPD5 Inhibitors Restore Telomerase Activity in Patient Stem Cells. *Cell stem cell*, *26*(6), 896-909 e898. https://doi.org/10.1016/j.stem.2020.03.016

Nakagawa, M., Koyanagi, M., Tanabe, K., Takahashi, K., Ichisaka, T., Aoi, T., Okita, K., Mochiduki, Y., Takizawa, N., & Yamanaka, S. (2008). Generation of induced pluripotent stem cells without Myc from mouse and human fibroblasts. *Nat Biotechnol*, *26*(1), 101-106. https://doi.org/10.1038/nbt1374

Nakagawa, M. M., Inagaki, R., Kuroda, Y., Nannya, Y., Zhao, L. Y., Ochi, Y., Takeda, J., Qi, X. X., Yoda, A., Kon, A., Kakiuchi, N., Makishima, H., Matsuda, S., & Ogawa, S. (2021). Distinct Pathogenesis of Clonal Hematopoiesis Revealed By Single Cell RNA Sequencing Integrated with Highly Sensitive Genotyping Method. *Blood*, *138*, 1092. https://doi.org/10.1182/blood-2021-152219

Neeper, M., Schmidt, A. M., Brett, J., Yan, S. D., Wang, F., Pan, Y. C., Elliston, K., Stern, D., & Shaw, A. (1992). Cloning and expression of a cell surface receptor for advanced glycosylation end products of proteins. *J Biol Chem*, *267*(21), 14998-15004. https://www.ncbi.nlm.nih.gov/pubmed/1378843

Nielsen, J., Hedeholm, R. B., Heinemeier, J., Bushnell, P. G., Christiansen, J. S., Olsen, J., Ramsey, C. B., Brill, R. W., Simon, M., & Steffensen, K. F. (2016). Eye lens radiocarbon reveals centuries of longevity in the Greenland shark (Somniosus microcephalus). *Science*, *353*(6300), 702-704.

Nowak, D. E., Tian, B., & Brasier, A. R. (2005). Two-step cross-linking method for identification of NF-kappaB gene network by chromatin immunoprecipitation. *Biotechniques*, *39*(5), 715-725. https://doi.org/10.2144/000112014

Núñez-Quintela, V., Chantrel, J., Prados, M. Á., Pedrosa, P., Lorandi, I., Lorenzo-Rodríguez, L., Chen, C., Paredes, R., Failde-Fiestras, A., & González-Pérez, D. (2026). Senomorphic effect of genetic and chemical partial reprogramming. *bioRxiv*, 2026.2001. 2013.699211.

Oberdoerffer, P., Michan, S., McVay, M., Mostoslavsky, R., Vann, J., Park, S.-K., Hartlerode, A., Stegmuller, J., Hafner, A., & Loerch, P. (2008). SIRT1 redistribution on chromatin promotes genomic stability but alters gene expression during aging. *Cell*, *135*(5), 907-918.

Ocampo, A., Reddy, P., Martinez-Redondo, P., Platero-Luengo, A., Hatanaka, F., Hishida, T., Li, M., Lam, D., Kurita, M., Beyret, E., Araoka, T., Vazquez-Ferrer, E., Donoso, D., Roman, J. L., Xu, J., Rodriguez Esteban, C., Nunez, G., Nunez Delicado, E., Campistol, J. M.,…Izpisua Belmonte, J. C. (2016). In Vivo Amelioration of Age-

Associated Hallmarks by Partial Reprogramming. *Cell*, *167*(7), 1719-1733 e1712. https://doi.org/10.1016/j.cell.2016.11.052
Ogata, J. D., Mu, W., Davis, E. S., Xue, B., Harrell, J. C., Sheffield, N. C., Phanstiel, D. H., Love, M. I., & Dozmorov, M. G. (2023). excluderanges: exclusion sets for T2T-CHM13, GRCm39, and other genome assemblies. *Bioinformatics*, *39*(4), btad198.
Oh, G., Ebrahimi, S., Carlucci, M., Zhang, A. P., Nair, A., Groot, D. E., Labrie, V., Jia, P. X., Oh, E. S., Jeremian, R. H., Susic, M., Shrestha, T. C., Ralph, M. R., Gordevicius, J., Koncevicius, K., & Petronis, A. (2018). Cytosine modifications exhibit circadian oscillations that are involved in epigenetic diversity and aging. *Nature communications*, *9*(1), 1-11. https://doi.org/10.1038/s41467-018-03073-7
Oh, G., Koncevicius, K., Ebrahimi, S., Carlucci, M., Groot, D. E., Nair, A., Zhang, A., Krisciunas, A., Oh, E. S., Labrie, V., Wong, A. H. C., Gordevicius, J., Jia, P., Susic, M., & Petronis, A. (2019). Circadian oscillations of cytosine modification in humans contribute to epigenetic variability, aging, and complex disease. *Genome Biol*, *20*(1), 2. https://doi.org/10.1186/s13059-018-1608-9
Oh, J. H., Hild, B., Yoshida, T., Badger, J. H., Seishima, J., McCulloch, J. A., Jung, M. K., Azar, S., Trinchieri, G., & Rehermann, B. (2025). Naturalized immune responses are stable over years in a colony of laboratory mice with wild-derived microbiota. *Immunity*, *58*(9), 2305-2319 e2305. https://doi.org/10.1016/j.immuni.2025.07.004
Ohnishi, K., Semi, K., Yamamoto, T., Shimizu, M., Tanaka, A., Mitsunaga, K., Okita, K., Osafune, K., Arioka, Y., Maeda, T., Soejima, H., Moriwaki, H., Yamanaka, S., Woltjen, K., & Yamada, Y. (2014). Premature termination of reprogramming in vivo leads to cancer development through altered epigenetic regulation. *Cell*, *156*(4), 663-677. https://doi.org/10.1016/j.cell.2014.01.005
Olova, N., Simpson, D. J., Marioni, R. E., & Chandra, T. (2019). Partial reprogramming induces a steady decline in epigenetic age before loss of somatic identity. *Aging cell*, *18*(1), e12877. https://doi.org/10.1111/acel.12877
Olshansky, S., Willcox, B., Demetrius, L., & Beltrán-Sánchez, H. (2024). Implausibility of radical life extension in humans in the twenty-first century. *4*, 1635–1642. https://doi.org/10.1038/s43587-024-00702-3
Onizuka, M., Imanishi, T., Harada, K., Aoyama, Y., Amaki, J., Toyosaki, M., Machida, S., Kikkawa, E., Yamada, S., & Nakabayashi, K. (2023). Donor cord blood aging accelerates in recipients after transplantation. *Scientific reports*, *13*(1), 2603.
Open2C, Abdennur, N., Fudenberg, G., Flyamer, I. M., Galitsyna, A. A., Goloborodko, A., Imakaev, M., & Venev, S. V. (2024). Pairtools: from sequencing data to chromosome contacts. *PLoS computational biology*, *20*(5), e1012164.
Osawa, M., Hanada, K., Hamada, H., & Nakauchi, H. (1996). Long-term lymphohematopoietic reconstitution by a single CD34-low/negative hematopoietic stem cell. *Science*, *273*(5272), 242-245. https://doi.org/10.1126/science.273.5272.242
Pang, W. W., Price, E. A., Sahoo, D., Beerman, I., Maloney, W. J., Rossi, D. J., Schrier, S. L., & Weissman, I. L. (2011). Human bone marrow hematopoietic stem cells are increased in frequency and myeloid-biased with age. *Proc Natl Acad Sci U S A*, *108*(50), 20012-20017. https://doi.org/10.1073/pnas.1116110108
Papaioannou, N. Y., Patsali, P., Naiisseh, B., Papasavva, P. L., Koniali, L., Kurita, R., Nakamura, Y., Christou, S., Sitarou, M., Mussolino, C., Cathomen, T., Kleanthous,

M., & Lederer, C. W. (2023). High-efficiency editing in hematopoietic stem cells and the HUDEP-2 cell line based on in vitro mRNA synthesis. *Front Genome Ed*, *5*, 1141618. https://doi.org/10.3389/fgeed.2023.1141618

Parasar, B., Venkatesh, A. R., Perera, J., Sosnick, L., Moghadami, S., Seo, Y., Shi, J., Chan, L., Takenawa, S., Akiyama, T., Sianto, O., Uenaka, T., Hadjipanayis, A., Wernig, M., Gitler, A. D., & Tan, L. (2026). Whole-genome 3D architectural screen reveals modulators of brain DNA structure. *bioRxiv*. https://doi.org/10.64898/2026.04.15.718501

Parras, A., Vílchez-Acosta, A., Desdín-Micó, G., Picó, S., Mrabti, C., Montenegro-Borbolla, E., Maroun, C. Y., Haghani, A., Brooke, R., & del Carmen Maza, M. (2023). In vivo reprogramming leads to premature death linked to hepatic and intestinal failure. *Nature Aging*, *3*(12), 1509-1520.

Parry, A., Rulands, S., & Reik, W. (2021). Active turnover of DNA methylation during cell fate decisions. *Nature Reviews Genetics*, *22*(1), 59-66.

Patrick, R., Naval-Sanchez, M., Deshpande, N., Huang, Y., Zhang, J., Chen, X., Yang, Y., Tiwari, K., Esmaeili, M., Tran, M., Mohamed, A. R., Wang, B., Xia, D., Ma, J., Bayliss, J., Wong, K., Hun, M. L., Sun, X., Cao, B.,…Nefzger, C. M. (2024). The activity of early-life gene regulatory elements is hijacked in aging through pervasive AP-1-linked chromatin opening. *Cell Metab*, *36*(8), 1858-1881 e1823. https://doi.org/10.1016/j.cmet.2024.06.006

Paul, K. C., Binder, A. M., Horvath, S., Kusters, C., Yan, Q., Rosario, I. D., Yu, Y., Bronstein, J., & Ritz, B. (2021). Accelerated hematopoietic mitotic aging measured by DNA methylation, blood cell lineage, and Parkinson's disease. *BMC Genomics*, *22*(1), 696. https://doi.org/10.1186/s12864-021-08009-y

Pawar, S. A., Shao, L., Chang, J., Wang, W., Pathak, R., Zhu, X., Wang, J., Hendrickson, H., Boerma, M., Sterneck, E., Zhou, D., & Hauer-Jensen, M. (2014). C/EBPdelta deficiency sensitizes mice to ionizing radiation-induced hematopoietic and intestinal injury. *Plos one*, *9*(4), e94967. https://doi.org/10.1371/journal.pone.0094967

Pedersen, T. (2025). ggraph: An Implementation of Grammar of Graphics for Graphs and Networks. (Version 2.2.2) [R package]. https://CRAN.R-project.org/package=ggraph

Pedrosa, P., Zhang, Z., Nunez-Quintela, V., Macias, D., Ge, J., Denholm, M., Dyas, A., Estevez-Souto, V., Lado-Fernandez, P., Gonzalez, P., Gomez, M., Martin, J. E., Da Silva-Alvarez, S., Collado, M., & Munoz-Espin, D. (2024). Inhibition of lung tumorigenesis by transient reprogramming in cancer cells. *Cell Death Dis*, *15*(11), 857. https://doi.org/10.1038/s41419-024-07207-2

Pei, X. Y., Liu, Z. J., Fu, Q., Lee, H. Y., Hu, Q., Zhao, X. S., Wei, Y., You, F. P., Sun, Y. Q., Xu, L. P., Wang, Y., Zhang, X. H., Zhao, X. Y., & Huang, X. J. (2026). Parvovirus B19 targets hematopoietic stem cells to disrupt multilineage differentiation and drive pancytopenia. *Cell Death Differ*. https://doi.org/10.1038/s41418-026-01671-3

Pereira, C. F., Chang, B., Qiu, J., Niu, X., Papatsenko, D., Hendry, C. E., Clark, N. R., Nomura-Kitabayashi, A., Kovacic, J. C., Ma'ayan, A., Schaniel, C., Lemischka, I. R., & Moore, K. (2013). Induction of a hemogenic program in mouse fibroblasts. *Cell stem cell*, *13*(2), 205-218. https://doi.org/10.1016/j.stem.2013.05.024

Pernomian, L., Waigi, E. W., Nguyen, V., Mohammed, A. D., Costa, T. J., Fontes, M. T., Kubinak, J. L., Aitken, A. V., Biancardi, V. C., Gleason, K., Shazly, T., Sinclair, D. A., McCarthy, C. G., Wang, Y., Tan, W., & Wenceslau, C. F. (2025). Single-Short Partial Reprogramming of the Endothelial Cells Decreases Blood Pressure via Attenuation of EndMT in Hypertensive Mice. *Circ Res*, *137*(8), 1092-1113. https://doi.org/10.1161/CIRCRESAHA.124.324909

Perrone, M., Chiodoni, C., Lecchi, M., Botti, L., Bassani, B., Piva, A., Jachetti, E., Milani, M., Lecis, D., Tagliabue, E., Verderio, P., Sangaletti, S., & Colombo, M. P. (2023). ATF3 Reprograms the Bone Marrow Niche in Response to Early Breast Cancer Transformation. *Cancer Res*, *83*(1), 117-129. https://doi.org/10.1158/0008-5472.CAN-22-0651

Peters, M., Teodorescu, P., Pasca, S., Zhang, X., Wang, R., Yegnasubramanian, S., Grimes, L. H., Salomonis, N., Gondek, L. P., & Ghiaur, G. (2025). Comprehensive characterization of human bone marrow microenvironment shows age-related changes. *haematologica*, *110*(11), 2844-2848. https://doi.org/10.3324/haematol.2025.287536

Petkovich, D. A., Podolskiy, D. I., Lobanov, A. V., Lee, S.-G., Miller, R. A., & Gladyshev, V. N. (2017). Using DNA methylation profiling to evaluate biological age and longevity interventions. *Cell Metabolism*, *25*(4), 954-960. e956.

Picó, S., Vílchez-Acosta, A., de Sousa, J. A., del Carmen Maza, M., Mrabti, C., Parras, A., Desdín-Micó, G., Maroun, C. Y., Branchina, C., & von Meyenn, F. (2025). Comparative analysis of mouse strains for in vivo induction of reprogramming factors. *Cell reports*, *44*(7).

Pietras, E. M., Mirantes-Barbeito, C., Fong, S., Loeffler, D., Kovtonyuk, L. V., Zhang, S. Y., Lakshminarasimhan, R., Chin, C. P., Techner, J. M., Will, B., Nerlov, C., Steidl, U., Manz, M. G., Schroeder, T., & Passegue, E. (2016). Chronic interleukin-1 exposure drives haematopoietic stem cells towards precocious myeloid differentiation at the expense of self-renewal. *Nature cell biology*, *18*(6), 607-+. https://doi.org/10.1038/ncb3346

Pio-Lopez, L., & Levin, M. (2024). Aging as a loss of morphostatic information: A developmental bioelectricity perspective. *Ageing Res Rev*, *97*, 102310. https://doi.org/10.1016/j.arr.2024.102310

Pioli, P. D., Casero, D., Montecino-Rodriguez, E., Morrison, S. L., & Dorshkind, K. (2019). Plasma Cells Are Obligate Effectors of Enhanced Myelopoiesis in Aging Bone Marrow. *Immunity*, *51*(2), 351-366 e356. https://doi.org/10.1016/j.immuni.2019.06.006

Piraino, S., Boero, F., Aeschbach, B., & Schmid, V. (1996). Reversing the life cycle: medusae transforming into polyps and cell transdifferentiation in Turritopsis nutricula (Cnidaria, Hydrozoa). *The Biological Bulletin*, *190*(3), 302-312.

Poulos, M. G., Ramalingam, P., Gutkin, M. C., Llanos, P., Gilleran, K., Rabbany, S. Y., & Butler, J. M. (2017). Endothelial transplantation rejuvenates aged hematopoietic stem cell function. *J Clin Invest*, *127*(11), 4163-4178. https://doi.org/10.1172/JCI93940

Purton, L. E. (2022). Adult murine hematopoietic stem cells and progenitors: an update on their identities, functions and assays. *Experimental Hematology*, *116*, 1-14. https://doi.org/10.1016/j.exphem.2022.10.005.

Qiu, J., Gjini, J., Arif, T., Moore, K., Lin, M., & Ghaffari, S. (2021). Using mitochondrial activity to select for potent human hematopoietic stem cells. *Blood Adv*, *5*(6), 1605-1616. https://doi.org/10.1182/bloodadvances.2020003658

Quinlan, A. R., & Hall, I. M. (2010). BEDTools: a flexible suite of utilities for comparing genomic features. *Bioinformatics*, *26*(6), 841-842.

Rackham, O. J. L., Firas, J., Fang, H., Oates, M. E., Holmes, M. L., Knaupp, A. S., Suzuki, H., Nefzger, C. M., Daub, C. O., Shin, J. W., Petretto, E., Forrest, A. R. R., Hayashizaki, Y., Polo, J. M., Gough, J., & Consortium, F. (2016). A predictive computational framework for direct reprogramming between human cell types. *Nature genetics*, *48*(3), 331-335. https://doi.org/10.1038/ng.3487

Raghavan, V., Zheng, Y., Li, Y., & Ding, J. (2025). Harnessing agent-based frameworks in CellAgentChat to unravel cell-cell interactions from single-cell and spatial transcriptomics. *Genome Res*, *35*(7), 1646-1663. https://doi.org/10.1101/gr.279771.124

Ramalingam, P., Gutkin, M. C., Poulos, M. G., Tillery, T., Doughty, C., Winiarski, A., Freire, A. G., Rafii, S., Redmond, D., & Butler, J. M. (2023). Restoring bone marrow niche function rejuvenates aged hematopoietic stem cells by reactivating the DNA Damage Response. *Nat Commun*, *14*(1), 2018. https://doi.org/10.1038/s41467-023-37783-4

Ramirez, F., Bhardwaj, V., Arrigoni, L., Lam, K. C., Gruning, B. A., Villaveces, J., Habermann, B., Akhtar, A., & Manke, T. (2018). High-resolution TADs reveal DNA sequences underlying genome organization in flies. *Nat Commun*, *9*(1), 189. https://doi.org/10.1038/s41467-017-02525-w

Ramunas, J., Yakubov, E., Brady, J. J., Corbel, S. Y., Holbrook, C., Brandt, M., Stein, J., Santiago, J. G., Cooke, J. P., & Blau, H. M. (2015). Transient delivery of modified mRNA encoding TERT rapidly extends telomeres in human cells. *FASEB J*, *29*(5), 1930-1939. https://doi.org/10.1096/fj.14-259531

Randhawa, V., & Kumar, M. (2021). An integrated network analysis approach to identify potential key genes, transcription factors, and microRNAs regulating human hematopoietic stem cell aging. *Mol Omics*, *17*(6), 967-984. https://doi.org/10.1039/d1mo00199j

Rao, S. S., Huntley, M. H., Durand, N. C., Stamenova, E. K., Bochkov, I. D., Robinson, J. T., Sanborn, A. L., Machol, I., Omer, A. D., Lander, E. S., & Aiden, E. L. (2014). A 3D map of the human genome at kilobase resolution reveals principles of chromatin looping. *Cell*, *159*(7), 1665-1680. https://doi.org/10.1016/j.cell.2014.11.021

Rasti, G., Becker, M., Vazquez, B. N., Espinosa-Alcantud, M., Fernandez-Duran, I., Gamez-Garcia, A., Gonzalez-Nieto, J., Bosch-Presegue, L., Marazuela-Duque, A., & Segura-Bayona, S. (2022). SIRT1 regulates DNA damage signaling through the PP4 phosphatase complex. *Nucleic Acids Res*, *51*(13), 6754-6769. https://doi.org/10.1093/nar/gkad504

Razavi-Mohseni, M., & Beer, M. A. (2024). MicroRNAs provide negative feedback and stability in gene regulatory network models of cell-state transitions. *Front Epigenet Epigenom*, *2*. https://doi.org/10.3389/freae.2024.1473789

Renders, S., Svendsen, A. F., Panten, J., Rama, N., Maryanovich, M., Sommerkamp, P., Ladel, L., Redavid, A. R., Gibert, B., Lazare, S., Ducarouge, B., Schonberger, K., Narr, A., Tourbez, M., Dethmers-Ausema, B., Zwart, E., Hotz-Wagenblatt, A.,

Zhang, D., Korn, C.,…Trumpp, A. (2021). Niche derived netrin-1 regulates hematopoietic stem cell dormancy via its receptor neogenin-1. *Nat Commun*, *12*(1), 608. https://doi.org/10.1038/s41467-020-20801-0

Reus, J. B., Trivino-Soto, G. S., Wu, L. I., Kokott, K., & Lim, E. S. (2020). SV40 Large T Antigen Is Not Responsible for the Loss of STING in 293T Cells but Can Inhibit cGAS-STING Interferon Induction. *Viruses*, *12*(2). https://doi.org/10.3390/v12020137

Revechon, G., Witasp, A., Viceconte, N., Helgadottir, H. T., Machtel, P., Stefani, F., Whisenant, D., Sola-Carvajal, A., McGuinness, D., Abutaleb, N. O., Artiach, G., Arzt, E. W., Soveri, I., Babler, A., Ziegler, S., Kramann, R., Back, M., Thorell, A., Truskey, G. A.,…Eriksson, M. (2025). Recurrent somatic mutation and progerin expression in early vascular aging of chronic kidney disease. *Nat Aging*, *5*(6), 1046-1062. https://doi.org/10.1038/s43587-025-00882-6

Robinson, M. D., McCarthy, D. J., & Smyth, G. K. (2010). edgeR: a Bioconductor package for differential expression analysis of digital gene expression data. *Bioinformatics*, *26*(1), 139-140. https://doi.org/10.1093/bioinformatics/btp616

Roisman, A., Adelman, E. R., Huang, H.-T., Wade, D., Bilbao, D., & Figueroa, M. E. (2019). Loss of KLF6 recapitulates molecular and functional changes associated with aging in human hematopoietic stem and progenitor cells. *Blood*, *134*, 447.

Romero-Tejeda, M., Fonoudi, H., Weddle, C. J., DeKeyser, J. M., Lenny, B., Fetterman, K. A., Magdy, T., Sapkota, Y., Epting, C. L., & Burridge, P. W. (2023). A novel transcription factor combination for direct reprogramming to a spontaneously contracting human cardiomyocyte-like state. *J Mol Cell Cardiol*, *182*, 30-43. https://doi.org/10.1016/j.yjmcc.2023.06.005

Rosalem, G., Assis, D. R. R., González Torres, L. A., Las Casas, E., Rodrigues, W. N., Gonçalves, R. S., Rabelo, R., Ruiz, J., & Carvalho, M. G. (2026). A Microfluidic Bone Marrow Model Combining CFD and Organ-on-a-Chip Technologies to Study Leukemia Niche Dynamics. *Frontiers in Bioengineering and Biotechnology*, *14*, 1766296.

Rossi, D. J., Bryder, D., Seita, J., Nussenzweig, A., Hoeijmakers, J., & Weissman, I. L. (2007). Deficiencies in DNA damage repair limit the function of haematopoietic stem cells with age. *Nature*, *447*(7145), 725-729. https://doi.org/10.1038/nature05862

Rossi, D. J., Bryder, D., Zahn, J. M., Ahlenius, H., Sonu, R., Wagers, A. J., & Weissman, I. L. (2005). Cell intrinsic alterations underlie hematopoietic stem cell aging. *Proc Natl Acad Sci U S A*, *102*(26), 9194-9199. https://doi.org/10.1073/pnas.0503280102

Roux, A. E., Zhang, C., Paw, J., Zavala-Solorio, J., Malahias, E., Vijay, T., Kolumam, G., Kenyon, C., & Kimmel, J. C. (2022). Diverse partial reprogramming strategies restore youthful gene expression and transiently suppress cell identity. *Cell Systems*, *13*(7), 574-587. e511.

Rube, C. E., Fricke, A., Widmann, T. A., Furst, T., Madry, H., Pfreundschuh, M., & Rube, C. (2011). Accumulation of DNA damage in hematopoietic stem and progenitor cells during human aging. *Plos one*, *6*(3), e17487. https://doi.org/10.1371/journal.pone.0017487

Rudnitsky, E., Braiman, A., Wolfson, M., Muradian, K. K., Gorbunova, V., Turgeman, G., & Fraifeld, V. E. (2025). Mesenchymal stem cells and their derivatives as potential

longevity-promoting tools. *Biogerontology*, *26*(3), 96. https://doi.org/10.1007/s10522-025-10240-z

Rundberg Nilsson, A., Hidalgo, I., Bryder, D., & Pronk, C. J. (2023). Temporal dynamics of TNF-mediated changes in hematopoietic stem cell function and recovery. *iScience*, *26*(4), 106341. https://doi.org/10.1016/j.isci.2023.106341

Rundberg Nilsson, A., Soneji, S., Adolfsson, S., Bryder, D., & Pronk, C. J. (2016). Human and murine hematopoietic stem cell aging is associated with functional impairments and intrinsic megakaryocytic/erythroid bias. *Plos one*, *11*(7), e0158369.

Rydstrom, A., Mansell, E., Sigurdsson, V., Sjoberg, J., Soneji, S., Miharada, K., & Larsson, J. (2023). MAC-1 marks a quiescent and functionally superior HSC subset during regeneration. *Stem cell reports*, *18*(3), 736-748. https://doi.org/10.1016/j.stemcr.2023.01.014

Saçma, M., Pospiech, J., Bogeska, R., de Back, W., Mallm, J.-P., Sakk, V., Soller, K., Marka, G., Vollmer, A., & Karns, R. (2019). Haematopoietic stem cells in perisinusoidal niches are protected from ageing. *Nature cell biology*, *21*(11), 1309-1320.

Saha, E., Ben Guebila, M., Fanfani, V., Shutta, K. H., DeMeo, D. L., Quackenbush, J., & Lopes-Ramos, C. M. (2025). Aging-associated alterations in gene regulatory networks associate with risk, prognosis and response to therapy in lung adenocarcinoma. *npj Aging*, *11*(1), 61. https://doi.org/10.1038/s41514-025-00247-8

Sahu, S. K., Reddy, P., Lu, J., Shao, Y., Wang, C., Tsuji, M., Delicado, E. N., Rodriguez Esteban, C., & Belmonte, J. C. I. (2024). Targeted partial reprogramming of age-associated cell states improves markers of health in mouse models of aging. *Sci Transl Med*, *16*(764), eadg1777. https://doi.org/10.1126/scitranslmed.adg1777

Sarkar, T. J., Quarta, M., Mukherjee, S., Colville, A., Paine, P., Doan, L., Tran, C. M., Chu, C. R., Horvath, S., Qi, L. S., Bhutani, N., Rando, T. A., & Sebastiano, V. (2020). Transient non-integrative expression of nuclear reprogramming factors promotes multifaceted amelioration of aging in human cells. *Nat Commun*, *11*(1), 1545. https://doi.org/10.1038/s41467-020-15174-3

Säwen, P., Eldeeb, M., Erlandsson, E., Kristiansen, T. A., Laterza, C., Kokaia, Z., Karlsson, G., Yuan, J., Soneji, S., & Mandal, P. K. (2018). Murine HSCs contribute actively to native hematopoiesis but with reduced differentiation capacity upon aging. *elife*, *7*, e41258.

Scherer, M., Singh, I., Braun, M. M., Szu-Tu, C., Sanchez Sanchez, P., Lindenhofer, D., Jakobsen, N. A., Korber, V., Kardorff, M., Nitsch, L., Kautz, P., Ruhle, J., Bianchi, A., Cozzuto, L., Fromel, R., Beneyto-Calabuig, S., Lareau, C., Satpathy, A. T., Beekman, R.,…Velten, L. (2025). Clonal tracing with somatic epimutations reveals dynamics of blood ageing. *Nature*, *643*(8071), 478-487. https://doi.org/10.1038/s41586-025-09041-8

Schoenfeldt, L., Paine, P. T., Pico, S., Kamaludeen, M. N., Phelps, G. B., Mrabti, C., Desdin-Mico, G., Del Carmen Maza, M., Perez, K., & Ocampo, A. (2025). Chemical reprogramming ameliorates cellular hallmarks of aging and extends lifespan. *EMBO Mol Med*, *17*(8), 2071-2094. https://doi.org/10.1038/s44321-025-00265-9

Schwab, J. D., Ikonomi, N., Werle, S. D., Weidner, F. M., Geiger, H., & Kestler, H. A. (2021). Reconstructing Boolean network ensembles from single-cell data for

unraveling dynamics in the aging of human hematopoietic stem cells. *Comput Struct Biotechnol J*, *19*, 5321-5332. https://doi.org/10.1016/j.csbj.2021.09.012

Sengstack, J., Zheng, J., Aghayev, T., Bieri, G., Mobaraki, M., Lin, J., Deng, C., Villeda, S. A., & Li, H. (2026). Systematic identification of single transcription factor perturbations that drive cellular and tissue rejuvenation. *Proc Natl Acad Sci U S A*, *123*(2), e2515183123. https://doi.org/10.1073/pnas.2515183123

Shen, Y., Benlabiod, C., Watson, E., Gurashi, K., Fower, A., Rodriguez-Romera, A., Reyat, J. S., Adnan-Awad, S., Hargreaves, R., Kemble, S., Smith, C. G., Croft, A. P., Oppermann, U., Welsh, A., Murphy, L., Murphy, E., Moetazedian, A., Jooss, N., Wong, Z. C.,…Khan, A. O. (2026). comBO: A combined human bone and lympho-myeloid bone marrow organoid for preclinical modeling of hematopoietic disorders. *Cell stem cell*, *33*(3), 421-437 e427. https://doi.org/10.1016/j.stem.2026.01.010

Shi, D., Toyonaga, S., & Anderson, D. G. (2023). In Vivo RNA Delivery to Hematopoietic Stem and Progenitor Cells via Targeted Lipid Nanoparticles. *Nano Lett*, *23*(7), 2938-2944. https://doi.org/10.1021/acs.nanolett.3c00304

Shibata, H., Komura, S., Yamada, Y., Sankoda, N., Tanaka, A., Ukai, T., Kabata, M., Sakurai, S., Kuze, B., Woltjen, K., Haga, H., Ito, Y., Kawaguchi, Y., Yamamoto, T., & Yamada, Y. (2018). In vivo reprogramming drives Kras-induced cancer development. *Nat Commun*, *9*(1), 2081. https://doi.org/10.1038/s41467-018-04449-5

Simon, M., Van Meter, M., Ablaeva, J., Ke, Z., Gonzalez, R. S., Taguchi, T., De Cecco, M., Leonova, K. I., Kogan, V., Helfand, S. L., Neretti, N., Roichman, A., Cohen, H. Y., Meer, M. V., Gladyshev, V. N., Antoch, M. P., Gudkov, A. V., Sedivy, J. M., Seluanov, A., & Gorbunova, V. (2019). LINE1 Derepression in Aged Wild-Type and SIRT6-Deficient Mice Drives Inflammation. *Cell Metab*, *29*(4), 871-885 e875. https://doi.org/10.1016/j.cmet.2019.02.014

Singh, P., Kacena, M. A., Orschell, C. M., & Pelus, L. M. (2020). Aging-related reduced expression of CXCR4 on bone marrow mesenchymal stromal cells contributes to hematopoietic stem and progenitor cell defects. *Stem cell reviews and reports*, *16*, 684-692.

Singovski, G., Bernal, C., Kuciak, M., Siegl-Cachedenier, I., Conod, A., & Ruiz i Altaba, A. (2016). In vivo epigenetic reprogramming of primary human colon cancer cells enhances metastases. *J Mol Cell Biol*, *8*(2), 157-173. https://doi.org/10.1093/jmcb/mjv034

Skinder, N., Sanz Fernandez, I., Dethmers-Ausema, A., Weersing, E., & de Haan, G. (2024). CD61 identifies a superior population of aged murine HSCs and is required to preserve quiescence and self-renewal. *Blood Adv*, *8*(1), 99-111. https://doi.org/10.1182/bloodadvances.2023011585

Smid, M., Coebergh van den Braak, R. R. J., van de Werken, H. J. G., van Riet, J., van Galen, A., de Weerd, V., van der Vlugt-Daane, M., Bril, S. I., Lalmahomed, Z. S., Kloosterman, W. P., Wilting, S. M., Foekens, J. A., JNM, I. J., group, M. s., Martens, J. W. M., & Sieuwerts, A. M. (2018). Gene length corrected trimmed mean of M-values (GeTMM) processing of RNA-seq data performs similarly in intersample analyses while improving intrasample comparisons. *BMC Bioinformatics*, *19*(1), 236. https://doi.org/10.1186/s12859-018-2246-7

Smith, M. A., Culver-Cochran, A. E., Adelman, E. R., Rhyasen, G. W., Ma, A., Figueroa, M. E., & Starczynowski, D. T. (2020). TNFAIP3 Plays a Role in Aging of the Hematopoietic System. *Front Immunol*, *11*, 536442. https://doi.org/10.3389/fimmu.2020.536442

Smits, J. G. A., Arts, J. A., Frolich, S., Snabel, R. R., Heuts, B. M. H., Martens, J. H. A., van Heeringen, S. J., & Zhou, H. (2023). scANANSE gene regulatory network and motif analysis of single-cell clusters. *F1000Res*, *12*, 243. https://doi.org/10.12688/f1000research.130530.1

Snabel, R. R., Cofino-Fabres, C., Baltissen, M., Schwach, V., Passier, R., & Veenstra, G. J. C. (2025). Cardiac differentiation roadmap for analysis of plasticity and balanced lineage commitment. *Stem cell reports*, *20*(3), 102422. https://doi.org/10.1016/j.stemcr.2025.102422

Sobrino, S., Magnani, A., Semeraro, M., Martignetti, L., Cortal, A., Denis, A., Couzin, C., Picard, C., Bustamante, J., Magrin, E., Joseph, L., Roudaut, C., Gabrion, A., Soheili, T., Cordier, C., Lortholary, O., Lefrere, F., Rieux-Laucat, F., Casanova, J. L.,…Six, E. (2023). Severe hematopoietic stem cell inflammation compromises chronic granulomatous disease gene therapy. *Cell Rep Med*, *4*(2), 100919. https://doi.org/10.1016/j.xcrm.2023.100919

Song, L., Zhang, J., Pan, L., Sun, S., Shi, B., Zhang, H., Li, H., Liu, Z., Li, L., Zhang, Y., & Ren, G. (2025). Small-scale in situ Hi-C protocol for early embryos to resolve the three-dimensional genome structure. *STAR Protoc*, *6*(3), 104064. https://doi.org/10.1016/j.xpro.2025.104064

Søraas, A., Matsuyama, M., de Lima, M., Wald, D., Buechner, J., Gedde-Dahl, T., Søraas, C. L., Chen, B., Ferrucci, L., & Dahl, J. A. (2019). Epigenetic age is a cell-intrinsic property in transplanted human hematopoietic cells. *Aging cell*, *18*(2), e12897.

Spangrude, G. J., Heimfeld, S., & Weissman, I. L. (1988). Purification and characterization of mouse hematopoietic stem cells. *Science*, *241*(4861), 58-62. https://doi.org/10.1126/science.2898810

Stark, R., & Brown, G. (2011). DiffBind: differential binding analysis of ChIP-Seq peak data. *R package version*, *100*(4.3), 2-21.

Steensma, D. P., Bejar, R., Jaiswal, S., Lindsley, R. C., Sekeres, M. A., Hasserjian, R. P., & Ebert, B. L. (2015). Clonal hematopoiesis of indeterminate potential and its distinction from myelodysplastic syndromes. *Blood, The Journal of the American Society of Hematology*, *126*(1), 9-16.

Stolzing, A., Jones, E., McGonagle, D., & Scutt, A. (2008). Age-related changes in human bone marrow-derived mesenchymal stem cells: consequences for cell therapies. *Mech Ageing Dev*, *129*(3), 163-173. https://doi.org/10.1016/j.mad.2007.12.002

Su, C., Lee, D., Jin, P., & Zhang, J. (2025). scMultiMap: Cell-type-specific mapping of enhancers and target genes from single-cell multimodal data. *Nat Commun*, *16*(1), 3941. https://doi.org/10.1038/s41467-025-59306-z

Su, T. Y., Hauenstein, J., Somuncular, E., Dumral, O., Leonard, E., Gustafsson, C., Tzortzis, E., Forlani, A., Johansson, A. S., Qian, H., Mansson, R., & Luc, S. (2024). Aging is associated with functional and molecular changes in distinct hematopoietic stem cell subsets. *Nat Commun*, *15*(1), 7966. https://doi.org/10.1038/s41467-024-52318-1

Sun, D. Q., Luo, M., Jeong, M., Rodriguez, B., Xia, Z., Hannah, R., Wang, H., Le, T., Faull, K. F., Chen, R., Gu, H. C., Bock, C., Meissner, A., Gottgens, B., Darlington, G. J., Li, W., & Goodell, M. A. (2014). Epigenomic Profiling of Young and Aged HSCs Reveals Concerted Changes during Aging that Reinforce Self-Renewal. *Cell stem cell*, *14*(5), 673-688. https://doi.org/10.1016/j.stem.2014.03.002

Sun, X., Cao, B., Naval-Sanchez, M., Pham, T., Sun, Y. B. Y., Williams, B., Heazlewood, S. Y., Deshpande, N., Li, J., Kraus, F., Rae, J., Nguyen, Q., Yari, H., Schroder, J., Heazlewood, C. K., Fulton, M., Hatwell-Humble, J., Das Gupta, K., Kapetanovic, R.,…Nilsson, S. K. (2021). Nicotinamide riboside attenuates age-associated metabolic and functional changes in hematopoietic stem cells. *Nat Commun*, *12*(1), 2665. https://doi.org/10.1038/s41467-021-22863-0

Sunchu, B., & Cabernard, C. (2020). Principles and mechanisms of asymmetric cell division. *Development*, *147*(13), dev167650.

Swanson, E. G., Mao, Y., Mallory, B. J., Vollger, M. R., Bohaczuk, S. C., Oliveira, C. B., Lyon, D. B., Ranchalis, J., Parmalee, N. L., Cohen, B. A., Bennett, J. T., & Stergachis, A. B. (2025). Mapping single-cell diploid chromatin fiber architectures using DAF-seq. *Nat Biotechnol*. https://doi.org/10.1038/s41587-025-02914-3

Taiwo, O., Wilson, G. A., Emmett, W., Morris, T., Bonnet, D., Schuster, E., Adejumo, T., Beck, S., & Pearce, D. J. (2013). DNA methylation analysis of murine hematopoietic side population cells during aging. *Epigenetics*, *8*(10), 1114-1122. https://doi.org/10.4161/epi.26017

Takahashi, K., & Yamanaka, S. (2006). Induction of pluripotent stem cells from mouse embryonic and adult fibroblast cultures by defined factors. *Cell*, *126*(4), 663-676. https://doi.org/10.1016/j.cell.2006.07.024

Tan, G., & Lenhard, B. (2016). TFBSTools: an R/bioconductor package for transcription factor binding site analysis. *Bioinformatics*, *32*(10), 1555-1556.

Tarum, J., Ball, G., Gustafsson, T., Altun, M., & Santos, L. (2024). Artificial neural network inference analysis identified novel genes and gene interactions associated with skeletal muscle aging. *J Cachexia Sarcopenia Muscle*, *15*(5), 2143-2155. https://doi.org/10.1002/jcsm.13562

Tasselli, L., Xi, Y., Zheng, W., Tennen, R. I., Odrowaz, Z., Simeoni, F., Li, W., & Chua, K. F. (2016). SIRT6 deacetylates H3K18ac at pericentric chromatin to prevent mitotic errors and cellular senescence. *Nature structural & molecular biology*, *23*(5), 434-440.

Thalheimer, F. B., Wingert, S., De Giacomo, P., Haetscher, N., Rehage, M., Brill, B., Theis, F. J., Hennighausen, L., Schroeder, T., & Rieger, M. A. (2014). Cytokine-regulated GADD45G induces differentiation and lineage selection in hematopoietic stem cells. *Stem cell reports*, *3*(1), 34-43. https://doi.org/10.1016/j.stemcr.2014.05.010

Thomas, E. D., Lochte, H. L., Jr., Lu, W. C., & Ferrebee, J. W. (1957). Intravenous infusion of bone marrow in patients receiving radiation and chemotherapy. *N Engl J Med*, *257*(11), 491-496. https://doi.org/10.1056/NEJM195709122571102

Thorvaldsdóttir, H., Robinson, J. T., & Mesirov, J. P. (2013). Integrative Genomics Viewer (IGV): high-performance genomics data visualization and exploration. *Briefings in bioinformatics*, *14*(2), 178-192.

Tian, B., Yang, J., & Brasier, A. R. (2012). Two-step cross-linking for analysis of protein-chromatin interactions. *Methods Mol Biol*, *809*, 105-120. https://doi.org/10.1007/978-1-61779-376-9_7

Tian, C., Zheng, G., Cao, Z., Li, Q., Ju, Z., Wang, J., Yuan, W., & Cheng, T. (2013). Hes1 mediates the different responses of hematopoietic stem and progenitor cells to T cell leukemic environment. *Cell Cycle*, *12*(2), 322-331. https://doi.org/10.4161/cc.23160

Tomas-Daza, L., Rovirosa, L., Lopez-Marti, P., Nieto-Aliseda, A., Serra, F., Planas-Riverola, A., Molina, O., McDonald, R., Ghevaert, C., Cuatrecasas, E., Costa, D., Camos, M., Bueno, C., Menendez, P., Valencia, A., & Javierre, B. M. (2023). Low input capture Hi-C (liCHi-C) identifies promoter-enhancer interactions at high-resolution. *Nat Commun*, *14*(1), 268. https://doi.org/10.1038/s41467-023-35911-8

Toppinen, M., Sajantila, A., Pratas, D., Hedman, K., & Perdomo, M. F. (2021). The Human Bone Marrow Is Host to the DNAs of Several Viruses. *Front Cell Infect Microbiol*, *11*, 657245. https://doi.org/10.3389/fcimb.2021.657245

Tran, A., Yang, P., Yang, J. Y. H., & Ormerod, J. T. (2022). scREMOTE: Using multimodal single cell data to predict regulatory gene relationships and to build a computational cell reprogramming model. *NAR Genom Bioinform*, *4*(1), lqac023. https://doi.org/10.1093/nargab/lqac023

Tremblay, B. J.-M. (2024). universalmotif: An R package for biological motif analysis. *Journal of Open Source Software*, *9*(100), 7012.

Trento, C., Marigo, I., Pievani, A., Galleu, A., Dolcetti, L., Wang, C. Y., Serafini, M., Bronte, V., & Dazzi, F. (2017). Bone marrow mesenchymal stromal cells induce nitric oxide synthase-dependent differentiation of CD11b(+) cells that expedite hematopoietic recovery. *haematologica*, *102*(5), 818-825. https://doi.org/10.3324/haematol.2016.155390

Valletta, S., Thomas, A., Meng, Y., Ren, X., Drissen, R., Sengul, H., Di Genua, C., & Nerlov, C. (2020). Micro-environmental sensing by bone marrow stroma identifies IL-6 and TGFbeta1 as regulators of hematopoietic ageing. *Nat Commun*, *11*(1), 4075. https://doi.org/10.1038/s41467-020-17942-7

Van Meter, M., Kashyap, M., Rezazadeh, S., Geneva, A. J., Morello, T. D., Seluanov, A., & Gorbunova, V. (2014). SIRT6 represses LINE1 retrotransposons by ribosylating KAP1 but this repression fails with stress and age. *Nature communications*, *5*(1), 1-10.

Van Meter, M., Simon, M., Tombline, G., May, A., Morello, T. D., Hubbard, B. P., Bredbenner, K., Park, R., Sinclair, D. A., & Bohr, V. A. (2016). JNK phosphorylates SIRT6 to stimulate DNA double-strand break repair in response to oxidative stress by recruiting PARP1 to DNA breaks. *Cell reports*, *16*(10), 2641-2650.

Varesi, A., Nagree, M. S., Di Biasio, I., Zeng, A. G. X., Shah, S., Zhang, M., Kim, H., Murison, A., Badami, R., Gan, O., Jin, L., McLeod, J., Abraham, S. A., Minden, M. D., Arruda, A., Novitzky-Basso, I., Mattsson, J., Dick, J. E., & Xie, S. Z. (2026). ATP2B1 expression identifies human hematopoietic stem cells with superior repopulation and self-renewal. *Proc Natl Acad Sci U S A*, *123*(19), e2604380123. https://doi.org/10.1073/pnas.2604380123

Vaziri, H., Dragowska, W., Allsopp, R. C., Thomas, T. E., Harley, C. B., & Lansdorp, P. M. (1994). Evidence for a mitotic clock in human hematopoietic stem cells: loss of

telomeric DNA with age. *Proc Natl Acad Sci U S A*, *91*(21), 9857-9860. https://doi.org/10.1073/pnas.91.21.9857

Velasco-Muñoz, V., Uribe-Gaviria, M., Suárez-Gómez, S. A., Villamizar-Romero, A., Ricaurte-Fajardo, A., Vásquez-Vélez, I. C., & Cano-Gutiérrez, C. A. (2025). Regenerative characteristics of the immortal jellyfish, Turritopsis dohrnii, and their potential implications for human aging. *Revista Española de Geriatría y Gerontología*, *60*(3), 101607.

Vierbuchen, T., Ostermeier, A., Pang, Z. P., Kokubu, Y., Sudhof, T. C., & Wernig, M. (2010). Direct conversion of fibroblasts to functional neurons by defined factors. *Nature*, *463*(7284), 1035-1041. https://doi.org/10.1038/nature08797

Vorontsov, I. E., Eliseeva, I. A., Zinkevich, A., Nikonov, M., Abramov, S., Boytsov, A., Kamenets, V., Kasianova, A., Kolmykov, S., & Yevshin, I. S. (2024). HOCOMOCO in 2024: a rebuild of the curated collection of binding models for human and mouse transcription factors. *Nucleic acids research*, *52*(D1), D154-D163.

Wahlestedt, M., Erlandsson, E., Kristiansen, T., Lu, R., Brakebusch, C., Weissman, I. L., Yuan, J., Martin-Gonzalez, J., & Bryder, D. (2017). Clonal reversal of ageing-associated stem cell lineage bias via a pluripotent intermediate. *Nat Commun*, *8*(1), 14533. https://doi.org/10.1038/ncomms14533

Wakayama, S., Ito, D., Inoue, R., Ooga, M., Toshishige, M., Satoh, Y., Shiura, H., Kohda, T., Uchimura, A., & Wakayama, T. (2026). Limitations of serial cloning in mammals. *Nature communications*, *17*(1), 2495.

Wakayama, S., Kohda, T., Obokata, H., Tokoro, M., Li, C., Terashita, Y., Mizutani, E., Kishigami, S., Ishino, F., & Wakayama, T. (2013). Successful serial recloning in the mouse over multiple generations. *Cell stem cell*, *12*(3), 293-297.

Walter, D., Lier, A., Geiselhart, A., Thalheimer, F. B., Huntscha, S., Sobotta, M. C., Moehrle, B., Brocks, D., Bayindir, I., Kaschutnig, P., Muedder, K., Klein, C., Jauch, A., Schroeder, T., Geiger, H., Dick, T. P., Holland-Letz, T., Schmezer, P., Lane, S. W.,…Milsom, M. D. (2015). Exit from dormancy provokes DNA-damage-induced attrition in haematopoietic stem cells. *Nature*, *520*(7548), 549-552. https://doi.org/10.1038/nature14131

Wang, J., Su, M., Wei, N., Yan, H., Zhang, J., Gong, Y., Wu, L., Suolitiken, D., Pi, Y., Song, D., Chen, L., Liu, H., Yang, S., Wang, X., & Wang, Z. (2024). Chronic active Epstein-Barr virus disease originates from infected hematopoietic stem cells. *Blood*, *143*(1), 32-41. https://doi.org/10.1182/blood.2023021074

Wang, J. C., Warner, J. K., Erdmann, N., Lansdorp, P. M., Harrington, L., & Dick, J. E. (2005). Dissociation of telomerase activity and telomere length maintenance in primitive human hematopoietic cells. *Proc Natl Acad Sci U S A*, *102*(40), 14398-14403. https://doi.org/10.1073/pnas.0504161102

Wang, R., Graham, S., Gao, L., Tam, J., & Levesque, M. C. (2021). Editing the immune system in vivo in mice using CRISPR/Cas9 ribonucleoprotein (RNP)-mediated gene editing of transplanted hematopoietic stem cells. *Methods*, *194*, 30-36. https://doi.org/10.1016/j.ymeth.2021.01.001

Wang, X. M., Ming, K., Wang, S., Wang, J., Li, P. L., Tian, R. F., Liu, S. Y., Cheng, X., Chen, Y., Shi, W., Wan, J., Hu, M., Tian, S., Zhang, X., She, Z. G., Li, H., Ding, Y., & Zhang, X. J. (2023). Network-based analysis identifies key regulatory

transcription factors involved in skin aging. *Exp Gerontol*, *178*, 112202. https://doi.org/10.1016/j.exger.2023.112202

Wang, Y., Lu, T., Sun, G., Zheng, Y., Yang, S., Zhang, H., Hao, S., Liu, Y., Ma, S., Zhang, H., Ru, Y., Gao, S., Yen, K., Cheng, H., & Cheng, T. (2019). Targeting of apoptosis gene loci by reprogramming factors leads to selective eradication of leukemia cells. *Nat Commun*, *10*(1), 5594. https://doi.org/10.1038/s41467-019-13411-y

Wang, Y., Zhang, W., Zhang, C., Van, H. Q. T., Seino, T., & Zhang, Y. (2025). Reducing functionally defective old HSCs alleviates aging-related phenotypes in old recipient mice. *Cell Res*, *35*(1), 45-58. https://doi.org/10.1038/s41422-024-01057-5

Warga, E., Anderson, J., Tucker, M., Harris, E., & Elmer, J. (2023). Transcriptomic analysis of the innate immune response to in vitro transfection of plasmid DNA. *Mol Ther Nucleic Acids*, *31*, 43-56. https://doi.org/10.1016/j.omtn.2022.11.025

Warren, L., Manos, P. D., Ahfeldt, T., Loh, Y.-H., Li, H., Lau, F., Ebina, W., Mandal, P. K., Smith, Z. D., & Meissner, A. (2010). Highly efficient reprogramming to pluripotency and directed differentiation of human cells with synthetic modified mRNA. *Cell stem cell*, *7*(5), 618-630.

Weeks, L. D., Niroula, A., Neuberg, D., Wong, W., Lindsley, R. C., Luskin, M., Berliner, N., Stone, R. M., DeAngelo, D. J., Soiffer, R., Uddin, M. M., Griffin, G., Vlasschaert, C., Gibson, C. J., Jaiswal, S., Bick, A. G., Malcovati, L., Natarajan, P., & Ebert, B. L. (2023). Prediction of risk for myeloid malignancy in clonal hematopoiesis. *NEJM Evid*, *2*(5). https://doi.org/10.1056/evidoa2200310

Weidner, C., Ziegler, P., Hahn, M., Brümmendorf, T., Ho, A., Dreger, P., & Wagner, W. (2015). Epigenetic aging upon allogeneic transplantation: the hematopoietic niche does not affect age-associated DNA methylation. *Leukemia*, *29*(4), 985-988.

Wickham, H. (2016). *ggplot2: Elegant Graphics for Data Analysis*. Springer-Verlag New York. https://ggplot2.tidyverse.org

Wickham, H., François, R., Henry, L., Müller, K., & Vaughan, D. (2023). dplyr: A grammar of data manipulation. (Version 1.1.4) [R package]. https://dplyr.tidyverse.org

Wickham, H., Hester, J., Francois, R., Bryan, J., Bearrows, S., Jylänki, J., & Jørgensen, M. (2024). readr: Read Rectangular Text Data. (Version 2.1.5) [R package]. https://readr.tidyverse.org

Wilkinson, A. C., Ishida, R., Nakauchi, H., & Yamazaki, S. (2020). Long-term ex vivo expansion of mouse hematopoietic stem cells. *Nat Protoc*, *15*(2), 628-648. https://doi.org/10.1038/s41596-019-0263-2

Wlodarczyk, T., Lun, A., Wu, D., Shi, M., Ye, X., Menon, S., Toneyan, S., Seidel, K., Wang, L., Tan, J., Chen, S. Y., Keyes, T., Chlebowski, A., Waddell, A., Zhou, W., Wang, Y., Yuan, Q., Guo, Y., Chen, L. F.,…Yao, X. (2025). Epiregulon: Single-cell transcription factor activity inference to predict drug response and drivers of cell states. *Nat Commun*, *16*(1), 7118. https://doi.org/10.1038/s41467-025-62252-5

Woolthuis, C. M., Mariani, N., Verkaik-Schakel, R. N., Brouwers-Vos, A. Z., Schuringa, J. J., Vellenga, E., de Wolf, J. T., & Huls, G. (2014). Aging impairs long-term hematopoietic regeneration after autologous stem cell transplantation. *Biol Blood Marrow Transplant*, *20*(6), 865-871. https://doi.org/10.1016/j.bbmt.2014.03.001

Xiao, D., Sahadevan, S., Mangala, M. M., Kim, H. J., Fredericks, A., Huang, H., Jothi, R., Tam, P., Gonzalez-Cordero, A., Zyner, K. G., & Yang, P. (2025). Refate identifies

chemical compounds to target trans-regulatory networks for cellular conversion. *bioRxiv*. https://doi.org/10.1101/2025.07.09.664003

Xie, M., Lu, C., Wang, J., McLellan, M. D., Johnson, K. J., Wendl, M. C., McMichael, J. F., Schmidt, H. K., Yellapantula, V., Miller, C. A., Ozenberger, B. A., Welch, J. S., Link, D. C., Walter, M. J., Mardis, E. R., Dipersio, J. F., Chen, F., Wilson, R. K., Ley, T. J., & Ding, L. (2014). Age-related mutations associated with clonal hematopoietic expansion and malignancies. *Nat Med*, *20*(12), 1472-1478. https://doi.org/10.1038/nm.3733

Xu, C., & Corces, V. G. (2018). Nascent DNA methylome mapping reveals inheritance of hemimethylation at CTCF/cohesin sites. *Science*, *359*(6380), 1166-1170.

Xu, Q., Georgiou, G., Frolich, S., van der Sande, M., Veenstra, G. J. C., Zhou, H., & van Heeringen, S. J. (2021). ANANSE: an enhancer network-based computational approach for predicting key transcription factors in cell fate determination. *Nucleic Acids Res*, *49*(14), 7966-7985. https://doi.org/10.1093/nar/gkab598

Xu, S., Liang, D., Wang, Q., Cheng, Y., Xie, D., Gui, Y., Zhang, H., Feng, C., Zhao, F., Ren, W., Sun, G., Yang, Y., Li, L., Lai, Y., Fu, B., Lu, Y., Wang, Z. J., & Wu, Y. (2026). In vivo genome editing of human haematopoietic stem cells for treatment of blood disorders using mRNA delivery. *Nat Biomed Eng*, *10*(3), 473-489. https://doi.org/10.1038/s41551-025-01480-y

Yamada, T., Fukasawa, K., Horie, T., Kadota, T., Lyu, J., Tokumura, K., Ochiai, S., Iwahashi, S., Suzuki, A., Park, G., Ueda, R., Yamamoto, M., Kitao, T., Shirahase, H., Ochi, H., Sato, S., Iezaki, T., & Hinoi, E. (2022). The role of CDK8 in mesenchymal stem cells in controlling osteoclastogenesis and bone homeostasis. *Stem cell reports*, *17*(7), 1576-1588. https://doi.org/10.1016/j.stemcr.2022.06.001

Yamamoto, R., Morita, Y., Ooehara, J., Hamanaka, S., Onodera, M., Rudolph, K. L., Ema, H., & Nakauchi, H. (2013). Clonal analysis unveils self-renewing lineage-restricted progenitors generated directly from hematopoietic stem cells. *Cell*, *154*(5), 1112-1126. https://doi.org/10.1016/j.cell.2013.08.007

Yamamoto, R., Wilkinson, A. C., Ooehara, J., Lan, X., Lai, C. Y., Nakauchi, Y., Pritchard, J. K., & Nakauchi, H. (2018). Large-Scale Clonal Analysis Resolves Aging of the Mouse Hematopoietic Stem Cell Compartment. *Cell stem cell*, *22*(4), 600-607 e604. https://doi.org/10.1016/j.stem.2018.03.013

Yang, B. A., Larouche, J. A., Sabin, K. M., Fraczek, P. M., Parker, S. C. J., & Aguilar, C. A. (2023). Three-dimensional chromatin re-organization during muscle stem cell aging. *Aging cell*, *22*(4), e13789. https://doi.org/10.1111/acel.13789

Yang, D., Skinder, N., Kao, Y. R., Chen, J., Thiruthuvanathan, V., Flohr Svendsen, A., Zhang, C., Dethmers-Ausema, B., Weersing, E., Maryanovich, M., Will, B., & de Haan, G. (2025). Aberrant engagement of P-selectin drives hematopoietic stem cell aging in mice. *Nat Aging*, *5*(6), 1010-1024. https://doi.org/10.1038/s43587-025-00880-8

Yang, J.-H., Hayano, M., Griffin, P. T., Amorim, J. A., Bonkowski, M. S., Apostolides, J. K., Salfati, E. L., Blanchette, M., Munding, E. M., & Bhakta, M. (2023a). Loss of epigenetic information as a cause of mammalian aging. *Cell*, *186*(2), p305-326.e327. https://doi.org/10.1016/j.cell.2022.12.027

Yang, J.-H., Petty, C. A., Dixon-McDougall, T., Lopez, M. V., Tyshkovskiy, A., Maybury-Lewis, S., Tian, X., Ibrahim, N., Chen, Z., Griffin, P. T., Arnold, M., Li, J.,

Martinez, O. A., Behn, A., Rogers-Hammond, R., Angeli, S., Gladyshev, V. N., & Sinclair, D. A. (2023b). Chemically induced reprogramming to reverse cellular aging. *Aging (Albany NY)*, *15*(13), 5966-5989. https://doi.org/10.18632/aging.204896

Yang, X., Gandhi, C., Rahman, M. M., Appleford, M., Sun, L. W., & Wang, X. (2015). Age-Related Effects of Advanced Glycation End Products (Ages) in Bone Matrix on Osteoclastic Resorption. *Calcif Tissue Int*, *97*(6), 592-601. https://doi.org/10.1007/s00223-015-0042-1

Yang, Z., Xu, F., Teschendorff, A. E., Zhao, Y., Yao, L., Li, J., & He, Y. (2022). Insights into the role of long non-coding RNAs in DNA methylation mediated transcriptional regulation. *Frontiers in molecular biosciences*, *9*, 1067406.

Young, K., Eudy, E., Bell, R., Loberg, M. A., Stearns, T., Sharma, D., Velten, L., Haas, S., Filippi, M. D., & Trowbridge, J. J. (2021). Decline in IGF1 in the bone marrow microenvironment initiates hematopoietic stem cell aging. *Cell stem cell*, *28*(8), 1473-1482 e1477. https://doi.org/10.1016/j.stem.2021.03.017

Young, K. A., Telpoukhovskaia, M. A., Hofmann, J., Mistry, J. J., Kokkaliaris, K. D., & Trowbridge, J. J. (2024). Variation in mesenchymal KITL/SCF and IGF1 expression in middle age underlies steady-state hematopoietic stem cell aging. *Blood*, *144*(4), 378-391. https://doi.org/10.1182/blood.2024024275

Young, N. S. (2018). Aplastic Anemia. *N Engl J Med*, *379*(17), 1643-1656. https://doi.org/10.1056/NEJMra1413485

Younis, S., Moutusy, S. I., Rasouli, S., Jahanbani, S., Pandit, M., Wu, X., Acharya, S., Sharpe, O., Wijeratne, T. U., Harris, M. L., Yang, E. Y., Chaichian, Y., Parsafar, S., Baker, M. C., Harley, J. B., Meffre, E., Steinman, L., Marshak-Rothstein, A., James, J. A.,…Robinson, W. H. (2025). Epstein-Barr virus reprograms autoreactive B cells as antigen-presenting cells in systemic lupus erythematosus. *Sci Transl Med*, *17*(824), eady0210. https://doi.org/10.1126/scitranslmed.ady0210

Yu, B., Roberts, M. B., Raffield, L. M., Zekavat, S. M., Nguyen, N. Q. H., Biggs, M. L., Brown, M. R., Griffin, G., Desai, P., Correa, A., Morrison, A. C., Shah, A. M., Niroula, A., Uddin, M. M., Honigberg, M. C., Ebert, B. L., Psaty, B. M., Whitsel, E. A., Manson, J. E.,…Blood Institute, T. C. (2021). Supplemental Association of Clonal Hematopoiesis With Incident Heart Failure. *J Am Coll Cardiol*, *78*(1), 42-52. https://doi.org/10.1016/j.jacc.2021.04.085

Yu, G. (2025). enrichplot: Visualization of Functional Enrichment Result. (Version 1.28.4) [R package]. Bioconductor. https://www.bioconductor.org/packages/release/bioc/html/enrichplot.html

Yu, G., Wang, L. G., Han, Y., & He, Q. Y. (2012). clusterProfiler: an R package for comparing biological themes among gene clusters. *OMICS*, *16*(5), 284-287. https://doi.org/10.1089/omi.2011.0118

Yu, J., Vodyanik, M. A., Smuga-Otto, K., Antosiewicz-Bourget, J., Frane, J. L., Tian, S., Nie, J., Jonsdottir, G. A., Ruotti, V., Stewart, R., Slukvin, II, & Thomson, J. A. (2007). Induced pluripotent stem cell lines derived from human somatic cells. *Science*, *318*(5858), 1917-1920. https://doi.org/10.1126/science.1151526

Yucel, D., Trembley, M. A., Ke, Q., Wu, Z., Kang, P., & Pu, W. T. (2025). Molecular Mechanisms of Cardiomyocyte Aging. *bioRxiv*. https://doi.org/10.1101/2025.07.29.666777

Yusa, K., Rad, R., Takeda, J., & Bradley, A. (2009). Generation of transgene-free induced pluripotent mouse stem cells by the piggyBac transposon. *Nat Methods*, *6*(5), 363-369. https://doi.org/10.1038/nmeth.1323

Yusa, K., Zhou, L., Li, M. A., Bradley, A., & Craig, N. L. (2011). A hyperactive piggyBac transposase for mammalian applications. *Proc Natl Acad Sci U S A*, *108*(4), 1531-1536. https://doi.org/10.1073/pnas.1008322108

Zaro, B. W., Noh, J. J., Mascetti, V. L., Demeter, J., George, B., Zukowska, M., Gulati, G. S., Sinha, R., Flynn, R. A., Banuelos, A., Zhang, A., Wilkinson, A. C., Jackson, P., & Weissman, I. L. (2020). Proteomic analysis of young and old mouse hematopoietic stem cells and their progenitors reveals post-transcriptional regulation in stem cells. *elife*, *9*. https://doi.org/10.7554/eLife.62210

Zhang, B., & Horvath, S. (2005). A general framework for weighted gene co-expression network analysis. *Stat Appl Genet Mol Biol*, *4*, Article17. https://doi.org/10.2202/1544-6115.1128

Zhang, C., Xu, Z., Yang, S., Sun, G., Jia, L., Zheng, Z., Gu, Q., Tao, W., Cheng, T., Li, C., & Cheng, H. (2020). tagHi-C Reveals 3D Chromatin Architecture Dynamics during Mouse Hematopoiesis. *Cell Rep*, *32*(13), 108206. https://doi.org/10.1016/j.celrep.2020.108206

Zhang, C. P., Qiu, H. Y., Zhang, C. X., Zhang, Y. M., Zhang, Y. Z., Yin, H., Zhang, K. Q., & Zhang, Y. (2023). Efficient non-viral delivery of macromolecules in human primary hematopoietic stem cells and lymphocytes. *J Mol Cell Biol*, *15*(3). https://doi.org/10.1093/jmcb/mjad018

Zhang, H., Liesveld, J. L., Calvi, L. M., Lipe, B. C., Xing, L., Becker, M. W., Schwarz, E. M., & Yeh, S. A. (2023). The roles of bone remodeling in normal hematopoiesis and age-related hematological malignancies. *Bone Res*, *11*(1), 15. https://doi.org/10.1038/s41413-023-00249-w

Zhang, J., Li, H., Li, L., Wu, J., Song, L., Liu, X., Pan, Z., Zhou, C., Li, W., Liu, Z., Jiao, M., Hu, M., Dong, Z., Zhang, H., Shi, B., Wang, Y., Wang, D., Carter, B., Zhao, S.,…Zhang, Y. (2025). Super RNA Pol II domains enhance minor ZGA through 3D interaction to ensure the integrity of major transcriptional waves in late-ZGA mammals. *Cell Genom*, *5*(6), 100856. https://doi.org/10.1016/j.xgen.2025.100856

Zhang, L., Dong, X., Lee, M., Maslov, A. Y., Wang, T., & Vijg, J. (2019). Single-cell whole-genome sequencing reveals the functional landscape of somatic mutations in B lymphocytes across the human lifespan. *Proc Natl Acad Sci U S A*, *116*(18), 9014-9019. https://doi.org/10.1073/pnas.1902510116

Zhang, W., Ou, G., Hamrick, M., Hill, W., Borke, J., Wenger, K., Chutkan, N., Yu, J., Mi, Q. S., Isales, C. M., & Shi, X. M. (2008). Age-related changes in the osteogenic differentiation potential of mouse bone marrow stromal cells. *J Bone Miner Res*, *23*(7), 1118-1128. https://doi.org/10.1359/jbmr.080304

Zhang, W. Q., Li, J. Y., Suzuki, K., Qu, J., Wang, P., Zhou, J. Z., Liu, X. M., Ren, R. T., Xu, X. L., Ocampo, A., Yuan, T. T., Yang, J. P., Li, Y., Shi, L., Guan, D., Pan, H. Z., Duan, S. L., Ding, Z. C., Li, M.,…Belmonte, J. C. I. (2015). A Werner syndrome stem cell model unveils heterochromatin alterations as a driver of human aging. *Science*, *348*(6239), 1160-1168. https://doi.org/10.1126/science.aaa1356

Zhang, Y., Amaral, M. L., Zhu, C., Grieco, S. F., Hou, X., Lin, L., Buchanan, J., Tong, L., Preissl, S., Xu, X., & Ren, B. (2022). Single-cell epigenome analysis reveals age-

associated decay of heterochromatin domains in excitatory neurons in the mouse brain. *Cell Res*, *32*(11), 1008-1021. https://doi.org/10.1038/s41422-022-00719-6

Zhang, Y., Liu, T., Meyer, C. A., Eeckhoute, J., Johnson, D. S., Bernstein, B. E., Nusbaum, C., Myers, R. M., Brown, M., & Li, W. (2008). Model-based analysis of ChIP-Seq (MACS). *Genome biology*, *9*(9), R137.

Zhao, X.-y., Li, W., Lv, Z., Liu, L., Tong, M., Hai, T., Hao, J., Wang, X., Wang, L., & Zeng, F. (2010). Viable fertile mice generated from fully pluripotent iPS cells derived from adult somatic cells. *Stem cell reviews and reports*, *6*, 390-397.

Zhao, Y., Ding, Y., He, L., Zhou, Q., Chen, X., Li, Y., Alfonsi, M. V., Wu, Z., Sun, H., & Wang, H. (2023). Multiscale 3D genome reorganization during skeletal muscle stem cell lineage progression and aging. *Sci Adv*, *9*(7), eabo1360. https://doi.org/10.1126/sciadv.abo1360

Zheng, Z., Zhou, H., Zhang, W., Wang, T., Swamiappan, S., Peng, X., & Zhou, Y. (2024). Effects of advanced glycation end products on stem cell. *Front Cell Dev Biol*, *12*, 1532614. https://doi.org/10.3389/fcell.2024.1532614

Zhou, C., Kuang, M., Liu, Z., Jia, X., Chen, Z., Liu, Y., Li, Z., Wu, W., Ma, L., Chen, J., & Hou, Y. (2022). Insufficiency of FZR1 disturbs HSC quiescence by inhibiting ubiquitin-dependent degradation of RUNX1 in aplastic anemia. *Leukemia*, *36*(3), 834-846. https://doi.org/10.1038/s41375-021-01445-5

Zhou, S., Greenberger, J. S., Epperly, M. W., Goff, J. P., Adler, C., Leboff, M. S., & Glowacki, J. (2008). Age-related intrinsic changes in human bone-marrow-derived mesenchymal stem cells and their differentiation to osteoblasts. *Aging cell*, *7*(3), 335-343. https://doi.org/10.1111/j.1474-9726.2008.00377.x

Zong, L., Tanaka-Yano, M., Park, B., Yanai, H., Turhan, F. T., Croteau, D. L., Tian, J., Fang, E. F., Bohr, V. A., & Beerman, I. (2021). NAD(+) augmentation with nicotinamide riboside improves lymphoid potential of Atm(-/-) and old mice HSCs. *NPJ Aging Mech Dis*, *7*(1), 25. https://doi.org/10.1038/s41514-021-00078-3